
**Synthesis of Novel Functionalised β -Ketoiminate and β -
Diketonate Metal Complexes for Their Use in Anti-Cancer
Treatment**

Rianne Michaela Lord

Submitted in accordance with the requirements for the degree of Doctor of
Philosophy

The University of Leeds
School of Chemistry

January 2014

The candidate confirms that the work submitted is her own, except where work which has formed part of jointly-authored publications has been included. The contribution of the candidate and the other authors to this work has been explicitly indicated below. The candidate confirms that appropriate credit has been given within the thesis where reference has been made to the work of others. The references for the jointly authored papers are stated below:

R. M. Lord, A. E. Nako, J. J. Mannion, A. J. Hebden, B. D. Crossley, M. W. McMullon, F. D. Janeway, R. M. Phillips and P. C. McGowan, ‘Mechanistic and Cytotoxicity studies of Group IV β -Diketonate Complexes’, *ChemMedChem*, **2014**, *accepted* (Metals in Medicine, special edition)

V. Brabec, S. E. Howson, R. A. Kaner, R. M. Lord, J. Malina, R. M. Phillips, Q. M. A. Abdallah, P. C. McGowan, A. Rodger and P. Scott, ‘Metallohelices with activity against cisplatin-resistant cancer cells; does the mechanism involve DNA binding?’ *Chem. Sci.*, **2013**, *4*, 4407-4416 (Hot paper September 2012)

S. J. Lucas, R. M. Lord, R. L. Wilson, R. M. Phillips, V. Sridharan and P. C. McGowan, ‘Synthesis of iridium and ruthenium complexes with (N,N), (N,O) and (O,O) coordinating bidentate ligands as potential anti-cancer agents’ *Dalton Trans.*, **2012**, *41*, 13800.13802 (top ten accessed journal September 2012)

In addition, following papers are pending publication:

A. Rodríguez-Bárzano, R. M. Lord, A. M. Basri, R. M. Phillips, A. J. Blacker and P. C. McGowan, **2014**, *Manuscript submitted*

S. J. Lucas, R. M. Lord, A. M. Basri, R. M. Phillips, A. J. Blacker and P. C. McGowan, **2014**, *Manuscript completed*

R. M. Lord, S. J. Lucas, A Rodríguez-Bárzano, S. J. Alison, R. M. Phillips, J. Fisher and P. C. McGowan, **2014**, *Manuscript in preparation*

Acknowledgements

I would like to say a huge thank you to Paddy for always having faith in me and for giving me the freedom to explore this project in my own way. I am very grateful for the opportunities you have given me, which have turned me into a keen biologist. I appreciate all your help and invaluable feedback, allowing me to finally gain confidence in both myself and my work. Also a thank you to Roger at the ICT in Bradford, you and your team have provided me with the knowledge to carry out all my own biology work and have always been there with a smile and a helping hand. Also a special thank you to Charlotte Willans for my initial cell line training.

Where would I be without Dr. Pask, not only have you been a huge inspiration and have always seen the better in me, but you have been an amazing friend. A massive thank you for all you do, your invaluable feedback and the masses of proof reading over the last 4 years. We would all be truly lost without you! Thank you to both past and present members of lab 1.29 who have made the past 4 years so enjoyable, for the many fun nights out, Christmas parties and for gaining lasting friendships. The McGowan group – Andrew, Ben, Adi, Felix, Andrea, Aida, Carlo and Laura, and the Halcrow group – Ame, Raf, Jonny, Tom and Laurence. It has truly been a pleasure working with you all and I am not sure I will ever find lab friends as ‘special’ as you guys! Last but not least I would like to say a massive thank you to my two best friends Stephie and Rufeida (FayFay). Thank you for all the laughs and nights out, some which are more memorable than others. Thank you for being there through the ups and downs with a bottle of rum at the ready!

The biggest thank you must go to my family... My parents, sister, grandma and nephew, you are my world and I wouldn't have made it here without you! Mum and Dad, I love you and words can never explain how thankful I am for everything you have done and continue to do for me. You have both always had so much faith in me no matter what. Thank you for always being on the other side of the phone and giving me words of encouragement and putting me back on track when things were rocky. Lastly, to my grandma who saw me start this degree but never got the chance to see me finish... I love you and miss you!

Abstract

This thesis is concerned with the synthesis, characterisation and evaluation of novel metal complexes for their application as anti-cancer agents. It contains the *in vitro* cell results, along with a range of other techniques to determine their biological relevance and their potential as anti-cancer agents.

Chapter 1 contains an introduction to the project including a literature search, previously synthesised complexes and project aims

Chapter 2 presents the synthesis and characterisation of novel β -diketonate and β -ketoiminate ligands. X-ray crystallographic data are analysed for some of the ligands.

Chapter 3 discusses the synthesis and characterisation of novel β -ketoiminate ruthenium chloride complexes. X-ray crystallographic data are analysed for all of the complexes.

Chapter 4 introduces the MTT technique for assessing cytotoxicity, and presents *in vitro* activities for the library of complexes synthesised in Chapter 3.

Chapter 5 looks at modifications of the previous ruthenium (II) complexes, introducing new ligands and iridium metal centres. X-ray crystallographic data for all of these complexes has been discussed, along with *in vitro* activity against a range of cell lines.

Chapter 6 introduces hypoxia and states the cytotoxicities of a range of complexes under 1.0% and 0.1% oxygen concentrations.

Chapter 7 discusses mechanistic studies on the complexes, including hydrolysis, hydrophobicity, Comet assay, apoptosis and thioredoxin reductase inhibition.

Chapter 8 introduces the previous group IV work within the group and an extension of the library by synthesis of β -ketoiminate titanium complexes. X-ray crystallographic analysis is discussed where applicable.

Chapter 9 contains experimental details and characterisation data for all compounds described in Chapters 2, 3, 5 and 8. Also protocols for all the biological studies.

Appendix presents a summary of X-ray crystallographic structure analysis for any crystals obtained within this work

Contents

ACKNOWLEDGEMENTS	II
ABSTRACT	III
CONTENTS.....	IV
ABBREVIATIONS.....	XI
1 INTRODUCTION	2
1.1 CANCER.....	2
1.2 METAL-BASED DRUGS	3
1.3 CISPLATIN	4
1.4 SECOND GENERATION OF PLATINUM COMPLEXES.....	6
1.5 TITANOCENE DICHLORIDE.....	8
1.5.1 Variations of the Chloride Ligands	9
1.5.2 Cyclopentadienyl Derivatives of Titanocene Dichloride	10
1.6 BUDOTITANE	13
1.7 RUTHENIUM.....	16
1.7.1 Ruthenium Red.....	17
1.7.2 NAMI-A.....	17
1.7.3 KP418 and KP1019.....	18
1.7.4 Organometallic Ruthenium Arenes.....	19
1.8 RESEARCH AIMS.....	23
1.9 REFERENCES.....	25
2 PREPARATION OF (<i>O,O</i>) AND (<i>N,O</i>) LIGANDS	32
2.1 PREPARATION OF β -DIKETONATE (<i>O,O</i>) LIGANDS	32
2.2 SYNTHESIS OF MONO-ARYL β -DIKETONATE LIGANDS.....	32
2.2.1 Characterisation of Mono-Aryl β -Diketonate Ligands	33
2.3 SYNTHESIS OF BIARYL β -DIKETONATE LIGANDS	34
2.3.1 Characterisation of Biaryl β -Diketonate Ligands	34
2.4 PREPARATION OF β -KETOIMINATE (<i>N,O</i>) LIGANDS	35
2.5 SYNTHESIS OF β -KETOIMINATE LIGANDS.....	36
2.5.1 NMR Characterisations for β -Ketoiminate Ligands	36

2.5.2	X-ray Crystallography for β -Ketoiminate.....	38
2.6	CHARACTERISATION OF NOVEL β -KETOIMINATE COMPOUNDS.....	38
2.6.1	X-ray Characterisation of C ₁₇ H ₁₇ NO (L11)	38
2.6.2	X-ray Characterisation of C ₁₆ H ₁₄ FNO (L12).....	40
2.6.3	X-ray Characterisation of C ₁₆ H ₁₃ Cl ₂ NO (L14).....	42
2.6.4	X-ray Characterisation of C ₁₆ H ₁₃ Cl ₂ NO (L15).....	44
2.6.5	X-ray Characterisation of C ₁₆ H ₁₂ Cl ₃ NO (L16).....	46
2.6.6	X-ray Characterisation of C ₁₈ H ₁₈ NO (L19)	48
2.6.7	X-ray characterisation for C ₁₈ H ₁₈ NO ₃ (L21).....	51
2.6.8	X-ray Characterisation of C ₁₈ H ₁₈ FNO ₂ (L22).....	54
2.6.9	X-ray Characterisation for C ₁₇ H ₁₅ NO ₃ (L24)	57
2.6.10	X-ray Characterisation of C ₁₉ H ₁₇ N ₃ O (L25).....	59
2.7	CONCLUSIONS	61
2.8	REFERENCES.....	61
3	RUTHENIUM ARENE COMPLEXES	63
3.1	RUTHENIUM (II) CHLORIDE COMPLEXES	66
3.2	NMR DATA FOR RUTHENIUM(II) CHLORIDE COMPLEXES.....	67
3.3	X-RAY CRYSTALLOGRAPHY FOR RUTHENIUM (II) CHLORIDE COMPLEXES	69
3.3.1	X-ray Characterisation for C ₂₆ H ₂₇ ClFNORu (1).....	69
3.3.2	X-ray Characterisation for C ₂₆ H ₂₇ ClFNORu (2).....	72
3.3.3	X-ray Characterisation for C ₂₆ H ₂₇ Cl ₂ NORu (3)	73
3.3.4	X-ray Characterisation for C ₂₆ H ₂₆ Cl ₃ NORu (4)	75
3.3.5	X-ray Characterisation for C ₂₆ H ₂₆ Cl ₃ NORu (5)	77
3.3.6	X-ray Characterisation for C ₂₆ H ₂₅ Cl ₄ NORu (6)	80
3.3.7	X-ray Characterisation for C ₂₆ H ₂₇ BrClNORu (7).....	83
3.3.8	X-ray Characterisation for C ₂₆ H ₂₇ BrClNORu (8).....	85
3.3.9	X-ray Characterisation for C ₂₆ H ₂₇ ClINORu (9)	87
3.3.10	X-ray Characterisation for C ₂₈ H ₃₂ ClNO ₂ Ru (10)	88
3.3.11	X-ray Characterisation for C ₂₇ H ₃₀ ClNORu (11).....	90
3.3.12	X-ray Characterisation for C ₃₀ H ₃₀ ClNORu (12).....	92
3.3.13	X-ray Characterisation for C ₂₆ H ₂₅ ClF ₃ NORu (13).....	95
3.4	CONCLUSIONS	98
3.5	REFERENCES.....	99

4	CYTOTOXICITY EVALUATION	98
4.1	MTT ASSAY	98
4.2	XTT ASSAY.....	99
4.3	SRB ASSAY.....	100
4.4	5-DAY MTT ASSAY	100
4.4.1	Conducting MTT Under Normoxic Conditions (21% O ₂).....	101
4.5	RESULTS AND DISCUSSION	101
4.5.1	β -Ketoiminate Ruthenium(II) Complexes	101
4.6	CONCLUSION	106
4.7	REFERENCES.....	107
5	MODIFIED COMPLEXES.....	109
5.1	SYNTHESIS OF ANILINE RUTHENIUM (II) DICHLORIDE (14).....	109
5.1.1	X-ray Characterisation of C ₁₆ H ₂₁ Cl ₂ NRu (14).....	110
5.2	SYNTHESIS OF DIPHENYL β -KETOIMINATE RUTHENIUM(II) CHLORIDE (15)	
	112	
5.2.1	X-ray Characterisation of C ₂₅ H ₂₆ ClNORu (15).....	112
5.3	SYNTHESIS OF β -DIKETONATE RUTHENIUM(II) CHLORIDE (16)	114
5.3.1	X-ray Characterisation of C ₂₀ H ₂₆ ClO ₂ Ru (16).....	114
5.4	SYNTHESIS OF β -KETOIMINATE RUTHENIUM ARENE CHLORIDE (17).....	116
5.4.1	X-ray Characterisation of C ₁₆ H ₁₄ ClFO ₂ Ru (17)	117
5.5	SYNTHESIS OF β -KETOIMINATE IRIDIUM Cp* CHLORIDE (C18).....	118
5.6	SYNTHESIS OF β -DIKETONATE IRIDIUM Cp* CHLORIDE (19).....	119
5.6.1	X-ray Characterisation of C ₂₀ H ₂₆ ClNORu (19)	119
5.7	CYTOTOXIC EVALUATION	122
5.8	CONCLUSION	124
5.9	REFERENCE	124
6	CYTOTOXICITY UNDER HYPOXIC CONDITIONS	126
6.1	HYPOXIA	126
6.2	EFFECTS OF HYPOXIA ON CANCER	126
6.3	HYPOXIA-INDUCIBLE FACTOR (HIF).....	127
6.4	HYPOXIA TARGETING DRUGS.....	128
6.4.1	Organic Hypoxia-activated Drugs.....	129

6.4.2	Transition Metal Complexes for Hypoxia.....	132
6.5	CONDUCTING THE MTT ASSAY UNDER HYPOXIC CONDITIONS ($\leq 1\% O_2$) 133	
6.6	RESULTS AND DISCUSSION	134
6.7	CONCLUSIONS	139
6.8	REFERENCES.....	140
7	BIOLOGICAL RELEVANCE.....	145
7.1	INTRODUCTION	145
7.2	HYDROLYSIS	145
7.3	HYDROPHOBICITY (LOG <i>P</i>).....	145
7.3.1	Conducting Hydrophobicity.....	146
7.3.2	Results and Discussion.....	146
7.4	COMET ASSAY.....	150
7.4.1	Conducting the Comet Assay.....	150
7.4.2	Results and Discussion.....	151
7.4.3	Results and Discussion.....	155
7.5	APOPTOSIS.....	157
7.5.1	Conducting the Annexin-V assay.....	157
7.5.2	Results and Discussion.....	158
7.6	THIOREDOXIN REDUCTASE.....	162
7.6.1	Conducting the Thioredoxin Reductase Assay	163
7.6.2	Results and Discussion.....	163
7.7	CONCLUSION	165
7.8	REFERENCES.....	166
8	SYNTHESIS AND CHARACTERISATION OF β- DIKETONATE AND β-KETOIMINATE GROUP IV CHLORIDE COMPLEXES	170
8.1	MECHANISTIC AND CYTOTOXICITY EVALUATION FOR β -DIKETONATE GROUP IV CHLORIDE COMPLEXES	170
8.2	ATTEMPTED SYNTHESIS OF β -DIKETONATE TITANIUM (IV) HALIDE COMPLEXES.....	175
8.3	β -DIKETONATE TITANIUM(IV) ISOPROPOXIDE COMPLEXES.....	176

8.3.1	¹ H NMR Data for Ti ₂ (C ₂₈ H ₂₀ N ₂ O ₄)(OCH ₃) ₆ (20)	176
8.3.2	X-ray Crystallography of Ti ₂ (C ₂₈ H ₂₀ N ₂ O ₄)(OCH ₃) ₆ (20)	178
8.4	<i>β</i> -KETOIMINATE TITANIUM(IV) CHLORIDE COMPLEXES	180
8.5	NMR DATA FOR TITANIUM(IV) CHLORIDE COMPLEXES	181
8.6	X-RAY CRYSTALLOGRAPHY FOR TITANIUM(IV) CHLORIDE COMPLEXES	182
8.6.1	X-Ray Characterisation for Ti(C ₃₂ H ₂₆ F ₂ N ₂ O ₂)Cl ₂ (21)	182
8.6.2	X-Ray Characterisation for Ti(C ₃₂ H ₂₆ Cl ₂ N ₂ O ₂)Cl ₂ (22).....	185
8.6.3	X-ray Crystallography for Ti(C ₃₂ H ₂₆ F ₂ N ₂ O ₂)Cl ₂ (23)	187
8.6.4	X-ray Crystallography for Ti(C ₃₄ H ₃₂ N ₂ O ₂)Cl ₂ (24).....	191
8.6.5	X-ray Crystallography for Ti(C ₃₆ H ₃₆ N ₂ O ₂)Cl ₂ (25).....	193
8.7	CONCLUSIONS AND FUTURE WORK.....	196
8.8	REFERENCES.....	197
9	EXPERIMENTAL.....	198
9.1	GENERAL EXPERIMENTAL PROCEDURES	198
9.2	INSTRUMENTATION.....	198
9.3	X-RAY CRYSTALLOGRAPHY.....	198
9.4	SYNTHESES OF FUNCTIONALISED <i>β</i> -DIKETONATE LIGANDS	199
9.4.1	Preparation of C ₁₄ H ₁₈ O ₂ (L1).....	199
9.4.2	Preparation of C ₁₂ H ₁₃ FO ₃ (L2).....	200
9.4.3	Preparation of C ₁₀ H ₈ F ₂ O ₂ (L3).....	200
9.4.4	Preparation of C ₉ H ₉ NO ₂ (L4).....	201
9.4.5	Preparation of C ₁₄ H ₁₁ NO ₂ (L5).....	202
9.4.6	Preparation of C ₁₄ H ₁₀ BrNO ₂ (L6).....	203
9.4.7	Preparation of C ₁₅ H ₁₃ NO ₃ (L7).....	203
9.4.8	Preparation of C ₁₅ H ₁₃ NO ₂ (L8).....	204
9.4.9	Preparation of C ₁₈ H ₁₃ NO ₂ (L9).....	205
9.4.10	Preparation of C ₁₄ H ₈ Cl ₃ NO ₂ (L10)	206
9.5	SYNTHESES OF FUNCTIONALISED <i>β</i> -KETOIMINATE LIGANDS	206
9.5.1	Preparation of C ₁₇ H ₁₇ NO (L11)	206
9.5.2	Preparation of C ₁₆ H ₁₄ FNO (L12)	207
9.5.3	Preparation of C ₁₆ H ₁₄ FNO (L13)	208
9.5.4	Preparation of C ₁₆ H ₁₃ Cl ₂ NO (L14)	208
9.5.5	Preparation of C ₁₆ H ₁₃ Cl ₂ NO (L15)	209
9.5.6	Preparation of C ₁₆ H ₁₂ Cl ₃ NO (L16)	210

9.5.7	Preparation of C ₁₆ H ₁₄ BrNO (L17).....	210
9.5.8	Preparation of C ₁₆ H ₁₄ INO (L18).....	211
9.5.9	Preparation of C ₁₈ H ₁₉ NO (L19)	212
9.5.10	Preparation of C ₁₇ H ₁₇ NO ₂ (L20).....	212
9.5.11	Preparation of C ₁₈ H ₁₉ NO ₃ (L21).....	213
9.5.12	Preparation of C ₁₈ H ₁₈ FNO ₂ (L22).....	214
9.5.13	Preparation of C ₁₈ H ₁₉ NO ₂ (L23)	214
9.5.14	Preparation of C ₁₇ H ₁₅ NO ₃ (L24)	215
9.5.15	Preparation of C ₁₇ H ₁₅ NO ₃ (L25)	216
9.5.16	Preparation of C ₂₀ H ₁₇ NO (L26)	216
9.5.17	Preparation of C ₁₆ H ₁₁ F ₃ NO (27).....	217
9.5.18	Preparation of C ₁₆ H ₁₃ F ₂ NO (L28).....	218
9.6	SYNTHESIS OF RUTHENIUM CHLORIDE COMPLEXES	219
9.6.1	Preparation of C ₂₆ H ₂₇ ClFNORu (1)	219
9.6.2	Preparation of C ₂₆ H ₂₇ ClFNORu (2)	220
9.6.3	Preparation of C ₂₆ H ₂₇ Cl ₂ NORu (3).....	221
9.6.4	Preparation of C ₂₆ H ₂₆ Cl ₃ NORu (4).....	222
9.6.5	Preparation of C ₂₆ H ₂₆ Cl ₃ NORu (5).....	223
9.6.6	Preparation of C ₂₆ H ₂₅ Cl ₄ NORu (6).....	224
9.6.7	Preparation of C ₂₆ H ₂₇ BrClINORu (7)	225
9.6.8	Preparation of C ₂₆ H ₂₇ BrClINORu (8).....	226
9.6.9	Preparation of C ₂₆ H ₂₇ ClINORu (9).....	226
9.6.10	Preparation of C ₂₈ H ₃₂ ClNO ₂ Ru (10).....	227
2.1.1	Preparation of C ₂₇ H ₃₀ ClINORu (11).....	228
9.6.11	Preparation of C ₃₀ H ₃₀ ClINORu (12)	229
9.6.12	Preparation of C ₃₀ H ₃₀ ClINORu (13)	230
9.7	RUTHENIUM AND IRIDIUM ADAPTATIONS.....	231
9.7.1	Preparation of RuC ₁₆ H ₂₁ Cl ₂ NO (14).....	231
9.7.2	Preparation of RuC ₂₅ H ₂₅ ClNO (15)	232
9.7.3	Preparation of RuC ₂₀ H ₂₂ ClFO ₂ (16).....	233
9.7.4	Preparation of C ₁₆ H ₁₄ ClFO ₂ Ru (17).....	233
9.7.5	Preparation of C ₂₀ H ₂₃ ClFO ₂ Ir (19).....	234
9.8	SYNTHESES OF TITANIUM(IV) β-DIKETONATE COMPLEXES.....	235
9.8.1	Preparation of Ti ₂ (C ₂₈ H ₂₀ N ₂ O ₄)(OCH ₃) ₆ (20).....	235
9.8.2	Preparation of Ti(C ₃₂ H ₂₆ F ₂ N ₂ O ₂)Cl ₂ (21)	235

9.8.3	Preparation of $\text{Ti}(\text{C}_{32}\text{H}_{26}\text{Cl}_2\text{N}_2\text{O}_2)\text{Cl}_2$ (22).....	235
9.8.4	Preparation of $\text{Ti}(\text{C}_{32}\text{H}_{26}\text{F}_2\text{N}_2\text{O}_2)\text{Cl}_2$ (23)	236
9.8.5	Preparation of $\text{Ti}(\text{C}_{34}\text{H}_{32}\text{N}_2\text{O}_2)\text{Cl}_2$ (24).....	236
9.8.6	Preparation of $\text{Ti}(\text{C}_{36}\text{H}_{36}\text{N}_2\text{O}_2)\text{Cl}_2$ (25).....	236
9.8.7	Preparation of $\text{Ti}(\text{C}_{32}\text{H}_{24}\text{Cl}_4\text{N}_2\text{O}_2)\text{Cl}_2$ (26).....	237
9.9	NORMOXIC CYTOTOXIC EVALUATION.....	239
9.9.1	General	239
9.9.2	Passaging Cells.....	239
9.9.3	Cell Counting	239
9.9.4	Conducting the 5-Day MTT Assay.....	240
9.9.5	Data Analysis	240
9.10	HYPOXIC CYTOTOXIC EVALUATION	241
9.11	HYDROPHOBICITY	241
9.12	DSB COMET ASSAY	241
9.12.1	Preparation of Comet assay slides:	241
9.12.2	Reagents	242
9.12.3	Sample Preparation:	242
9.12.4	Conducting the Assay:	243
9.13	SSB AND CROSS-LINKING COMET ASSAY.....	244
9.13.1	Preparation of Comet assay slides:	244
9.13.2	Reagents	244
9.13.3	Sample Preparation:	245
9.13.4	Conducting the Assay:	245
9.14	APOPTOSIS.....	246
9.14.1	Cell counting	246
9.14.2	Harvesting	246
9.15	DATA ANALYSIS.....	246
9.16	THIOREDOXIN REDUCTASE.....	247
9.16.1	Reaction Reagents:.....	247
9.16.2	Conducting the assay.....	247
9.16.3	Analysis of Results.....	247
9.17	REFERENCES.....	248
APPENDIX.....		243

Abbreviations

η	hapticity
2D	two dimensional
Å	Angstrom, 1×10^{-10} m
A2780/A2780cis	human ovarian carcinoma (cisplatin resistance)
AFM	Atomic Force Microscopy
br. d	broad doublet
br. t	broad triplet
br. s	broad singlet
BSA	Bovine Serum Albumin
$[C]_{\text{org}} / [C]_{\text{aq}}$	concentration organic / concentration aqueous
Cisplatin	cis-diamminedichloroplatinum(II)
Cg	Centroid
COSY	correlation spectroscopy
Cp	cyclopentadiene
Cp*	pentamethylcyclopentadiene
d/ dd	doublet/ doublet of doublets
D...A	donor to acceptor distance
DCM	dichloromethane
DMSO	dimethylsulfoxide
DSB	Double Strand Break
dt	doublet of triplets
EDTA	ethylenediaminetetraacetic acid
ES MS	Electro Spray Mass Spectrometry
EtG	ethyl guanine
gmin^{-1}	grams per minute
HBSS	HANKS Balanced Salt Solution
HCR	Hypoxic Cytotoxic Ratio
HIF	Hypoxia-Inducible Factor
HMQC	Heteronuclear Multi-Quantum Correlation spectroscopy
HPDC	Hypoxia-activated Prodrugs of Diffusible Cytotoxins
HT-29	human colon adenocarcinoma
[I]	concentration inhibition
IC ₅₀	concentration at which 50% growth is inhibited

<i>in vitro</i>	in glass
<i>in vivo</i>	in life
LD ₅₀	concentration causing 50% population death
LLC-PK	pig kidney epithelial cells
LMPA	Low Melting Point Agarose
LoVo	human colon adenocarcinoma
LS 174T	human colon adenocarcinoma
[M ⁺]	parent molecular ion
m	multiplet
MCF-7	human breast adenocarcinoma
MTT	3-(4,5-dimethylthiazol-2-yl)-2,5-diphenyl tetrazolium bromide
<i>m/z</i>	mass to charge ratio
NADPH	reduced nicotinamide adenine dinucleotide phosphate
NAMI	New Anti-tumour Metastasis Inhibitor
NHS	National Health Service
NMR	Nuclear Magnetic Resonance
PBS	Phosphate Buffer Solution
<i>p</i> -cymene	<i>para</i> cymene
RPMI	Roswell Park Memorial Institute medium
SARs	Structural Activity Relationships
SD	standard deviation
SRB	Sulforhodamide B
SSB	Single Strand Break
t	triplet
TAP	Tumour-activated Prodrug
THF	tetrahydrofuran
TPZ	Tirapazamine
Trx	Thioredoxin
TrxR	Thioredoxin Reductase
UV- <i>vis</i>	Ultraviolet-Visible Spectroscopy
V	voltage
X	one electron donor
XTT	3'-[1-[(phenylamino)-carbonyl]-3,4-tetrazolium]-bis(4-methoxy-6-nitro)benzene-sulfonic acid hydrate

Chapter 1

Introduction

1 Introduction

This thesis describes the synthesis and evaluation of novel ruthenium complexes as potential anticancer agents, with some further work on titanium complexes. The complexes feature substituted β -ketoiminate ligands with differing electronic and steric properties and adaptations of these complexes. This chapter will present a review of previous research in the area of metal based anticancer agents, with particular emphasis on ruthenium, titanium and iridium based complexes.

1.1 Cancer

Since the mid 1970s, incidence rates for cancer in Great Britain in the UK have increased by 22% in men and 42% in women. However, over the last ten years, these incidence rates have increased by just 2% in men and 6% in women. Cancer occurs predominantly in older people, with the chance of developing cancer increasing rapidly from 50 years of age. More than three in five cancers (63%) were diagnosed in people aged 65 and over, and more than a third (36%) were diagnosed in the elderly (aged 75 and over). The most common cancer found in men is prostate cancer, which accounts for a quarter (25%) of all male cancer cases. In females, the most common is breast cancer and accounts for nearly a third (31%) of all cancers in women. In both males and females the second and third most common cancers are lung cancer and bowel cancer respectively.¹ The majority of deaths occur in older generations, with the rates increasing at the age of 60. More than three quarters (77%) of deaths occur in patients 65 and over, whilst over half of these (52%) occur in patients over 75 years of age.¹ Recent statistics show that in 2010, 324,579 people in the UK were diagnosed with cancer² costing £9.4 billion across the NHS, private and voluntary sectors.³ In 2011, 159,178 people died from cancer in the UK.⁴

Cancer is the term given to a group of diseases resulting from mutations in our cells which can cause them to undergo uncontrollable cell division.⁵ The cells divide through a process known as mitosis, which is controlled by two ‘cancer genes’ known as oncogenes and tumour gene suppressor genes. However, if one or more of these genes has a mutation the cell uncontrollably divides causing a lump of tissue known as a tumour. Normal cells frequently undergo a process known as programmed cell death. However, these activated oncogenes can cause a cell that

ought to die to survive and enter cell proliferation.⁶ This can cause one of two types of tumour, known as benign or malignant. A benign tumour does not invade other tissues, is usually not life-threatening and is easily treated. Whereas malignant tumours can undergo metastasis, in which the initial tumour can migrate to a secondary site producing a secondary tumour. These are usually hard to treat and can be life threatening.⁷ The risk of developing cancer can be increased by exposure to carcinogens, a high fat diet or genetic susceptibility.⁸ Cancers are different depending on what cells are affected and therefore different types of cancer treatment are used to maximise treatability, these include surgery, radiotherapy, immunotherapy, chemotherapy and gene therapy.⁹ Often several types of treatment are used simultaneously to give maximum effects.¹⁰

1.2 Metal-Based Drugs

Transition metal complexes are well known in biological processes and play a vital role in the human anatomy. The use of metal-based complexes has been understood since as early as 1910, when Salvarsan (Arsphenamine), an arsenic containing therapeutic agent, was used in the treatment of syphilis, and was the first known chemotherapeutic agent.¹¹ The structure of this complex was thought to contain an As=As double bond. However, in 2005 work by Nicholson *et al.* provided evidence that Salvarsan in fact exists as cyclic trimers and pentamers (**Figure 1.1**).¹²

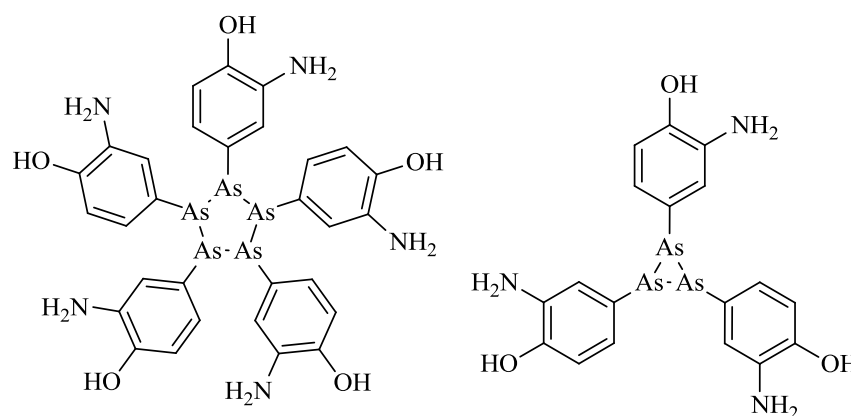


Figure 1.1 Cyclic Salvarsan structures

Since the discovery of Salvarsan, therapeutic agents have been established across the periodic table, including a gold containing complex Auranofin (Ridura) which is used to treat rheumatoid arthritis, by reducing tender joints and morning stiffness commonly caused by arthritis (**Figure 1.2**).¹³

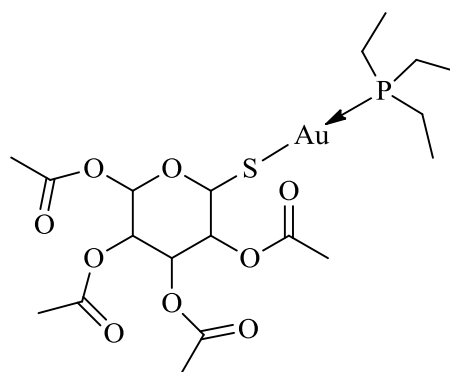


Figure 1.2 Auranofin (Ridura)

Another modern example is Tetrofosmin (**Figure 1.3**), a ^{99m}Tc based cardiac imaging agent better known as MyoviewTM, which is used to enable the diagnosis and localisation of regions of reversible myocardial ischemia.¹⁴

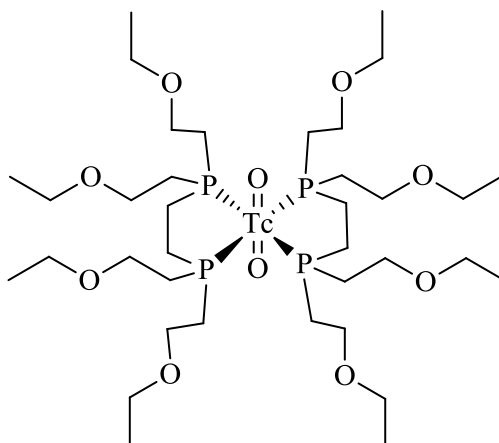


Figure 1.3 Tetrofosmin

1.3 Cisplatin

Cisplatin [*cis*-dichlorodiammine platinum(II)] was first discovered by Peyrone in 1845 and was known as Peyrone's salt.¹⁵ Its structure (**Figure 1.4**) was later elucidated in 1893 by Werner, when he proposed the theory of coordination chemistry, showing that ammonia can in fact bind to the Pt(II) by donating its lone pair in a dative or coordination bond.^{16, 17} However, the anti-cancer properties of cisplatin were not discovered until over a century after its initial discovery, by Rosenberg *et al.* in 1965.¹⁸ The discovery was made whilst researching electric field effects on cell growth in *E. coli* using an aqueous solution of NH_4Cl and platinum electrodes. Since then it entered clinical phase trials in 1971 and was approved for pharmaceutical use in 1978.¹⁹ It has since become the world's leading

anti-cancer drug in treating neck, bladder, ovarian and testicular cancers.²⁰

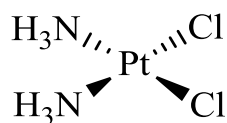
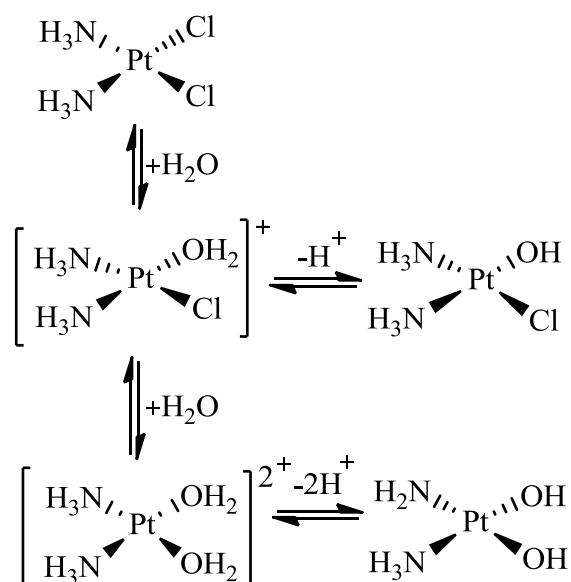


Figure 1.4 Structure of cisplatin

Once cisplatin enters the body and reaches the desired organs, it diffuses through the cell membrane by passive transport. This is due to a chloride ion concentration deficiency in the cytoplasm of the cells, which enables the labile chloride ligands of cisplatin to dissociate and be replaced by water molecules (**Scheme 1.1**).²¹



Scheme 1.1 Hydrolysis of Cisplatin

The water ligand is easily displaced by the basic nitrogen atoms on DNA, specifically the N7 position on guanine residues. Once it is bound to the DNA, the second chloride ligand is replaced by another nitrogen atom from either the same DNA strand (intrastrand) or an adjacent DNA strand (interstrand) (**Figure 1.5**). Incorporation of this platinum centre causes irreversible dehydration and induces structural changes to the DNA strand preventing replication. The cross-linking prevents cell division and stops tumour growth. This DNA damage in tumour cells causes the strands to ‘kink’; this is not recognised and results in programmed cell death (apoptosis). It is crucial that the *cis* isomer is used as it has the correct geometry for cross-linking; whereas transplatin is thought to be deactivated before it reaches the DNA.¹⁶ However, this is a non-specific process and affects healthy

cells as well as cancerous cells, causing severe physiological side effects such as nausea, and nephrotoxicity. Current research has now led to second-generation derivatives of cisplatin, in the hope to achieve higher activity with reduced toxicity.²²

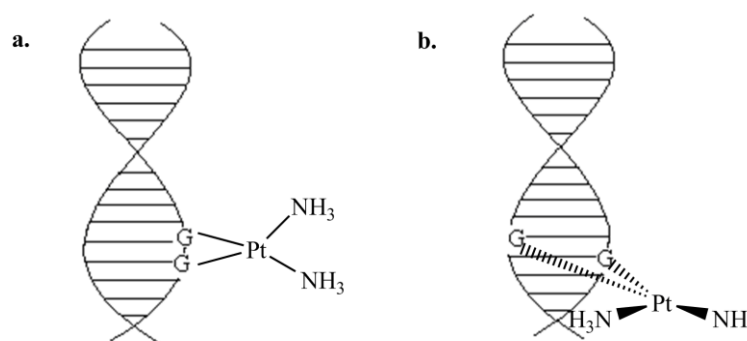


Figure 1.5 Representation of a. intrastrand and b. interstrand cross-linking

1.4 Second Generation of Platinum Complexes

The most successful cisplatin analogue is *cis*-diammine (1,1-cyclobutanedicarboxylato)platinum(II) (carboplatin) (**Figure 1.6**). It has shown similar activity to cisplatin against lung and ovarian tumours but with lower cytotoxic behaviour.²¹

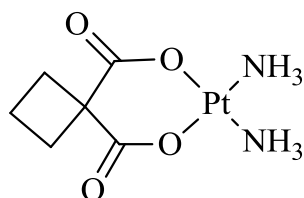


Figure 1.6 Carboplatin

Its activity is due to the cyclobutanedicarboxylate ligand being more stable than the chloride ligands of cisplatin, causing slower *in vivo* hydrolysis and allowing more time for the complex to reach target cells before the ligand is displaced.²³ A significant advantage is that carboplatin has much lower toxic side effects, allowing the drug to be administered in much higher dosages when compared to cisplatin. However, the main disadvantage of this drug is that it induces greater bone marrow toxicity.²⁴ Other platinum complexes have been synthesised with either platinum(II) or platinum(IV) centres (**Figure 1.7**), many of which have entered into clinical trials.

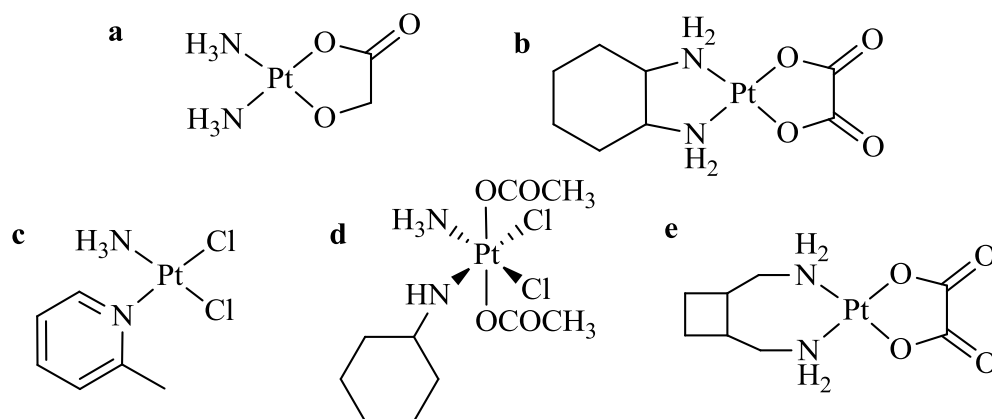


Figure 1.7 Molecular structures of **a** nedaplatin, **b** oxaliplatin, **c** ZN0473, **d** JM216 and **e** Lobaplatin.

Nedaplatin (**a**) was found to have the highest anti-cancer activity of this second generation, possessing lower nephrotoxicity in comparison to cisplatin, and has been approved for clinical use in Japan.²⁵ Oxaliplatin (**b**) was found to be effective in cisplatin-resistant cells for a range of different cancers and has since been approved for clinical use in France.²⁶⁻²⁸ ZN0473 (**c**) is sterically hindered and hydrolyses around 4 times slower than cisplatin and this is thought to be a factor contributing to its high activity against cisplatin-resistant cell lines.²⁹ JM216 (**d**) was the first orally administered platinum complex and was found to form at least six metabolites, with no parent compound being detected after 20 minutes of administration.³⁰ Finally, Lobaplatin (**e**) was introduced in 1992 and is currently in phase II clinical trials for cisplatin-resistant ovarian cancer, head and neck cancers and small-cell lung cancer.³¹⁻³³

Research groups are still investigating the group 10 metals for their use in anti-cancer treatment. However, in more recent years researchers have begun to investigate a larger range of transition metals. Therefore this chapter discusses some key complexes currently being investigated, with a closer look into current titanium, ruthenium and iridium complexes.

1.5 Titanocene Dichloride

The anti-cancer properties of dichlorobis(η^5 -cyclopentadienyl)titanium(IV) (titanocene dichloride) were discovered in 1979 by Köpf and Köpf-Maier (**Figure 1.8**).³⁴ Its cytotoxic potential was investigated due to the similarities in structure between titanocene dichloride and cisplatin; both contain *cis*-dichloro ligands in the neutral complex. Titanocene dichloride was tested on a group of CF₁ mice implanted with Ehrlich ascites tumour cells, and was found to give a cure rate of over 80%. It was both the first metallocene and the first titanium-based compound to exhibit cytotoxic properties.

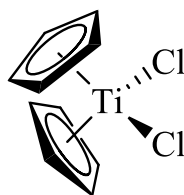
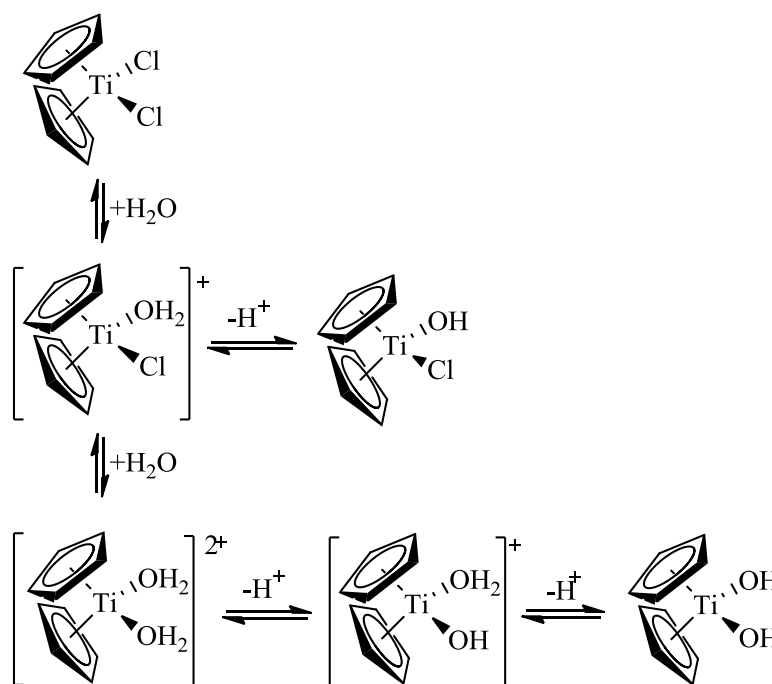


Figure 1.8 Structure of Titanocene Dichloride

Titanocene dichloride has been shown to be effective against several carcinomas and does not exhibit the same toxicological profile as cisplatin, but it does exhibit liver damage (hepatotoxicity).³⁵ It entered phase I clinical trials in 1991 but was rejected during phase II clinical trials as it produced responses too small to justify its use in single-agent therapy against both renal and breast cancer.^{36, 37} The *in vivo* aqueous chemistry is thought to be similar to that of cisplatin involving hydrolysis of the chloride ligands (**Scheme 1.2**), with mechanistic findings by Marks *et al.* showing the substitution of the chloride ligands occurred faster than in the case of cisplatin.³⁸ Titanocene dichloride can also be taken up by transferrin at blood plasma pH (7.35-7.45) and proton-induced loss of the Cp rings occurs. This is thought to be a key step in the mechanism, with the rate at which the Cp is lost controlling the activity of the complexes.³⁹ Once inside the cell, the complex is transported to the nucleus *via* interaction with ATP, where it is then free to interact with the DNA.⁴⁰⁻⁴²



Scheme 1.2 Hydrolysis of Titanocene Dichloride

1.5.1 Variations of the Chloride Ligands

Köpf-Maier *et al.* investigated modifications of titanocene dichloride, including substituting the chloride ligands for different halides and *pseudo* halides i.e. X = F, Br, I, NCS and N₃. These complexes showed similar activities to both titanocene dichloride and cisplatin, with the *pseudo* halide being displaced during hydrolysis in all cases.⁴³ The introduction of the hydrophilic trichloroacetate or pentafluorophenoxy (**Figure 1.9a** and **b** respectively) saw a significant decrease in toxicity (LD₅₀ = 440 mg/kg and 480 mg/kg respectively) compared to titanocene dichloride (LD₅₀ = 100 mg/kg).

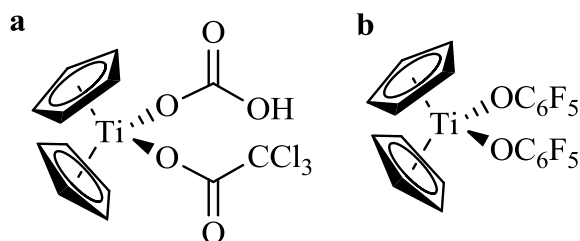


Figure 1.9 Variations of titanocene dichloride containing; **a** trichloroacetate and **b** pentafluorophenoxy

Other modifications have included neutral and charged moieties in addition to both monodentate and bidentate ligands. These included a range of ionic, salt like derivatives (**Figure 1.10**), which have showed good water solubility. This has led to further research aimed towards increasing both the solubility and hydrophilic character, as both have proven to be beneficial in the design of active titanium anti-cancer drugs.^{44, 45}

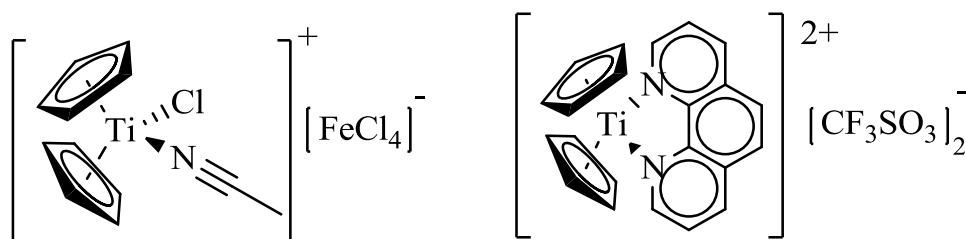


Figure 1.10 Ionic derivatives of titanocene dichloride

1.5.2 Cyclopentadienyl Derivatives of Titanocene Dichloride

As well as alterations to the chloride ligands, research has since moved onto modification of the Cp ligand by addition of either a small group or larger pendant arms. Köpf and Köpf-Maier proved that addition of electron donating groups to the Cp ring did not lead to an increase in cytotoxic properties.⁴⁶ Baird *et al.* conversely added electron withdrawing groups to the Cp ring in an attempt to increase cytotoxicity.⁴⁷ It was hoped that a more stable Ti-Cp bond would form, which under physiological pH would give an electrophilic titanium centre. This would increase the Lewis acidity of the titanium centre and effectively increase the binding to DNA, which is a Lewis base. When pendant arms were added on to the Cp ring, lower IC₅₀ values were observed in comparison to titanocene dichloride. These were extensively researched by Tacke *et al.* with bis-[(4-methoxybenzyl)cyclopentadienyl]titanium dichloride (Titanocene Y) (**Figure 1.11**) showing an IC₅₀ value of 21 μM when tested on LLC-PK, in comparison to an IC₅₀ value of 2 mM for titanocene dichloride.⁴⁸

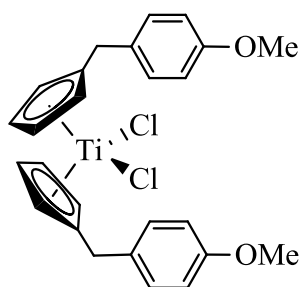


Figure 1.11 Structure of Titanocene Y

Tacke *et al.* have also synthesised a range of Titanocene Y analogues with the corresponding difluoride derivatives, some showing higher activity than the dichloride complexes.⁵ Substituting the chloride ligands for a bidentate oxalate ligand (Oxali-Titanocene Y) showed around a 13-fold increase in activity against LLC-PK, giving an IC_{50} value of $1.6 \mu\text{M}$ (**Figure 1.12**).⁴⁹ Due to the success of these complexes, it was necessary to conduct research into a library of carboxylate anion-substituted derivatives of Titanocene Y. Some improvements were seen in cytotoxicity when compared to titanocene dichloride, but Titanocene Y still remains the leading drug candidate of this library.⁴⁸

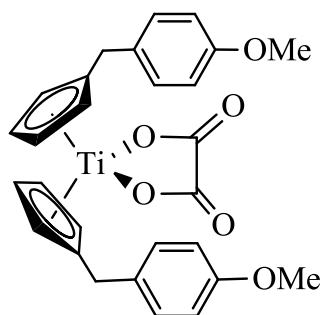


Figure 1.12 Oxali-Titanocene Y

McGowan *et al.* have studied the addition of amino functionalised pendant arms, and have synthesised the following classes of substituted titanocenes (**Figure 1.13**). In the case of the monocationic complexes (**Figure 1.13a**), additional methyl and silyl groups have been added to the non-pendant cyclopentadienyl ring to improve lipophilicity and hence the ability to cross the cell membrane. *In vitro* testing on cell lines MCF7, LoVo, LS 174T, A2780 and A2780cis showed the mono- and dicationic species to be potent cytotoxic agents, with the most active complexes outperforming titanocene dichloride by 10-fold. Upon addition of one silyl group onto the non-pendant cyclopentadienyl ligand showed little effect on the IC_{50} ,

whereas the addition of two silyl groups led to a marked decrease in IC_{50} . It was seen that these complexes were sensitive to cisplatin-resistance cell lines, supporting the theories of these complexes acting *via* a different mechanism to cisplatin, although in the case of these ionic complexes there is evidence of significant DNA cross-linking.⁵⁰⁻⁵⁴

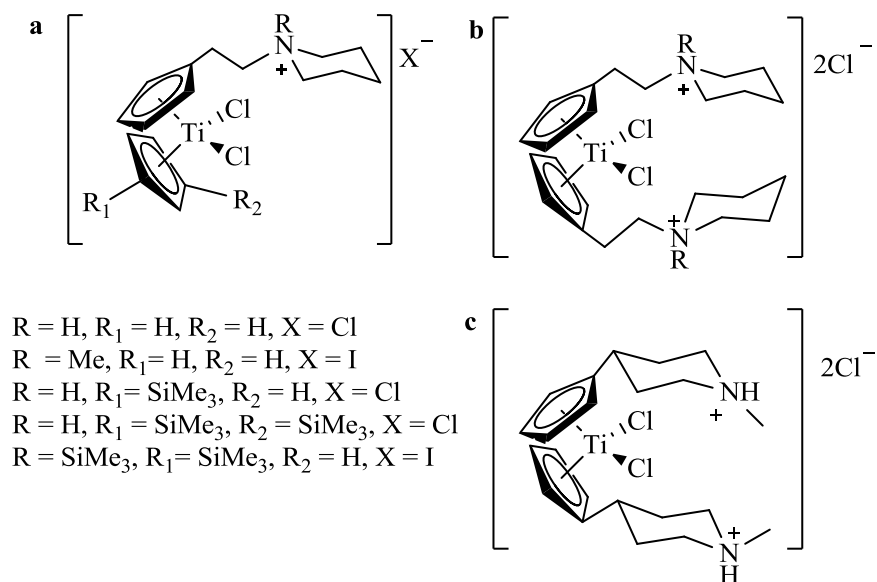


Figure 1.13 a. Mono- b and c bifunctionalised pendant-arm titanocene dichlorides

The lead complex of this type is $[C_5H_4(CH_2)_2N(CH_2)_5]_2TiCl_2 \cdot 2HCl$, which was shown to have increased activity in comparison to Cp_2TiCl_2 (**Figure 1.14**).^{50, 51, 54}

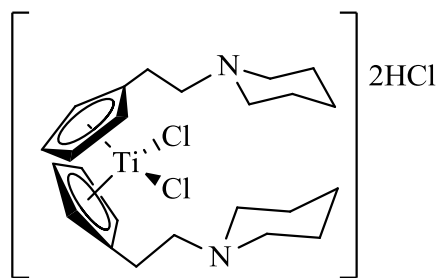


Figure 1.14 Ionic piperidine functionalised titanocene dichloride

1.6 Budotitane

Along with titanocene dichloride, another library of complexes known as the *bis* (β -diketonate) titanium complexes has undergone extensive research as potential anti-cancer drugs. The first to enter phase trials was $\text{Ti}(\text{bzac})_2(\text{OEt})_2$ (Budotitane) (**Figure 1.15**). The complex and its anti-cancer potential have been studied by Keppler *et al.* and has been shown to be effective against sarcoma 180 ascitic tumours, Walker 256 carcinosarcoma ascitic tumours, and induced colorectal tumours in mice.⁵⁵⁻⁵⁹

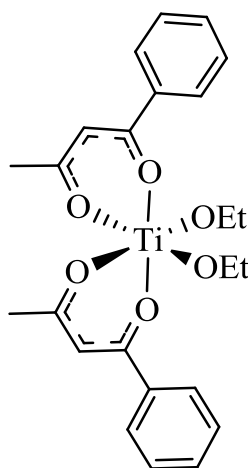
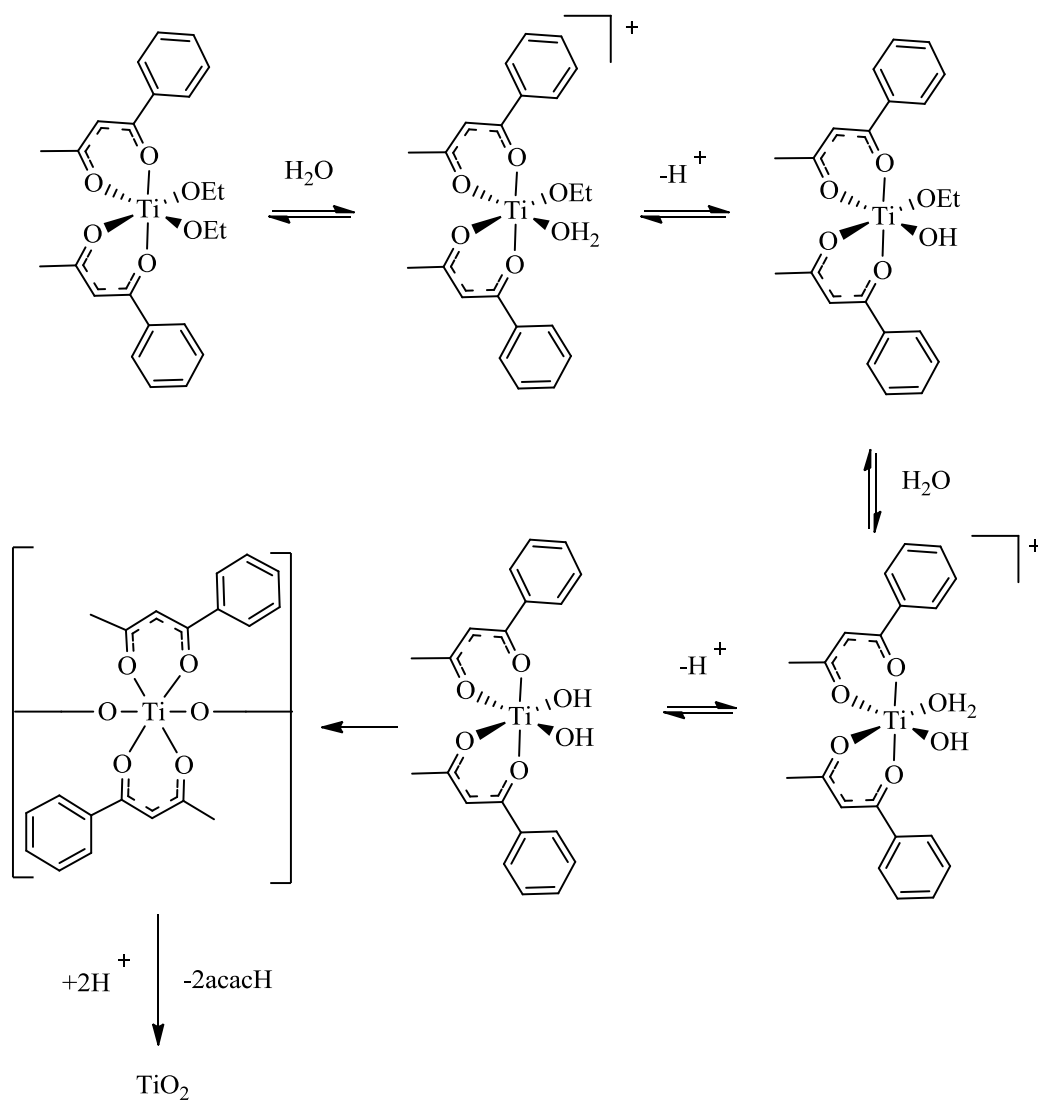


Figure 1.15 Budotitane

Budotitane entered phase I clinical trials stating a maximum tolerated dosage of 230 mg/m^2 with the dose-limiting toxicity being cardiac arrhythmia, and a biweekly dose of 180 mg/m^2 was recommended for further treatment.⁶⁰ However, phase II and III clinical trials were postponed due to problems with formulation.^{61, 62} The issues associated with this complex included poor solubility and stability in water, which is a significant limiting factor. Attempts were made to encapsulate the active species within a micelle containing glycerine polyethylene-glycolericinoleate and 1,2-propylene glycol in water-free ethanol; this protective micelle is formed when dissolved in water.⁶³ However, this formulation provided hydrolytic stability for only a few hours, and has proved problematic to characterise.⁶⁴ It has been proposed that budotitane loses the ethoxide ligands initially, followed by the acac ligands, to form titanium dioxide (**Scheme 1.3**). However, to date the mechanism is poorly understood.^{57, 60, 65}



Scheme 1.3 Proposed pathway for the hydrolysis of budotitane

A major issue with budotitane is that it can exist as five different isomers (**Figure 1.16**) and this makes it difficult to determine which isomer is key for the observed activity. Dubler *et al.* showed crystallographically evidence that budotitane adopted a *cis-cis-trans* (**b**) geometry in the solid state, in comparison to the titanium chloride derivative which adopted a *cis-trans-cis* (**a**) configuration.⁶⁶

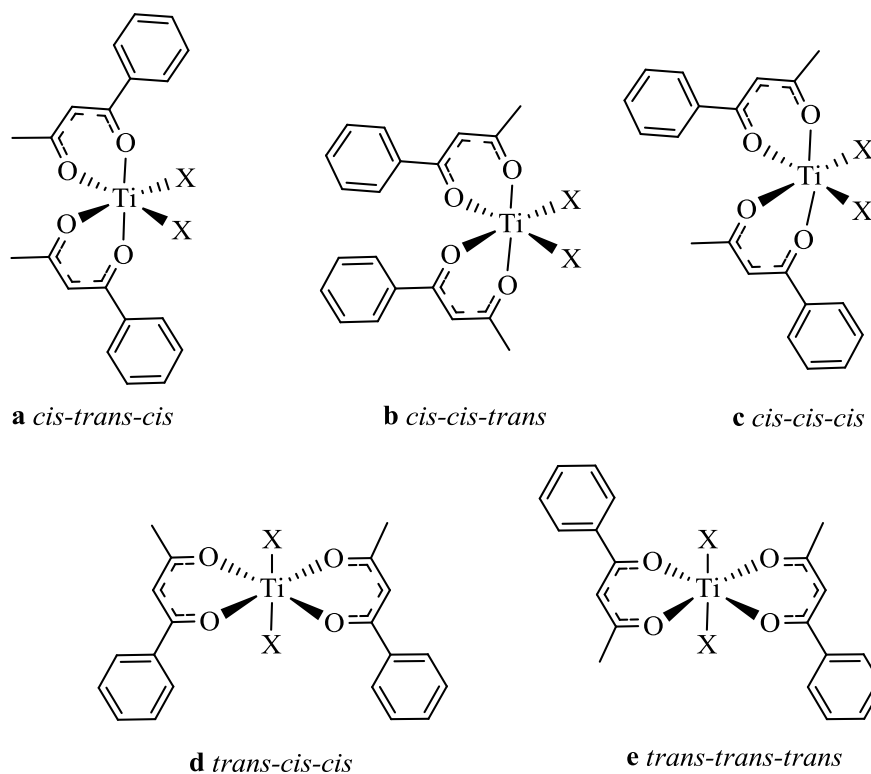


Figure 1.16 Five possible isomers of budotitane

Solution studies have shown broad ^1H NMR signals for the presence of multiple isomers, which were thought to be the *cis* geometries, with the *cis-cis-cis* (**c**) being the most abundant at 60%, the *cis-trans-cis* (**a**) at 21% and then the *cis-cis-trans* (**b**) at 19%. A further issue is that (**a**) and (**b**) are found as enantiomeric pairs, further complicating the purification and separation. The presence of the phenyl rings is thought to be the key to the activity of these complexes, as replacement with methyl groups destroyed the activity, but this has not yet been proven and recent studies have shown no DNA damage during both *in vivo* or *in vitro* studies.⁶⁷

Aside from titanium, research has continued in the group IV metals, where Keppler *et al.* were amongst the first to show their potential as anti-cancer complexes. Analogues of budotitane were made, incorporating either zirconium or hafnium with β -diketonate ligands, showing that the titanium gave the most promising results *in vivo*.⁶⁸ These libraries have been extended within the McGowan *et al.* showing the *in vitro* testing of these metal complexes actually have a reversed activity where compared to *in vivo* studies by Keppler. Whereby we show that the hafnium analogues are the most active complexes (discussed in Chapter 8).⁶⁹

1.7 Ruthenium

The use of ruthenium as potential anti-cancer complexes has emerged due to the following three properties;

1. Ligand Exchange

When considering both ruthenium(II) and (III) complexes, it has been shown that the ligand exchange in aqueous conditions is relatively slow and is similar to that seen for the platinum(II) complexes.⁷⁰ It is thought that ligand exchange is a key process in the drug's activity and that most complexes in fact alter their structure before interaction with the biological targets.^{71, 72}

2. Oxidation State

Ruthenium has variable oxidation states that are easily accessible under physiological conditions, meaning that it can be easily reduced by one electron transfer proteins and thus have potential under hypoxic or anoxic conditions. Due to the increased metabolic rates of cancer cells there is an increase in lactic acid being produced, which decreases the pH within the cancer cells and lowers the concentration of O₂ at the cell, leading to a preference of ruthenium(II) species over ruthenium (III).^{72, 73}

According to the “activation by reduction” hypothesis, ruthenium (II) complexes are more available for binding to cellular components than ruthenium (III).⁶³ The relatively inert and non-toxic ruthenium(III) complexes, which have no effect on healthy cells, may be administered, and are then biologically activated by reduction to the more active ruthenium(II) complexes. As a result, the ruthenium complexes are more selective for cancer cells and decrease the toxicity.^{70, 72}

3. Iron Mimicking

Another advantage is ruthenium's capacity to mimic iron in binding *in vivo* to different biomolecules, including protein albumin and transferrin. It is known that cancer cells have more transferrin receptors on the surface of the cell membrane and therefore more ruthenium complexes are able to enter the cell. Radio-labelling studies have shown this increase ranges from 2-12 fold, depending on the cell type, therefore reducing the toxicity.^{63, 72, 74}

1.7.1 Ruthenium Red

One of the most common forms of ruthenium complex is “ruthenium red” $[(\text{NH}_3)_5\text{Ru}(\text{III})\text{ORu}(\text{IV})(\text{NH}_3)_4\text{ORu}(\text{III})(\text{NH}_3)_5]^{6+}$ (**Figure 1.17**), a polycationic red dye used to selectively stain mitochondria by binding to the calcium channels and inhibiting calcium ion uptake.⁷³ The use of ruthenium red as an anti-cancer agent is also known, although its high toxicity has prevented further research.^{75, 76}

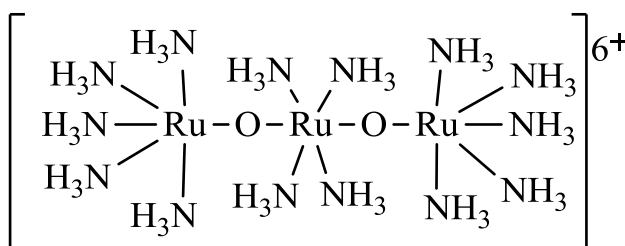


Figure 1.17 Ruthenium Red

In 1976, Durig *et al.* discovered that *fac*- $[\text{Cl}_3(\text{NH}_3)_3\text{Ru}]$ worked in a similar way to cisplatin and in fact inhibited *E. coli* growth, however its low water solubility prevented clinical use.^{77, 78} In order to increase solubility, the use of labile ligands were suggested and the complex $[\text{cis-RuCl}_2(\text{DMSO})_4]$ was synthesised and was the earliest ruthenium complex to exhibit anti-cancer properties.⁷⁹ Not only was it active against several metastatic tumours, it also forms covalent bonds to the N7 position on the guanine residue.^{80, 81}

1.7.2 NAMI-A

Imidazolium $[\text{trans-imidazoledimethylsulfoxidetetrachlororuthenate}(\text{III})]$ (NAMI-A) was discovered by Sava *et al.* and is the most successful ruthenium anti-cancer drug to date and the first to enter phase I clinical trials (**Figure 1.18**).⁸²

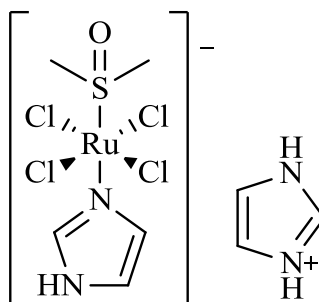


Figure 1.18 NAMI-A

The complex NAMI contains a sodium counterion and replacement of this with an imidazolium cation gives NAMI-A. NAMI-A is easier to reproduce synthetically than NAMI and is air stable. Both of these complexes have shown activity against reducing lung metastasis formation on mice and the anti-metastatic activity of both complexes has been shown to have no relation to their cytotoxicity against cancerous cells.⁸² It has been suggested they have a different mode of activity in comparison to cisplatin and other ruthenium complexes, where their action involves extracellular activity which is unique to both agents.⁸²⁻⁸⁴ It was shown that they are able to treat metastatic tumours at doses which are not toxic for the liver, lung or kidney,^{82, 85} and have the advantage of being administered orally. The reduction of NAMI-A by ascorbic acid prior to administration led to NAMI-AR. It was found that this complex improves the efficiency against the metastasis growth, according to the “activation by reduction” hypothesis.⁸⁵

1.7.3 KP418 and KP1019

Imidazolium [*trans*-tetrachlorobis(imidazole)-ruthenate(III)] (KP418) (**Figure 1.19**), has shown to be much less toxic than its indazole analogue, however it still shows high activity against colorectal carcinoma models in mice.⁸⁷

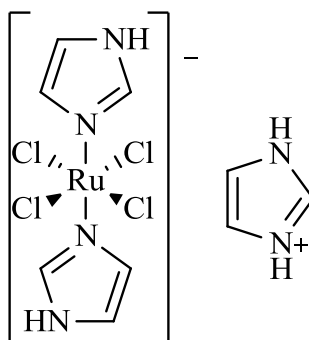


Figure 1.19 Imidazolium [*trans*-tetrachlorobis(imidazole)-ruthenate(III)] (KP418)

Indazolium [*trans*-tetrachlorobis(indazole)-ruthenate(III)] (KP1019) (**Figure 1.20**) was discovered by Keppler *et al.* and has shown high activity against a range of cell lines. Unlike NAMI-A, which exhibited activity against metastasis processes, KP1019 is active against colon carcinomas and primary human tumours. Inhibiting approximately one third of tumours, the only side-effect of KP1019 is the increased production of red blood cells (erythropoiesis), with clinical reports suggesting no severe side effects.⁸⁹

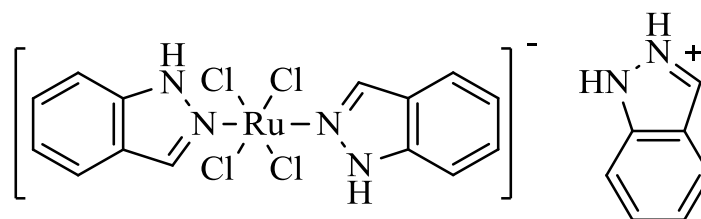


Figure 1.20 Indazolium [*trans*-tetrachlorobis(indazole)-ruthenate(III)] (KP1019)

Although KP1019 has poor water solubility, the substitution of the indazolium cation with sodium increases its water solubility, improving its potential for clinical use.⁸⁸ The active species of both these complexes have been shown to be the hydrolysed species of the chloride precursor, with KP418 hydrolysing at a rate comparable to cisplatin. However, KP1019 hydrolyses more slowly and *via* a different pathway and is dependent upon both temperature and pH. Following hydrolysis both complexes interact with the nucleophilic sites on DNA. They are also active against cisplatin-resistant cell lines and therefore it is thought that binding of ruthenium complexes will have different cytotoxic effects in comparison to cisplatin.^{75,89, 90}

It has been shown that colorectal tumour uptake for KP418 was 10-fold lower than KP1019, leading to lower anti-cancer activity. KP1019 has been shown to be active against cisplatin-resistant tumours and this could be due to a different mechanism of action. It is thought that ruthenium complexes target the N7 position of guanine or adenine and shows that KP1019 has less interstrand cross-linking in comparison to cisplatin.⁸⁹

1.7.4 Organometallic Ruthenium Arenes

Organometallic complexes were once restricted to ruthenocene, until Sheldrick *et al.* reported the biological use of organometallic η^6 -arene ruthenium complexes. This organometallic work was based on his previous coordination work and the reported activity of *cis*-[RuCl₂(DMSO)₄].⁹¹ Sheldrick made a range of η^6 -ruthenium organometallic complexes, with the most promising ones taking the form $[(\eta^6\text{-arene})\text{Ru(II)(en)X}]^+$ (X = halide, en = ethylenediamine) (**Figure 1.21**). It was shown that differing the arene substituents lead to differences in activity both *in vitro* and *in vivo* against a range of cancer cell lines, including cisplatin-resistant cell lines.⁹²⁻⁹⁴

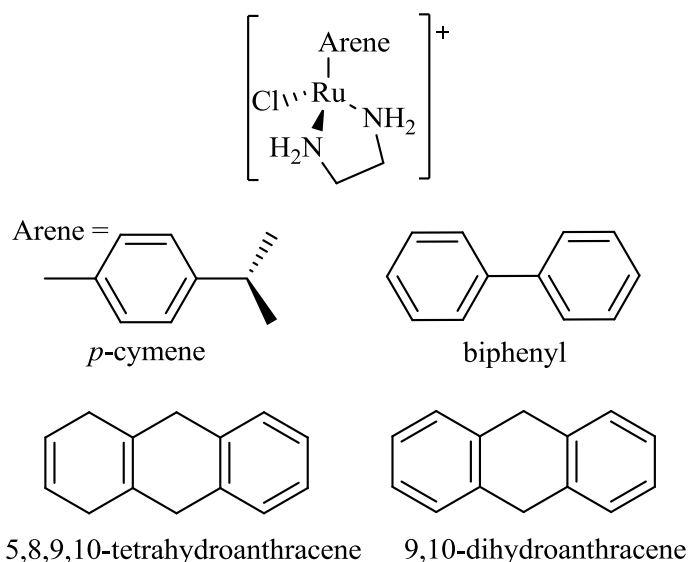
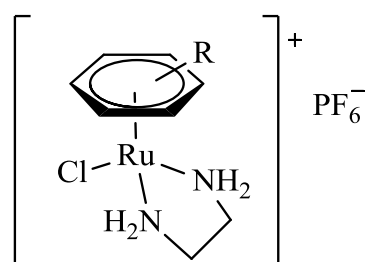


Figure 1.21 Examples of $[(\eta^6\text{-arene})\text{Ru}(\text{II})(\text{en})\text{X}]^+$ complexes

These types of complex have also been studied by Sadler *et al.* (**Figure 1.22**) and the 2-phenoxy derivatives showed the highest cytotoxicity amongst the polar substituents, but further results showed the non polar substituents had higher activity than polar groups.⁹⁴ They also showed that polycyclic arenes on average had higher activity than monocyclic arenes. It is thought that increasing the number of arenes increases hydrophobicity, allowing easier passive transport into the cell.⁹²⁻⁹⁴ To achieve better DNA binding the neutral ethylenediamine ligand was replaced with an anionic β -diketonate ligand, which exhibited high activity due to rapid hydrolysis in water and a change in binding specificity. They show selective binding to adenosine, with very little binding to other residues.⁹⁵



R = Polar or Non-polar substituent

Figure 1.22 $[(\eta^6\text{-arene})\text{Ru}(\text{II})(\text{en})\text{X}]\cdot\text{PF}_6^-$ complexes

It is thought that these types of ruthenium complexes hydrolyse at a faster rate than cisplatin, resulting in $[(\eta^6\text{-arene})\text{Ru}(\text{en})(\text{H}_2\text{O})]^{2+}$ which reacts rapidly with guanosine monophosphate (5'-GMP).⁹⁶ The interaction of these complexes with

guanine derivatives *in vitro* were studied by Sadler *et al.*⁹⁷ A crystal structure was determined and shows π - π arene-nucleobase stacking of $[(\eta^6\text{-dha})\text{Ru}(\text{en})9\text{EtG-N7}]^{2+}$ and $[(\eta^6\text{-tha})\text{Ru}(\text{en})9\text{EtG-N7}]^{2+}$ (9EtG-N7 = N7 bound 9-ethyl guanine). It was also shown that there is intermolecular π - π stacking between the pendant phenyl ring and the guanine base, and a hydrogen bond interaction between the ligand NH and guanine O6.⁹⁷

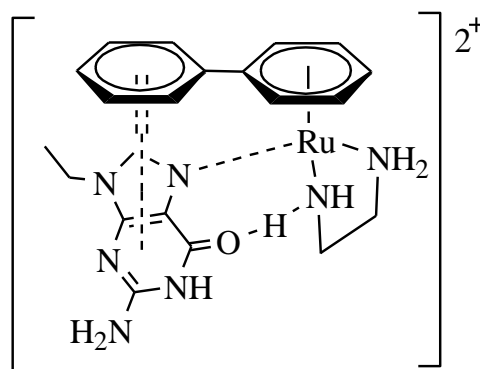


Figure 1.23 Interactions between $[\eta^6\text{-dhaRu}(\text{en})]^{2+}$ and 9EtG

McGowan *et al.* have carried out extensive work on arene ruthenium complexes to try and produce higher activity against cancerous cells and cisplatin-resistant cell lines. These include a range of picolinamide and quinaldamide complexes (**Figure 1.24**), that have been synthesised by reactions with the *p*-cymene ruthenium(II) chloride dimer.⁹⁸

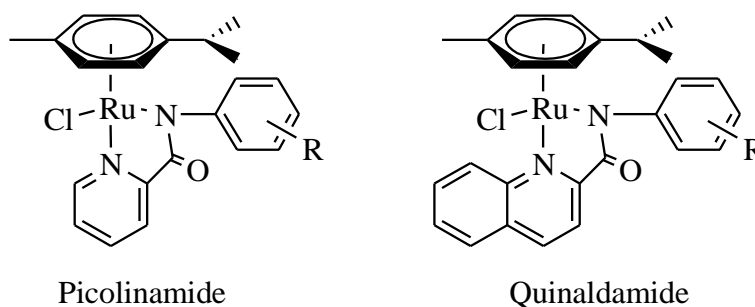


Figure 1.24 Ruthenium picolinamides and quinaldamides

The lead drug within this type of complex is the charged ruthenium (II) chloride 2,5-dichloropicolinamide complex, which is made by filtering the uncharged complex onto NH_4PF_6 (**Figure 1.25**). These types of (*N,N*) chelating ligands are of high interest due to previous results discussed within the work of Sheldrick *et al.* and they also have the advantage of coordinating as (*N,O*) chelating ligands, giving them potential to target different organelles within the cancerous cells.

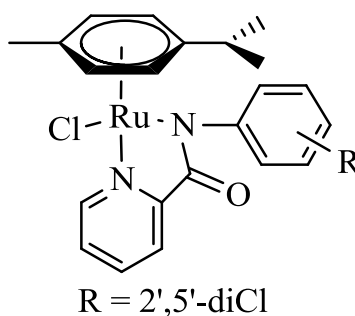


Figure 1.25 McGowan *et al.* lead compound

NMR studies have shown that equilibrium between the (*N,O*) and (*N,N*) coordination can be altered by changes in temperature and pH.⁹⁹ The ruthenium complexes with 3-nitro, 4-nitro and 4-fluoro picolinamide have shown IC₅₀ values against a range of tumour cells in the same order of magnitude as cisplatin and carboplatin, with the added advantage of being active against a cisplatin resistant cell line. It was shown that the binding mode of these complexes is essential to its cytotoxic behaviour. Studies showed that the more cytotoxic (*N,N*) complexes have rapid hydrolysis and bind preferentially to guanine, whereas switching the binding mode to (*N,O*) slows the rate of hydrolysis and switches off the activity.⁹⁹⁻¹⁰¹

Work has since continued on ruthenium and iridium arene complexes incorporating either a picolinamide (*N,N*), ketoiminate (*N,O*) or a naphthoquinone (*O,O*) ligand, where the IC₅₀ values against both HT-29 and MCF-7 show the difference in binding mode is key for the cytotoxic values seen.¹⁰² The most significant result was seen for the ketoiminate (*N,O*) complexes for both ruthenium and iridium and activity followed the general trend (*N,O*) > (*O,O*) > (*N,N*). Part of the work in this thesis helps to explore further structural activity relationships.

Since the start of this project, Dyson *et al.* have also started working on ruthenium β -ketoiminate complexes (**Figure 1.26**). They show that altering the Ru-arene substituent can tune the activity of the complexes, whereby the *p*-cymene ligand gave the highest activities. Upon minor alterations of the β -ketominate ligand, large differences were noted in the cytotoxicities observed. It was also noted that all ruthenium β -ketominate complexes were less active than cisplatin against A2780, but they were more active than cisplatin against A2780*cis*, suggesting these complexes are activated *via* a different mechanism to cisplatin.¹⁰³

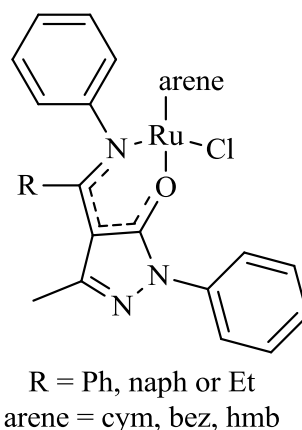
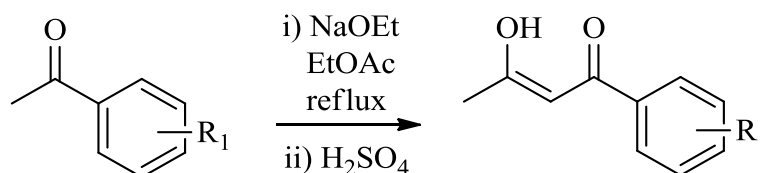


Figure 1.26 Ruthenium β -ketoiminato complexes reported by Dyson *et al.*¹⁰³

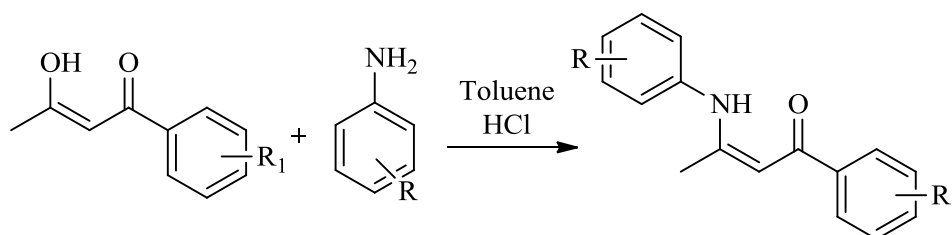
1.8 Research Aims

The aims of the project were to synthesise a range of β -ketoinate ruthenium chloride complexes, altering both the electronics and sterics of the β -ketoinate ligand in order to gain structural activity relationships and assess their potential as anti-cancer compounds.

- Firstly, the β -diketonate ligands¹⁰⁴ and β -keiminato ligands¹⁰⁵ will be synthesised according to **Scheme 1.4** and **Scheme 1.5** respectively.

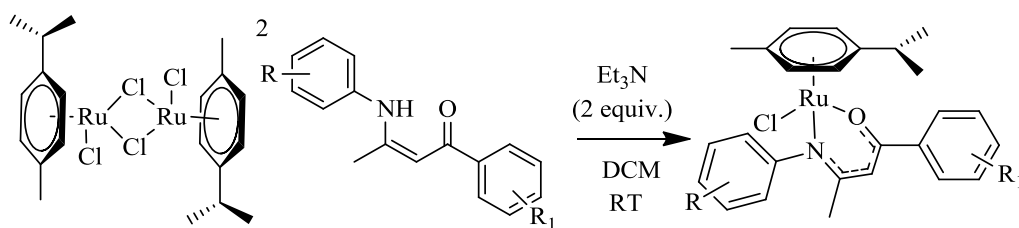


Scheme 1.4 Synthetic route for β -diketonate ligands¹⁰⁴



Scheme 1.5 Synthetic route for β -ketoiminato ligands¹⁰⁵

- The complexes will be synthesised according to **Scheme 1.6**.



Scheme 1.6 Synthetic route of β -ketominate ruthenium chloride complexes

Complexes synthesised will include the following components which have been shown to be important:

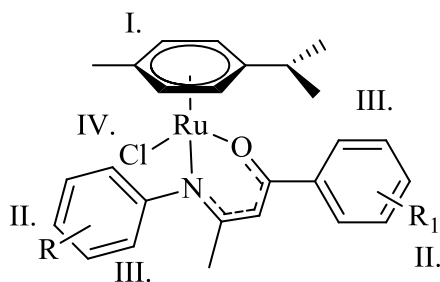


Figure 1.27 Target ruthenium complexes

- I. The *p*-cymene moiety may stabilise the ruthenium centre towards hydrolysis and increase the hydrophobic character of the complex, allowing the complex to remain intact *in vivo* and facilitating passive transport across cell membranes.
- II. Varying the substituents R and R₁ may increase the water solubility of the complex as well as increasing the anti-cancer activity of the complex.
- III. Planar aromatic groups may provide a potential site for π -stacking with nucleobases within the DNA chain (intercalation).
- IV. The presence of a labile halide ligand could allow rapid hydrolysis of the complex at the low intracellular chloride levels, forming the more reactive species which can then form covalent bonds with nucleophilic sites on the DNA chain.

The complexes will be assessed for their anti-cancer potential by determining their cytotoxicities using several biological assays and gaining structure activity relationships (SARs).

1.9 References

1. Cancer Research UK,
[http://publications.cancerresearchuk.org/downloads/Product/CS_REPORT
_TOP10INCMORT.pdf](http://publications.cancerresearchuk.org/downloads/Product/CS_REPORT_TOP10INCMORT.pdf), Accessed 17.12.2013.
2. Cancer Research UK,
<http://www.cancerresearchuk.org/cancer-info/cancerstats/incidence/>,
Accessed 17.12.2013.
3. NHS, [http://www.nhs.uk/news/2011/12December/Pages/cancer-treatment-
cost-may-increase.aspx](http://www.nhs.uk/news/2011/12December/Pages/cancer-treatment-cost-may-increase.aspx), Accessed 17th December, 2013.
4. Cancer Research UK,
<http://www.cancerresearchuk.org/cancer-info/cancerstats/mortality/>,
Accessed 17th December, 2013.
5. T. Huhn, M. Tacke, S. Eger, T. A. Immel, J. Claffey, H. Muller-Bunz and
U. Groth, *Inorg. Chem.*, 2010, **49**, 1292.
6. V. J. Bykov and K. G. Wiman, *Ann Med*, 2003, **35**, 458-465.
7. D. Voet and J. G. Voet, *Biochemistry*, 2 edn., John Wiley & Sons Inc.,
1995.
8. N. C. Turner and J. S. Reis, *Oncogene*, 2006, **25**, 5846-5853.
9. Cancer Research UK, 2009.
10. D. Hoffmann, J.-M. Bangen, W. Bayer and O. Wildner, *Gene therapy*,
2006, **13**, 1534-1544.
11. S. Riethmiller, *Bull. Hist. Chem.*, 1999, **23**, 28.
12. N. C. Lloyd, H. W. Morgan, B. K. Nicholson and R. S. Ronimus, *Angew.
Chem., Int. Ed.*, 2005, **44**, 941-944.
13. T. A. S. o. H.-S. Pharmacists, *Medline Plus*, Accessed 29th December,
2013.
14. J. D. Kelly, A. M. Forster, B. Higley, C. M. Archer, F. S. Booker, L. R.
Canning, K. W. Chiu, B. Edwards, H. K. Gill, M. McPartlin, K. R. Nagle, I.
A. Latham, R. D. Pickett, A. E. Storey and P. M. Webbon, *J. Nucl. Med.*,
1993, **34**, 222-227.
15. M. Peyrone, *Ann. Chemie. Pharm. (Med. Times)*, 1844, **51 (10)**, 1-29 (381).
16. Chemistry World,
[http://www.rsc.org.uk/chemistryworld/podcast/CIIEcompounds/transcripts/
cisplatin.asp](http://www.rsc.org.uk/chemistryworld/podcast/CIIEcompounds/transcripts/cisplatin.asp), Accessed 29.12.2013

17. S. Trzaska, *Chem. Eng. News*, 2005, **83**, 25.
18. B. Rosenberg, L. Van Camp and T. Krigas, *Nature (London)*, 1965, **205**, 698-699.
19. C. Moucheron, *New J. Chem.*, 2009, **33**, 235-245.
20. M. J. Cleare, *Coord. Chem. Rev.*, 1974, **12**, 349-405.
21. W. Kaim and B. Schwederski, *Bioinorganic Chemistry: Inorganic Elements in the Chemistry of Life*, Wiley, New York, 1998.
22. W. A. Schroyens, J. B. Meeker, P. Dodion, P. A. Stryckmans and M. Rozenzweig, *Eur. J. Cancer Clin. Oncol.*, 1988, **24**, 1309-1312.
23. K. R. Herrap, *Cancer Treat. Rev.*, 1985, **12 (supl. A)**, 21.
24. K. R. Kelland, *Problems with Carboplatin*, Chapman and Hall, 1994.
25. N. Uchida, Y. Takeda and P. J. Sadler, *Inorg. Chem. (Wash., D. C.)*, 1993, **32**, 1333.
26. I. Monnet, P. Soulie, H. de Cremoux, S. Saltiel-Voisin, M. Bekradda, J.-C. Saltiel, E. Brain, G. Dupont-Andre and E. Cvitkovic, *J. Clin. Oncol.*, 2001, **19**, 458.
27. L. Zelek, P. Cottu, M. Tubiana-Hulin, J. M. Vannetzel, P. Chollet, J. L. Misset, N. Chouaki, M. Marty, E. Gamelin, S. Culine, V. Dieras, S. Mackenzie and M. Spielmann, *J. Clin. Oncol.*, 2002, **20**, 2551.
28. V. Dieras, P. Bougnoux, T. Petit, P. Chollet, P. Beuzeboc, C. Borel, F. Husseini, A. Goupil, P. Kerbrat, J. L. Misset, A. Bensmaine, I. Tabah-Fisch and P. Pouillart, *Ann. Oncol.*, 2002, **13**, 258.
29. Y. Chen, Z. Guo, S. Parsons and P. J. Sadler, *Chem.- A Euro. J.*, 1998, **4**, 672-676.
30. F. I. Raynaud, P. Mistry, A. Donaghue, G. K. Poon, L. R. Kelland, C. F. J. Barnard, B. A. Murrer and K. R. Harrap, *Cancer Chemoth. Pharm.*, 1996, **38**, 155-162.
31. M. Degardin, J. P. Armand, B. Chevallier, P. Cappelaere, M.-A. Lentz, M. David and H. Roche, *Invest. New Drugs*, 1995, **13**, 253-255.
32. J. A. Gietema, G. J. Veldhuis, H. J. Guchelaar, P. H. Willemse, D. R. Uges, A. Cats, H. Boonstra, W. T. van der Graaf, D. T. Sleijfer and E. G. de Vries, *Br. J. Cancer*, 1995, **71**, 1302-1307.
33. J. Welink, E. Boven, J. B. Vermorken, H. E. Gall and W. J. F. Van der Vijgh, *Clin. Cancer Res.*, 1999, **5**, 2349-2358.

34. H. Kopf and P. Kopf-Maier, *Angew. Chem.*, 1979, **18**, 477-478.
35. K. O'Connor, C. Gill, M. Tacke, F. J. K. Rehmman, K. Strohfeltdt, N. Sweeney, J. M. Fitzpatrick and R. W. G. Watson, *Apop.*, 2006, **11**, 1205-1214.
36. G. Lummen, H. Sperling, H. Luboldt, T. Otto and H. Rubben, *Cancer Chemoth. Pharm.*, 1998, **42**, 415-417.
37. N. Kroger, U. R. Kleeberg, K. Mross, L. Edler, G. Sass and D. Hossfeld, *Onkologie*, 2000, 60-62.
38. J. H. Toney and T. J. Marks, *J. Am. Chem. Soc.*, 1985, **107**, 947-953.
39. S. S. Yun, I.-H. Suh, S.-S. Choi, T.-H. Kim and S. Lee, *J. Coord. Chem.*, 1999, **47**, 315-318.
40. M. M. Harding and G. Mokdsi, *Curr. Med. Chem.*, 2000, **7**, 1289-1303.
41. P. Kopf-Maier, *J. Struct. Biol.*, 1990, **105**, 35-45.
42. Z. Guo and P. J. Sadler, *Adv. Inorg. Chem.*, 2000, **49**, 183-306.
43. M. C. Valadares and M. L. S. Queiroz, *Eur. J. Pharmacol.*, 2002, **439**, 35-42.
44. P. Kopf-Maier, E. Neuse, T. Klapotke and H. Kopf, *Cancer Chemoth. Pharm.*, 1989, **24**, 23-27.
45. H. Yasuda, T. Yasuhara, H. Yamamoto, K. Takei and A. Nakamura, *Chem. Express*, 1988, **3**, 375-378.
46. H. Kopf and P. Kopf-Maier, *Transition and main-group metal cyclopentadienyl complexes: Preclinical studies on a series of antitumor agents of different structural type*, Springer Berlin/Heidelberg, 1988.
47. M. C. Baird, J. R. Boyles, B. G. Campling and N. Jain, *J. Inorg. Biochem.*, 2001, **84**, 159.
48. J. Claffey, M. Hogan, H. Mueller-Bunz, C. Pampillon and M. Tacke, *J. Organomet. Chem.*, 2008, **693**, 526-536.
49. M. Tacke, J. Claffey, M. Hogan, H. Muller-Bunz and C. Pampillon, *Chemmed. Chem.*, 2008, **3**, 729.
50. M. A. D. McGowan and P. C. McGowan, *Inorg. Chem. Comm.*, 2000, **3**, 337-340.
51. O. R. Allen, L. Croll, A. L. Gott, R. J. Knox and P. C. McGowan, *Organometallics*, 2004, **23**, 288-292.

52. O. R. Allen, A. L. Gott, J. A. Hartley, J. M. Hartley, R. J. Knox and P. C. McGowan, *Dalton Trans.*, 2007, 5082-5090.
53. P. C. McGowan and R. J. Know, *WO* 2004/005305, 2004.
54. P. C. McGowan and M. D. McGowan, *WO* 2001/042260, 2001.
55. H. J. Keller, B. Keppler and D. Schmahl, *Jouranal of Cancer Research Clinical Oncology*, 1983, **105**, 109-110.
56. H. J. Keller, B. K. Keppler and D. Schmahl, *Arzneim.-Forsch. (Drug Res.)*, 1982, **32 (II)**, 806-807.
57. B. K. Keppler, C. Friesen, H. G. Moritz, H. Vongerichten and E. Vogel, *Struct. Bond.*, 1991, **78**, 97-127.
58. B. K. Keppler and M. Hartmann, *Metal-Based Drugs*, 1994, **1**, 169-173.
59. B. K. Keppler and M. E. Heim, *Drugs Future*, 1988, **13**, 637-652.
60. T. Schilling, B. K. Keppler, M. E. Heim, G. Niebch, H. Dietzfelbinger, J. Rastetter and A.-R. Hanauske, *Invest. New Drugs*, 1996, **13**, 327-332.
61. P. Kopf-Maier, *Eur. J. Clin. Pharmacol.*, 1994, **47**, 1-16.
62. T. Schilling, K. B. Keppler, M. E. Heim, G. Niebch, H. Dietzfelbinger, J. Rastetter and A. R. Hanauske, *Invest. New Drugs*, 1996, **13**, 327-332.
63. M. J. Clarke, F. Zhu and D. R. Frasca, *Chem. Rev.*, 1999, **99**, 2511-2533.
64. B. K. Keppler, *Metal Complexes in Cancer Chemotherapy*, Wiley - VCH, Weinheim, Germany, 1993.
65. L. M. Gao, R. Hernandez, J. Matta and E. Melendez, *J. Biol. Inorg. Chem.*, 2007, **12**, 959-967.
66. E. Dubler, R. Buschmann and H. W. Schmalte, *J. Inorg. Biochem.*, 2003, **95**, 97-104.
67. S. Fruhauf and W. J. Zeller, *Cancer Res.*, 1991, **51**, 2943-2948.
68. B. K. Keppler and K. Michels, *Arzneim.-Forsch. (Drug Res.)*, 1985, **35(II)**, 1837-1839.
69. R. M. Lord, J. J. Mannion, A. J. Hebden, A. E. Nako, B. D. Crossley, M. W. McMullon, F. D. Janeway, R. M. Phillips and P. C. McGowan, *Submitted Manuscript*, 2014.
70. G. Suss-Fink, *Dalton Trans.*, 2010, **39**, 1673-1688.
71. J. Reedijk, *Platinum Met. Rev.*, 2008, **52**, 2-11.
72. C. S. Allardyce and P. J. Dyson, *Platinum Met. Rev.*, 2001, **45**, 62-69.
73. M. J. Clarke, *Coord. Chem. Rev.*, 2003, **236**, 209-233.

74. C. S. Allardyce, A. Dorcier, C. Scolaro and P. J. Dyson, *Appl. Organomet. Chem.*, 2005, **19**, 1-10.
75. C. S. Allardyce, P. J. Dyson, D. J. Ellis and S. L. Heath, *Chem. Commun.*, 2001, **15**, 1396-1397.
76. K. C. Reed and F. L. Bygrave, *J. Biochem.*, 1974, **2**, 143-155.
77. J. R. Durig, J. Danneman, W. D. Behnke and E. E. Mercer, *Chem. Biol. Interact.*, 1976, **13**, 287-294.
78. M. J. Clarke, *Prog. Clin. Biochem. Med.*, 1989, **10**, 25-39.
79. E. Alessio, G. Mestroni, G. Nardin, W. M. Attia, M. Calligaris, G. Sava and S. Zorzets, *Inorg. Chem.*, 1988, **27**, 4099-4106.
80. G. Sava, S. Zorzets, T. Giralidi, G. Mestroni and G. Zassinovich, *Eur. J. Cancer Clin. Oncol.*, 1984, **20**, 841-847.
81. S. Cauci, E. Alessio, G. Mestroni and F. Quadrifoglio, *Inorg. Chim. Acta*, 1987, **137**, 19-24.
82. G. Sava, I. Capozzi, K. Clerici, G. Gagliardi, E. Alessio and G. Mestroni, *Clin. Exp. Met.*, 1998, **16**, 371-379.
83. G. Sava, S. Pacor, A. Bergamo, M. Cocchietto, G. Mestroni and E. Alessio, *Chem. Biol. Interact.*, 1995, **95**, 109-126.
84. C. A. Smith, A. J. Sutherland-Smith, B. K. Keppler, F. Kratz and E. N. Baker, *J. Biol. Inorg. Chem.*, 1996, **1**, 424-431.
85. G. Sava, A. Bergamo, S. Zorzet, B. Gava, C. Casarsa, M. Cocchietto, A. Furlani, V. Scarcia, B. Serli, E. Iengo, E. Alessio and G. Mestroni, *Eur. J. Cancer*, 2002, **38**, 427-435.
86. L. Trynda-Lemiesz, A. Karaczyn, B. K. Keppler and H. Kozłowski, *J. Inorg. Biochem.*, 2000, **78**, 341-346.
87. B. K. Keppler, W. Rupp, U. M. Juhl, H. Endres, R. Niebl and W. Balzer, *Inorg. Chem.*, 1987, **26**, 4366-4370.
88. W. Peti, T. Pieper, M. Sommer, B. K. Keppler and G. Giester, *Eur. J. Inorg. Chem.*, 1999, **1999**, 1551-1555.
89. C. G. Hartinger, S. Zorbas-Seifried, M. A. Jakupec, B. Kynast, H. Zorbas and B. K. Keppler, *J. Inorg. Biochem.*, 2006, **100**, 891-904.
90. A. Kung, T. Pieper, R. Wissiack, E. Rosenberg and B. K. Keppler, *J. Inorg. Biochem.*, 2001, **6**, 292-299.
91. W. S. Sheldrick and S. Heeb, *Inorg. Chim. Acta*, 1990, **168**, 93-100.

92. R. E. Morris, R. E. Aird, P. d. S. Murdoch, H. Chen, J. Cummings, N. D. Hughes, S. Parsons, A. Parkin, G. Boyd, D. I. Jodrell and P. J. Sadler, *J. Med. Chem.*, 2001, **44**, 3616-3621.
93. R. E. Aird, J. Cummings, A. A. Ritchie, M. Muir, R. E. Morris, H. Chen and P. J. Sadler, *J. Br. Cancer*, 2002, **86**, 1652-1657.
94. A. Habtemariam, M. Melchart, R. Fernandez, S. Parsons, I. D. H. Oswald, A. Parkin, F. P. A. Fabbiani, J. E. Davidson, A. Dawson, R. E. Aird, D. I. Jodrell and P. J. Sadler, *J. Med. Chem.*, 2006, **49**, 6858-6868.
95. R. Fernandez, M. Melchart, A. Habtemariam, S. Parsons and P. J. Sadler, *Chem. Eur. J.*, 2004, **10**, 5173-5179.
96. H. Chen, J. A. Parkinson, R. E. Morris and P. J. Sadler, *J. Am. Chem. Soc.*, 2003, **125**, 173-186.
97. H. M. Chen, J. A. Parkinson, S. Parsons, R. A. Coxall, R. O. Gould and P. J. Sadler, *J. Am. Chem. Soc.*, 2002, **124**, 3064-3082.
98. Z. Almodares, 2010.
99. S. H. van Rijt, A. J. Hebden, T. Amaresekera, R. J. Deeth, G. J. Clarkson, P. Parsons, P. C. McGowan and P. J. Sadler, *J. Med. Chem.*, 2009, **52**, 7753-7764.
100. K. D. Camm, A. El-Sokkary, A. L. Gott, P. G. Stockley, T. Belyaeva and P. C. McGowan, *Dalton Trans.*, 2009, 10914-10925.
101. K. Rafferty, Ph.D Thesis, University of Leeds, 2008.
102. S. J. Lucas, R. M. Lord, R. L. Wilson, R. M. Phillips, V. Sridharana and P. C. McGowan, *Dalton Trans.*, 2012, **41**, 13800-13802.
103. R. Pettinari, C. Pettinari, F. Marchetti, C. M. Clavel, R. Scopelliti and P. J. Dyson, *Organometallics*, 2012, **32**, 309-316.
104. J. J. Hollick, B. T. Golding, I. R. Hardcastle, N. Martin, C. Richardson, L. J. M. Rigoreau, G. C. M. Smith and R. J. R. J. Griffin, *Bioorg. Med. Chem. Lett.*, 2003, **13**, 3083-3086.
105. L.-M. Tang, Y.-Q. Duan, X.-F. Li and Y.-S. Li, *J. Organomet. Chem.*, 2006, **691**, 2023-2030.

Chapter 2

Synthesis and Characterisation of β -Diketonate and β - Ketoiminate Ligands

2 Preparation of (*O,O*) and (*N,O*) Ligands

2.1 Preparation of β -Diketonate (*O,O*) Ligands

This section extends the previous library of 4-hydroxy-4-phenyl-3-buten-2-one (β -diketonate) ligands which have previously been reported within the research group.^{1, 2} The library was first extended by the synthesis of novel mono-aryl β -diketonate ligands (**L1-L4**) and also novel bi-aryl β -diketonate ligands (**L5-L10**) (**Figure 2.1**). All compounds have been synthesised and fully characterised by the author using ¹H NMR, ¹H-¹H COSY, ¹³C{¹H} NMR, ¹H-¹³C{¹H} HMQC spectroscopy, mass spectrometry and micro-analysis.

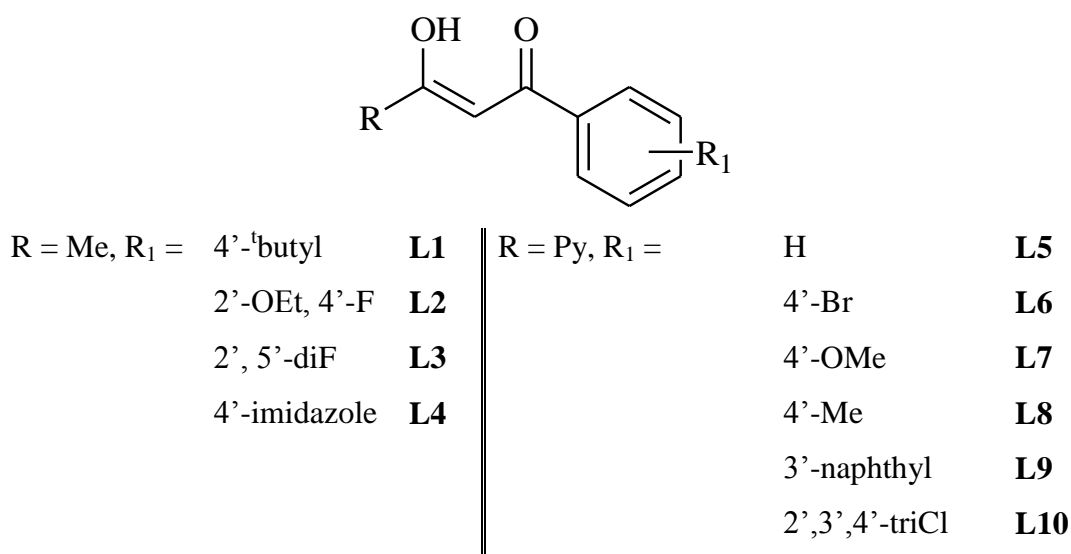
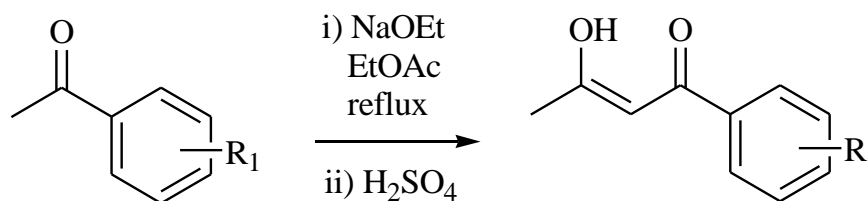


Figure 2.1 Novel β -diketonate ligands synthesised within this chapter

2.2 Synthesis of Mono-Aryl β -Diketonate Ligands

There are several different synthetic routes for the preparation of these mono-aryl ligands. In this work, a Claisen condensation reaction was carried out by reacting a substituted acetophenone with ethyl acetate in the presence of sodium ethoxide (**Scheme 2.1**).³



Scheme 2.1 Synthetic route for mono-aryl β -diketonate ligands

2.2.1 Characterisation of Mono-Aryl β -Diketonate Ligands

The ^1H NMR spectra of these mono-aryl ligands (**Figure 2.2**) are all very similar with the aromatic hydrogens (**f-h**) having the highest chemical shifts (an example for **L4** is seen in **Figure 2.3**), all appearing in the region 6.6-8.1 ppm. The methine hydrogen (**c**) is the most characteristic peak and appears as a one proton singlet in the region 6.1-6.5 ppm. The methyl hydrogens (**a**) appear as a three proton singlet in the region 2.1-2.3 ppm. In some ligands a peak for the OH can be seen at approximately 16 ppm.

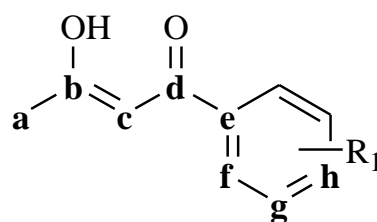


Figure 2.2 General structure of mono-aryl β -diketonate

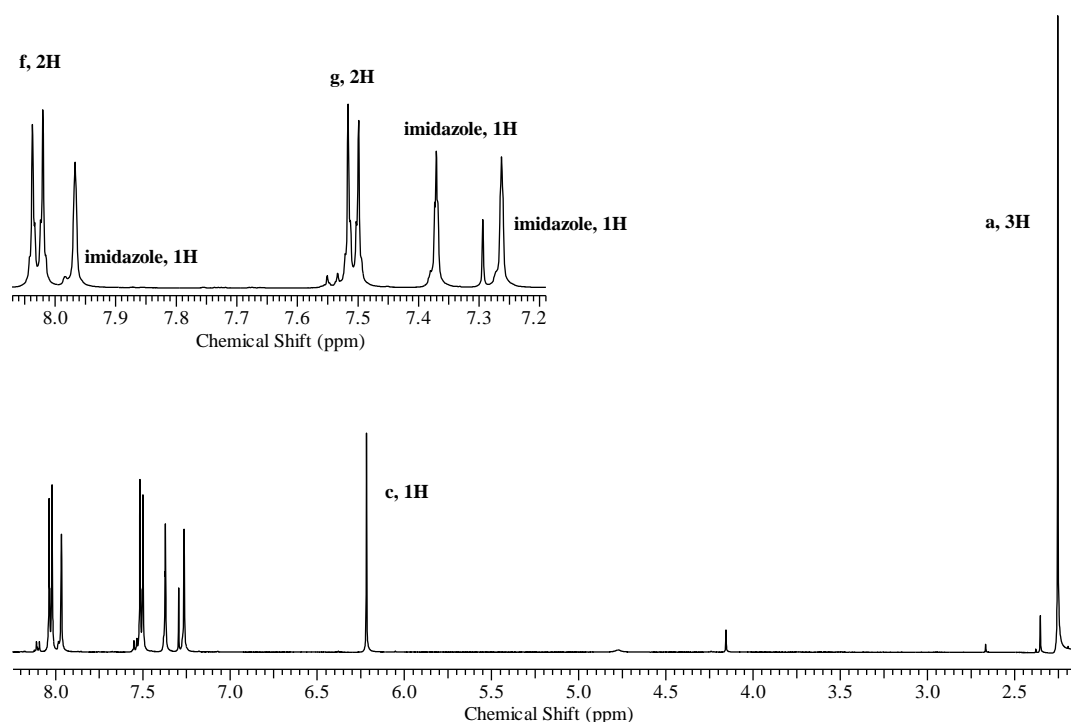


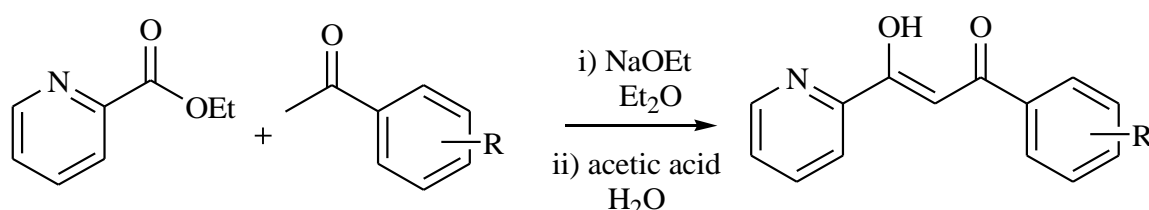
Figure 2.3 ^1H NMR spectrum for ligand **L4** (CDCl_3 , 500 MHz, 300K)

The $^{13}\text{C}\{^1\text{H}\}$ NMR spectra show the highest chemical shifts for the quaternary carbonyl/enol carbons (**b** and **d**), these appear in the range 175-195 ppm. All aromatic quaternary carbons are in the region 130-160 ppm and aromatic CH seen between 100-130 ppm and these values differ depending on the substituent R. The

methine carbon (**c**) is in the region 95-105 ppm and finally the methyl carbon (**a**) is usually seen between 25-27 ppm.

2.3 Synthesis of Biaryl β -Diketonate Ligands

The biaryl β -diketonate ligands were also prepared *via* a Claisen condensation reaction of a substituted aromatic ketone with a substituted pyridine ester in the presence of sodium ethoxide, acetic acid and water (**Scheme 2.2**). This is a modification of a previously published literature route by Levine *et al.* and goes *via* a similar mechanistic pathway to the mono-aryl ligands.⁴



Scheme 2.2 Synthetic route for biaryl β -diketonate ligands

2.3.1 Characterisation of Biaryl β -Diketonate Ligands

The ¹H NMR spectra for these biaryl ligands (**Figure 2.4**) are very similar, but show significant differences when compared to the mono-aryl ligands. The protons **a-d** appear slightly higher in at a chemical region of 7.4-8.8 ppm. The aromatic protons **j-l** are within the region 6-8 ppm. The methine hydrogen (**g**) is seen at a much higher chemical shift when compared to the mono-aryl ligands and appears as a one hydrogen singlet between 7.2-7.7 ppm (example for **L5** seen in **Figure 2.5**)

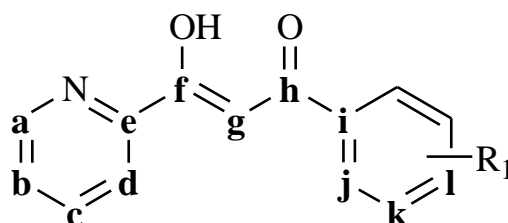


Figure 2.4 General structure of a biaryl β -diketonate

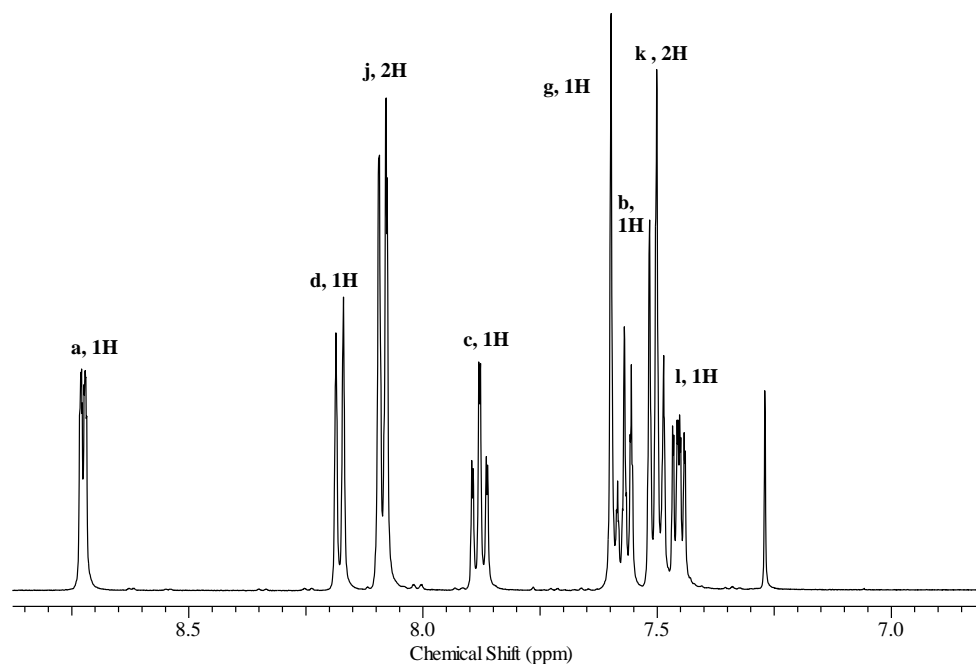


Figure 2.5 ^1H NMR spectra example of the biaryl ligand **L5** (CDCl_3 , 500 MHz, 300K)

The $^{13}\text{C}\{^1\text{H}\}$ NMR spectra are similar to the mono-aryl β -diketonate ligands, with the highest shifts seen between 180-190 ppm for the quaternary carbons **f** and **h**. All the pyridine and aromatic CH signals appear between 120-150 ppm and were assigned using a 2D ^1H - $^{13}\text{C}\{^1\text{H}\}$ COSY spectra. The quaternary pyridine carbon **e** is typically seen between 150-160 ppm and the aromatic quaternary carbon **i** between 127-135 ppm. Finally, the methane carbon **g** has the lowest chemical shift and can be found between 90-95 ppm.

2.4 Preparation of β -Ketoiminate (*N,O*) Ligands

This section expands on previously synthesised phenyl-3(phenylamino)-2-buten-1-one (β -ketoiminate) ligands.⁵ The novel ligands shown in **Figure 2.6** have been synthesised and characterised by the author using ^1H NMR, ^1H - ^1H COSY, $^{13}\text{C}\{^1\text{H}\}$ NMR, ^1H - $^{13}\text{C}\{^1\text{H}\}$ COSY spectroscopy, mass spectrometry, microanalysis. In addition single X-ray crystallography data has been obtained for ligands **L11**, **L12**, **L14-16**, **L19**, **L21**, **L22**, **L24** and **L25**.

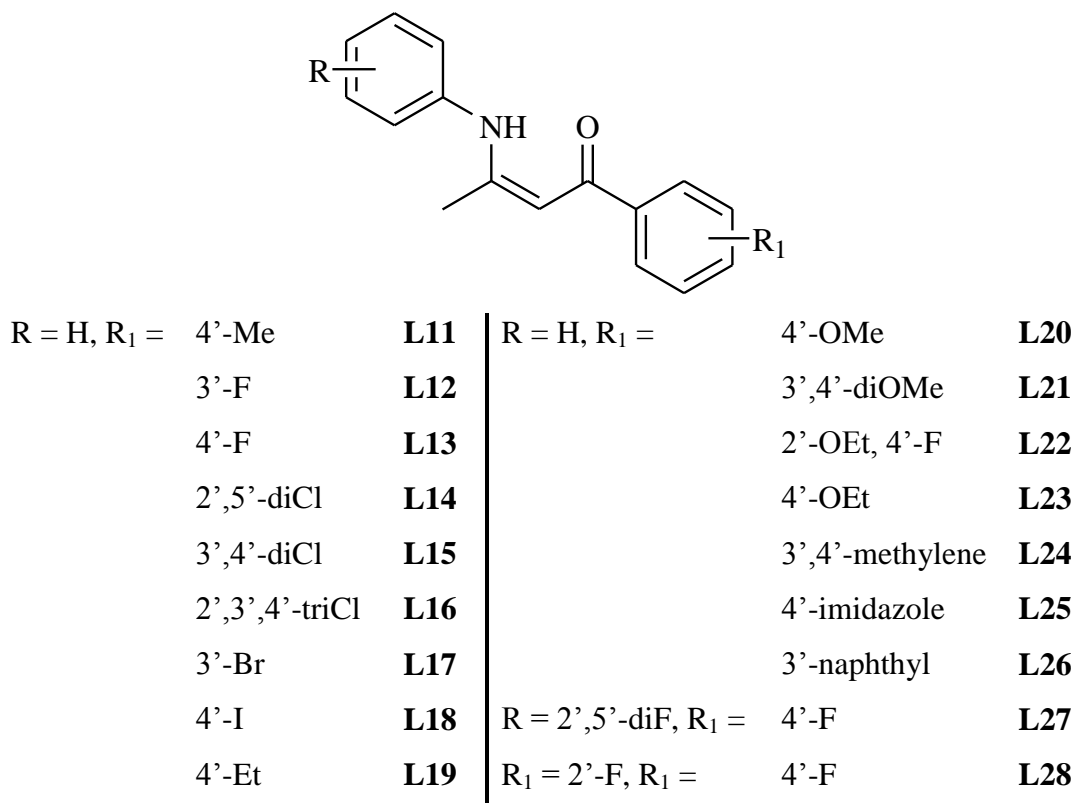
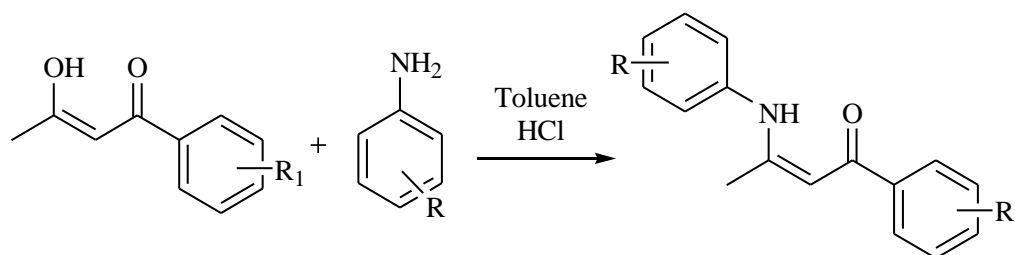


Figure 2.6 Novel β -ketoiminate ligands synthesised within this chapter

2.5 Synthesis of β -Ketoiminate Ligands

The β -ketoiminate ligands were synthesised using an adaptation of a previously established method by Tang *et al.*⁶ The corresponding functionalised β -diketonate ligand was reacted with the relevant aniline in the presence of toluene and HCl (Scheme 2.3).



Scheme 2.3 General synthetic route for the β -ketoiminate ligands

2.5.1 NMR Characterisations for β -Ketoiminate Ligands

The ¹H NMR spectra for the β -ketoiminate ligands (Figure 2.7) show a characteristic broad singlet between 12.7-13.2 ppm corresponding to the NH. In general, the aniline aromatic protons are usually within the range 7.1-7.5 ppm, with the *meta* hydrogens (c) usually appearing as a broad triplet and the *para* hydrogens

(**d**) as a multiplet. These are at higher ppm values and generally more deshielded than the *ortho* hydrogens (**b**) which often appear as broad doublets. The methyl hydrogens (**e**) appear as a three proton singlet between 2.1-2.2 ppm and the methine hydrogen (**g**) is a one proton singlet in the region of 5.4-6.1 ppm and is shifted upfield approximately 0.5 ppm from the corresponding β -diketonate ligand. The protons from the aromatic ring (**j-l**) all differ depending on the substituent R_1 and can be seen within the region 6-8 ppm (example for **L11** seen in **Figure 2.8**).

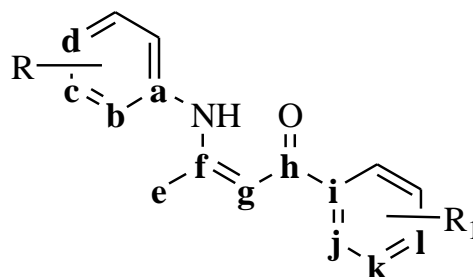


Figure 2.7 General structure of the β -ketoiminate ligand

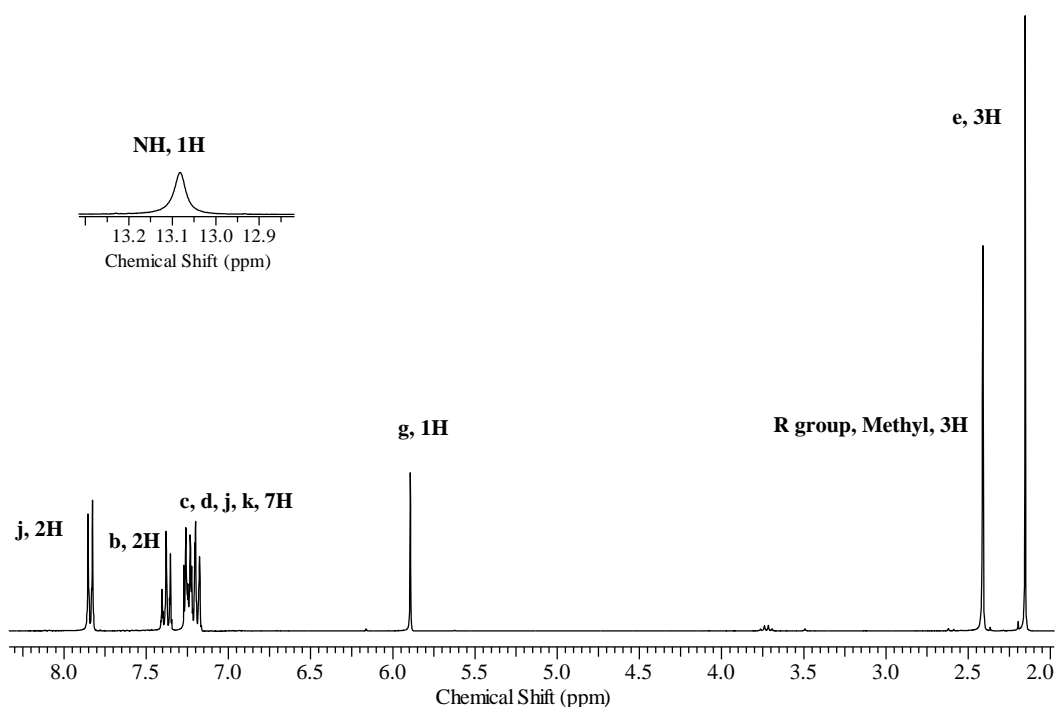


Figure 2.8 ^1H NMR spectra example for ligand **L11** (CDCl_3 , 300 MHz, 300K)

The $^{13}\text{C}\{^1\text{H}\}$ spectrum for ligands are all similar, with the highest peaks for the quaternary carbonyl carbon (**h**) and quaternary carbon *ipso* to NH (**f**), these are usually seen in the region of 160-188 ppm. All aromatic carbons are in the range 100-135 ppm and the order differs depending on the substituent R. The methine carbon (**g**) appears in the region 93-100 ppm and the methyl carbon (**e**) is seen in

the region 19-21 ppm.

2.5.2 X-ray Crystallography for β -Ketoiminate

Single crystals suitable for X-ray crystallography were obtained by slow evaporation from hot ethanol. Structural solutions were performed in a monoclinic (**L11**, **L12**, **L14**, **L16**, **L19**, **L24** and **L25**), orthorhombic (**L15**) or triclinic (**L21** and **L22**) space group. All angles around the central atoms are between 118-125°, showing this section of the ligand is planar, with the atoms held together by an intramolecular hydrogen bonding interaction between N-H...O, this interaction is seen in all crystal structures. Most of the ligands have intermolecular interactions holding pairs of molecules together and have a distinctive herringbone arrangement when viewed along an axis.

2.6 Characterisation of Novel β -Ketoiminate Compounds

2.6.1 X-ray Characterisation of C₁₇H₁₇NO (**L11**)

L11 has been previously synthesised,⁵ however, colourless crystals suitable for X-ray crystallographic analysis were obtained by slow evaporation in hot ethanol over a period of 3 days. The molecular structure is given in **Figure 2.9**, and selected bond lengths and angles are stated in **Table 2.1**. Ligand **L11** was solved in a monoclinic cell and structural solution was performed in the space group $P2_1/n$, with two molecules in the asymmetric unit.

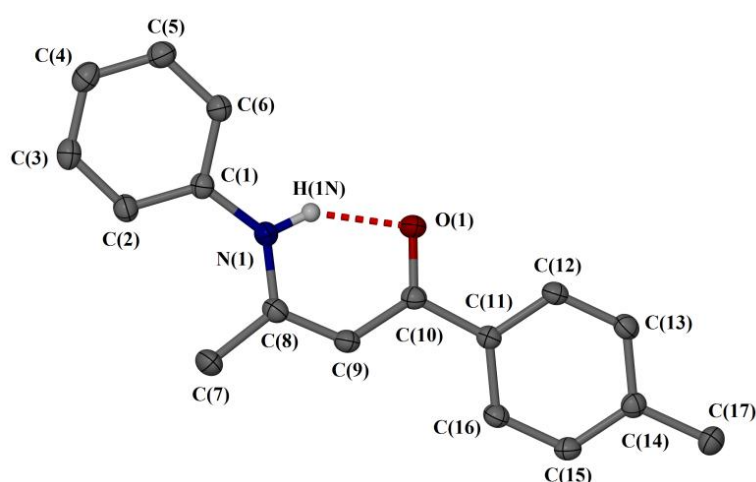


Figure 2.9 Molecular structure of **L11**, displacement ellipsoids are at the 50% probability level and hydrogen atoms are omitted for clarity.

Table 2.1 Selected bond lengths and angles for both molecules of **L11**

Bond	Distance (Å)	Bond	Angle (°)
C(1)-N(1)	1.4104(13)	C(1)-N(1)-C(8)	133.39(9)
N(1)-C(8)	1.3543(13)	N(1)-C(8)-C(9)	119.60(9)
C(7)-C(8)	1.4996(14)	C(8)-C(9)-C(10)	124.15(10)
C(8)-C(9)	1.3805(15)	O(1)-C(10)-C(9)	122.67(10)
C(9)-C(10)	1.4298(14)	O(1)-C(10)-C(11)	117.81(9)
O(1)-C(10)	1.2552(12)		
C(10)-C(11)	1.4988(14)		
C(14)-C(17)	1.5092(15)		
Bond	Distance (Å)	Bond	Angle (°)
C(1')-N(1')	1.4147(13)	C(1')-N(1')-C(8')	130.88(8)
N(1')-C(8')	1.3499(13)	N(1')-C(8')-C(9')	119.79(9)
C(7')-C(8')	1.5018(14)	C(8')-C(9')-C(10')	123.66(9)
C(8')-C(9')	1.3797(14)	O(1')-C(10')-C(9')	122.56(10)
C(9')-C(10')	1.4265(14)	O(1')-C(10')-C(11')	117.67(9)
O(1')-C(10')	1.2610(12)		
C(10')-C(11')	1.4967(14)		
C(14')-C(17')	1.5114(15)		

The packing diagram for **L11** shows the molecules pack in pairs of alternating molecules with a head-tail-tail-head arrangement when viewed along the *c* axis there is a slight herringbone structure. Intramolecular hydrogen bonding can be seen between N-H...O of both molecules and an intermolecular hydrogen bond between C(3)-H(3)...O(1') which is contributing to the packing of this molecule. The packing diagram and intermolecular interactions are presented in **Figure 2.10**, with D...A distances and torsion angles are stated in **Table 2.2**.

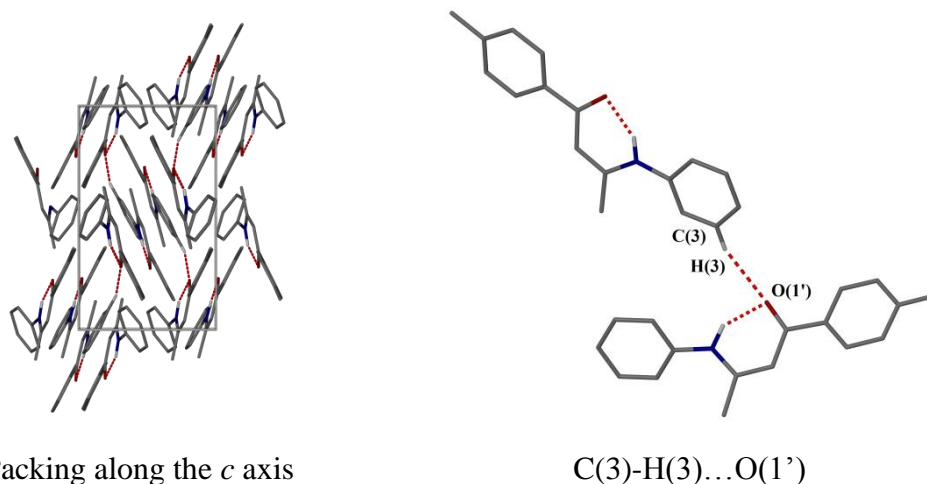


Figure 2.10 Packing diagrams and intermolecular interaction of **L11**, and hydrogen atoms are omitted for clarity.

Table 2.2 Bond lengths and torsion angles of ligand **L11**

Interaction	Atoms	Bond Lengths and Angles
Intramolecular	N(1)-H(1)...O(1)	2.6286(12) Å
	N(1')-H(1')...O(1')	2.6107(12) Å
Intermolecular	C(3)-H(3)...O(1')	3.3190(14) Å
Torsion	Cg(1)-Centre	15.49°
	Centre-Cg(2)	15.00°

2.6.2 X-ray Characterisation of C₁₆H₁₄FNO (**L12**)

Yellow plates of **L12** suitable for X-ray crystallographic analysis were obtained by slow evaporation in hot ethanol over a period of several days. The molecular structure is given in **Figure 2.11**, and selected bond lengths and angles are stated in **Table 2.2**. Ligand **L12** was solved in a monoclinic cell and structural solution was performed in the space group $P2_1/c$, with one molecule in the asymmetric unit.

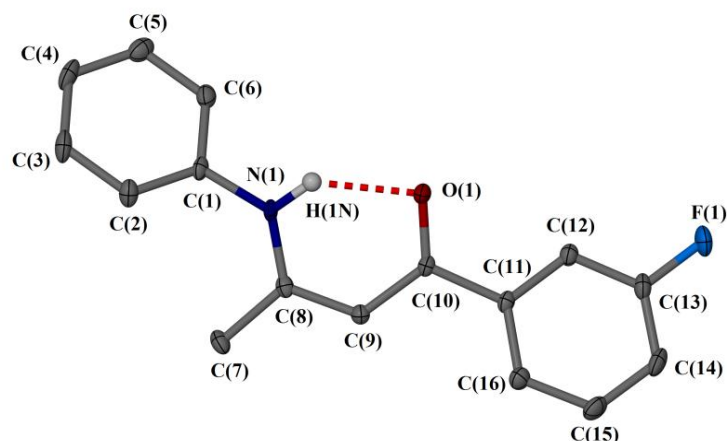
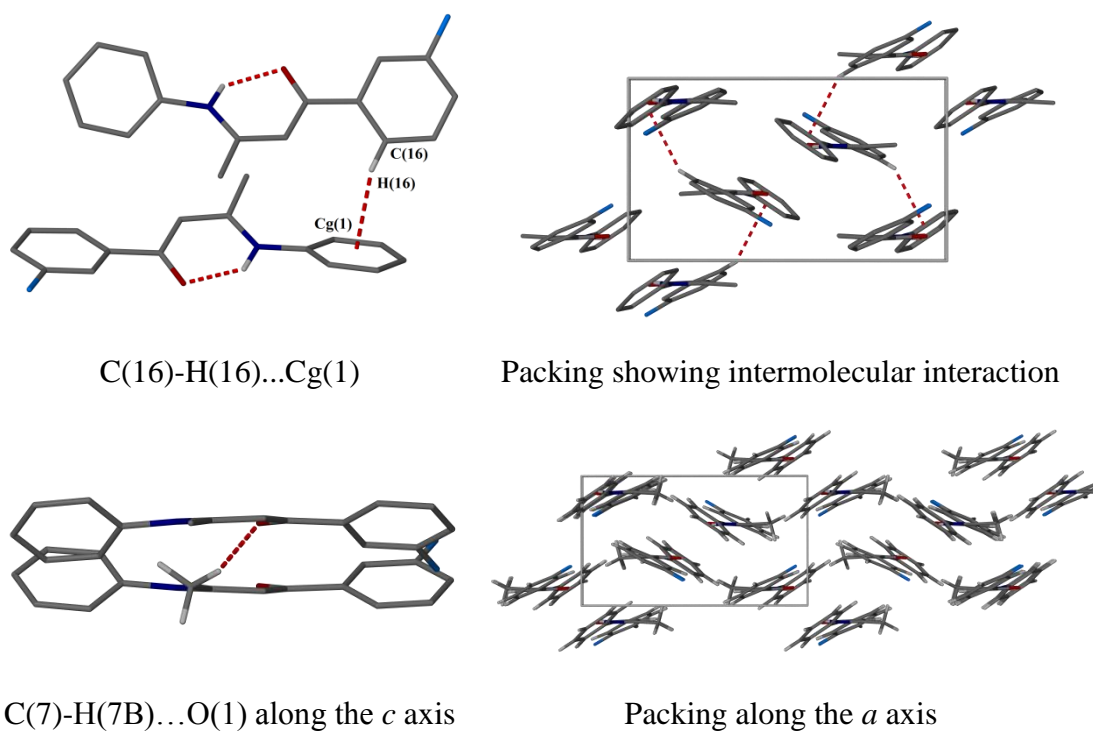


Figure 2.11 Molecular structure of **L12**, displacement ellipsoids are at the 50% probability level and hydrogen atoms are omitted for clarity.

Table 2.3 Selected bond lengths and angles of **L12**

Bond	Distance (Å)	Bond	Angle (°)
C(1)-N(1)	1.4235(14)	C(1)-N(1)-C(8)	130.54(9)
N(1)-C(8)	1.3457(14)	N(1)-C(8)-C(9)	120.17(9)
C(7)-C(8)	1.5049(14)	C(8)-C(9)-C(10)	123.34(10)
C(8)-C(9)	1.3963(15)	O(1)-C(10)-C(9)	123.39(10)
C(9)-C(10)	1.4286(15)	O(1)-C(10)-C(11)	118.88(9)
O(1)-C(10)	1.2583(13)		
C(10)-C(11)	1.5105(14)		
C(13)-F(1)	1.3622(13)		

The packing diagrams for **L12** show that when viewed along the *a* axis there is a herringbone arrangement with intermolecular interactions holding rows of molecules together. Intramolecular hydrogen bonding can be seen between N(1)-H(1N)...O(1) and an intermolecular T-stacking interaction is seen between C(16)-H(16)...Cg(1). The interactions and packing diagrams are presented in **Figure 2.12**, with D...A distances and torsion angles stated in **Table 2.4**.

**Figure 2.12** Intermolecular interactions and packing diagram of **L12****Table 2.4** Bond lengths and torsion angles of **L12**

Interaction	Atoms	Bond Lengths and Angles
Intramolecular	N(1)-H(1N)...O(1)	2.6434(14) Å
Intermolecular	C(16)-H(16)...Cg(1)	3.5834 Å
	N(1)-H(1N)...O(1)	3.1450(13) Å
	C(7)-H(7B)...O(1)	3.3968(14) Å
Torsion	Cg(1)-Centre	34.83°
	Centre-Cg(2)	24.74°

2.6.3 X-ray Characterisation of $C_{16}H_{13}Cl_2NO$ (**L14**)

Yellow plates of **L14** suitable for X-ray crystallographic analysis were obtained by slow evaporation in hot ethanol over a period of several days. The molecular structure is given in **Figure 2.13**, and selected bond lengths and angles are stated in **Table 2.5**. Ligand **L15** was solved in a monoclinic cell and structural solution was performed in the space group $P2_1/n$, with one molecule in the asymmetric unit.

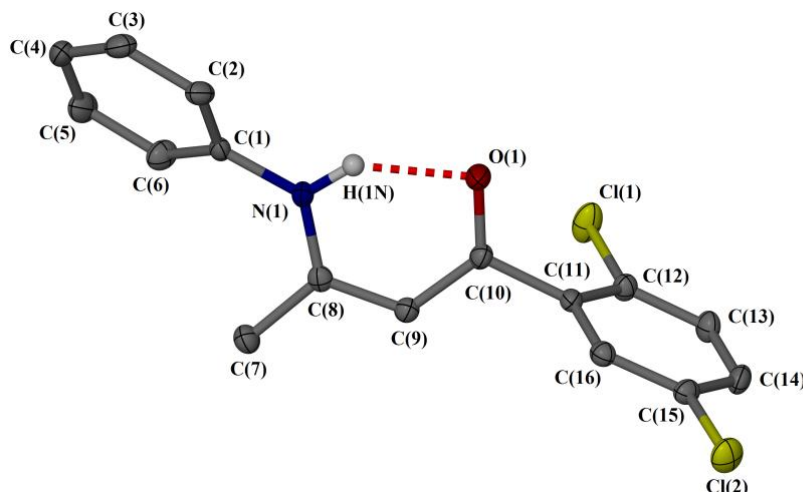
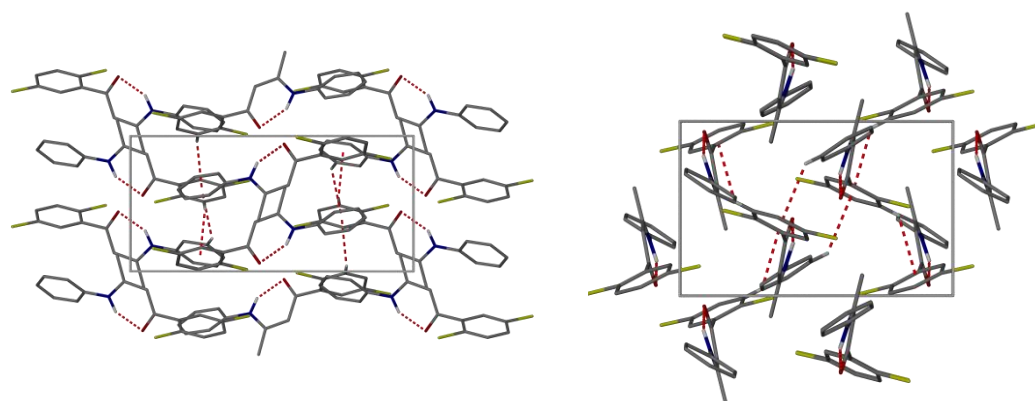
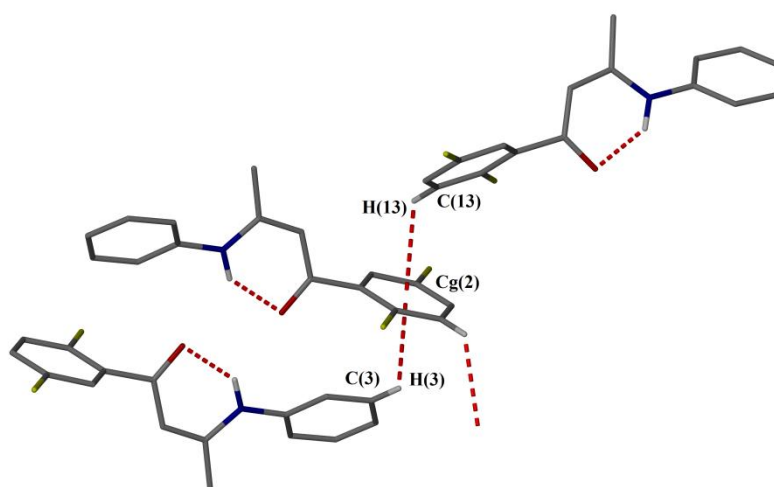


Figure 2.13 Molecular structure of **L14**, displacement ellipsoids are at the 50% probability level and hydrogen atoms are omitted for clarity.

Table 2.5 Selected bond lengths and angles of **L14**

Bond	Distance (Å)	Bond	Angle (°)
C(1)-N(1)	1.4232(15)	C(1)-N(1)-C(8)	128.29(11)
N(1)-C(8)	1.3460(16)	N(1)-C(8)-C(9)	119.87(11)
C(7)-C(8)	1.4987(17)	C(8)-C(9)-C(10)	123.80(11)
C(8)-C(9)	1.3883(16)	O(1)-C(10)-C(9)	125.41(11)
C(9)-C(10)	1.4158(18)	O(1)-C(10)-C(11)	118.14(11)
O(1)-C(10)	1.2480(16)		
C(10)-C(11)	1.5146(16)		
C(12)-Cl(1)	1.7412(12)		
C(15)-Cl(2)	1.7380(12)		

The packing diagrams show the molecules pack in a head-tail arrangement and when viewed along both the *a* and *c* axes there is a herringbone structure, with intermolecular T-stacking interactions holding rows of molecules together. Intramolecular hydrogen bonding can be seen between N(1)-H(1N)...O(1), and two intermolecular T-stacking interactions are seen between C(3)-H(3)...Cg(2) and C(13)-H(13)...Cg(2). The packing diagrams and T-stacking interactions and are presented in **Figure 2.14**, with D...A distances and torsion angles stated in **Table 2.6**.

Packing along the *a* axisPacking along the *c* axis

T-stacking between C(3)-H(3)...Cg(2)...H(13)-C(13)

Figure 2.14 Packing diagrams and T-stacking interactions of **L14****Table 2.6** Bond lengths and torsion angles of **L14**

Interaction	Atoms	Bond Lengths and Angles
Intramolecular	N(1)-H(1N)...O(1)	2.6788(14) Å
Intermolecular	C(3)-H(3)...Cg(2)	3.5000 Å
	C(13)-H(13)...Cg(2)	3.5220 Å
Torsion	Cg(1)-Centre	45.61°
	Centre-Cg(2)	81.99°

2.6.4 X-ray Characterisation of $C_{16}H_{13}Cl_2NO$ (**L15**)

Yellow fragments of **L15** suitable for X-ray crystallographic analysis were obtained by slow evaporation in hot ethanol over a period of several days. The molecular structure is given in **Figure 2.15**, and selected bond lengths and angles are stated in **Table 2.7**. Ligand **L15** was solved in an orthorhombic cell and

structural solution was performed in the space group *Pbca*, with one molecule in the asymmetric unit.

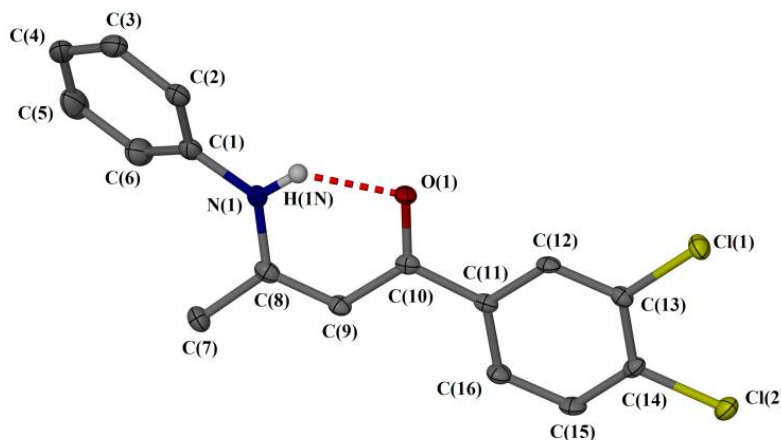
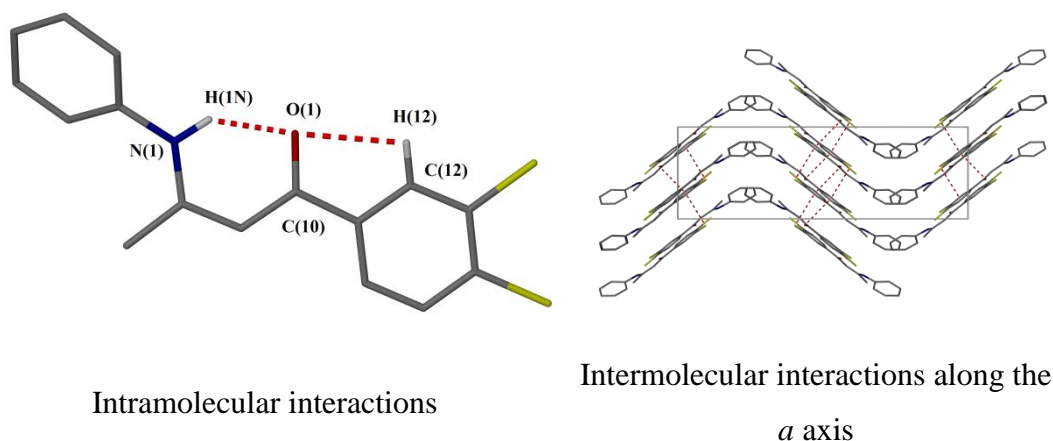


Figure 2.15 Molecular structure of **L15**, displacement ellipsoids are at the 50% probability level and hydrogen atoms are omitted for clarity.

Table 2.7 Selected bond lengths and angles of **L15**

Bond	Distance (Å)	Bond	Angle (°)
C(1)-N(1)	1.4107(3)	C(1)-N(1)-C(8)	129.75(22)
N(1)-C(8)	1.3528(3)	N(1)-C(8)-C(9)	120.22(23)
C(7)-C(8)	1.4997(4)	C(8)-C(9)-C(10)	123.29(24)
C(8)-C(9)	1.3759(4)	O(1)-C(10)-C(9)	122.67(23)
C(9)-C(10)	1.4236(4)	O(1)-C(10)-C(11)	117.26(22)
O(1)-C(10)	1.2564(3)		
C(10)-C(11)	1.5003(3)		
C(13)-Cl(1)	1.7391(3)		
C(14)-Cl(2)	1.7353(3)		

The packing diagrams for **L15** show the molecules pack in a head-tail-tail-head herringbone arrangement when viewed along the *a* axis, with intermolecular T-stacking interactions holding rows of molecules together. Intramolecular hydrogen bonding interactions can be seen between N(1)-H(1N)...O(1) and C(12)-H(12)...O(1). There are intermolecular T-stacking interaction between C(13)-Cl(1)...Cg(2) and C(10)-O(1)...Cg(2). These interactions and the packing diagram are presented in **Figure 2.16**, with D...A distances and torsion angles stated in **Table 2.8**.

**Figure 2.16** Intra-/Intermolecular interactions and packing diagram of **L15****Table 2.8** Bond lengths and torsion angles of **L15**

Interaction	Atoms	Bond Lengths and Angles
Intramolecular	N(1)-H(1N)...O(1)	2.607(3) Å
	C(12)-H(12)...O(1)	2.733(3)
Intermolecular	C(13)-C(1)...Cg(2)	3.911 Å
	C(10)-O(1)...Cg(2)	3.478 Å
	C(15)-H(15)...O(1)	3.175(3) Å
Torsion	Cg(1)-Centre	45.61°
	Centre-Cg(2)	81.99°

2.6.5 X-ray Characterisation of C₁₆H₁₂Cl₃NO (**L16**)

Brown fragments of **L17** suitable for X-ray crystallographic analysis were obtained by slow evaporation in hot ethanol over a period of several days. The molecular structure is given in **Figure 2.17**, and selected bond lengths and angles are stated in **Table 2.9**. Ligand **L17** was solved in a monoclinic cell and structural solution was performed in the space group $P2_1/c$, with one molecule in the asymmetric unit.

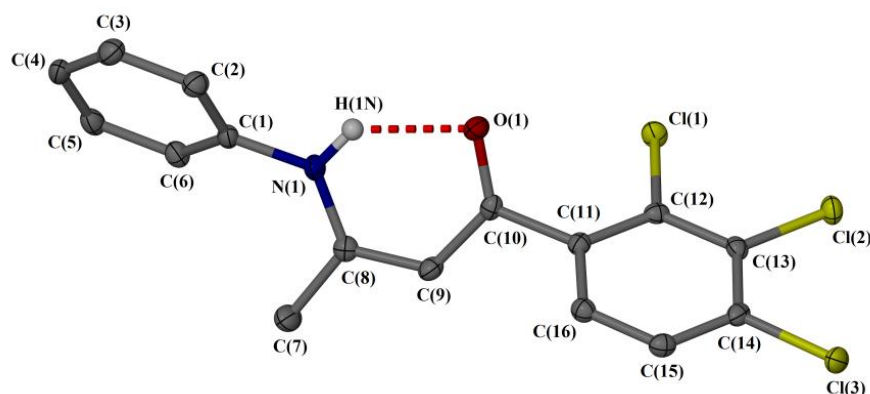
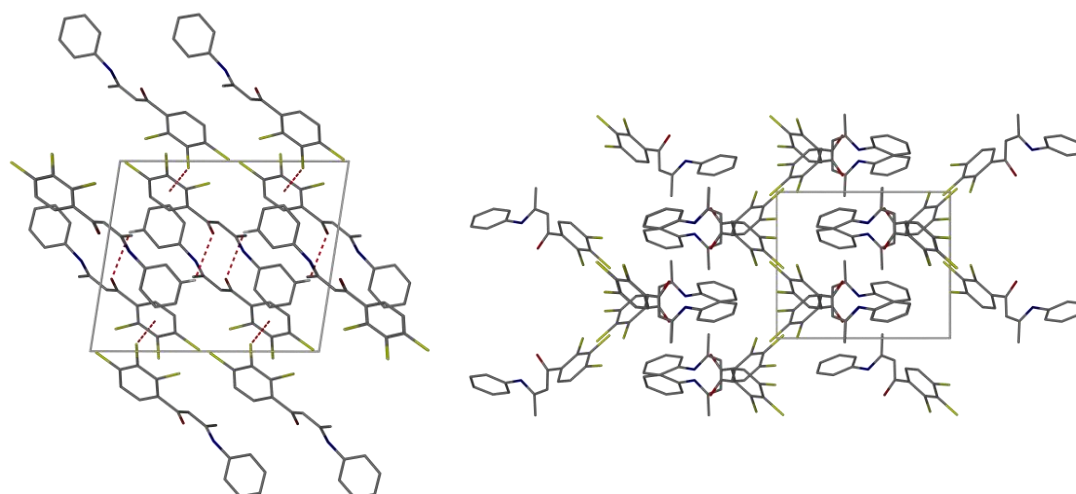


Figure 2.17 Molecular structure of L16, displacement ellipsoids are at the 50% probability level and hydrogen atoms are omitted for clarity.

Table 2.9 Selected bond lengths and angles for L16

Bond	Distance (Å)	Bond	Angle (°)
C(1)-N(1)	1.411(3)	C(1)-N(1)-C(8)	128.72(15)
N(1)-C(8)	1.346(2)	N(1)-C(8)-C(9)	120.35(16)
C(7)-C(8)	1.494(2)	C(8)-C(9)-C(10)	123.85(16)
C(8)-C(9)	1.380(2)	O(1)-C(10)-C(9)	125.19(15)
C(9)-C(10)	1.418(2)	O(1)-C(10)-C(11)	118.99(15)
O(1)-C(10)	1.245(2)		
C(10)-C(11)	1.510(2)		
C(12)-Cl(1)	1.7326(17)		
C(13)-Cl(2)	1.7153(17)		
C(14)-Cl(3)	1.7304(17)		

The packing diagrams for **L16** show that when viewed along the *c* axis they have a slight herringbone arrangement. An intramolecular hydrogen bonding interaction can be seen between N(1)-H(1N)...O(1) and an intermolecular interaction between C(13)-Cl(1)...Cg(2) and C(5)-H(5)...O(1). These interactions and the packing diagram are presented in **Figure 2.18**, with D...A distances and torsion angles stated in **Table 2.10**.

Packing along the *b* axisPacking along the *c* axis**Figure 2.18** Intra-/Intermolecular interactions and packing diagram for **L16****Table 2.10** Bond lengths and torsions angles for **L16**

Interaction	Atoms	Bond Lengths and Angles
Intramolecular	N(1)-H(1N)...O(1)	2.6792(19) Å
Intermolecular	C(13)-Cl(2)...Cg(2)	4.8661 Å
	C(5)-H(5)...O(1)	3.473(2) Å
Torsion	Cg(1)-Centre	45.42°
	Centre-Cg(2)	59.40°

2.6.6 X-ray Characterisation of C₁₈H₁₈NO (L19)

Brown crystals of **L19** suitable for X-ray crystallographic analysis were obtained by slow evaporation from hot ethanol over a period of 2-3 weeks. The molecular structure is given in **Figure 2.19**, and selected bond lengths and angles are stated in **Table 2.11**. Ligand **L19** was solved in a monoclinic cell and structural solution was performed in the space group $P2_1/n$, with a two molecules in the asymmetric unit.

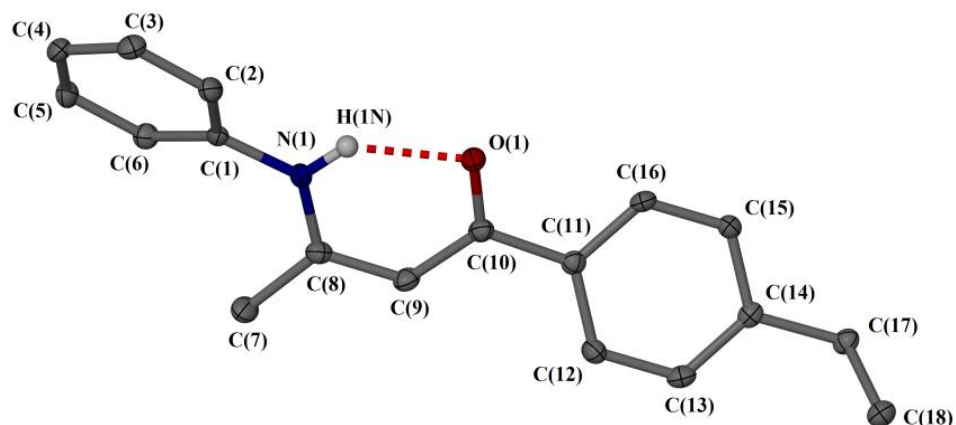


Figure 2.19 Molecular structure of **L19**, displacement ellipsoids are at the 50% probability level, hydrogen atoms and the second molecule are omitted for clarity.

Table 2.11 Selected bond lengths and angles for both molecules of **L19**

Bond	Distance (Å)	Bond	Angle (°)
C(1)-N(1)	1.4148(2)	C(1)-N(1)-C(8)	129.79(16)
N(1)-C(8)	1.3461(2)	N(1)-C(8)-C(9)	119.78(18)
C(7)-C(8)	1.4958(3)	C(8)-C(9)-C(10)	123.71(17)
C(8)-C(9)	1.3809(3)	O(1)-C(10)-C(9)	122.80(17)
C(9)-C(10)	1.4220(3)	O(1)-C(10)-C(11)	117.6(17)
O(1)-C(10)	1.2581(2)		
C(10)-C(11)	1.4970(3)		
Bond	Distance (Å)	Bond	Angle (°)
C(1)-N(1)	1.4104(2)	C(1)-N(1)-C(8)	131.97(16)
N(1)-C(8)	1.3505(2)	N(1)-C(8)-C(9)	119.83(17)
C(7)-C(8)	1.4941(3)	C(8)-C(9)-C(10)	124.36(17)
C(8)-C(9)	1.3729(3)	O(1)-C(10)-C(9)	122.58(16)
C(9)-C(10)	1.4288(3)	O(1)-C(10)-C(11)	118.11(17)
O(1)-C(10)	1.2503(2)		
C(10)-C(11)	1.4970(3)		

The packing diagram when viewed along both the b axis shows the molecules packing in a head-tail-tail-head arrangement within each plane of molecules. When viewed along the c axis the molecules pack in pairs and give a herringbone arrangement. Intramolecular interactions are seen between the N-H...O of both molecules, along with several intermolecular T-stacking interactions. The packing diagrams are presented in **Figure 2.20**, with D...A distances and torsion angles stated in **Table 2.12**.

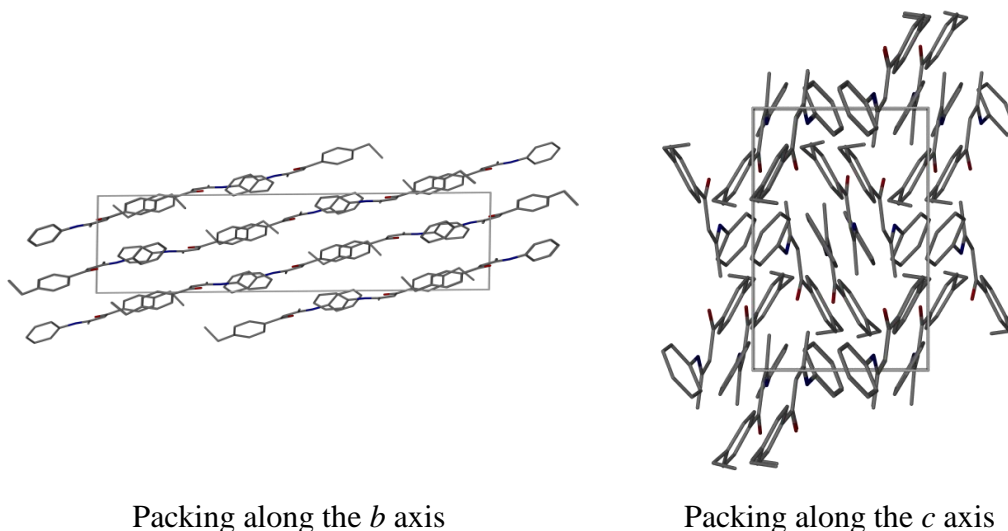


Figure 2.20 Packing diagrams of **L19** when viewed along the b and c axis

Table 2.12 Bond lengths and torsion angles for **L19**

Interaction	Atoms	Bond Lengths and Angles
Intramolecular	N(1)-H(1N)...O(1)	2.614(2) Å
	N(1')-H(1'N)...O(1')	2.6346(19) Å
Intermolecular	C(2')-H(2')...Cg(2)	3.6518 Å
	C(6)-H(6)...Cg(2)	3.7445 Å
	C(12)-H(12)...Cg(1)	3.6236 Å
	C(12')-H(12')...Cg(1)	3.6315 Å
	C(15)-H(15)...Cg3	3.6671 Å
	C(17')-H(17C)...Cg(3)	3.5166 Å
	C(18')-H(18A)...O(1)	3.386(2) Å
Torsion	Cg(1)-Centre	35.75°
	Centre-Cg(2)	23.36°
	Cg(3)-Centre'	25.37°
	Centre'-Cg(4)	24.43°

2.6.7 X-ray characterisation for C₁₈H₁₈NO₃ (L21)

Yellow fragments of **L21** suitable for X-ray crystallographic analysis were obtained by slow evaporation in hot ethanol over a period of several days. The molecular structure is given in **Figure 2.21**, and selected bond lengths and angles are stated in **Table 2.13**. Ligand **L21** was solved in a triclinic cell and structural solution was performed in the space group *P*1, with two molecules in the asymmetric unit.

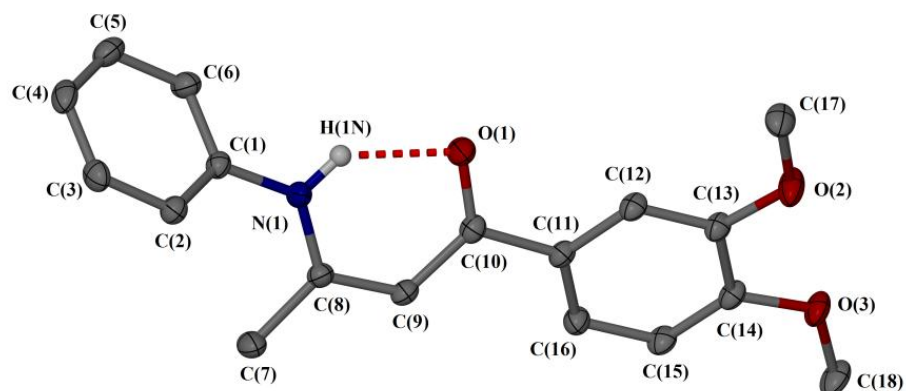
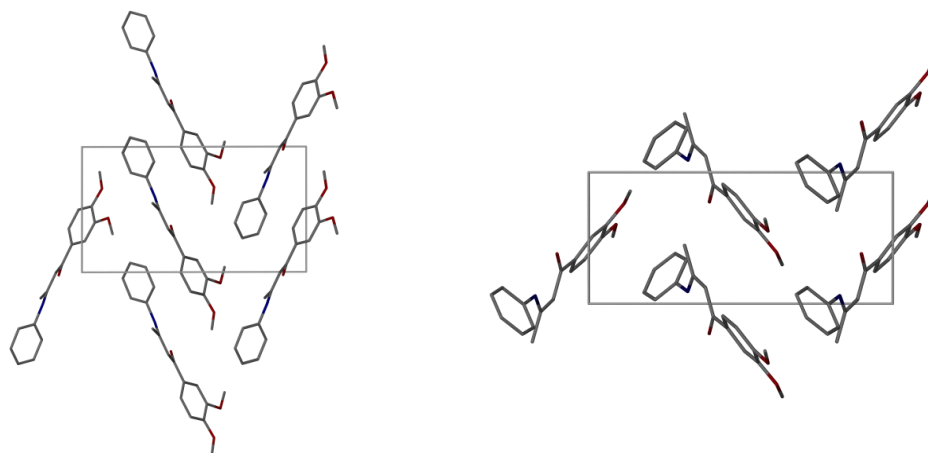


Figure 2.21 Molecular structure of **L21**, displacement ellipsoids are at the 50% probability level, the hydrogen atoms and second molecule are omitted for clarity.

Table 2.13 Selected bond lengths and angles for both molecules of **L21**

Bond	Distance (Å)	Bond	Angle (°)
C(1)-N(1)	1.431(3)	N(1)-C(8)-C(9)	120.1(2)
N(1)-C(8)	1.362(3)	C(8)-C(9)-C(10)	123.3(2)
C(7)-C(8)	1.511(4)	O(1)-C(10)-C(9)	122.7(2)
C(8)-C(9)	1.403(3)	O(1)-C(10)-C(11)	117.8(2)
C(9)-C(10)	1.439(4)		
O(1)-C(10)	1.271(3)		
C(10)-C(11)	1.515(3)		
Bond	Distance (Å)	Bond	Angle (°)
C(1')-N(1')	1.430(3)	N(1')-C(8')-C(9')	120.8(2)
N(1')-C(8')	1.361(3)	C(8')-C(9')-C(10')	123.0(2)
C(7')-C(8')	1.526(4)	O(1')-C(10')-C(9')	122.2(3)
C(8')-C(9')	1.270(3)	O(1')-C(10')-C(11')	118.4(2)
C(9')-C(10')	1.449(4)		
O(1')-C(10')	1.390(4)		
C(10')-C(11')	1.503(4)		

The packing diagrams when viewed along the both the *a* and *b* axis show there is a herringbone arrangement. Intramolecular hydrogen bonding interactions can be seen between N(1)-H(1)...O(1), the packing also has a large number of intermolecular interactions, all contributing to the packing of these molecules. The packing diagrams are presented in **Figure 2.22**, with D...A distances and torsion angles stated in **Table 2.14**.

Packing diagram along the a axisPacking along the b axis**Figure 2.22** Packing diagrams of **L21** when viewed along the a and b axes**Table 2.14** Bond lengths and torsion angles for both molecules of **L21**

Interaction	Atoms	Bond Lengths and Angles
Intramolecular	N(1)-H(1N)...O(1)	2.642(3) Å
	N(1')-H(1N')...O(1')	2.633(3) Å
Intermolecular	C(2)-H(2)...Cg(2)	3.639 Å
	C(2')-H(2')...Cg(4)	3.635 Å
	C(12)-H(12)...Cg(1)	3.605 Å
	C(12')-H(12')...Cg(3)	3.614 Å
	C(17)-H(17A)...Cg(3)	3.585 Å
	C(17)-H(17D)...Cg(1)	3.573 Å
	C(7)-H(7B)...O(1)	3.310(4) Å
	C(7')-H(7'B)...O(1')	3.300(4) Å
	C(6)-H(6)...O(2')	3.324(4) Å
	C(6')-H(6')...O(2)	3.319(4) Å
	C(6)-H(6)...O(3')	3.407(4) Å
	C(6')-H(6')...O(3)	3.411(4) Å
	C(17)-H(17C)...O(1)	3.332(4) Å
	C(17')-H(17'C)...O(1')	3.346(4) Å
Torsion	Cg(1)-Centre	48.92°
	Centre-Cg(2)	27.30°
	Cg(3) Centre'	49.14°
	Centre'-Cg(4)	27.23°

2.6.8 X-ray Characterisation of C₁₈H₁₈FNO₂ (L22)

Yellow crystals of compound **L22** suitable for X-ray crystallographic analysis were obtained by slow evaporation in hot ethanol over a period of 2-3 weeks. The molecular structure is given in **Figure 2.23**, and selected bond lengths and angles are stated in **Table 2.15**. Ligand **L22** was solved in a triclinic cell and structural solution was performed in the space group $P\bar{1}$, with two molecules in the asymmetric unit.

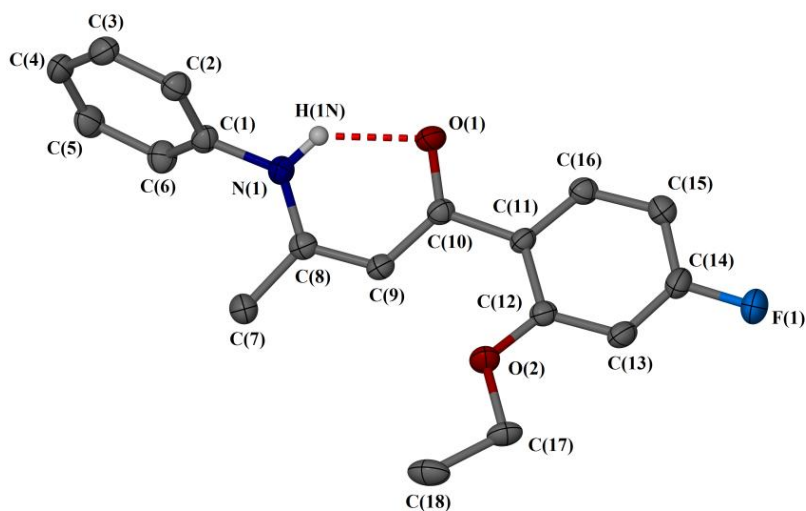
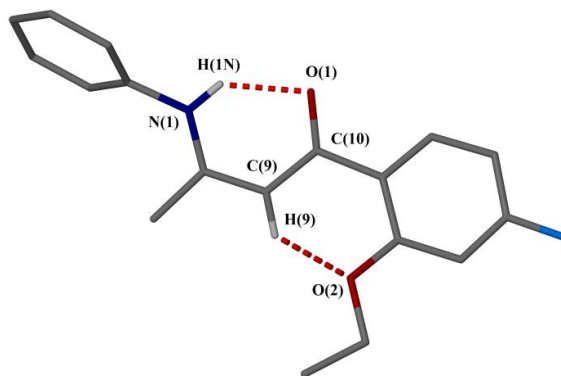


Figure 2.23 Molecular structure of **L22**, displacement ellipsoids are at the 50% probability level. Hydrogen atoms omitted for clarity.

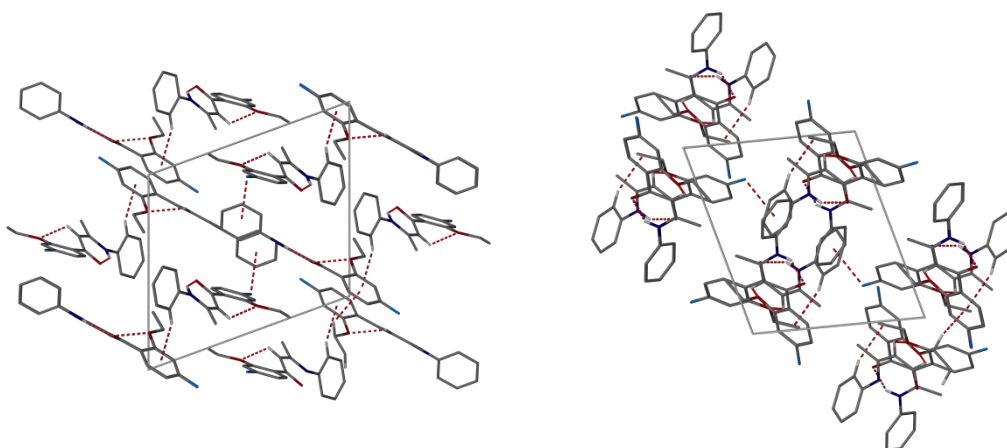
Table 2.15 Selected bond lengths and angles for both molecules of **L22**

Bond	Distance (Å)	Bond	Angle (°)
C(1)-N(1)	1.431(3)	N(1)-C(8)-C(9)	121.1(2)
N(1)-C(8)	1.346(4)	C(8)-C(9)-C(10)	123.5(3)
C(7)-C(8)	1.501(4)	O(1)-C(10)-C(9)	123.4(2)
C(8)-C(9)	1.394(4)	O(1)-C(10)-C(11)	117.1(2)
C(9)-C(10)	1.427(4)		
O(1)-C(10)	1.258(3)		
C(10)-C(11)	1.509(4)		
Bond	Distance (Å)	Bond	Angle (°)
C(1')-N(1')	1.430(4)	N(1')-C(8')-C(9')	120.9(3)
N(1')-C(8')	1.350(4)	C(8')-C(9')-C(10')	123.2(3)
C(7')-C(8')	1.514(5)	O(1')-C(10')-C(9')	122.8(3)
C(8')-C(9')	1.388(4)	O(1')-C(10')-C(11')	116.4(3)
C(9')-C(10')	1.425(5)		
O(1')-C(10')	1.264(4)		
C(10')-C(11')	1.513(4)		

When viewed along the *a* axis the molecules pack in pairs with a tail-head-head-tail arrangement and alternate in each row. Intramolecular hydrogen bonding is seen between N(1)-H(1N)...O(1) and C(9)-H(9)...O(2) of both molecules. There are observable intermolecular T-stacking interactions between C(2')-H(2')...Cg(2), C(17)-H(17B)...Cg(2) and C(14')-F(1')...Cg(1). The interactions and packing diagrams are presented in **Figure 2.24**, with D...A distance and torsion angles stated in **Table 2.16**.



Intramolecular interactions N(1)-H(1N)...O(1) and C(9)-H(9)...O(2)

Intermolecular interactions along the *c* axisIntermolecular interactions along the *a* axis**Figure 2.24** Intra-/Intermolecular packing along the *a* and *c* axes for **L22****Table 2.16** Bond lengths and torsion angles for **L22**

Interaction	Atoms	Bond Lengths and Angles
Intramolecular	N(1)-H(1N)...O(1)	2.667(3) Å
	N(1')-H(1N')...O(1')	2.632(5) Å
	C(9)-H(9)...O(2)	2.852(3) Å
	C(9')-H(9')...O(2')	2.867(4) Å
Intermolecular	C(2')-H(2')...Cg(2)	3.758 Å
	C(17)-H(17B)...Cg(2)	3.618 Å
	C(14')-F(1')...Cg(1)	4.423 Å
Torsion	Cg(1)-Centre	54.31°
	Centre-Cg(2)	28.91°

2.6.9 X-ray Characterisation for C₁₇H₁₅NO₃ (L24)

Green crystals of **L24** suitable for X-ray crystallographic analysis were obtained by slow evaporation from hot ethanol over a period of 2 weeks and further washing with diethyl ether. The molecular structure is given in **Figure 2.25**, selected bond lengths and angles are stated in **Table 2.17**. Ligand **L24** was solved in a monoclinic cell and structural solution was performed in the space group $P2_1$, with a single molecule in the asymmetric unit.

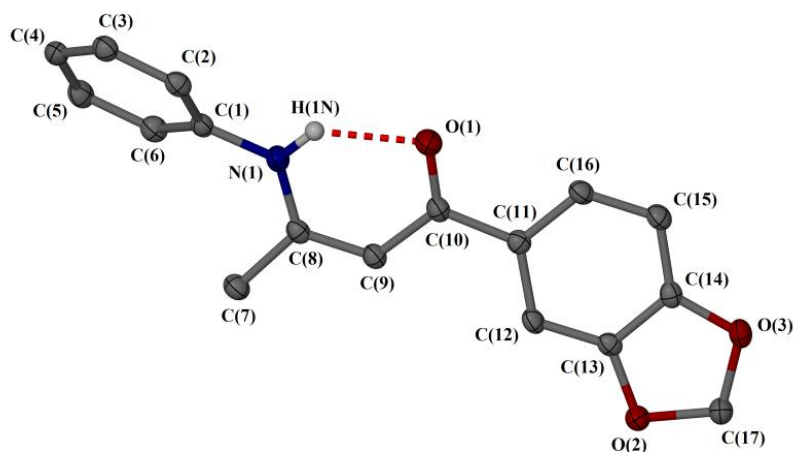
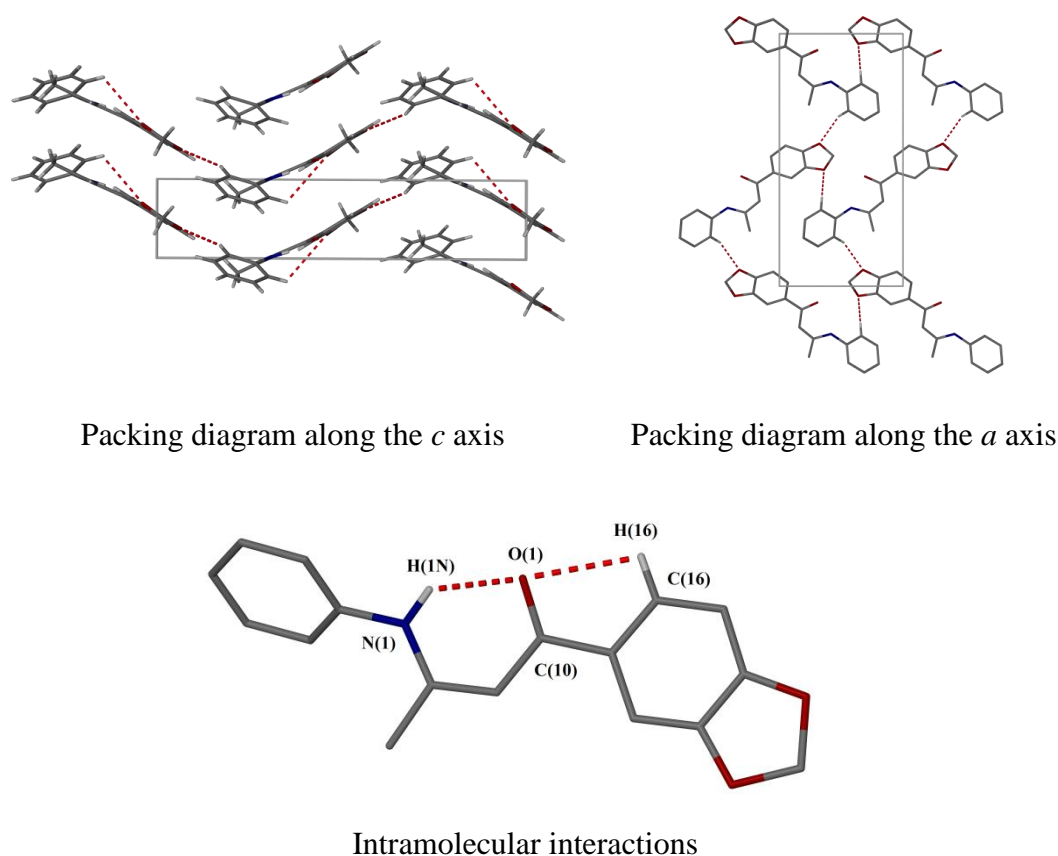


Figure 2.25 Molecular structure of **L24**, displacement ellipsoids are at the 50% probability level and hydrogen atoms omitted for clarity.

Table 2.17 Selected bond lengths and angles of **L24**

Bond	Distance (Å)	Bond	Angle (°)
C(1)-N(1)	1.433(2)	C(6)-C(1)-N(1)	118.17(17)
N(1)-C(8)	1.361(3)	C(2)-C(1)-N(1)	121.7(2)
C(7)-C(8)	1.515(3)	N(1)-C(8)-C(9)	121.60(18)
C(8)-C(9)	1.389(3)	C(8)-C(9)-C(10)	124.02(19)
C(9)-C(10)	1.452(3)	O(1)-C(10)-C(9)	122.34(19)
O(1)-C(10)	1.259(2)	O(1)-C(10)-C(11)	119.02(17)
C(10)-C(11)	1.509(3)	C(10)-C(11)-C(12)	118.34(17)
		C(10)-C(11)-C(17)	122.14(17)

The packing diagram shows that when viewed along both the *a* and *c* axes the molecules pack in a herringbone arrangement. Intramolecular hydrogen bonding can be seen between N(1)-H(1N)...O(1) and C(16)-H(16)...O(1). Intermolecular hydrogen bonding interactions are seen between the molecules within the same plane and also between different planes of molecules. The interactions and packing diagrams are presented in **Figure 2.26**, with a D...A distances and torsion angles stated in **Table 2.18**.

**Figure 2.26** Interactions and packing diagrams of **L24****Table 2.18** Bond lengths and torsion angles of **L24**

Interaction	Atoms	Bond Lengths and Angles
Intramolecular	N(1)-H(1N)...O(1)	2.693(2) Å
	C(16)-H(16)...O(1)	2.798(3) Å
Intermolecular	C(2)-H(2)...O(2)	3.486(3) Å
	C(6)-H(6)...O(3)	3.491(3) Å
Torsion	Cg(1)-Centre	44.39°
	Centre-Cg(2)	10.00°

2.6.10 X-ray Characterisation of C₁₉H₁₇N₃O (L25)

Green crystals of ligand **L25** suitable for X-ray crystallographic analysis were obtained by slow evaporation from hot ethanol over a period of 2-3 weeks and further washing with diethyl ether. Molecular structure is given in **Figure 2.27**, selected bond lengths and angles are stated in **Table 2.19**. Ligand **L25** was solved in a monoclinic cell and structural solution was performed in the space group $P2_1$, with a single molecule in the asymmetric unit.

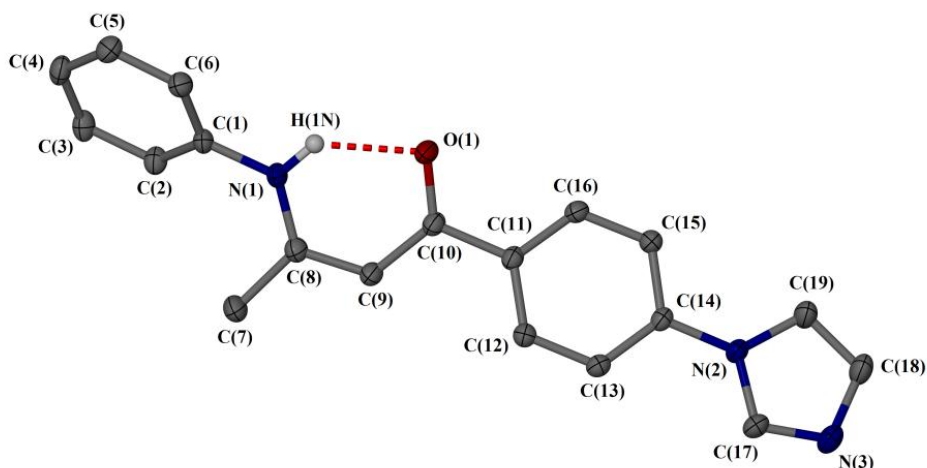


Figure 2.27 Molecular structure of **L25**, displacement ellipsoids are at the 50% probability level and hydrogen atoms omitted for clarity.

Table 2.19 Selected bond lengths and angles of **L25**

Bond	Distance (Å)	Bond	Angle (°)
C(1)-N(1)	1.4420(13)	N(1)-C(8)-C(9)	121.36(10)
N(1)-C(8)	1.3567(14)	C(8)-C(9)-C(10)	124.18(10)
C(7)-C(8)	1.5179(16)	O(1)-C(10)-C(9)	123.27(10)
C(8)-C(9)	1.4048(15)	O(1)-C(10)-C(11)	118.39(9)
C(9)-C(10)	1.4401(15)		
O(1)-C(10)	1.2772(13)		
C(10)-C(11)	1.5178(14)		

The packing diagrams show the molecules pack in pairs with intermolecular interactions between each plane of molecules. Also when viewed along the c axis the molecules pack in a herringbone arrangement. An intramolecular hydrogen bonding interaction is observed between N(1)-H(1N)...O(1) and an intermolecular hydrogen bonding interaction between C(17)-H(17)...O(1). The packing diagrams are present in **Figure 2.28**, with D...A distances and torsion angles are stated in **Table 2.20**.

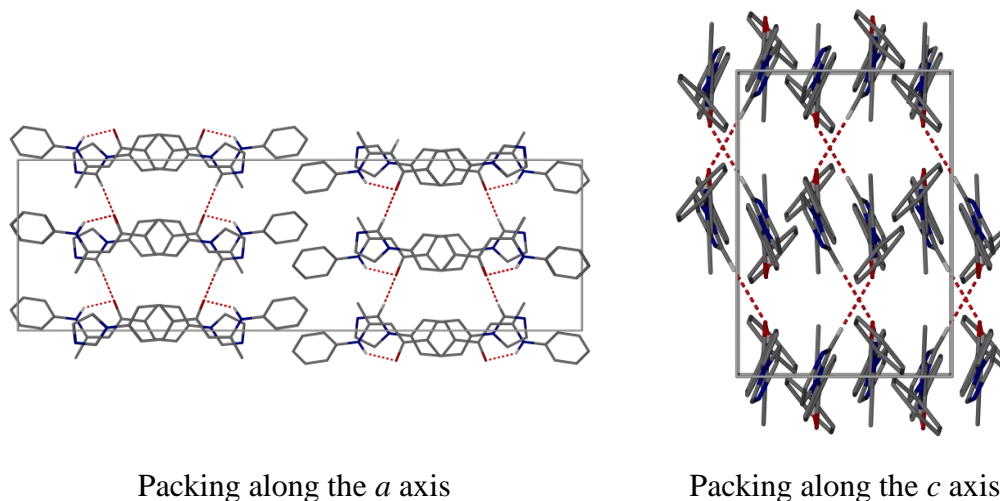


Figure 2.28 Interactions and packing diagram of **L25**

Table 2.20 Bond lengths and torsion angles of **L25**

Interaction	Atoms	Bond Lengths and Angles
Intramolecular	N(1)-H(1N)...O(1)	2.7179(11) Å
Intermolecular	C(17)-H(17)...O(1)	3.2994(14) Å
Torsion	Cg(1)-Centre	44.95°
	Centre-Cg(2)	23.24°

2.7 Conclusions

A range of novel mono-aryl and biaryl β -diketonate and β -ketoiminate ligands have been synthesised and fully characterised, including X-ray crystallography data for several of the β -ketoiminate ligands. All ligands show similar ^1H and $^{13}\text{C}\{^1\text{H}\}$ NMR spectra with a distinctive methine proton that is characteristic of ligand formation. The ligands were obtained as single crystals, with structural solutions performed in a monoclinic (**L11**, **L12**, **L14**, **L16**, **L19**, **L24** and **L25**), orthorhombic (**L15**) or triclinic (**L21** and **L22**) space groups. All ligands show an intramolecular hydrogen bonding interaction between N-H...O which holds the centre of the molecule in a planar orientation. The tables of torsion angles show that both the aniline and aromatic rings are bent out of this plane, with the size of the torsion angle depending on the nature and electronics of the aromatic substituents. A range of compounds were synthesised to include different electronic and steric properties in order to gain structure activity relationships upon complexations; these complexes are presented in Chapters 3, 5 and 8.

2.8 References

1. J. J. Mannion, Ph.D Thesis, University of Leeds, 2008.
2. B. D. Crossley, Ph.D Thesis, University of Leeds, 2011.
3. J. J. Hollick, B. T. Golding, I. R. Hardcastle, N. Martin, C. Richardson, L. J. M. Rigoreau, G. C. M. Smith and R. J. Griffin, *Bioorg. Med. Chem. Lett.*, 2003, **13**, 3083-3086.
4. R. Levine and J. K. Sneed, *J. Am. Chem. Soc.*, 1951, **73**, 5614-5616.
5. A. J. Hebden, Ph.D Thesis, University of Leeds, 2010.
6. L.-M. Tang, Y.-Q. Duan, X.-F. Li and Y.-S. Li, *J. Organomet. Chem.*, 2006, **691**, 2023.

Chapter 3

Synthesis and Characterisation of Functionalised β - Ketoiminate Ruthenium (II) Chloride Complexes

3 Ruthenium Arene Complexes

The work within this chapter builds on the libraries of ruthenium compounds with (*N,N*), (*N,O*) and (*O,O*) chelating ligands. This area has been extensively studied by the Sadler, Keppler and Dyson research groups. Sadler *et al.* first reported the cationic ruthenium arene complexes (**Figure 3.1**) incorporating neutral ethylenediamine (*N,N*) chelating ligands, along with a range of derivatives containing different Ru-halides and different arene substituents (**A-C**).¹ Cytotoxic values were all comparable to cisplatin against A2780 (human ovarian carcinomas), with the most hydrophobic arene substituent (**C**) giving the most promising results. It was observed that rates of hydrolysis were independent of ionic strength but proportional to the size of the arene substituent.¹ Sadler has also investigated the interactions with DNA models and found that these ruthenium ethylenediamine compounds preferentially bind to the N7 position of guanine; this has been studied by solid state X-ray crystallography and in solution by 2D NMR, with all studies confirming this preferential binding.² A range of ruthenium (*N,O*) and (*O,O*) chelating compounds (**D-F**), all showing moderate cytotoxicity and again preferential binding to the N7 position of guanine (**Figure 3.1**).³

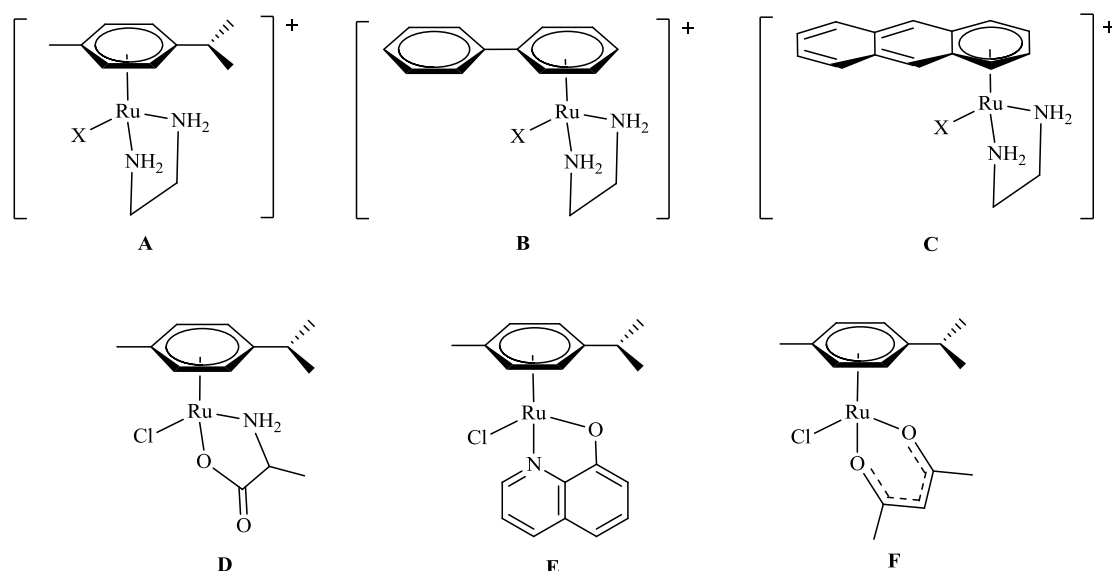


Figure 3.1 Compounds previously synthesised by Sadler *et al.*

Dyson *et al.* have carried out extensive work in this area, with particular interest in multinuclear ruthenium arene clusters and their ability to form host-guest type structures. The water-soluble metallaprism cages were shown to deliver the

hydrophobic dendrimer guest to the cells, with noticeably increased cytotoxicity for the host-guest molecules against A2780 (human ovarian carcinomas) and A2780cis (cisplatin resistant human ovarian carcinomas), when compared to the empty host molecule.^{4, 5} They have also carried out studies using hexa-osmium cages (**Figure 3.2**) and their delivery systems compare favourably with the ruthenium arene analogues.⁶

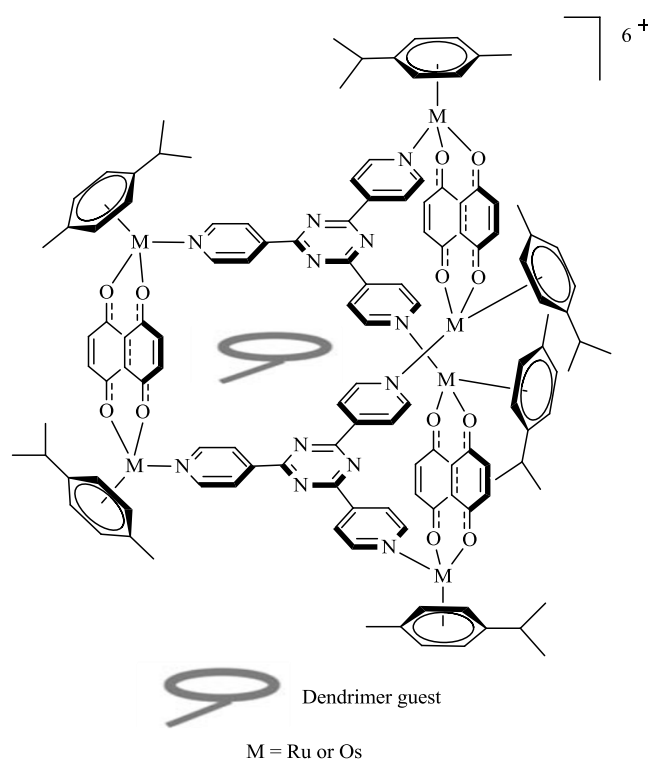


Figure 3.2 Ruthenium and osmium host-guest molecules synthesised by Dyson *et al.*

Keppler *et al.* have coupled known enzyme inhibitors (**G**),^{7, 8} pain relief molecules (**H**)⁹ and antibacterial agents (**I**)^{10, 11} (**Figure 3.3**) to ruthenium/osmium arenes and carried out extensive research into their antiproliferative activities, apoptosis, cell cycling kinetics and measured DNA shrinkage using AFM measurements.

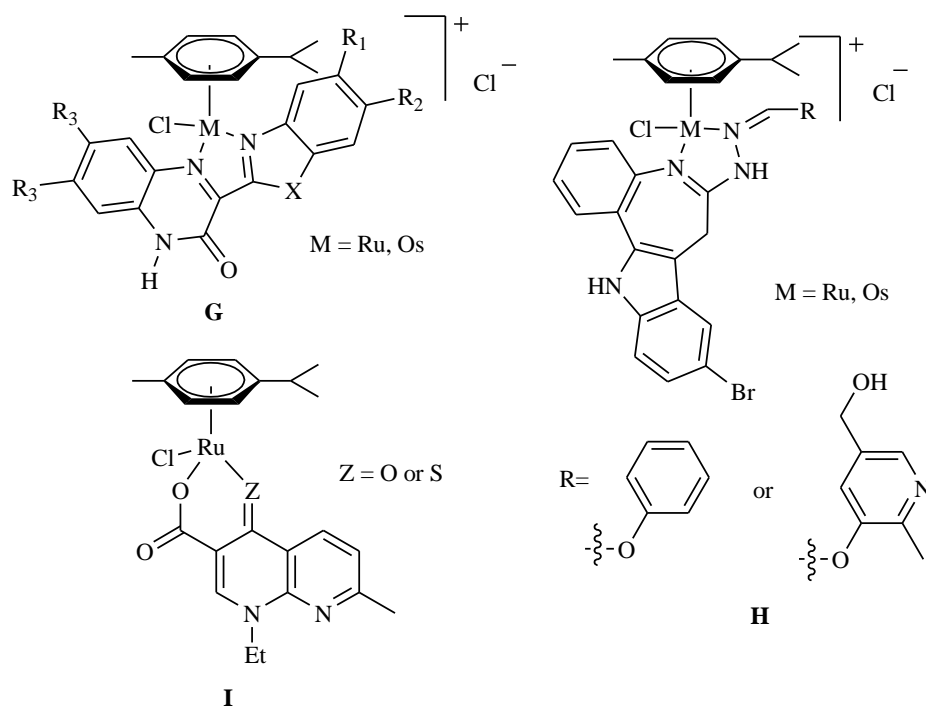


Figure 3.3 Ruthenium and osmium compounds synthesised by Keppler *et al.*

The McGowan research group has since carried out work on ruthenium arenes incorporating picolinamide and quinaldamide ligands (**Figure 3.4**), which show high cytotoxicity and significant binding to 9-EtG. Results showed a reversible inter-conversion in the binding of these ligands, either (*N,N*) or (*N,O*); the differences in cytotoxicity showed potential in tuning the ligands for biological application^{12, 13}

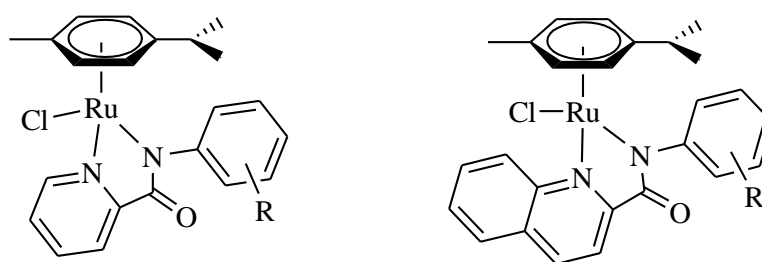


Figure 3.4 Picolinamide and quinaldamide compounds by McGowan *et al.*

Since these results, the group started work into incorporating β -ketoiminate (*N,O*) ligands and has since produced a library of compounds stated within this chapter. Cell line testing against a range of human carcinomas has been completed and biological evaluations into the modes of action will be discussed in chapters 4-6. In addition work was published on an iridium(III) Cp* analogue incorporating a β -ketoiminate ligand that has also been synthesised, along with a small library of

(*N,N*), (*N,O*) and (*O,O*) iridium compounds, with cell line data being compared to that of complex **1** (see synthesis within this Chapter). These showed a trend in binding mode, whereby the activity followed the trend *N,O* > *O,O* > *N,N* (**Figure 3.5**).^{14,15}

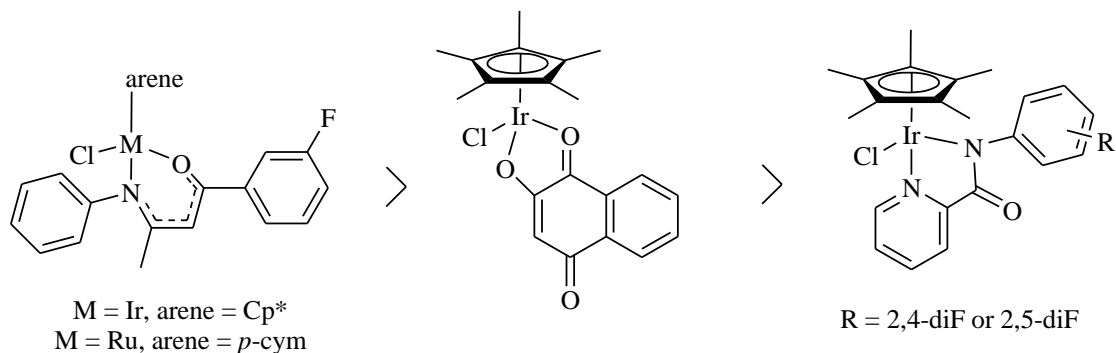
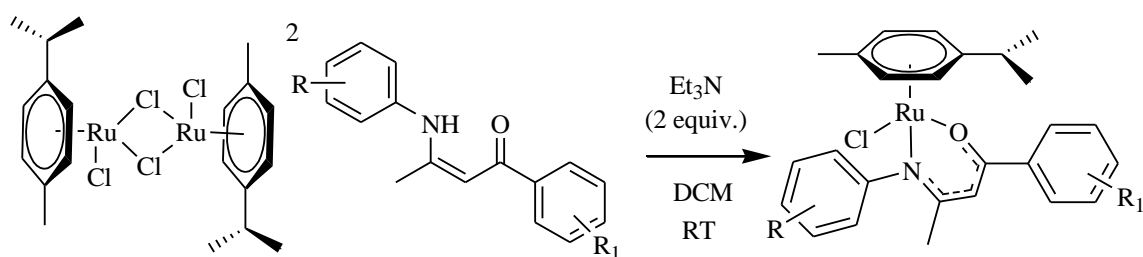


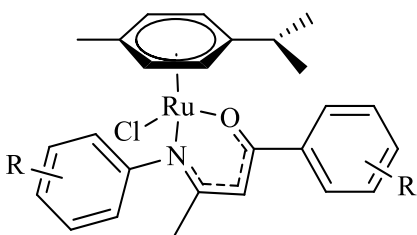
Figure 3.5 List of complexes previously synthesised by McGowan *et al.*

3.1 Ruthenium (II) Chloride Complexes

All β -ketoiminate ruthenium complexes were prepared according to **Scheme 3.1**, by reacting two equivalents of a functionalised β -ketoiminate ligand, two equivalents of triethylamine and [*p*-cymRuCl₂]₂ in dichloromethane overnight at room temperature, followed by recrystallisation by slow evaporation from a methanolic solution.



Scheme 3.1 General synthetic pathway for ruthenium(II) arene compounds



R ₁ = 3'-F	R = H	1	R ₁ = 4'-Br	R = H	8
R ₁ = 4'-F	R = H	2	R ₁ = 4'-I	R = H	9
R ₁ = 4'-Cl	R = H	3	R ₁ = 4'-OEt	R = H	10
R ₁ = 2',4'-diCl	R = H	4	R ₁ = 4'-Me	R = H	11
R ₁ = 2',5'-diCl	R = H	5	R ₁ = 3'-naphthyl	R = H	12
R ₁ = 2',3',4'-triCl	R = H	6	R ₁ = 4'-F	R = 2',4'-diF	13
R ₁ = 3'-Br	R = H	7			

Figure 3.6 List of complexes synthesised within this Chapter

Complexes **1-13** (**Figure 3.6**) were synthesised and characterised by the author, with full experimental data described in Chapter 9. All of the compounds were obtained as analytically pure solids and have been characterised by ¹H NMR, ¹H-¹H COSY, ¹³C{¹H}NMR, ¹H-¹³C{¹H} HMQC spectroscopy, mass spectrometry and micro-analysis. In addition X-ray crystallographic data has been obtained for all complexes.

3.2 NMR Data for Ruthenium(II) Chloride Complexes

The ¹H NMR spectra for [*p*-cymRuCl₂]₂ shows the aromatic *p*-cymene protons (**c**, **d**, **f** and **g**, **Figure 3.7**) as two doublets at 5.35 and 5.48 ppm for two protons each. Upon complexation to a β-ketoiminato ligand they separate into four broad doublets ranging from 3.68-5.35 ppm, each peak one proton each (shown for compound **7** in **Figure 3.8**). The chemical shifts for **l-n** and **t-v** remain within the same range as the starting ligand but are frequently seen in a different order, their chemical shift ranges depending on the substituent R. The characteristic shift for complexation is seen when monitoring proton **q**, which is shifted upfield upon complexation. In the case of compound **C7**, proton **q** is a singlet at 5.84 ppm in the free ligand and it shifts upfield to 5.36 ppm upon complexation. Also the *p*-cymene proton **h**, which appears as a broad septet, usually shows a significant upfield chemical shift from 2.93 ppm to 2.67 ppm upon complexation. The broad singlet at around 13 ppm seen for the NH in the free ligand disappears indicating the reaction has gone to completion.

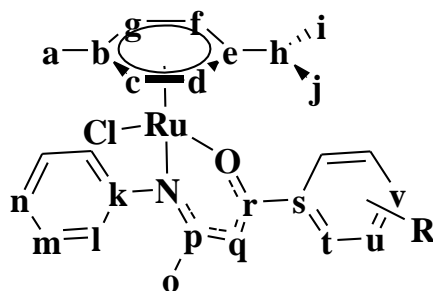


Figure 3.7 General ruthenium(II) β -ketoiminato structure

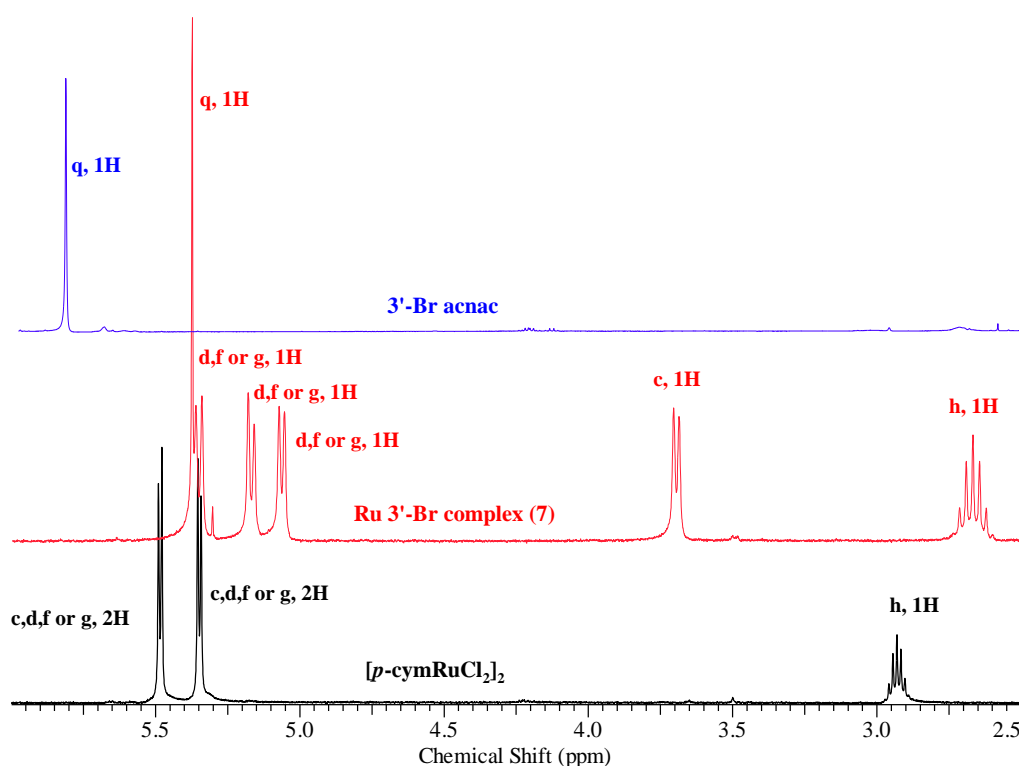


Figure 3.8 ^1H NMR for $[p\text{-cymRuCl}_2]_2$ (black), free ligand (blue) and complex **7** (red) (CDCl_3 , 300 MHz, 300K)

When analysing the $^{13}\text{C}\{^1\text{H}\}$ NMR spectra for the β -ketoiminato complexes, they have similar trends with the highest shifts seen for the quaternary carbons **p** and **r** which are typically in the range 170-190 ppm. All CH peaks for the β -ketoiminato ligand are in the range 100-150 ppm. The aromatic *p*-cymene quaternary carbons (**b** and **e**) have higher chemical shifts of 96-102 ppm, whilst the CH carbons (**c**, **d**, **f** and **g**) are between 78-90 ppm. The methine CH (**q**) from the β -ketoiminato ligand is also within this range and typically seen at 93-95 ppm. The remaining carbon atoms have low chemical shifts between 18-31 ppm.

3.3 X-ray Crystallography for Ruthenium (II) Chloride Complexes

X-ray crystallographic data was analysed for complexes **1-13** and all crystals were obtained using slow evaporation from a methanolic solution, appearing as orange/red single crystals. Solutions were performed in either a monoclinic *Cc* (**4** and **7**) or triclinic $P\bar{1}$ (**1-3**, **5**, **6** and **8-13**) space groups. All of the angles around the metal centre show the geometry expected for *pseudo* octahedral compounds which is common for half-sandwich “piano-stool” structures. The angles between the N-Ru-O, N-Ru-Cl and O-Ru-Cl are expected to be 90° and complexes here show angles ranging between 83-90°. The smaller angles can be explained due to the restrictions caused by the bidentate ligand. The remaining three coordination sites are occupied by the bulky *p*-cymene ligand and when considering the restriction from the β -ketoiminate ligand the angles observed for Cg-Ru-Cl, Cg-Ru-N and Cg-Ru-O are within the range 124-133°.

When comparing the ruthenium β -ketoiminate complexes, intramolecular interactions are typically seen between a *p*-cymene C-H and either the centroid of the aniline ring or the Ru-Cl bond. This is thought to correspond to the upfield shift seen for one of the *p*-cymene C-H protons upon analysis of the ^1H NMR spectra. The intramolecular T-stacking interactions can be seen in compounds **1**, **2**, **4-7**, **10**, **12** and **13**, with D...A distances ranging between 3.4-3.6 Å. However, complexes **3**, **8** and **11** have the *p*-cymene ligand rotated away from the aniline ring and D...A distances are too large to be considered as a T-stacking interaction. This is due to an additional intramolecular hydrogen interaction between the methyl group of the *p*-cymene and the chloride of the Ru-Cl bond, causing restricted rotation of the *p*-cymene ligand.

3.3.1 X-ray Characterisation for $\text{C}_{26}\text{H}_{27}\text{ClFNORu}$ (**1**)

Red fragments of **1** suitable for X-ray crystallographic analysis were obtained using slow evaporation from a methanolic solution over a period of several days. The molecular structure is shown in **Figure 3.9** and selected bond lengths and angles are stated in **Table 3.1**. Complex **1** crystallised in a triclinic cell and structural solution was performed in the space group $P\bar{1}$, with a single molecule in the asymmetric unit.

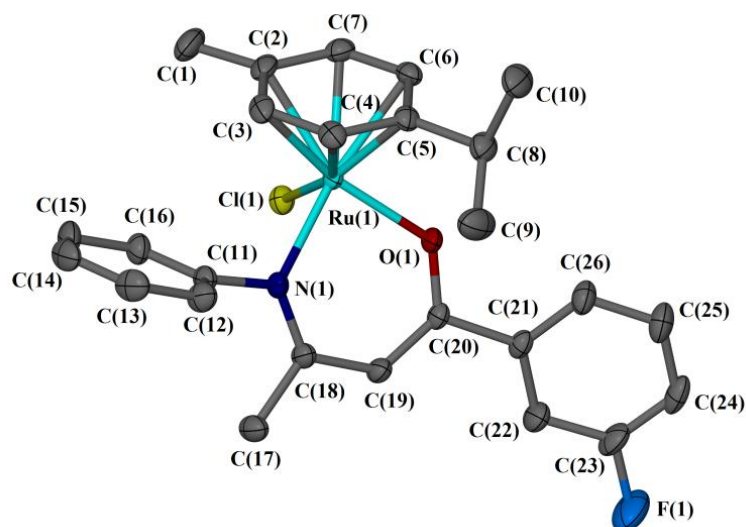
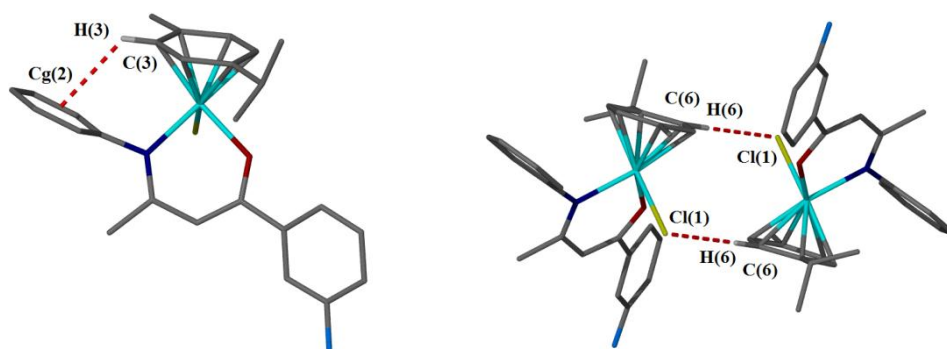


Figure 3.9 Molecular structure of **1**, displacement ellipsoids are at the 50% probability level and hydrogen atoms are omitted for clarity.

Table 3.1 Selected bond lengths and angles for **1**

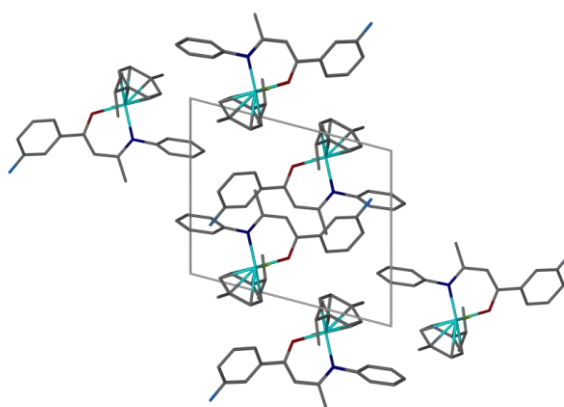
Bond	Distance (Å)	Bond	Angle (°)
Ru(1)-N(1)	2.0870(17)	N(1)-Ru(1)-O(1)	88.40(6)
Ru(1)-O(1)	2.0683(13)	N(1)-Ru(1)-Cl(1)	83.65(5)
Ru(1)-Cl(1)	2.4384(6)	O(1)-Ru(1)-Cl(1)	87.14(4)
Ru(1)-Cg(3)	1.6673(8)	Cg(1)-Ru(1)-O(1)	124.22(5)
C(23)-F(1)	1.340(3)	Cg(1)-Ru(1)-N(1)	131.97(5)
		Cg(1)-Ru(1)-Cl(1)	127.07(3)

The packing diagram for complex **1** shows the molecules pack in pairs about a centre of inversion, in alternating rows, with evidence of intermolecular hydrogen bonding between these pairs of molecules. There is also a suggested intramolecular T-stacking interaction between the *p*-cymene H(3) and aniline centroid Cg(3). These interactions and packing diagram are presented in **Figure 3.10**, with D...A distance and torsion angles stated in **Table 3.2**.



Intramolecular
C(3)-H(3)...Cg(1)

Intermolecular
C(6)-H(6)...Cl(1)



Packing diagram when viewed along the *a* axis

Figure 3.10 Interactions and packing diagram for **1**

Table 3.2 Bond lengths and torsion angles for **1**

Interaction	Atoms	Bond Lengths and Angles
Intramolecular	C(3)-H(3)...Cg(2)	3.458 Å
Intermolecular	C(6)-H(6)...Cl(1)	3.622(2) Å
Torsion	Cg(2)-Centre	77.28°
	Centre-Cg(3)	29.31°

3.3.2 X-ray Characterisation for C₂₆H₂₇ClFNORu (2)

Red fragments of **2** suitable for X-ray crystallographic analysis were obtained using slow evaporation from a methanolic solution over a period of several days. The molecular structure is shown in **Figure 3.11** and selected bond lengths and angles are stated in **Table 3.3**. Complex **2** crystallised in a triclinic cell and structural solution was performed in the space group $P\bar{1}$, with a single molecule in the asymmetric unit.

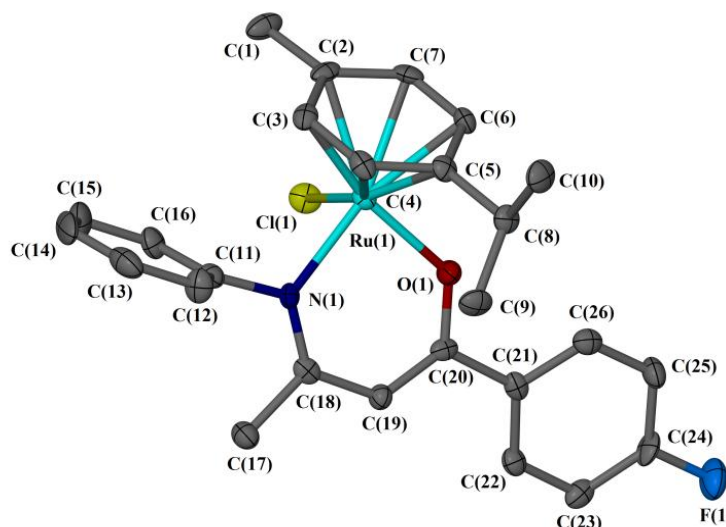


Figure 3.11 Molecular structure of **2**, displacement ellipsoids are at the 50% probability level and hydrogen atoms are omitted for clarity.

Table 3.3 Selected bond lengths and angles for **2**

Bond	Distance (Å)	Bond	Angle (°)
Ru(1)-N(1)	2.088(3)	N(1)-Ru(1)-O(1)	89.08(12)
Ru(1)-O(1)	2.059(3)	N(1)-Ru(1)-Cl(1)	83.86(11)
Ru(1)-Cl(1)	2.4362(13)	O(1)-Ru(1)-Cl(1)	85.01(9)
Ru(1)-Cg(1)	1.6680(19)	Cg(1)-Ru(1)-O(1)	124.71(11)
C(24)-F(1)		Cg(1)-Ru(1)-N(1)	130.90(12)
		Cg(1)-Ru(1)-Cl(1)	128.44(8)

The packing diagram for complex **2** shows the molecules pack in pairs about a centre of inversion, in alternating rows, with evidence of intermolecular hydrogen bonding between these pairs of molecules. There is also a suggested intramolecular T-stacking interaction between the *p*-cymene H(3) and aniline centroid Cg(2) and also between H(1A) and Cl(1). These interactions and packing diagram are

presented in **Figure 3.12**, with D...A distance and torsion angles stated in **Table 3.4**.

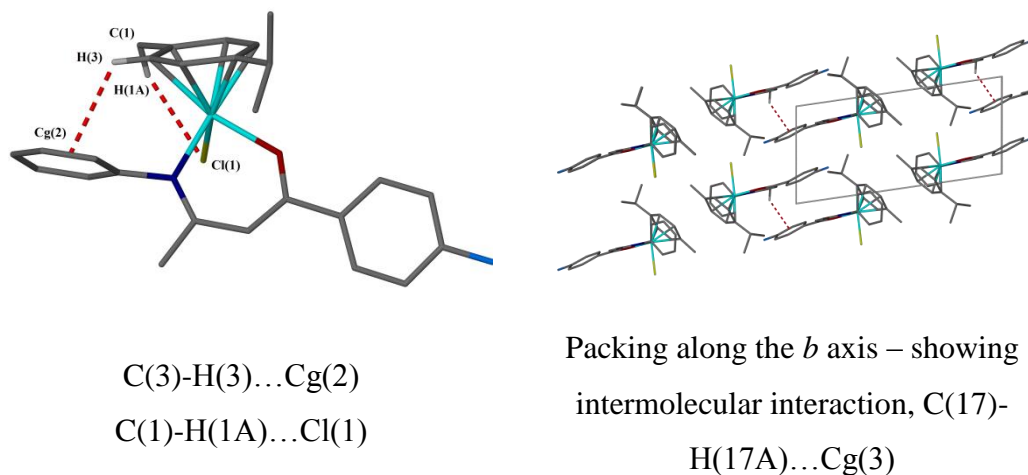


Figure 3.12 Interactions and packing diagram for **2**

Table 3.4 Bond lengths and torsion angles for **2**

Interaction	Atoms	Bond Lengths and Angles
Intramolecular	C(3)-H(3)...Cg(2)	3.571 Å
	C(1)-H(1A)...Cl(1)	3.437(5) Å
Intermolecular	C(17)-H(17A)...Cg(3)	3.590 Å
	Ru(1)-Cl(1)...Cg(1)	3.711 Å
	C(4)-H(4)...Cl(1)	3.505(5) Å
	C(8)-H(8)...F(1)	3.229(5) Å
Torsion	Cg(1)-centre	78.34°
	centre-Cg(2)	17.11°

3.3.3 X-ray Characterisation for C₂₆H₂₇Cl₂NORu (**3**)

Red fragments of **3** suitable for X-ray crystallographic analysis were obtained using slow evaporation from a methanolic solution over a period of three days. The molecular structure is shown in **Figure 3.13**, selected bond lengths and angles are stated in **Table 3.5**. Complex **3** crystallised in a triclinic cell and structural solution was performed in the space group $P\bar{1}$, with a single molecule in the asymmetric unit.

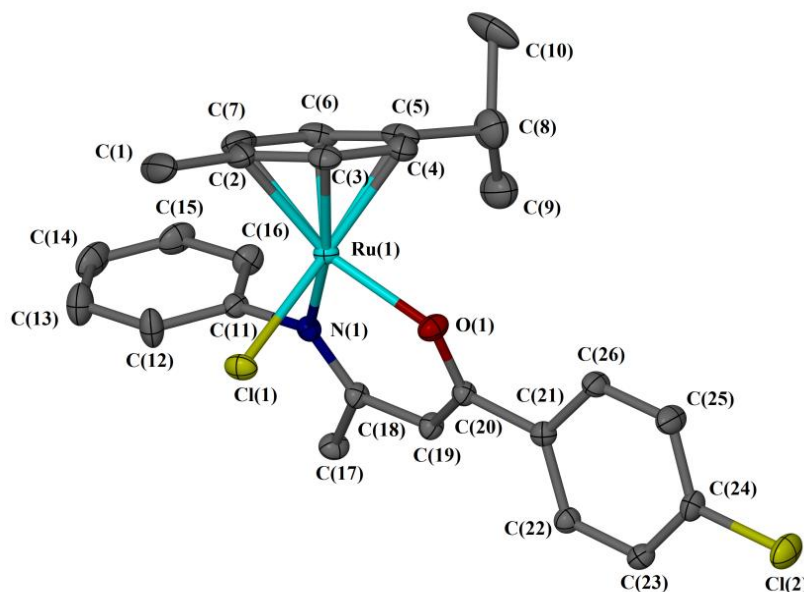
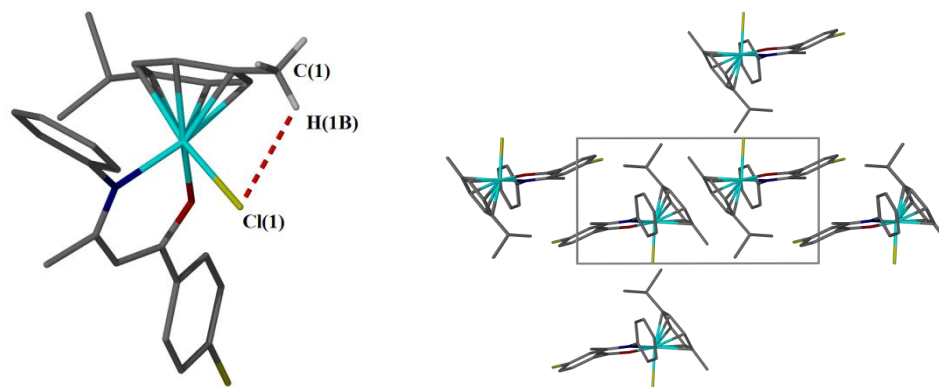


Figure 3.13 Molecular structure of **3**, displacement ellipsoids are at the 50% probability level and hydrogen atoms are omitted for clarity.

Table 3.5 Selected bond lengths and bond angles for **3**

Bond	Distance (Å)	Bond	Angle (°)
Ru(1)-N(1)	2.099(4)	N(1)-Ru(1)-O(1)	89.45(15)
Ru(1)-O(1)	2.068(3)	N(1)-Ru(1)-Cl(1)	84.03(12)
Ru(1)-Cl(1)	2.4513(13)	O(1)-Ru(1)-Cl(1)	84.90(11)
Ru(1)-Cg(1)	1.677(2)	Cg(1)-Ru(1)-O(1)	124.02(13)
C(24)-Cl(2)	1.755(4)	Cg(1)-Ru(1)-N(1)	130.73(14)
		Cg(1)-Ru(1)-Cl(1)	129.02(9)

The packing diagram for complex **3** shows the molecules pack in alternating rows, with no evidence of intermolecular interactions suggesting the packing of molecules is due to crystal packing interactions only. There is an intramolecular hydrogen bond between H(1B) and Cl(1), however, no T-stacking interaction is observed between the *p*-cymene and aniline ring. The intramolecular interaction and packing are presented in **Figure 3.14**, with the D...A distance and torsion angles stated in **Table 3.6**.



Intramolecular C(1)-H(1B)...Cl(1)

Packing along the *b* axis**Figure 3.14** Intramolecular interaction and packing diagram for **3****Table 3.6** Bond lengths and torsion angles for **3**

Interaction	Atoms	Bond Lengths and Angles
Intramolecular	C(1)-H(1B)...Cl(1)	3.393(7) Å
Torsion	Cg(2)-Centre	76.49°
	Centre-Cg(3)	24.36°

3.3.4 X-ray Characterisation for C₂₆H₂₆Cl₃NORu (**4**)

Red fragments of **4** suitable for X-ray crystallographic analysis were obtained by slow evaporation in methanol over a period of several days. The molecular structure is shown in **Figure 3.15** with selected bond lengths and angles stated in **Table 3.7**. Complex **4** crystallised in a monoclinic cell and structural solution was performed in the space group *Cc*, with a single molecule in the asymmetric unit.

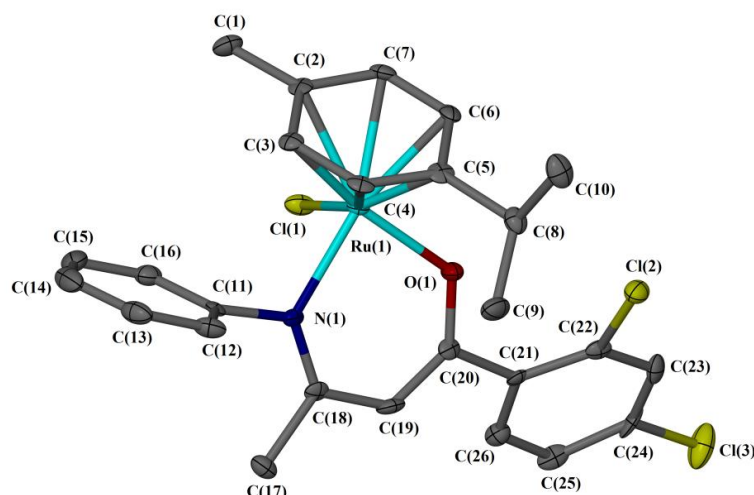
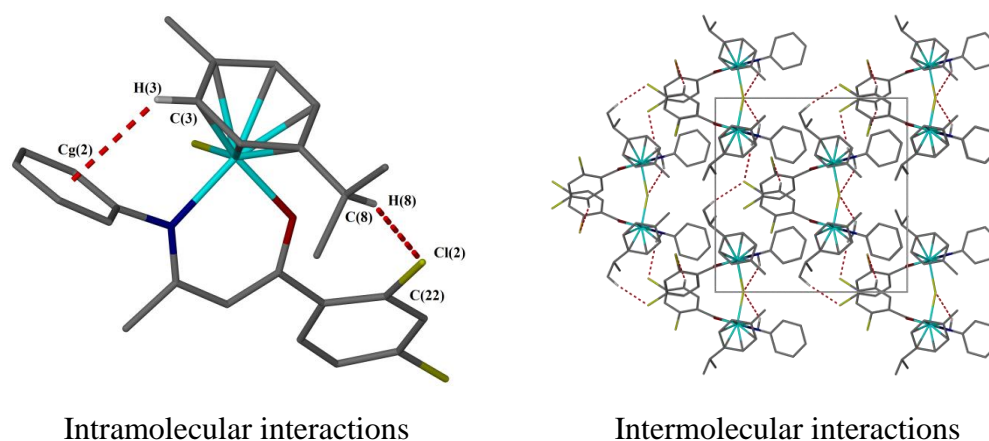


Figure 3.15 Molecular structure of **4**, displacement ellipsoids are at the 50% probability level and hydrogen atoms are omitted for clarity.

Table 3.7 Selected bond lengths and bond angles for **4**

Bond	Distance (Å)	Bond	Angle (°)
Ru(1)-N(1)	2.095(5)	N(1)-Ru(1)-O(1)	89.61(15)
Ru(1)-O(1)	2.077(3)	N(1)-Ru(1)-Cl(1)	85.74(12)
Ru(1)-Cl(1)	2.4314(12)	O(1)-Ru(1)-Cl(1)	82.74(9)
Ru(1)-Cg(1)	1.670(2)	Cg(1)-Ru(1)-O(1)	125.63(12)
C(22)-Cl(2)	1.745(5)	Cg(1)-Ru(1)-N(1)	129.19(14)
C(24)-Cl(3)	1.736(5)	Cg(1)-Ru(1)-Cl(1)	129.07(8)

The packing diagram for complex **4** shows the molecules pack in head-to-tail pairs, with intermolecular interactions between each pair and also holding together alternate rows of molecules. There are intramolecular hydrogen bonds between H(8)-Cl(2), and also an intramolecular T-stacking interaction is observed between the *p*-cymene H(3) and the aniline ring Cg(2). The intramolecular interactions and packing diagram are presented in **Figure 3.16**, with the D...A distance and torsion angles stated in **Table 3.8**.



Intramolecular interactions

Intermolecular interactions

Figure 3.16 Intramolecular interactions and packing diagram for **4****Table 3.8** Bond lengths and torsion angles for **4**

Interaction	Atoms	Bond Lengths and Angles
Intramolecular	C(3)-H(3)...Cg(2)	3.445 Å
	C(8)-H(8)...Cl(2)	3.695(6) Å
Intermolecular	Ru(1)-Cl(1)...Cg(1)	1.670 Å
	C(10)-H(10C)...Cl(3)	3.672(6) Å
	C(17)-H(17B)...Cl(3)	3.539(6) Å
	C(17)-H(17C)...Cl(1)	3.649(6) Å
	C(25)-H(25)...Cl(2)	3.670(5) Å
Torsion	Cg(2)-Centre	78.85°
	Centre-Cg(3)	41.28°

3.3.5 X-ray Characterisation for $C_{26}H_{26}Cl_3NORu$ (**5**)

Red fragments of **5** suitable for X-ray crystallographic analysis were obtained using slow evaporation from a methanolic solution over a period of several days. The molecular structure is shown in **Figure 3.17** with selected bond lengths and angles stated in **Table 3.9**. Complex **5** crystallised in a triclinic cell and structural solution was performed in the space group $P\bar{1}$, with two molecules in the asymmetric unit.

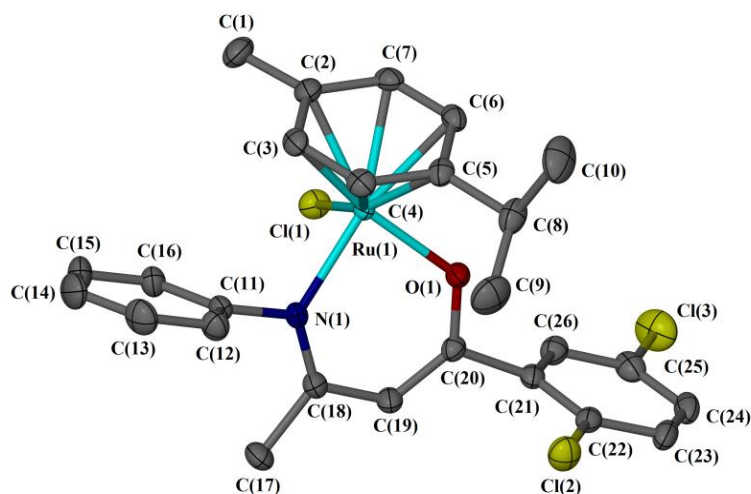


Figure 3.17 Molecular structure of **5**, displacement ellipsoids are at the 50% probability level. Hydrogen atoms and the second molecule are omitted for clarity

Table 3.9 Selected bond lengths and angles for both molecules of **5**

Bond	Distance (Å)	Bond	Angle (°)
Ru(1)-N(1)	2.1223(15)	N(1)-Ru(1)-O(1)	88.06(5)
Ru(1)-O(1)	2.0762(12)	N(1)-Ru(1)-Cl(1)	84.56(4)
Ru(1)-Cl(1)	2.4587(5)	O(1)-Ru(1)-Cl(1)	85.35(4)
Ru(1)-Cg(1)	1.6836(8)	Cg(1)-Ru(1)-O(1)	124.74(4)
C(22)-Cl(2)	1.7580(19)	Cg(1)-Ru(1)-N(1)	132.30(5)
C(25)-Cl(3)	1.756(2)	Cg(1)-Ru(1)-Cl(1)	126.88(3)
Bond	Distance (Å)	Bond	Angle (°)
Ru(1')-N(1')	2.1198(14)	N(1')-Ru(1')-O(1')	88.25(5)
Ru(1')-O(1')	2.0874(12)	N(1')-Ru(1')-Cl(1')	88.09(4)
Ru(1')-Cl(1')	2.4477(5)	O(1')-Ru(1')-Cl(1')	84.91(4)
Ru(1')-Cg(4)	1.6790(7)	Cg(4)-Ru(1')-O(1')	125.49(4)
C(22')-Cl(2')	1.754(2)	Cg(4)-Ru(1')-N(1')	130.12(5)
C(25')-Cl(3')	1.759(2)	Cg(4)-Ru(1')-Cl(1')	126.02(3)

The packing diagram for complex **5** shows the molecules pack in a head-tail-tail-head arrangement, within alternating rows. There are several intermolecular interactions contributing to the packing of the molecules. There is evidence of a T-stacking interaction between the *p*-cymene H(3) and the centroid of the aniline ring Cg(1). Interactions and the packing diagram are present in **Figure 3.18**, with D...A

distances and torsion angles stated in **Table 3.10**.

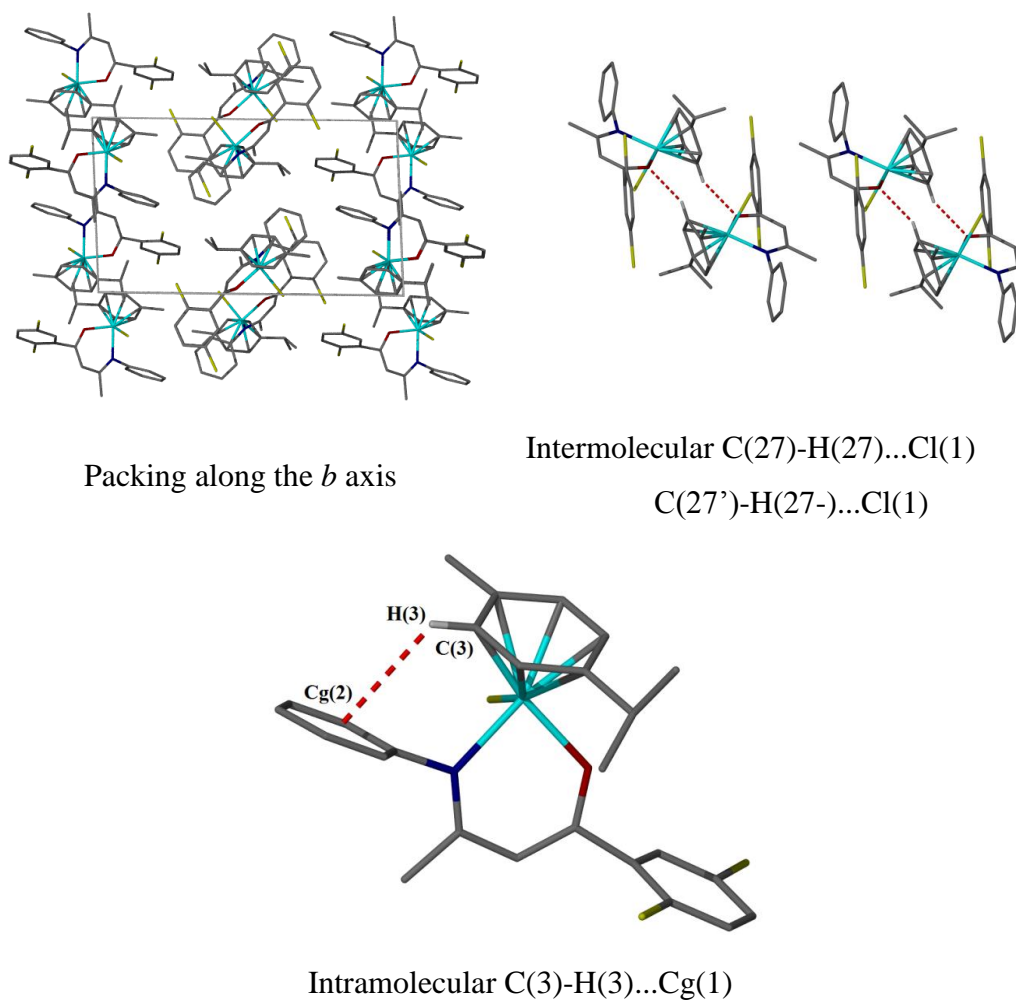


Figure 3.18 Interactions and packing diagram for **5**

Table 3.10 Bond lengths and torsion angles for both molecules of **5**

Interaction	Atoms	Bond Lengths and Angles
Intramolecular	C(3)-H(3)...Cg(2)	3.620 Å
Intermolecular	C(25)-Cl(3)...Cg(1)	4.180 Å
	C(25')-Cl(3')...Cg(4)	4.148 Å
	C(17')-H(17'B)...Cl(1')	3.570(2) Å
	C(7)-H(7)...O(1)	3.312(2) Å
	C(7')-H(7')...O(1')	3.198(2) Å
Torsion	Cg(2)-Centre	87.58°
	Centre-Cg(3)	75.01°
	Cg(5)-Centre	75.88°
	Centre-Cg(6)	59.41°

3.3.6 X-ray Characterisation for C₂₆H₂₅Cl₄NORu (6)

Red fragments of **6** suitable for X-ray crystallographic analysis were obtained by slow evaporation in methanol over a period of three days. The molecular structure is shown in **Figure 3.19**, selected bond lengths and angles are stated in **Table 3.11**. Complex **6** crystallised in a triclinic cell and structural solution was performed in the space group $P\bar{1}$, with two complex molecules and two molecules of methanol in the asymmetric unit.

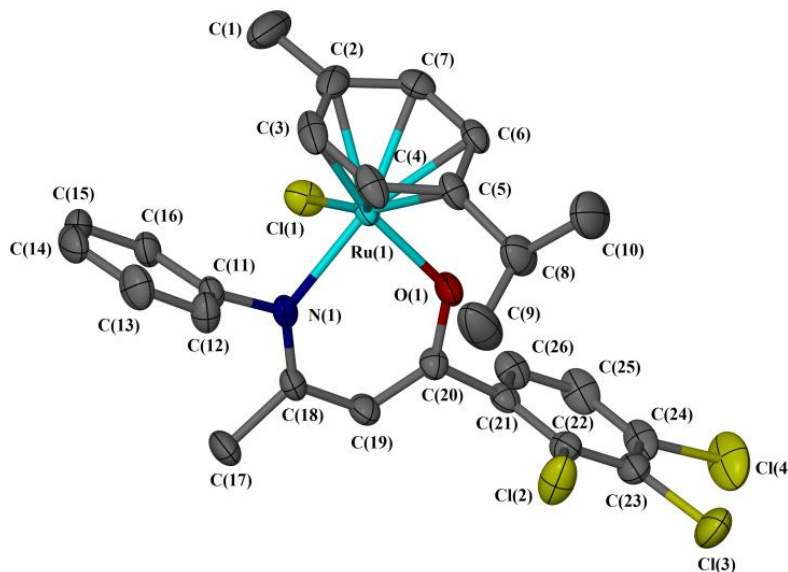
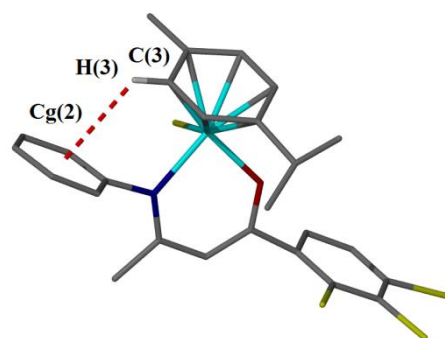


Figure 3.19 Molecular structure of **6**, displacement ellipsoids are at the 50% probability level. Hydrogen atoms, disorder, the second molecule and solvent molecules are omitted for clarity.

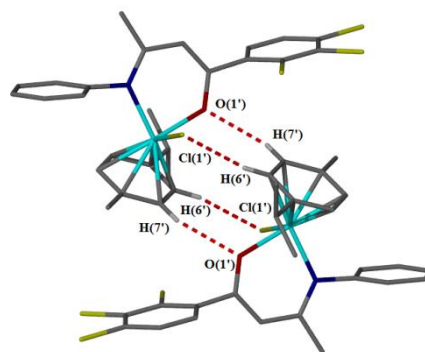
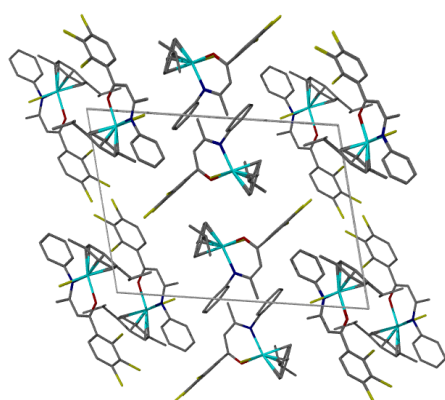
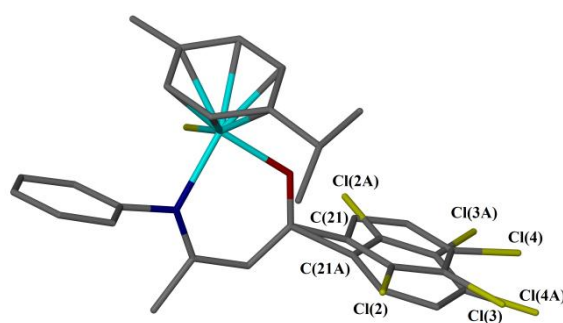
Table 3.11 Selected bond lengths and angles for both molecules of **6**

Bond	Distance (Å)	Bond	Angle (°)
Ru(1)-N(1)	2.128(3)	N(1)-Ru(1)-O(1)	88.66(10)
Ru(1)-O(1)	2.086(3)	N(1)-Ru(1)-Cl(1)	84.23(8)
Ru(1)-Cl(1)	2.4622(10)	O(1)-Ru(1)-Cl(1)	84.54(7)
Ru(1)-Cg(1)	1.6839(16)	Cg(1)-Ru(1)-O(1)	124.50(9)
		Cg(1)-Ru(1)-N(1)	131.23(10)
		Cg(1)-Ru(1)-Cl(1)	128.64(6)
Bond	Distance (Å)	Bond	Angle (°)
Ru(1')-N(1')	2.125(3)	N(1')-Ru(1')-O(1')	88.48(11)
Ru(1')-O(1')	2.102(3)	N(1')-Ru(1')-Cl(1')	84.56(9)
Ru(1')-Cl(1')	2.4700(11)	O(1')-Ru(1')-Cl(1')	85.59(9)
Ru(1')-Cg(4)	1.6914(15)	Cg(4)-Ru(1')-O(1')	124.54(11)
		Cg(4)-Ru(1')-N(1')	131.55(9)
		Cg(4)-Ru(1')-Cl(1')	127.45(9)

The packing diagram for complex **6** shows the molecules pack in a head-tail-tail-head pairs, alternating in each row. There are several intermolecular interactions contributing to the packing of the molecules. There is also evidence of a T-stacking interaction between the *p*-cymene and the centroid of the aniline ring. In one of the molecules, the substituted phenyl ring is disordered and the molecule was solved with each atom set at half the occupancy. These interactions and packing diagram are presented in **Figure 3.20**, with D...A distances and torsion angles are stated in **Table 3.12**.



Intramolecular C(3)-H(3)...Cg(2)

Intermolecular C(6')-H(6')...Cl(1')
C(7')-H(7')...O(1')Packing diagram along the *a* axis

Disorder around Cg(3)

Figure 3.20 Interactions and packing diagram for **6****Table 3.12** Bond lengths and torsion angles for both molecules of **6**

Interaction	Atoms	Bond Lengths and Angles
Intramolecular	C(3)-H(3)...Cg(2)	3.552(5) Å
Intermolecular	C(3)-H(3)...Cl(4)	3.370(5) Å
	C(14')-H(14')...Cg(2)	3.809 Å
	C(6)-H(6)...O(1)	3.269(2) Å
	C(6')-H(6')...Cl(1')	3.632(5) Å
	C(7')-H(7')...O(1')	3.257(5) Å
Torsion	Cg(2)-Centre	83.11°
	Centre-Cg(3)	76.29°

3.3.7 X-ray Characterisation for C₂₆H₂₇BrClNORu (7)

Red fragments of **7** suitable for X-ray crystallographic analysis were obtained using slow evaporation from a methanolic solution over a period of several days. The molecular structure is shown in **Figure 3.21**, selected bond lengths and angles are stated in **Table 3.13**. Complex **7** crystallised in a monoclinic cell and structural solution was performed in the space group *Cc*, with one molecule in the asymmetric unit.

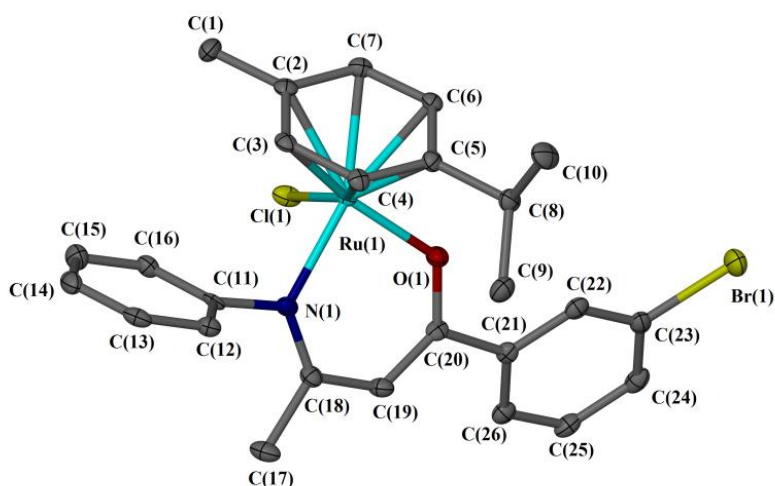


Figure 3.21 Molecular structure of **7**, displacement ellipsoids are at the 50% probability level and hydrogen atoms are omitted for clarity

Table 3.13 Selected bond lengths and angles for **7**

Bond	Distance (Å)	Bond	Angle (°)
Ru(1)-N(1)	2.101(2)	N(1)-Ru(1)-O(1)	89.10(8)
Ru(1)-O(1)	2.0516(19)	N(1)-Ru(1)-Cl(1)	85.01(7)
Ru(1)-Cl(1)	2.4281(7)	O(1)-Ru(1)-Cl(1)	83.27(6)
Ru(1)-Cg(1)	1.6661(12)	Cg(1)-Ru(1)-O(1)	125.24(7)
C(23)-Br(1)	1.902(3)	Cg(1)-Ru(1)-N(1)	129.73(8)
		Cg(1)-Ru(1)-Cl(1)	129.44(4)

The packing diagram for complex **7** shows the molecules pack in head-to-tail arrangement with the molecules alternating in each row. There are several intermolecular interactions contributing to the packing of the molecules. There is also evidence of a T-stacking interaction between the *p*-cymene H(3) and the centroid of the aniline ring Cg(2). These interactions and packing diagrams are presented in **Figure 3.22**, with D...A distances and torsion angles are stated in **Table 3.16**.

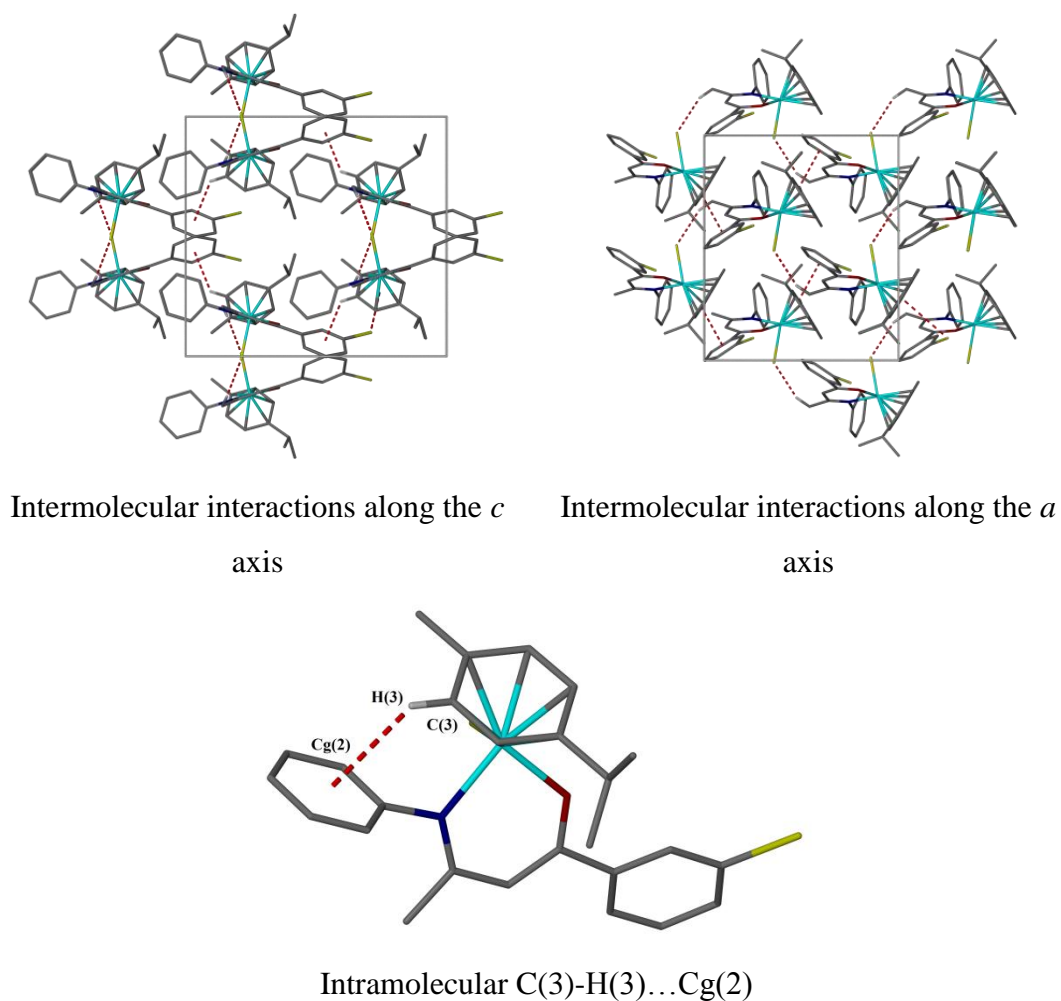


Figure 3.22 Intra/intermolecular interactions and packing diagrams for **7**

Table 3.14 Bond lengths and torsion angles for **7**

Interaction	Atoms	Bond Lengths and Angles
Intramolecular	C(3)-H(3)...Cg(2)	3.471(3) Å
Intermolecular	C(3)-H(3)...Cg(3)	3.484 Å
	C(23)-Br(1)...Cg(1)	3.932 Å
	Ru(1)-Cl(1)...Cg(1)	1.6661 Å
	C(17)-H(17B)...Cl(1)	3.588(3) Å
Torsion	Cg(2)-Centre	74.99°
	Centre-Cg(3)	31.76°

3.3.8 X-ray Characterisation for C₂₆H₂₇BrClNORu (**8**)

Red fragments of **8** suitable for X-ray crystallographic analysis were obtained using slow evaporation from a methanolic solution over a period of several days. The molecular structure is shown in **Figure 3.23**, selected bond lengths and angles are stated in **Table 3.15**. Complex **8** crystallised in a triclinic cell and structural solution was performed in the space group $P\bar{1}$, with one molecule in the asymmetric unit.

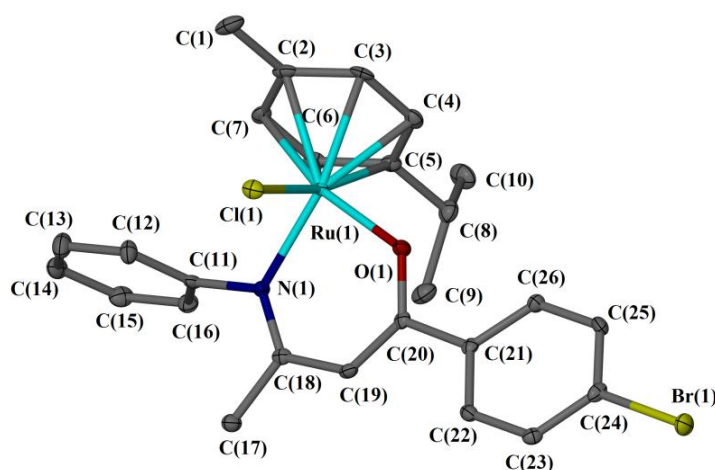
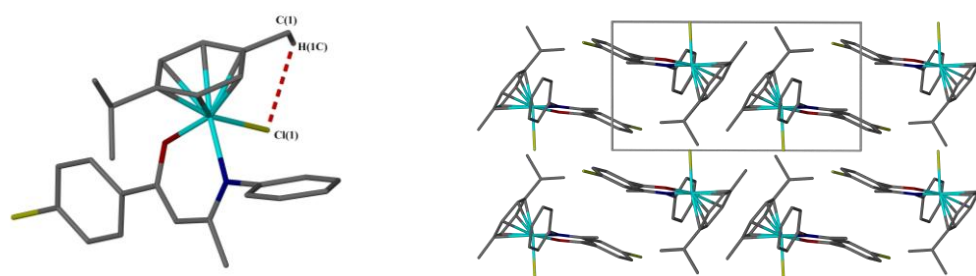


Figure 3.23 Molecular structure of **8**, displacement ellipsoids are at the 50% probability level and hydrogen atoms are omitted for clarity

Table 3.15 Selected bond lengths and angles for **8**

Bond	Distance (Å)	Bond	Angle (°)
Ru(1)-N(1)	2.086(2)	N(1)-Ru(1)-O(1)	89.42(8)
Ru(1)-O(1)	2.0518(17)	N(1)-Ru(1)-Cl(1)	83.68(7)
Ru(1)-Cl(1)	2.4377(8)	O(1)-Ru(1)-Cl(1)	84.85(5)
Ru(1)-Cg(1)	1.6661(11)	Cg(1)-Ru(1)-O(1)	124.54(7)
C(24)-Br(1)	1.906(3)	Cg(1)-Ru(1)-N(1)	130.71(8)
		Cg(1)-Ru(1)-Cl(1)	128.82(5)

The packing diagram for complex **8** shows the molecules pack in head-to-tail arrangement with the molecules alternating in each rows around a centre of inversion. There is evidence of an intramolecular interaction between the *p*-cymene H(1C)-Cl(1). The interactions and packing diagram are presented in **Figure 3.22**, with D...A distances and torsion angles are stated in **Table 3.14**.



Intramolecular C(1)-H(1C)...Cl(1)

Packing along the *b* axis**Figure 3.24** Intra/intermolecular interactions and packing diagrams for **8****Table 3.16** Bond lengths and torsion angles for **8**

Interaction	Atoms	Bond Lengths and Angles
Intramolecular	C(1)-H(1C)...Cl(1)	3.374(3) Å
Torsion	Cg(2)-centre	46.49°
	Centre-Cg(3)	63.43°

3.3.9 X-ray Characterisation for C₂₆H₂₇ClINORu (9)

Orange needles of **9** suitable for X-ray crystallographic analysis were obtained using slow evaporation from a methanolic solution over a period of several days. The molecular structure is shown in **Figure 3.25**, selected bond lengths and angles are stated in **Table 3.17**. Complex **9** crystallised in a triclinic cell and structural solution was performed in the space group $P\bar{1}$, with one molecule in the asymmetric unit.

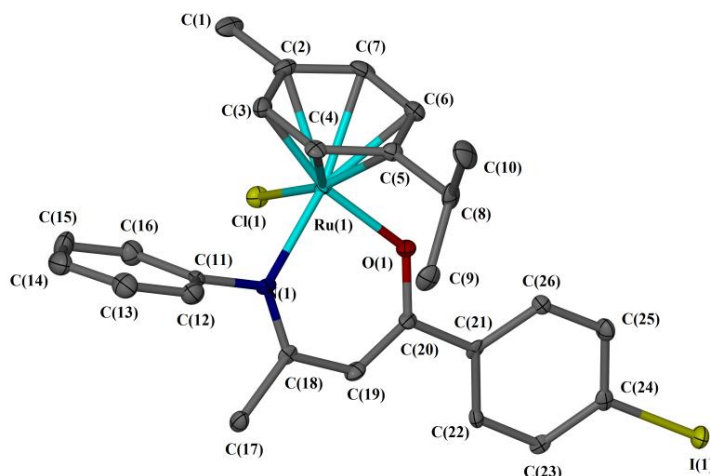


Figure 3.25 Molecular structure of **9**, displacement ellipsoids are at the 50% probability level and hydrogen atoms are omitted for clarity

Table 3.17 Selected bond lengths and angles for **9**

Bond	Distance (Å)	Bond	Angle (°)
Ru(1)-N(1)	2.088(3)	N(1)-Ru(1)-O(1)	89.44(13)
Ru(1)-O(1)	2.063(3)	N(1)-Ru(1)-Cl(1)	84.07(11)
Ru(1)-Cl(1)	2.4422(13)	O(1)-Ru(1)-Cl(1)	84.75(10)
Ru(1)-Cg(1)	1.6663(19)	Cg(1)-Ru(1)-O(1)	124.54(11)
C(24)-I(1)	2.109(4)	Cg(1)-Ru(1)-N(1)	130.49(13)
		Cg(1)-Ru(1)-Cl(1)	128.81(8)

The packing diagram for complex **9** shows the molecules pack in rows, with each pair of molecules around a centre of inversion. Packing along the *a* axis shows the pairs of molecules around the centre of inversion, whilst the packing along the *b* axis shows they pack in a herringbone arrangement. There is no evidence of either intramolecular or intermolecular interactions contributing to the packing of the molecules and therefore they pack by crystal packing interactions only. The

packing diagram are presented in **Figure 3.26**, and torsion angles are stated in **Table 3.18**.

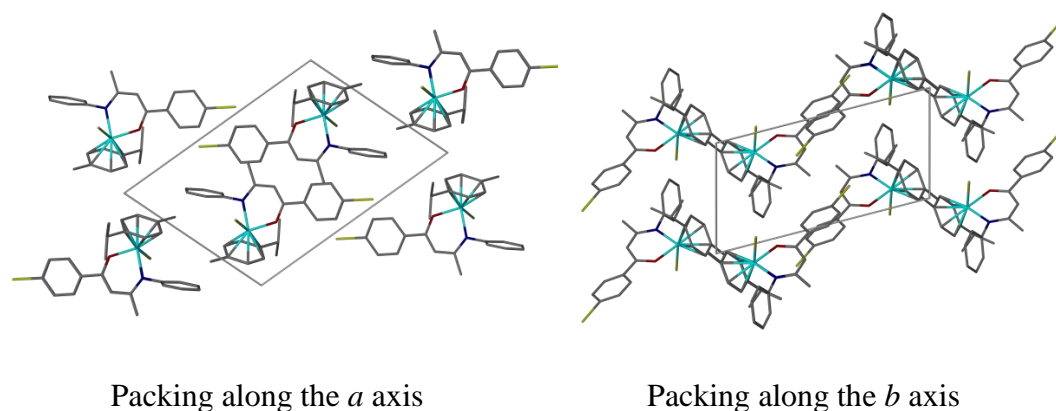


Figure 3.26 Packing diagrams for complex **9** when viewed along both the *a* and *b* axis

Table 3.18 Torsion angles for **9**

Interaction	Atoms	Bond Lengths and Angles
Torsion	Cg(2)-centre	76.87°
	Centre-Cg(3)	23.63°

3.3.10 X-ray Characterisation for C₂₈H₃₂ClNO₂Ru (**10**)

Orange needles of **10** suitable for X-ray crystallographic analysis were obtained using slow evaporation from a methanolic solution over a period of several days. The molecular structure is shown in **Figure 3.27**, selected bond lengths and angles are stated in **Table 3.19**. Complex **10** crystallised in a triclinic cell and structural solution was performed in the space group $P\bar{1}$, with one molecule in the asymmetric unit.

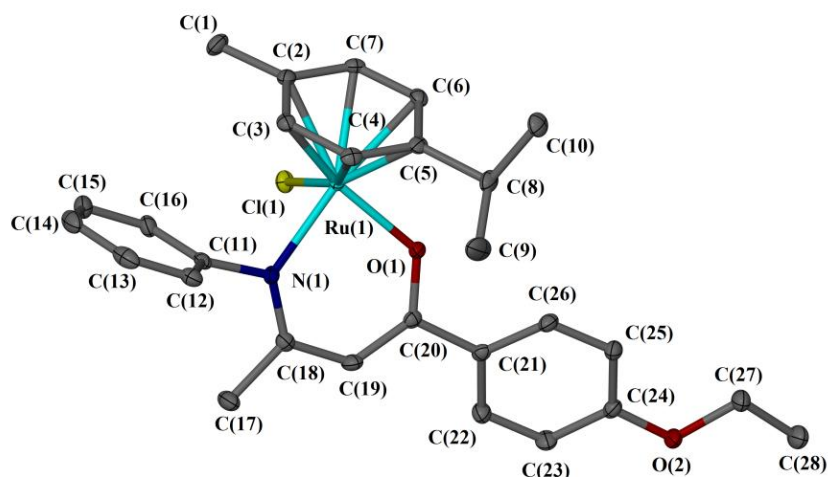


Figure 3.27 Molecular structure of **10**, displacement ellipsoids are at the 50% probability level and hydrogen atoms are omitted for clarity

Table 3.19 Selected bond lengths and angles for **10**

Bond	Distance (Å)	Bond	Angle (°)
Ru(1)-N(1)	2.0891(19)	N(1)-Ru(1)-O(1)	88.30(6)
Ru(1)-O(1)	2.0676(14)	N(1)-Ru(1)-Cl(1)	83.62(5)
Ru(1)-Cl(1)	2.4268(6)	O(1)-Ru(1)-Cl(1)	86.95(5)
Ru(1)-Cg(1)	1.6654(9)	Cg(1)-Ru(1)-O(1)	124.64(5)
C(24)-O(2)	1.370(2)	Cg(1)-Ru(1)-N(1)	132.54(5)
		Cg(1)-Ru(1)-Cl(1)	126.20(3)

The packing diagram for complex **10** shows the molecules pack in rows, with each pair of molecules around a centre of inversion. There is evidence an intramolecular T-stacking interaction between H(3) and the centroid of the aniline ring Cg(2). There are also several intermolecular interactions contributing to the packing of these molecules. The packing diagram are presented in **Figure 3.28**, and torsion angles are stated in **Table 3.20**.

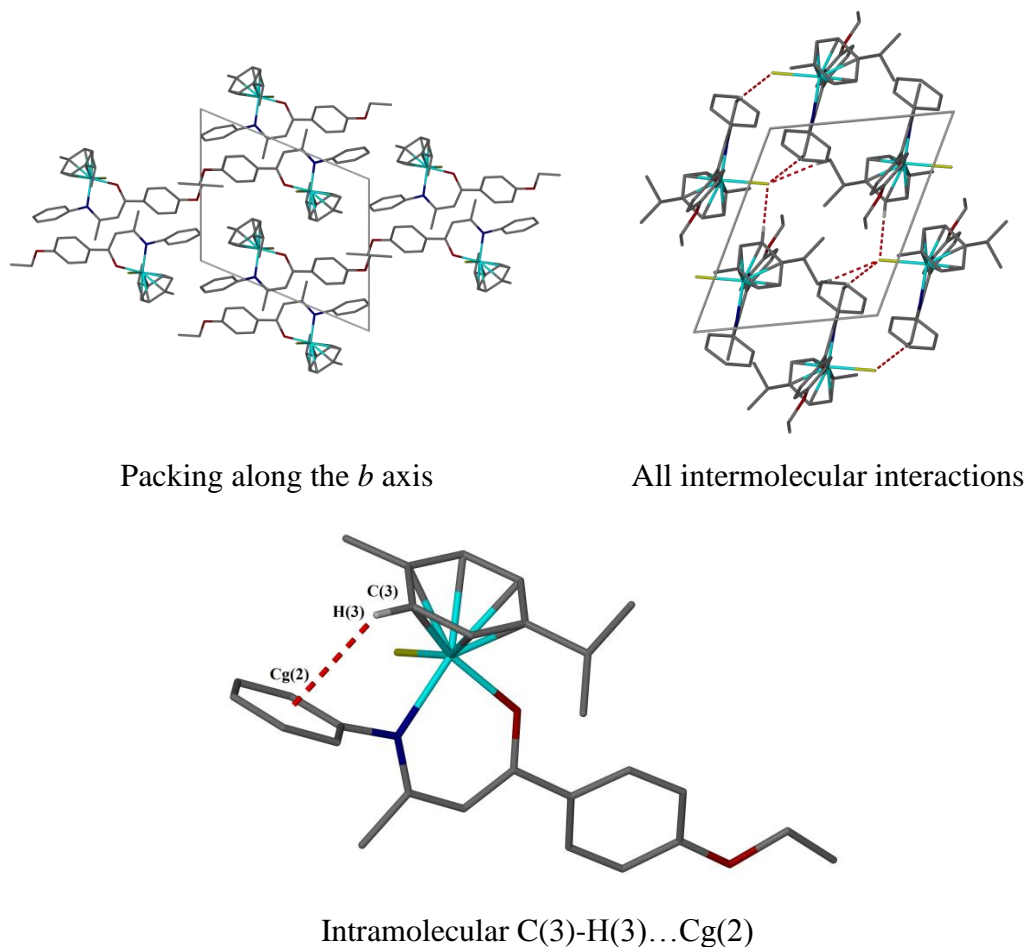


Figure 3.28 Intra-/Intermolecular interactions and packing diagrams for **10**

Table 3.20 Bond lengths and torsion angles for **10**

Interaction	Atoms	Bond Lengths and Angles
Intramolecular	C(3)-H(3)...Cg(2)	3.498 Å
Intermolecular	C(17)-H(17B)...Cl(1)	3.620(2) Å
	C(6)-H(6)...Cl(1)	3.481(2) Å
	C(9)-H(9B)...Cl(1)	3.681(3) Å
Torsion	Cg(2)-centre	78.18°
	Centre-Cg(3)	31.57

3.3.11 X-ray Characterisation for C₂₇H₃₀ClNORu (**11**)

Red fragments of **11** suitable for X-ray crystallographic analysis were obtained by slow evaporation in methanol over a period of one day. The molecular structure is shown in **Figure 3.29**, selected bond lengths and angles are stated in **Table 3.21**. Complex **11** crystallised in a triclinic cell and structural solution was performed in the space group $P\bar{1}$, with a single molecule in the asymmetric unit.

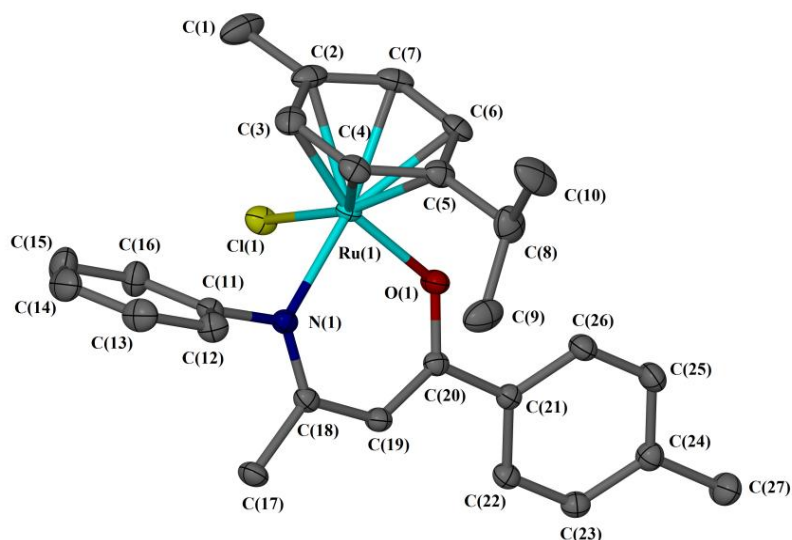
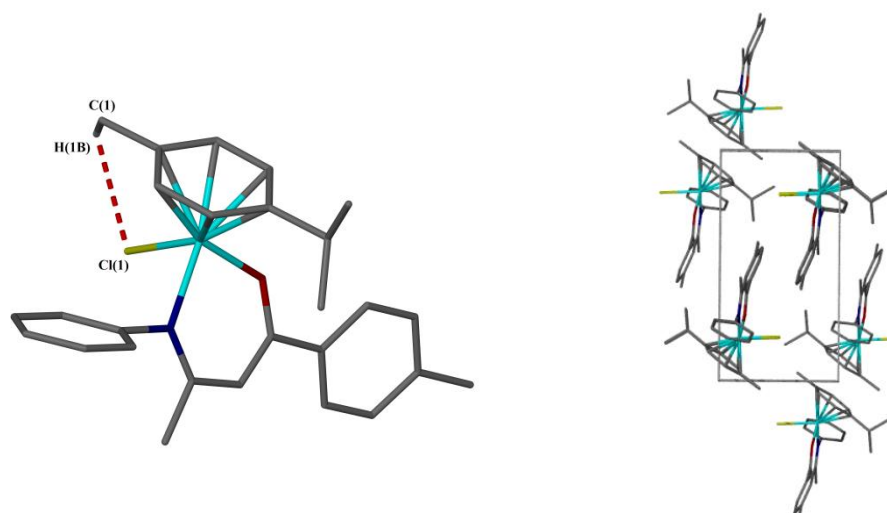


Figure 3.29 Molecular structure of **11**. Displacement ellipsoids are at the 50% probability level and hydrogen atoms are omitted for clarity

Table 3.21 Selected bond lengths and angles for **11**

Bond	Distance (Å)	Bond	Angle (°)
Ru(1)-N(1)	2.1064(14)	N(1)-Ru(1)-O(1)	89.41(5)
Ru(1)-O(1)	2.0711(13)	N(1)-Ru(1)-Cl(1)	83.90(4)
Ru(1)-Cl(1)	2.4623(5)	O(1)-Ru(1)-Cl(1)	84.84(4)
Ru(1)-Cg(1)	1.6830(7)	Cg(1)-Ru(1)-O(1)	124.31(5)
C(24)-C(27)	1.528(3)	Cg(1)-Ru(1)-N(1)	130.72(5)
		Cg(1)-Ru(1)-Cl(1)	128.90(3)

The packing diagram for complex **11** shows the molecules pack in head-tail-tail-head pairs, alternating in each row, with evidence of an intramolecular interaction between C(1)-H(1B)...Cl(1). The intramolecular interaction and packing diagram are presented in **Figure 3.30**, with D...A distances and torsion angles stated in **Table 3.22**.



Intramolecular C(1)-H(1B)...Cl(1)

Packing diagram along the *b* axis

Figure 3.30 Intramolecular interaction and packing along the *b* axis for **11**

Table 3.22 Bond lengths and torsion angles for **11**

Interaction	Atoms	Bond Lengths and Angles
Intramolecular	C(1)-H(1B)...Cl(1)	3.399(2) Å
Torsion	Cg(2)-Centre	75.05°
	Centre-Cg(3)	23.41°

3.3.12 X-ray Characterisation for C₃₀H₃₀ClNORu (**12**)

Red fragments of **12** suitable for X-ray crystallographic analysis were obtained using slow evaporation from a methanolic solution over a period of one day. The molecular structure is shown in **Figure 3.31**, selected bond lengths and angles are stated in **Table 3.23**. Complex **12** crystallised in a triclinic cell and structural solution was performed in the space group $P\bar{1}$, with two molecules in the asymmetric unit.

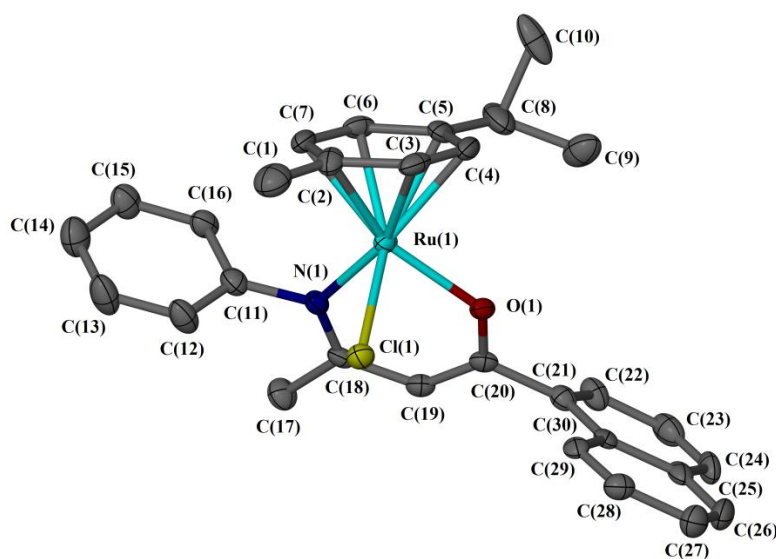


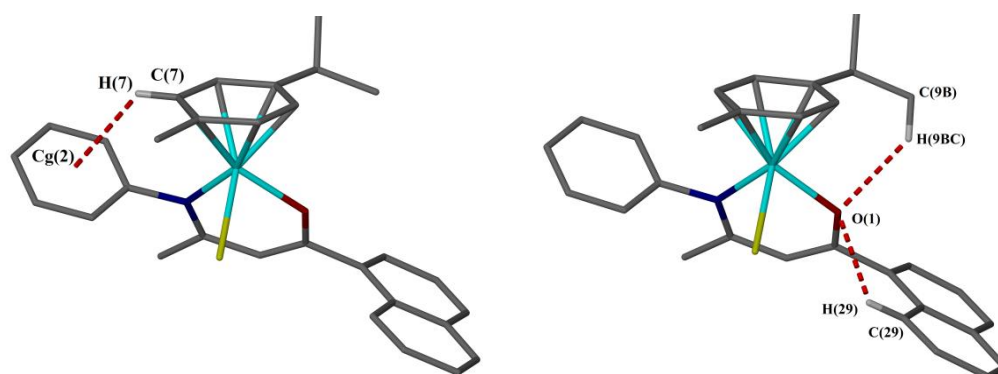
Figure 3.31 Molecular structure of **12**. Displacement ellipsoids are at the 50% probability level and hydrogen atoms and the second molecule are omitted for clarity.

Table 3.23 Selected bond lengths and angles for both molecules of **12**

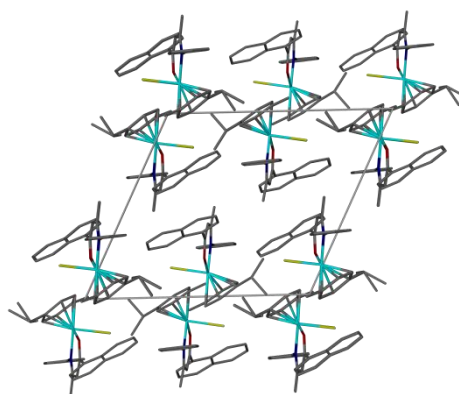
Bond	Distance (Å)	Bond	Angle (°)
Ru(1)-N(1)	2.094(6)	N(1)-Ru(1)-O(1)	88.4(2)
Ru(1)-O(1)	2.069(4)	N(1)-Ru(1)-Cl(1)	85.71(16)
Ru(1)-Cl(1)	2.4340(18)	O(1)-Ru(1)-Cl(1)	83.33(12)
Ru(1)-Cg(1)	1.675(3)	Cg(1)-Ru(1)-O(1)	126.30(16)
		Cg(1)-Ru(1)-N(1)	129.91(19)
		Cg(1)-Ru(1)-Cl(1)	128.09(13)
Bond	Distance (Å)	Bond	Angle (°)
Ru(1')-N(1')	2.101(5)	N(1')-Ru(1')-O(1')	88.8(2)
Ru(1')-O(1')	2.070(5)	N(1')-Ru(1')-Cl(1')	85.79(16)
Ru(1')-Cl(1')	2.4365(19)	O(1')-Ru(1')-Cl(1')	84.25(13)
Ru(1')-Cg(5)	1.674(3)	Cg(5)-Ru(1')-O(1')	125.07(15)
		Cg(5)-Ru(1')-N(1')	129.78(17)
		Cg(5)-Ru(1')-Cl(1')	128.57(13)

The packing diagram for complex **12** shows the molecules pack in pairs about a centre of inversion. There is evidence of intramolecular interactions in both molecules of **12** and evidence of several intermolecular interactions between these molecules. The *p*-cymene is rotated and a T-stacking interactions is now seen

between the *p*-cymene H(7) and aniline ring Cg(2). The interaction and packing diagram are presented in **Figure 3.32**, with D...A distances and torsion angles stated in **Table 3.24**.



Intramolecular interactions



Packing diagram along the *b* axis

Figure 3.32 Intramolecular interaction and packing along the *b* axis for **12**

Table 3.24 Bond lengths and torsion angles for **12**

Interaction	Atoms	Bond Lengths and Angles
Intramolecular	C(9B)-H(9BC)...O(1)	3.336(13) Å
	C(29)-H(29)...O(1)	3.041(8) Å
	C(29')-H(29')...O(1')	3.077(8) Å
	C(7)-H(7)...Cg(2)	3.547(9) Å
Intermolecular	C(24)-H(24)...Cg(7)	3.526(8) Å
	Ru(1')-Cl(1')...Cg(5)	1.674(3) Å
	C(3)-H(3)...O(1)	3.256(10) Å
	C(7')-H(7')...O(1')	3.144(9) Å
Torsion	Cg(2)-Centre	83.88(22)°
	Centre-Cg(3)	56.95(19)°
	Cg(6)-Centre	80.49(19)°
	Centre-Cg(7)	64.07(2)°

3.3.13 X-ray Characterisation for C₂₆H₂₅ClF₃NORu (**13**)

Red fragments of **13** suitable for X-ray crystallographic analysis were obtained using slow evaporation from a methanolic solution over a period of two days. The molecular structure is shown in **Figure 3.33**, selected bond lengths and angles are stated in **Table 3.25**. Complex **13** crystallised in a monoclinic cell and structural solution was performed in the space group *Cc*, with a single molecule in the asymmetric unit.

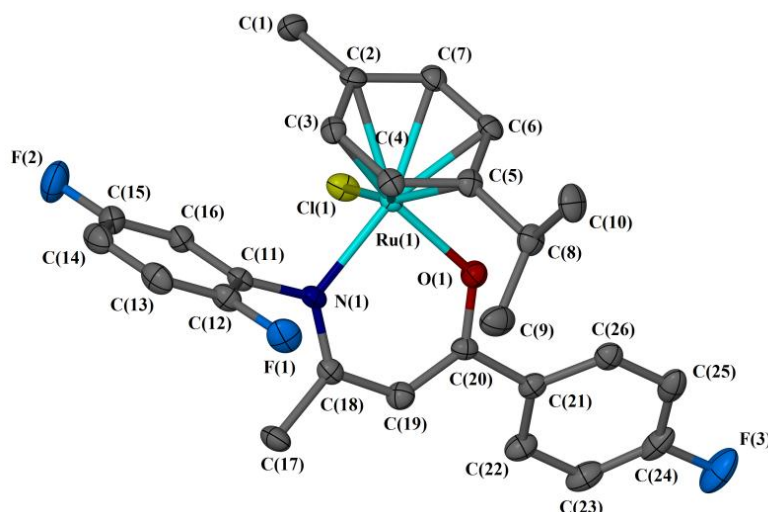
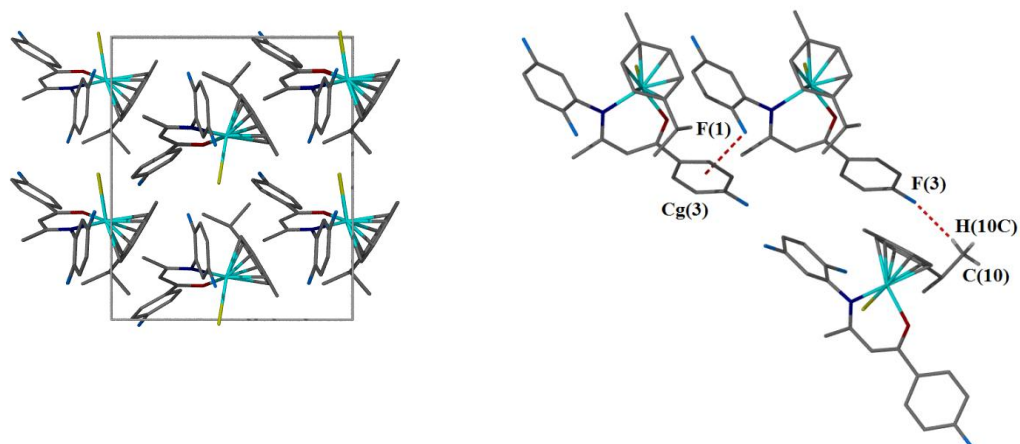


Figure 3.33 Molecular structure of **13**, displacement ellipsoids are at the 50% probability level and hydrogen atoms are omitted for clarity.

Table 3.25 Selected bond lengths and bond angles for **13**

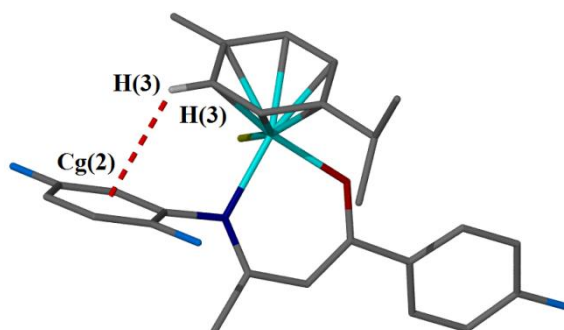
Bond	Distance (Å)	Bond	Angle (°)
Ru(1)-N(1)	2.131(2)	N(1)-Ru(1)-O(1)	89.32(8)
Ru(1)-O(1)	2.0930(18)	N(1)-Ru(1)-Cl(1)	86.24(6)
Ru(1)-Cl(1)	2.4661(7)	O(1)-Ru(1)-Cl(1)	83.86(5)
Ru(1)-Cg(1)	1.6861(10)	Cg(1)-Ru(1)-O(1)	124.53(6)
C(12)-F(1)	1.370(3)	Cg(1)-Ru(1)-N(1)	129.46(7)
C(15)-F(2)	1.370(3)	Cg(1)-Ru(1)-Cl(1)	128.98(4)
C(24)-F(3)	1.381(3)		

The packing diagram for compound **13** shows the molecules pack in alternating rows with T-stacking between one row and a hydrogen bond linking the two rows together. There is evidence of several intermolecular interactions contributing to the packing of the molecule and a possible intramolecular T-stacking interaction seen between the *p*-cymene hydrogen H(3) and the centroid of the aniline ring Cg(2). These interactions are presented in **Figure 3.34**, with D...A distances and torsion angles stated in **Table 3.26**.

Packing diagram along the *a* axis

Intermolecular C(12)-F(1)...Cg(3)

C(10)-H(10C)...F(3)



Intramolecular C(3)-H(3)...Cg(2)

Figure 3.34 Interactions and packing diagram for **13****Table 3.26** Bond lengths and torsion angles for **13**

Interaction	Atoms	Bond Lengths and Angles
Intramolecular	C(3)-H(3)...Cg(2)	3.576 Å
Intermolecular	Ru(1)-Cl(1)...Cg(1)	1.6861 Å
	C(12)-F(1)...Cg(3)	4.021 Å
	C(10)-H(10C)...F(3)	3.405(4) Å
Torsion	Cg(1)-Cg(2)	76.38°
	Cg(2)-Cg(3)	33.47°

3.4 Conclusions

A range of novel functionalised β -ketoiminate ruthenium(II) chloride *pseudo* octahedral “piano-stool” complexes has been synthesised and fully characterised, with X-ray crystallographic analysis obtained for all complexes. All of these complexes crystallised as orange/red single crystals and structural solutions were performed in either a monoclinic Cc (**4** and **7**) or a triclinic $P\bar{1}$ (**1-3**, **5**, **6** and **8-13**) space groups. The complexes all show similar ^1H and $^{13}\text{C}\{^1\text{H}\}$ NMR spectra, with a distinctive upfield shift for one of the *p*-cymene hydrogens seen when analysing the ^1H NMR spectra. Apart from **9**, which shows no intramolecular interactions, X-ray crystallographic analysis shows all compounds have an intramolecular interaction with the *p*-cymene ring. Complexes **1**, **2**, **4-7**, **10**, **12** and **13** all show an intramolecular T-stacking interaction between a *p*-cymene C-H and the centroid of the aniline ring. Complexes **3**, **8** and **11** all have the *p*-cymene twisted and instead have an intramolecular interaction between the *p*-cymene C-H and the Ru-Cl. Both of these types of interaction are thought to be the cause of the upfield shift seen in the ^1H NMR spectra. The β -ketoiminate ligands were functionalised to include electron withdrawing groups, electron donating groups and increased steric bulk, these were to allow conclusive structure activity relationships to be determined and to allow relationships in IC_{50} to be determined (see Chapter 4).

3.5 References

1. F. Wang, A. Habtemariam, E. P. L. van der Geer, R. Fernández, M. Melchart, R. J. Deeth, R. Aird, S. Guichard, F. P. A. Fabbiani, P. Lozano-Casal, I. D. H. Oswald, D. I. Jodrell, S. Parsons and P. J. Sadler, *Proc. Natl. Acad. Sci. U.S.A.*, 2005, **102**, 18269-18274.
2. T. Bugarcic, A. Habtemariam, R. J. Deeth, F. P. A. Fabbiani, S. Parsons and P. J. Sadler, *Inorg. Chem.*, 2009, **48**, 9444-9453.
3. R. Fernández, M. Melchart, A. Habtemariam, S. Parsons and P. J. Sadler, *Chem. Eur. J.*, 2004, **10**, 5173-5179.
4. A. Pitto-Barry, N. P. E. Barry, O. Zava, R. Deschenaux, P. J. Dyson and B. Therrien, *Chem. Eur. J.*, 2011, **17**, 1966-1971.
5. A. Pitto-Barry, O. Zava, P. J. Dyson, R. Deschenaux and B. Therrien, *Inorg. Chem.*, 2012, **51**, 7119-7124.
6. N. P. E. Barry, O. Zava, P. J. Dyson and B. Therrien, *J. Organomet. Chem.*, 2012, **705**, 1-6.
7. I. N. Stepanenko, A. Casini, F. Edafe, M. S. Novak, V. B. Arion, P. J. Dyson, M. A. Jakupec and B. K. Keppler, *Inorg. Chem.*, 2011, **50**, 12669-12679.
8. W. Ginzinger, G. Mühlgassner, V. B. Arion, M. A. Jakupec, A. Roller, M. Galanski, M. Reithofer, W. Berger and B. K. Keppler, *J. Med. Chem.*, 2012, **55**, 3398-3413.
9. G. Mühlgassner, C. Bartel, W. F. Schmid, M. A. Jakupec, V. B. Arion and B. K. Keppler, *J. Inorg. Biochem.*, 2012, **116**, 180-187.
10. R. Hudej, J. Kljun, W. Kandioller, U. Repnik, B. Turk, C. G. Hartinger, B. K. Keppler, D. Miklavčič and I. Turel, *Organometallics*, 2012, **31**, 5867-5874.
11. J. Kljun, A. K. Bytzeck, W. Kandioller, C. Bartel, M. A. Jakupec, C. G. Hartinger, B. K. Keppler and I. Turel, *Organometallics*, 2011, **30**, 2506-2512.
12. S. H. van Rijt, A. J. Hebden, T. Amaresekera, R. J. Deeth, G. J. Clarkson, S. Parsons, P. C. McGowan and P. J. Sadler, *J. Med. Chem.*, 2009, **52**, 7753-7764.
13. K. D. Camm, A. El-Sokkary, A. L. Gott, P. G. Stockley, T. Belyaeva and P. C. McGowan, *Dalton Trans*, 2009, **0**, 10914-10925.

14. S. J. Lucas, Ph. D Thesis, University of Leeds, 2013.
15. S. J. Lucas, R. M. Lord, R. L. Wilson, R. M. Phillips, V. Sridharan and P. C. McGowan, *Dalton Trans.*, 2012, **41**, 13800-13802.

Chapter 4

Evaluation of *In Vitro* Cytotoxicity of β -Ketoiminate

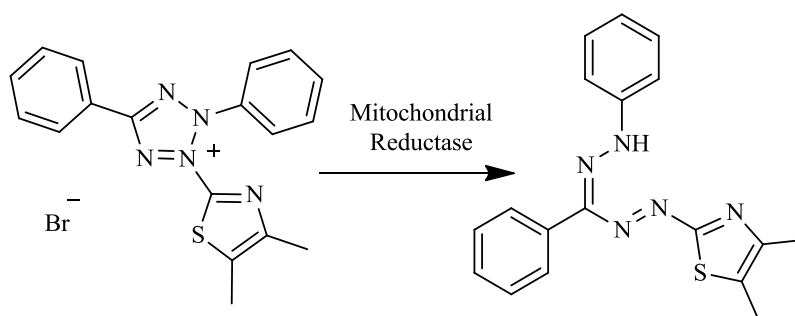
Ruthenium (II) Chloride Complexes

4 Cytotoxicity Evaluation

Biological assays require a technique to measure the amount of cell survival or proliferation of mammalian cells. This can be carried out by either counting cells using a dye, measuring the release of ^{51}Cr -labelled proteins after cell lysis or incorporation of radioactive nucleotides during proliferation.¹ Tetrazolium salts are good candidates as they are used to measure the activity of various dehydrogenase enzymes.² Current research requires assays which are quantitative and rapid and which are able to handle large amounts of data on a daily basis.

4.1 MTT Assay

The MTT assay was developed by Mosmann in 1983 and is a method of measuring the survival of mammalian cells, in which the yellow 3-(4,5-dimethylthiazol-2-yl)-2,5-diphenyl tetrazolium bromide (MTT) is reduced to the purple formazan in living cells (**Scheme 4.1**)^{3,4}

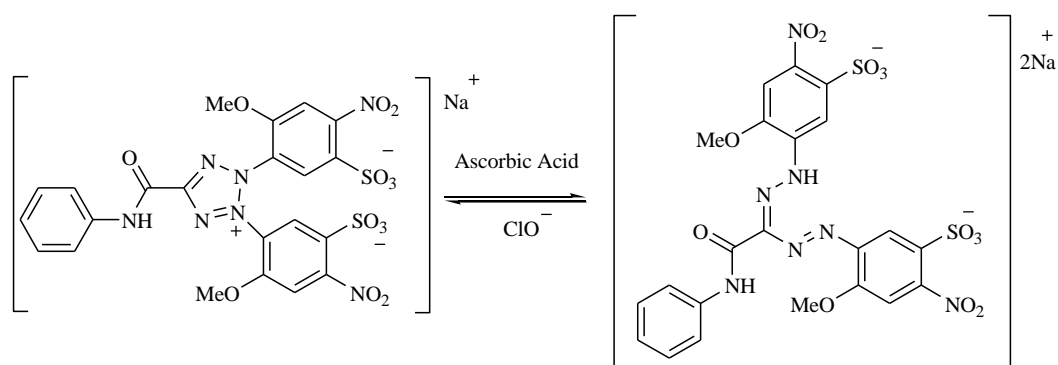


Scheme 4.1 Reduction of MTT to Formazan

The cancer cells are incubated with the potential drug for a period of 3-5 days at 37°C. A solution of MTT in distilled water (5 mg/ mL) is added and the cells incubated for a further 3-4 hours to allow for the reduction to the purple formazan. The reduction occurs due to the transfer of electrons to the MTT ($E_0' = -0.11 \text{ V}$) from oxidising substrates such as NADH and NADPH ($E_0' = -0.317 \text{ V}$).⁵ The primary source for the reduction is thought to start within the mitochondria, however there is no evidence indicating it is confined here.^{6,7} The purple formazan crystals can be separated by removing the MTT/medium *via* pipette and dissolving the crystals in DMSO. The absorbance is then measured at a wavelength of 540 nm using a multi-well scanning spectrophotometer.

4.2 XTT Assay

A variation of the MTT assay known as XTT was developed by Paull *et al.* in 1988. The sodium 3'-[1-[(phenylamino)-carbonyl]-3,4-tetrazolium]-bis(4-methoxy-6-nitro)benzene-sulfonic acid hydrate (XTT) undergoes a bioreduction in the presence of ascorbic acid, in which the charged sulfonic acid groups are key for its water solubility (**Scheme 4.2**).⁸ The XTT in pre-warmed medium (1 mg/ mL), without serum, is mixed with PMS in phosphate buffered saline (PBS) (1.53 mg/ mL). Once added to the plate and incubated for a period of time, a mechanical shaker is used to mix the solutions and the readings taken at 450 nm. The assay time is reduced due to the elimination of the solubilising step, shortening the culture assay procedure.



Scheme 4.2 Reduction of XTT to a water-soluble formazan

In the late 1980's the US National Cancer Institute (NCI) noted problems with both MTT and XTT assays which made them unsuitable for use on large scale drug screening.⁹ MTT reduction varied depending on both the specific cell line and the age of the cell culture. Vistica *et al.* noticed a correlation with the amount of D-glucose within the cell medium and that cells with increased metabolic rates for sugar demonstrated lower reduction of MTT.⁶ XTT also had problems with either the absence/ inhibition of reduction without the presence of an electron-coupling agent such as phenazine methosulfate.⁹ This was thought to be due to the presence of a disulfonate which has shown to have difficulty permeating the cell membrane.^{10, 11}

4.3 SRB Assay

This assay was developed by Skehan *et al.* in 1990 after investigating the suitability of a series of different dyes for providing cell density measurements.¹² It utilises an aminoxanthene dye, Sulforhodamide B (SRB) (**Figure 4.1**), which under mildly acidic conditions binds electrostatically to amino acids through the charged sulfonic acid group. Cultures fixed with trichloroacetic acid are stained and incubated for 30 minutes with SRB (0.4%, w/v) and dissolved in acetic acid (1%). The unbound dye is removed by four washes with acetic acid (1%) and the bound dye extracted with an unbuffered base (10 mM). The absorbance is measured at a wavelength between 490-530 nm using a microtiter plate reader. The SRB assay has shorter incubation times than the previous assays and gives more consistent results over a greater number of cell lines. At present this is the only assay used for large scale measurements, where several million culture wells are run per year.

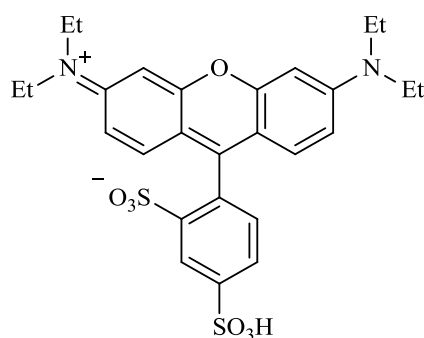


Figure 4.1 Sulforhodamide B (SRB) Dye

4.4 5-Day MTT Assay

The complexes to be tested are firstly dissolved in DMSO, control assays have previously been carried out using only DMSO to investigate the effect on cytotoxicity with differing concentrations.¹³ Using HT-29 cells, the rate of cell survival remained high for all concentrations of DMSO, falling to only 73% at a concentration of 2.0% DMSO. For the MCF-7 cell line, the cytotoxic effect of DMSO was more significant, with a 52% cell survival at the same concentration of DMSO. The A2780 cell line exhibited the highest sensitivity to DMSO, with significant cell death observed with 63% cell survival at 2.0% DMSO and 76% cell survival at 1.0% DMSO.¹³ The complexes stated within this chapter had IC_{50} values under the thresholds stated and it was decided that the DMSO-related toxicity would not interfere significantly with the assay.

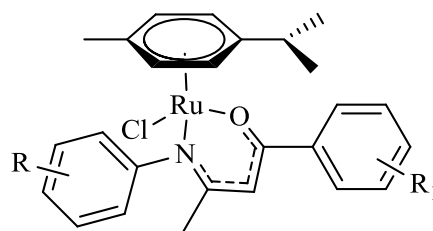
4.4.1 Conducting MTT Under Normoxic Conditions (21% O₂)

A series of complexes were incubated with the cancer cells at ten different concentrations, each one a double dilution of the previous one. To obtain these concentrations the drugs were diluted in DMSO to give an initial concentration of 25 mM, followed by dilutions in cell media to give a range of concentrations between 250-0.48 μ M. Firstly, the cell plates are incubated for 24-hours, followed by addition of the drug dilutions on day two and then a 5-day incubation period. After the 5-day incubation, MTT solution (5 mg/ mL) was added to the plates, incubated for a further 3 hours and then absorbance measured at 540 nm, using a Thermo Scientific Multiskan EX microplate photometer. All IC₅₀ values were taken from an average of three different assays with good repeatability; any measurements not correlating were repeated until they were within a 10% error. The full protocol for this procedure is stated within Chapter 9.

4.5 Results and Discussion

4.5.1 β -Ketoiminate Ruthenium(II) Complexes

The series of novel ruthenium(II) β -ketoinate chloride complexes previously reported in Chapter 3 (**Figure 4.2**) and cisplatin as a control, were tested against a range of cell lines including; HT-29 (human colon adenocarcinoma), MCF-7 (human breast carcinoma), A2780 (human ovarian adenocarcinoma) and A2780cis (cisplatin resistant human ovarian adenocarcinoma). Assays were carried out using a 5-day drug exposure and during this period were incubated at 37 °C with a 5.0% CO₂ concentration.



R ₁ = 3'-F	R = H	1	R ₁ = 4'-Br	R = H	8
R ₁ = 4'-F	R = H	2	R ₁ = 4'-I	R = H	9
R ₁ = 4'-Cl	R = H	3	R ₁ = 4'-OEt	R = H	10
R ₁ = 2',4'-diCl	R = H	4	R ₁ = 4'-Me	R = H	11
R ₁ = 2',5'-diCl	R = H	5	R ₁ = 2'-naphthyl	R = H	12
R ₁ = 2',3',4'-triCl	R = H	6	R ₁ = 4'-F	R = 2',4'-diF	13
R ₁ = 3'-Br	R = H	7			

Figure 4.2 Ruthenium (II) chloride complexes tested *in vitro* using the MTT assay

Once the incubated cells had been treated with the MTT solution (5mg/ mL), the amount of living cells could be determine due to the change in MTT colour. The living cells are able to reduce the MTT to the purple formazan and so the amount of purple coloration seen is proportional to cell survival. To calculate the IC₅₀ values of the complexes, graphs were plotted of % cell survival versus drug concentration (μM) and the concentration found at 50% cell survival. The graph in **Figure 4.3** shows the % cell survival versus drug concentration (μM) for cisplatin, **1** and **12** against HT-29 cell line. The values were calculated by plotting two points, one above and one below the 50% cell survival value, then plotting a line of best fit and rearrangement of the equation to find the concentration (μM).

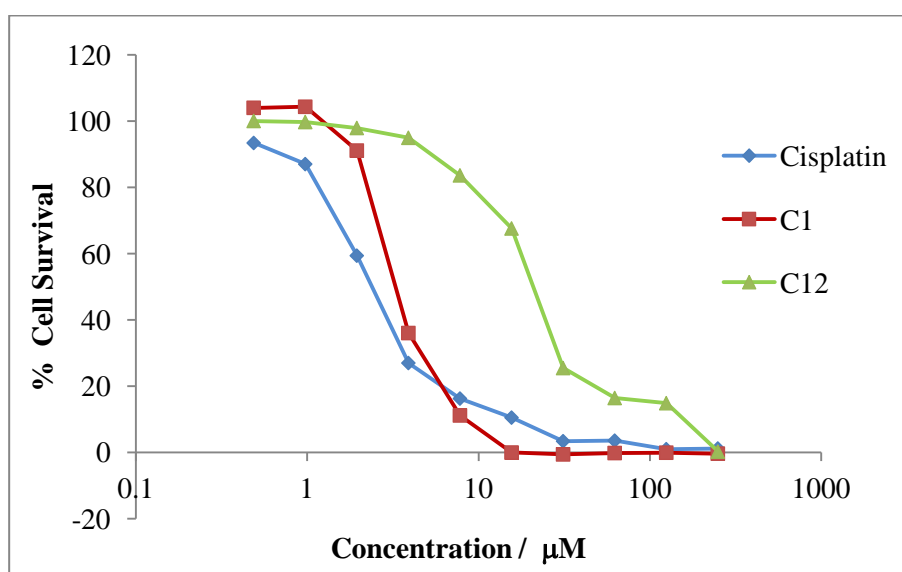


Figure 4.3 % Cell survival versus concentration (μM) for cisplatin, **1** and **12**

The values are stated in **Table 4.1** and have also been summarised as a bar-chart in **Figure 4.4**. It can be seen that all the complexes tested have moderate to high activities against all cell lines. Complexes **1**, **3** and **4** have the most consistent IC_{50} values over all four cell lines, with significantly higher cytotoxic values against the cisplatin resistant ovarian cell line A2780cis then the other cell lines. Against HT-29 and A2780cis there are differences in IC_{50} when comparing the different electronic properties of the complex, where increasing the withdrawing nature decreased the cytotoxicity of the complex. Whereas, against MCF-7 and A2780 cell lines all of the complexes have high cytotoxicity and no clear trend can be seen between electronic or steric properties versus cytotoxic behaviour.

Table 4.1 Summary of IC₅₀ values for cisplatin and ruthenium complexes using a 5-day exposure

Complex	HT-29		MCF 7		A2780		A2780cis	
	IC ₅₀ (μM)	± SD (μM)	IC ₅₀ (μM)	± SD (μM)	IC ₅₀ (μM)	± SD (μM)	IC ₅₀ (μM)	± SD (μM)
Cisplatin	2.4	0.1	1.07	0.10	0.94	0.04	10.5	0.2
[<i>p</i> -cymRuCl ₂] ₂	197.09	4.5	183.6	2.9	195.4	4.5	216.6	9.2
1	3.5	0.3	1.9	0.1	2.60	0.08	3.13	0.09
2	10.5	0.4	5.07	0.09	2.8	0.1	3.37	0.07
3	5.40	0.09	3.0	0.2	1.6	0.1	3.8	0.1
4	4.3	0.5	3.22	0.09	2.35	0.04	5.59	0.05
5	11.4	0.6	3.5	0.2	2.5	0.1	6.4	0.1
6	12.6	0.2	3.27	0.08	2.84	0.04	11.5	0.3
7	6.1	0.3	3.55	0.09	2.5	0.2	3.69	0.09
8	10.3	0.6	6.2	0.2	2.3	0.2	7.00	0.04
9	11.8	0.8	-	-	-	-	-	-
10	12.8	0.5	-	-	-	-	-	-
11	10.21	0.09	2.9	0.1	2.87	0.05	9.1	0.1
12	22	2	13.0	0.2	-	-	-	-
13	6.3	0.3	7.2	0.2	1.9	0.1	3.80	0.09

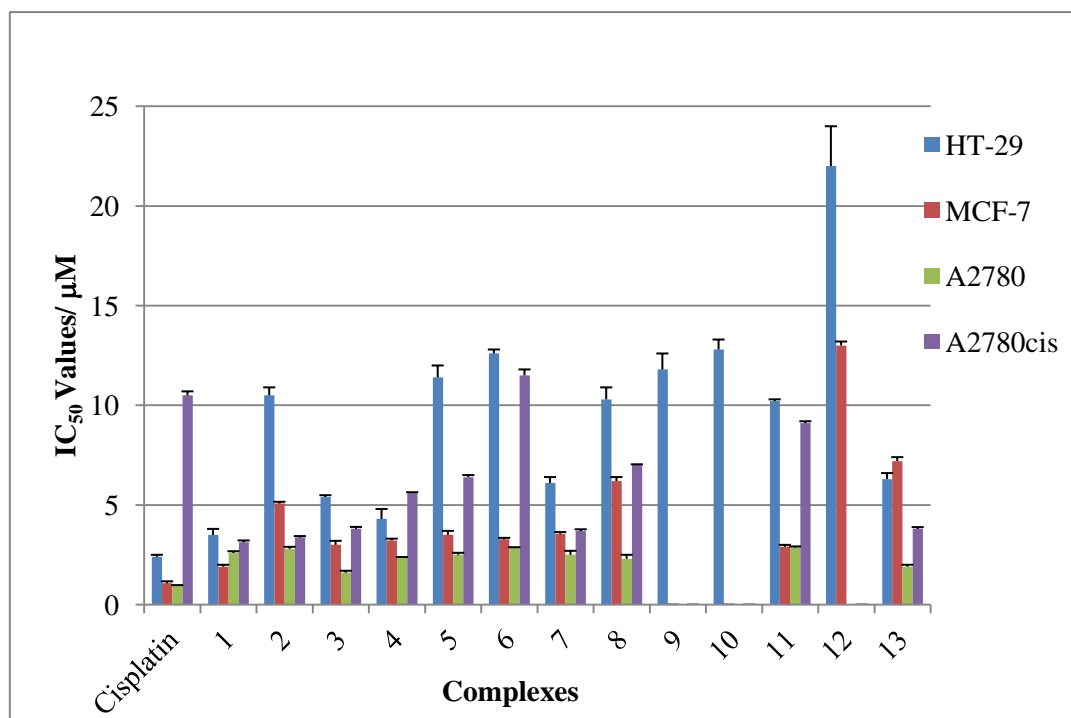


Figure 4.4 Bar chart of IC₅₀ values for cisplatin and complexes 1-13

Previously within the McGowan group it was found that *para* substituted β -diketonate titanium complexes gave the greatest cytotoxic behaviour, with the 4-fluoro- β -diketonate titanium complex giving the highest cytotoxicity values.^{13, 14} Therefore the following bar-chart (**Figure 4.5**) shows the difference in cytotoxic behaviour of the *para* β -ketoiminate ruthenium chloride complexes (C2=4F, C3=4Cl, C8=4Br and C9=4I).

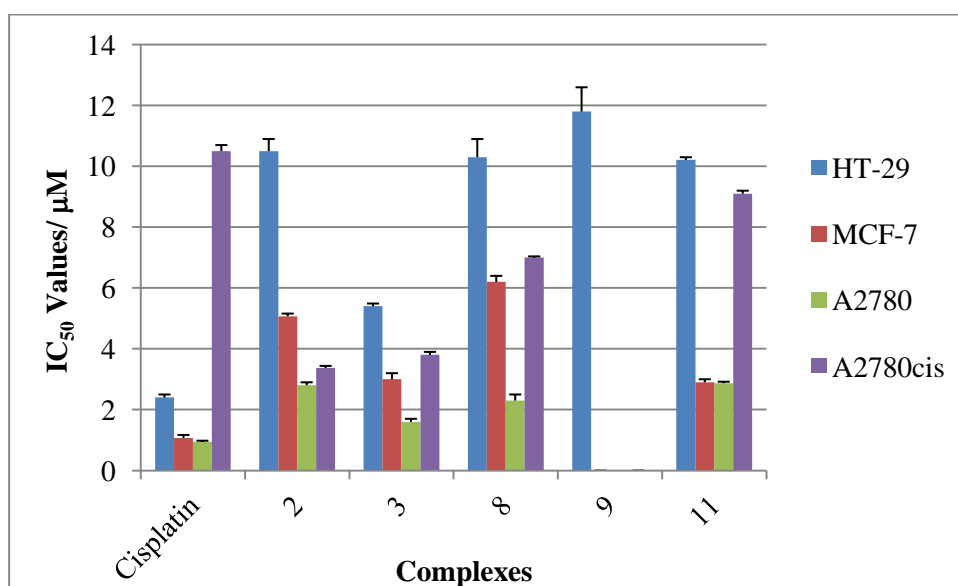


Figure 4.5 Bar-chart showing comparisons with the *para* ruthenium complexes

There is no overall trend seen with most cell lines but it appears the *para* chloro- β -ketoiminate complex (**3**) has the most potential against all four cell lines. When considering the cytotoxicities against the cisplatin resistant ovarian A2780cis it can be seen there is a slight trend, with the most electron withdrawing fluoro complex (**2**) having the highest activity and this activity decreases down the periodic table, with all complexes showing higher activity than cisplatin. The *para* methyl complex (**11**) was synthesised and tested to see if substituting an electron donating group had any effects on the cytotoxicity. In most cases this complex had similar activity to the electron withdrawing substituents, except against MCF-7, where complex **11** gave the highest cytotoxicity. A larger library of compounds must be synthesised to gain more conclusive structure activity relationships, but so far this data suggests there is a limited relationship between the electronics of the complex and its cytotoxic behaviour.

4.6 Conclusion

The library of ruthenium chloride complexes characterised in Chapter 3 has been tested under normoxic (21% O₂) conditions using the well know MTT assay. This enables measurements of cytotoxic behaviour and gives an indication of the complexes potential as an anti-cancer compound. The assays, data manipulation and evaluation of results have been completed by the author at the Institute of Cancer Therapeutics, Bradford. The library tested shows that these (*N,O*) β -ketoiminate ruthenium (II) chloride complexes have moderate to high cytotoxicity behaviour, with some of the complexes showing great potential for future biological studies, which will be discussed in Chapters 6 and 7. These easily tuneable complexes allow for a wider library to be synthesised and future work would require a larger library to be tested in order to gain more extensive structure activity relationships and to optimise the potential of these complexes.

4.7 References

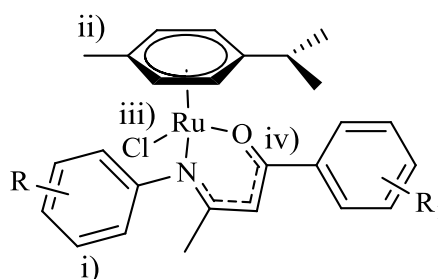
1. T. Mosmann, *J. Immunol. Meth.*, 1983, **65**, 55-63.
2. T. F. Slater, B. Sawyer and U. D. Strauli, *Biochim. Biophys. Acta*, 1963, **77**, 383-393.
3. T. Mosmann, *J. Immunol. Meth.*, 1983, **65**, 55.
4. R. D. Lillie, *H. J. Conn's Biological Stains*, Willians and Wilkins, Baltimore, 1977.
5. D. T. Vistica, P. Skehan, D. Scudiero, A. Monks, A. Pittman and M. R. Boyd, *Cancer Res.*, 1991, **51**, 2515-2520.
6. D. T. Vistica, P. Skehan, D. Scudiero, A. Monks, A. Pittman and M. R. Boyd, *Cancer Res.*, 1991, **51**, 2515.
7. A. G. E. Pearse, *Histochemistry, Theoretical and Applied*, Churchill Livingstone, Edinburgh, 1972.
8. K. D. Paull, R. H. Shoemaker, M. R. Boyd, J. L. Parsons, P. A. Risbood, W. A. Barbera, M. N. Sharma, D. C. Baker, E. Hand, D. A. Scudiero, A. Monks, M. C. Alley and M. Grote, *J. Heterocycl. Chem.*, 1988, **25**, 911-914.
9. D. A. Scudiero, R. H. Shoemaker, K. D. Paull, A. Monks, S. Tierney, T. H. Nofziger, M. J. Currens, D. Seniff and M. R. Boyd, *Cancer Res.*, 1988, **48**, 4827-4833.
10. P. A. Knauf and A. Rothstein, *J. Gen. Physiol.*, 1971, **58**, 211.
11. P. A. Knauf and A. Rothstein, *J. Gen. Physiol.*, 1971, **58**, 190.
12. P. Skehan, R. Storeng, D. Scudiero, A. Monks, J. McMahon, D. Vistica, J. T. Warren, H. Bokesch, S. Kenney and M. R. Boyd, *J. Natl. Cancer Inst.*, 1990, **82**, 1107-1112.
13. B. D. Crossley, Ph. D Thesis, University of Leeds, 2011.
14. J. J. Mannion, Ph. D Thesis, University of Leeds, 2008.

Chapter 5

Synthesis, Characterisation and Cytotoxic Evaluation of Modified Ruthenium Complexes

5 Modified Complexes

Previously in Chapters 3 and 4, a range of β -ketoiminate ruthenium(II) chloride complexes were synthesised and showed very promising cytotoxic behaviour, with many values comparable or higher than cisplatin against A2780cis. Due to the success of these complexes, an effort has been made to tune the structure of the complexes by either;

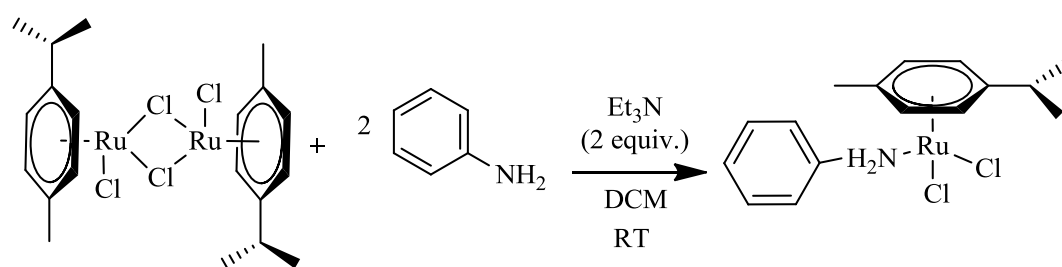


- i) eliminating part of the ligand
- ii) altering the sterics of the arene ring
- iii) changing the metal centre, or
- iv) changing the binding mode of the ligand.

This chapter discusses the synthesis, characterisation and cytotoxic behaviour of these complexes, with comparisons made to the previous complexes, discussed in Chapter 4.

5.1 Synthesis of Aniline Ruthenium (II) Dichloride (14)

It was postulated that the T-stacking interactions commonly seen with the aniline ring may be key for the compounds activity. Complex **14** was synthesised to eliminate the β -ketoiminate ligand. The synthesis of this complex was reported in 2006 by Govindaswamy *et al.* but for the purpose of cytotoxic comparisons has been resynthesised by the author.¹ This complex was synthesised according to **Scheme 5.1**, where $[p\text{-cymRuCl}_2]_2$ was added to aniline and Et_3N in dichloromethane.



Scheme 5.1 Synthetic route to complex **14**

5.1.1 X-ray Characterisation of C₁₆H₂₁Cl₂NRu (14)

Red fragments of **14** suitable for X-ray crystallographic analysis were obtained using slow evaporation from a methanolic solution over a period of several days. The molecular structure is shown in **Figure 5.1** and selected bond lengths and angles are stated in **Table 5.1**. Complex **14** crystallised in a triclinic cell and structural solution was performed in the space group $P\bar{1}$, with a single molecule in the asymmetric unit.

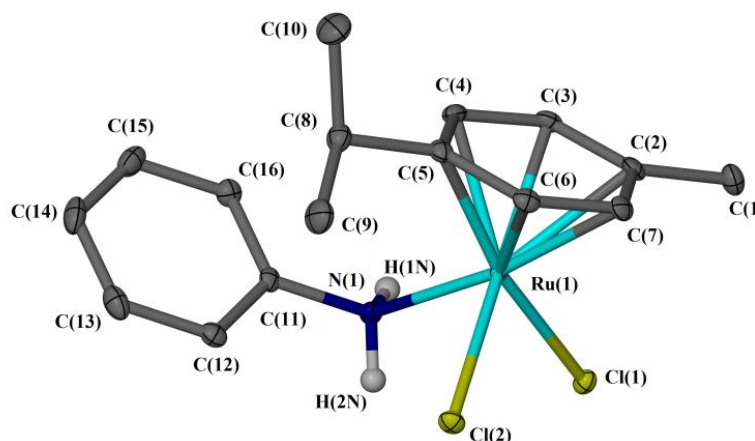


Figure 5.1 Molecular structure of **14**, displacement ellipsoids are at the 50% probability level and hydrogen atoms are omitted for clarity.

Table 5.1 Selected bond lengths and angles for **14**

Bond	Distance (Å)	Bond	Angle (°)
Ru(1)-N(1)	2.1932(13)	Cl(1)-Ru(1)-Cl(2)	87.70(1)
Ru(1)-Cl(1)	2.4407(5)	N(1)-Ru(1)-Cl(1)	80.23(4)
Ru(1)-Cl(2)	2.4250(5)	N(1)-Ru(1)-Cl(2)	83.80(4)
Ru(1)-Cg(1)	1.6684(7)	Cg(1)-Ru(1)-N(1)	132.29(4)
		Cg(1)-Ru(1)-Cl(1)	128.55(2)
		Cg(1)-Ru(1)-Cl(2)	127.62(3)

The packing diagram along the *a* axis shows the molecules pack head-tail and alternate in each plane, with intermolecular N-H...Cl holding the two pairs in the head-tail-tail-head arrangement and the C-H...Cg interactions between each plane. When viewed along the *c* axis two hydrogen's of the NH₂ form N-H...Cl interaction with adjacent molecules giving a head-tail-tail-head arrangement. There is one intramolecular interaction seen between the *p*-cymene CH₃ and the centroid of the

aniline ring. The intermolecular interactions and packing diagrams are presented in **Figure 5.2**, with D...A distances stated in **Table 5.2**.

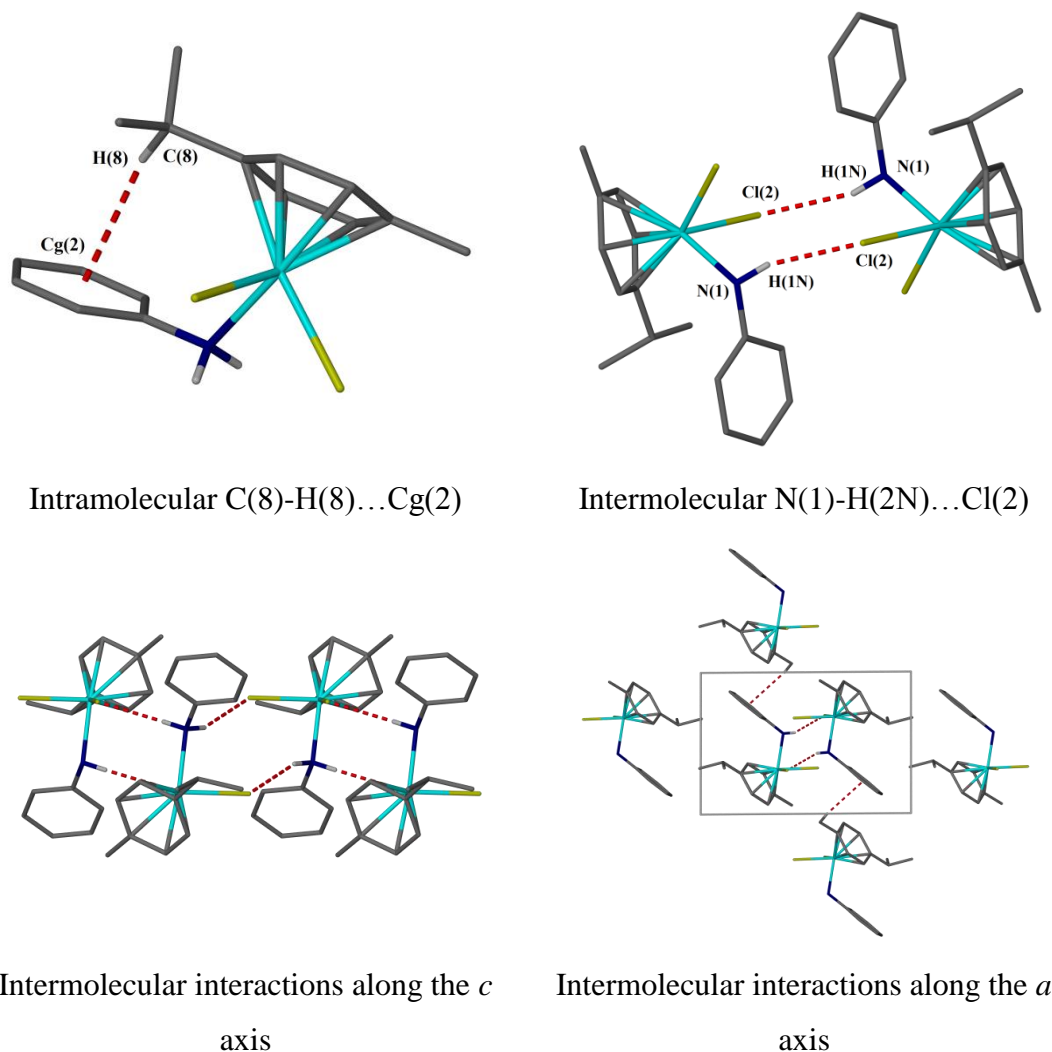


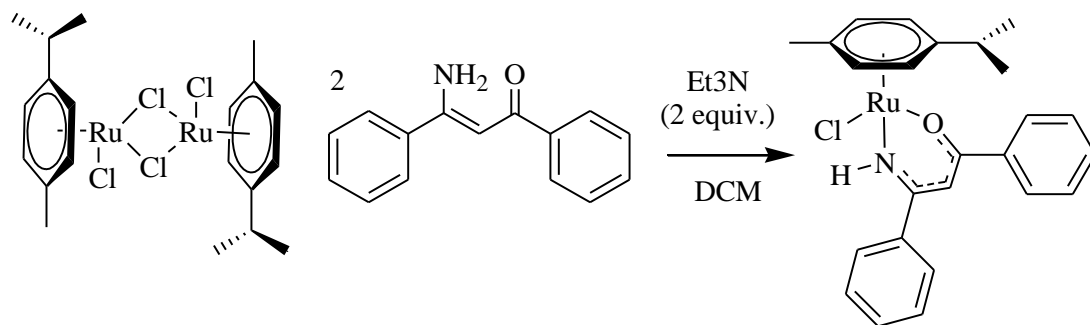
Figure 5.2 Interactions and packing diagrams along the *c* and *a* axes for **14**

Table 5.2 Bond lengths for complex **14**

Interaction	Atoms	Bond Lengths and Angles
Intramolecular	C(8)-H(8)...Cg(2)	3.7156 Å
Intermolecular	C(1)-H(1C)...Cg(2)	3.8084 Å
	Ru(1)-Cl(1)...Cg(1)	1.6684 Å
	N(1)-H(1N)...Cl(1)	3.2954(17) Å
	N(1)-H(2N)...Cl(2)	3.3424(16) Å
	C(7)-H(7)...Cl(1)	3.7261(16) Å
	C(12)-H(12)...Cl(1)	3.5939(17) Å

5.2 Synthesis of Diphenyl β -Ketoiminate Ruthenium(II) Chloride (**15**)

This complex was designed to move the position of the phenyl ring of the aniline group and so comprises of an β -ketoiminate ligand with the ligand binding *via* a NH. Complex **15** was synthesised according to **Scheme 5.2**, where $[p\text{-cymRuCl}_2]_2$ was added to the diphenyl β -ketoiminate ligand and Et_3N in dichloromethane.



Scheme 5.2 Synthetic route to complex **15**

5.2.1 X-ray Characterisation of $\text{C}_{25}\text{H}_{26}\text{ClNORu}$ (**15**)

Red fragments of **15** suitable for X-ray crystallographic analysis were obtained using slow evaporation from a methanolic solution over a period of several days. The molecular structure is shown in **Figure 5.3** and selected bond lengths and angles are stated in **Table 5.3**. Complex **15** crystallised in a monoclinic cell and structural solution was performed in the space group $P2_1/c$, with a single molecule in the asymmetric unit.

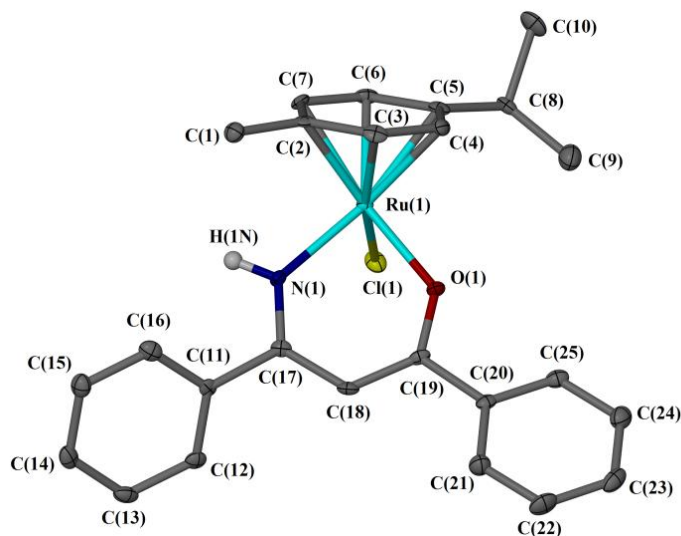


Figure 5.3 Molecular structure of **15**, displacement ellipsoids are at the 50% probability level and hydrogen atoms are omitted for clarity.

Table 5.3 Selected bond lengths and angles for **15**

Bond	Distance (Å)	Bond	Angle (°)
Ru(1)-N(1)	2.052(3)	N(1)-Ru(1)-O(1)	87.52(11)
Ru(1)-O(1)	2.058(3)	N(1)-Ru(1)-Cl(1)	86.25(8)
Ru(1)-Cl(1)	2.4413(10)	O(1)-Ru(1)-Cl(1)	85.80(8)
Ru(1)-Cg(1)	1.6481(17)	Cg(1)-Ru(1)-O(1)	126.41(10)
		Cg(1)-Ru(1)-N(1)	129.40(10)
		Cg(1)-Ru(1)-Cl(1)	127.19(6)

The packing diagrams show the molecules pack in head-tail-tail-head pairs on all axes, with intermolecular C-H...Cl interactions holding the molecules together. When viewed along the *c* axis intermolecular T-stacking interactions can be seen between the *p*-cymene and the centroid of the aromatic ring C(10)-H(10B)...Cg(2), these interactions hold two planes of molecules together. The intermolecular interactions and packing diagrams are presented in **Figure 5.4**, with D...A distances and torsion angles stated in **Table 5.4**.

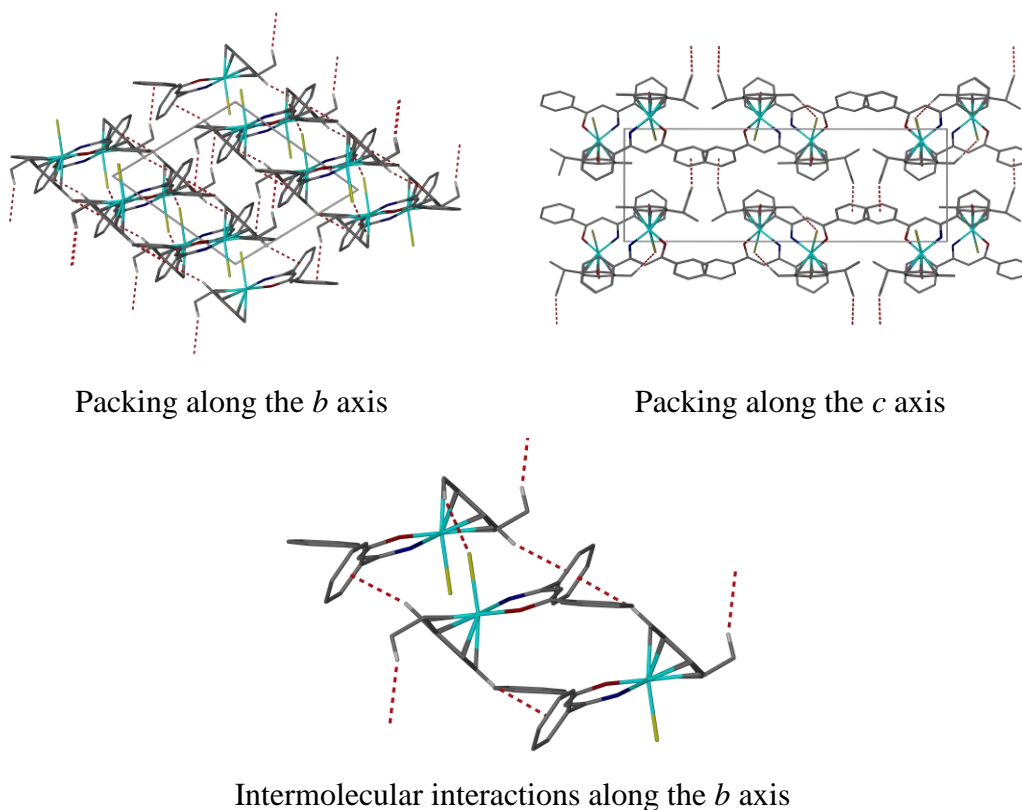
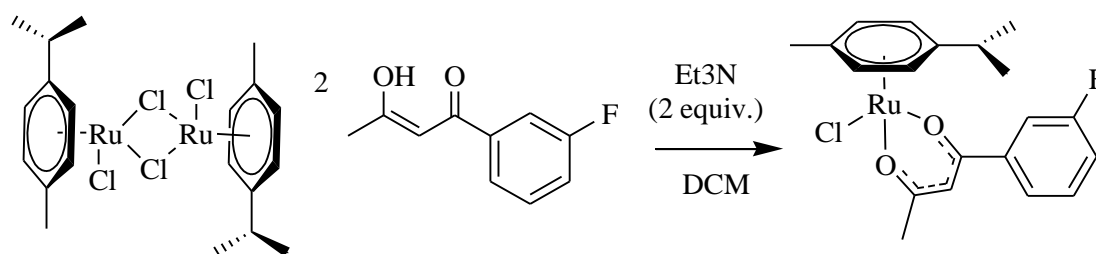
**Figure 5.4** Packing diagrams showing intermolecular interactions along the *b* and *c* axes for **15**

Table 5.4 Bond lengths and torsion angles for **15**

Interaction	Atoms	Bond Lengths and Angles
Intermolecular	C(3)-H(3)...Cg(2)	3.633 Å
	C(6)-H(6)...Cg(2)	3.553 Å
	C(10)-H(10C)...Cg(3)	3.628 Å
	C(1)-H(1B)...Cl(1)	3.629(4) Å
Torsion	Cg(2)-Centre	77.28°
	Centre-Cg(3)	29.31°

5.3 Synthesis of β -Diketonate Ruthenium(II) Chloride (**16**)

It was seen during synthesis that the β -ketoiminate ligands can sometimes dissociate back to the starting β -diketonate ligand. Complex **16** was synthesised to incorporate the starting ligand. As the previous chapters shows that the *meta* fluoro β -ketoiminate ruthenium complex (**1**) was active against all four cell lines, the *meta* fluoro β -diketonate ruthenium (II) chloride complex was synthesised. Complex **16** was synthesised according to **Scheme 5.3**, where $[p\text{-cymRuCl}_2]_2$ was added to the *meta* fluoro β -diketonate ligand and Et₃N in dichloromethane.

**Scheme 5.3** Synthetic route to complex **16**

5.3.1 X-ray Characterisation of C₂₀H₂₆ClO₂Ru (**16**)

Orange plates of **16** suitable for X-ray crystallographic analysis were obtained using slow evaporation from a methanolic solution over a period of several days. The molecular structure is shown in **Figure 5.5** and selected bond lengths and angles are stated in **Table 5.5**. Complex **16** crystallised in a monoclinic cell and structural solution was performed in the space group $P2_1/c$, with a single molecule in the asymmetric unit.

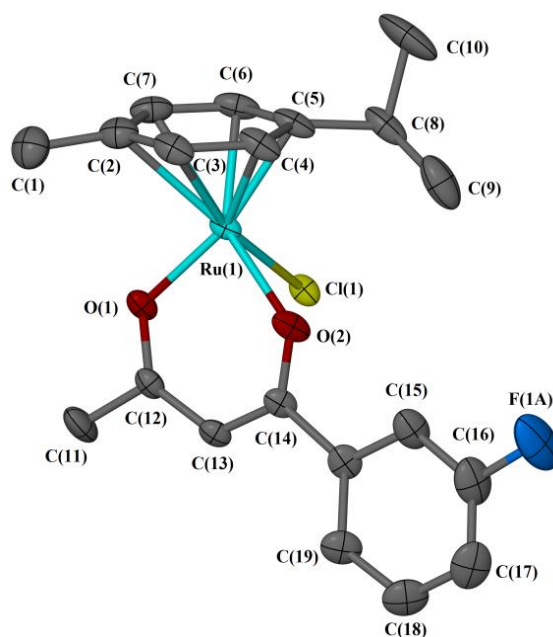
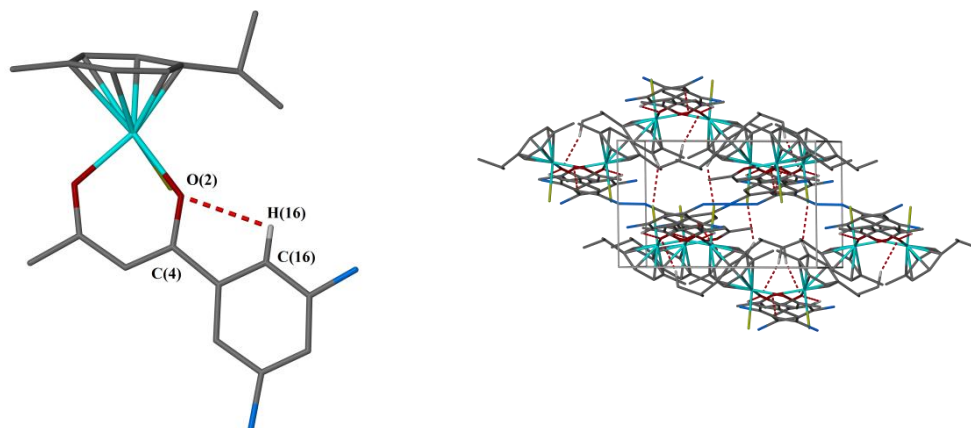


Figure 5.5 Molecular structure of **16**, displacement ellipsoids are at the 50% probability level and hydrogen atoms are omitted for clarity.

Table 5.5 Selected bond lengths and angles for **16**

Bond	Distance (Å)	Bond	Angle (°)
Ru(1)-O(1)	2.069(2)	O(1)-Ru(1)-O(2)	85.21(9)
Ru(1)-O(2)	2.217(2)	O(1)-Ru(1)-Cl(1)	87.76(7)
Ru(1)-Cl(1)	2.5340(8)	O(2)-Ru(1)-Cl(1)	65.31(7)
Ru(1)-Cg(1)	1.8681(15)	Cg(1)-Ru(1)-O(1)	123.30(8)
C(16)-F(1A)	1.395(6)	Cg(1)-Ru(1)-O(2)	139.34(8)
		Cg(1)-Ru(1)-Cl(1)	135.39(5)

The packing diagram show the molecules pack in pairs with intermolecular interactions holding the molecules together and when viewed along the *c* axis this gives a herringbone arrangement. There are also intermolecular interactions between C-H...Cl which holds the molecules between each plane. The intramolecular interaction and packing diagrams are presented in **Figure 5.6**, with D...A distances and torsion angles stated in **Table 5.6**.



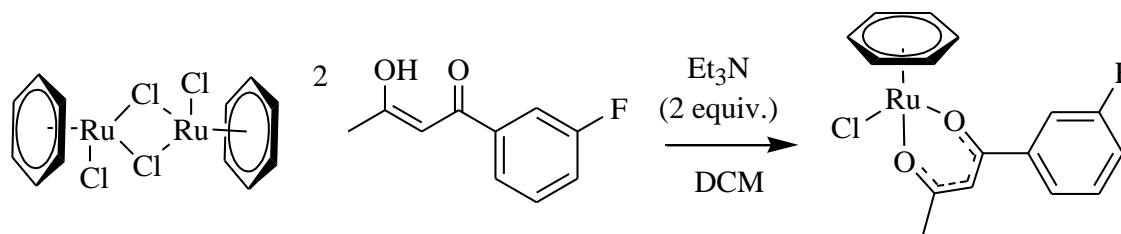
Intramolecular C(16)-H(16)...O(2)

Packing along the *c* axis**Figure 5.6** Intramolecular interactions and packing diagrams for **16****Table 5.6** Bond lengths and torsion angles for **16**

Interaction	Atoms	Bond Lengths and Angles
Intramolecular	C(16)-H(16)...O(2)	2.917(5) Å
Intermolecular	C(18)-H(18)...O(1)	2.951(5) Å
	C(3)-H(3)...Cl(1)	3.323(3) Å
	C(10)-H(10A)...O(2)	3.449(7) Å
	C(7)-H(7)...Cg(1)	3.585 Å
Torsion	Centre-Cg(2)	1.30°

5.4 Synthesis of β -Ketoiminate Ruthenium Arene Chloride (**17**)

Complex **17** was synthesised to incorporate the *meta* fluoro β -diketonate and the *p*-cymene ligand is substituted for an phenyl ring. Complex **17** was synthesised according to **Scheme 5.3**, where [areneRuCl₂]₂ was added to the *meta* fluoro β -diketonate ligand and Et₃N in dichloromethane.

**Scheme 5.4** Synthetic route to complex **17**

5.4.1 X-ray Characterisation of C₁₆H₁₄ClFO₂Ru (17)

Orange plates of **17** suitable for X-ray crystallographic analysis were obtained using slow evaporation from a methanolic solution over a period of several days. The molecular structure is shown in **Figure 5.7** and selected bond lengths and angles are stated in **Table 5.7**. Complex **17** crystallised in a monoclinic cell and structural solution was performed in the space group $P2_1/c$, with a single molecule in the asymmetric unit.

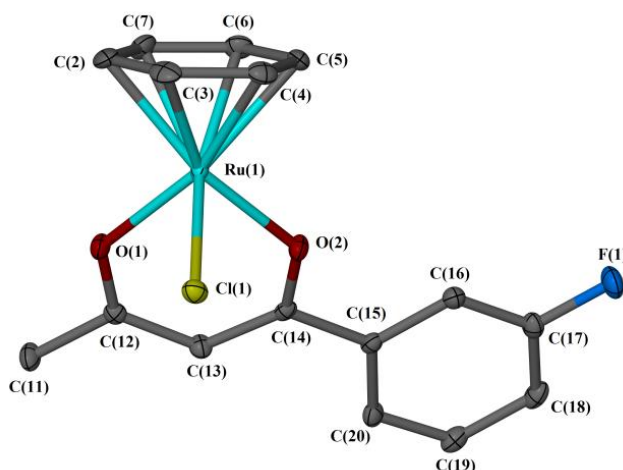


Figure 5.7 Molecular structure of **17** displacement ellipsoids are at the 50% probability level and hydrogen atoms are omitted for clarity.

Table 5.7 Selected bond lengths and angles for **17**

Bond	Distance (Å)	Bond	Angle (°)
Ru(1)-O(1)	2.0689(18)	O(1)-Ru(1)-O(2)	88.62(7)
Ru(1)-O(2)	2.0622(19)	O(1)-Ru(1)-Cl(1)	84.82(5)
Ru(1)-Cl(1)	2.4148(7)	O(2)-Ru(1)-Cl(1)	86.10(5)
Ru(1)-Cg(1)	1.6403(12)	Cg(1)-Ru(1)-O(1)	128.34(7)
C(17)-F(1A)	1.358(3)	Cg(1)-Ru(1)-O(2)	126.51(7)
		Cg(1)-Ru(1)-Cl(1)	128.22(5)

The packing diagram shows the molecules pack in a head-tail-tail-head arrangement along the a axis, with intermolecular C-H...Cl interactions between each plane of atoms. The intramolecular interaction and packing diagrams are presented in **Figure 5.8**, with D...A distances and torsion angles stated in **Table 5.8**.

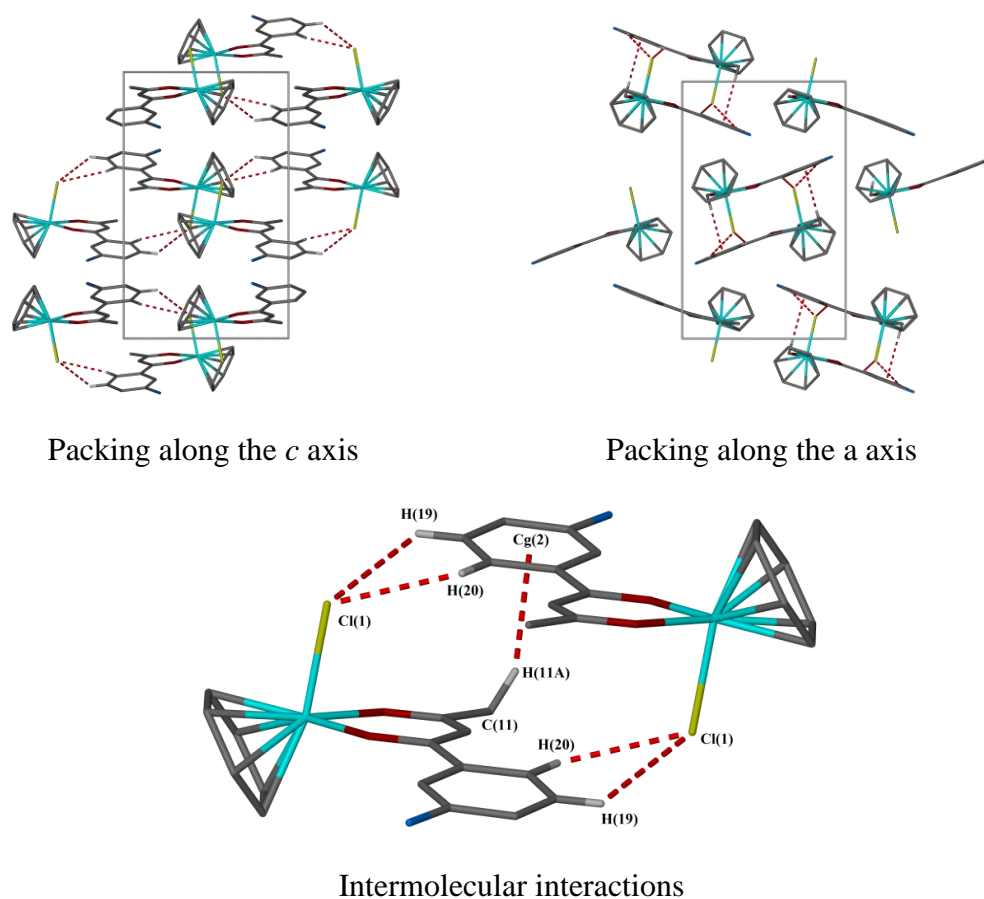


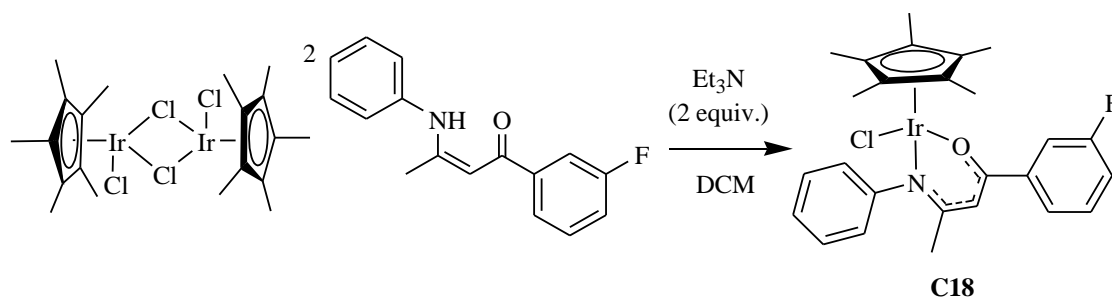
Figure 5.8 Intramolecular interactions and packing diagrams for **17**

Table 5.8 Bond lengths and torsion angles for **17**

Interaction	Atoms	Bond Lengths and Angles
Intermolecular	C(11)-H(11A)...Cg(2)	3.607 Å
	C(19)-H(19)...Cl(1)	3.582(3) Å
	C(20)-H(20)...Cl(1)	3.444(3) Å
Torsion	Centre-Cg(2)	9.81(7)°

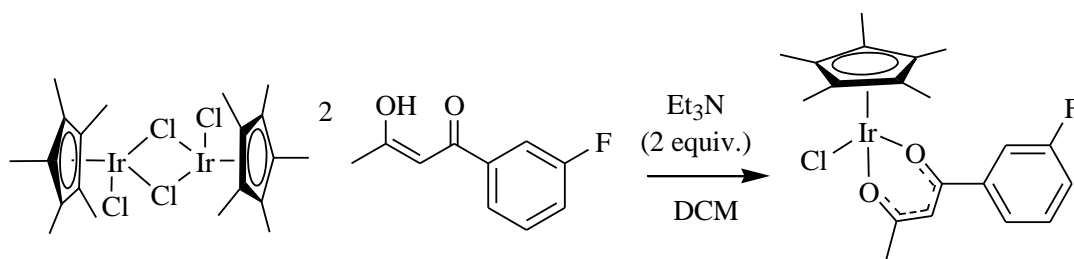
5.5 Synthesis of β -Ketoiminate Iridium Cp* Chloride (C18)

Complex **18** was first synthesised within the research group for its catalytic potential,² as it is analogous to complex **1** it was tested for its cytotoxic potential. It was synthesised according to **Scheme 5.5**, initial cytotoxic results have since been published³ and it is stated within this chapter as future cytotoxic and biological studies have been assessed using this complex.

Scheme 5.5 Synthetic route to **18**³

5.6 Synthesis of β -Diketonate Iridium Cp* Chloride (**19**)

Complex **19** was synthesised as it is analogous to complex **C16** and allows comparisons to be made between binding modes of the ligands and changing the metal source. Complex **19** was synthesised according to **Scheme 5.6**, where $[\text{Cp}^*\text{IrCl}_2]_2$ is added to the 3-fluoro β -diketonate ligand and Et_3N in dichloromethane.

Scheme 5.6 Synthetic route to complex **19**

5.6.1 X-ray Characterisation of $\text{C}_{20}\text{H}_{26}\text{ClINORu}$ (**19**)

Yellow fragments of **19** suitable for X-ray crystallographic analysis were obtained using slow evaporation from a methanolic solution over a period of several days. The molecular structure is shown in **Figure 5.9** and selected bond lengths and angles are stated in **Table 5.9**. Compound **19** crystallised in an orthorhombic cell and structural solution was performed in the space group $P2_12_12_1$, with a single molecule in the asymmetric unit.

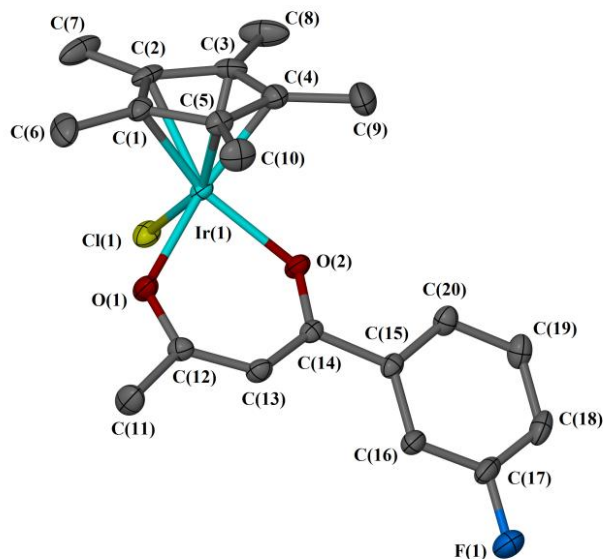
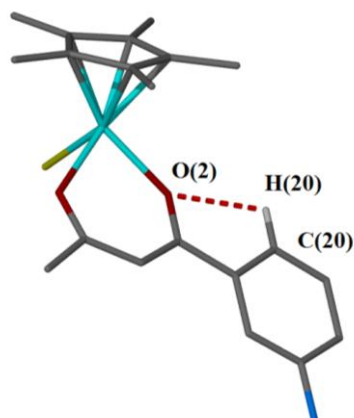


Figure 5.9 Molecular structure of **19**, displacement ellipsoids are at the 50% probability level and hydrogen atoms are omitted for clarity.

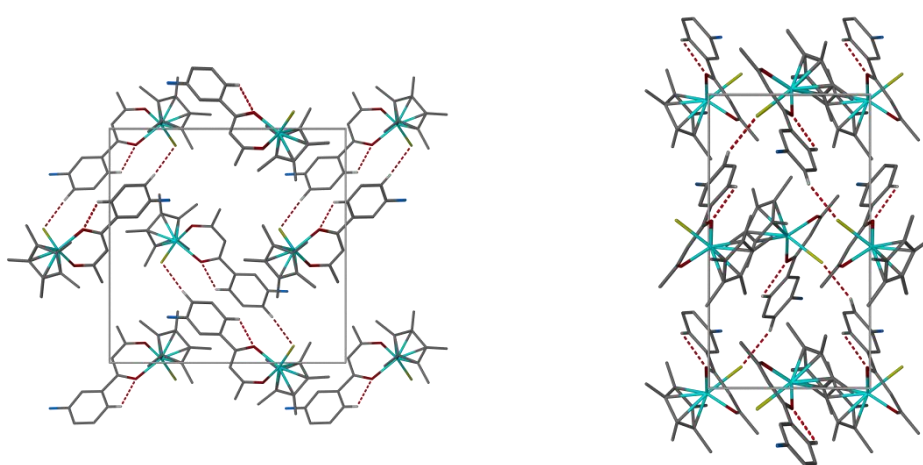
Table 5.9 Selected bond lengths and angles for **19**

Bond	Distance (Å)	Bond	Angle (°)
Ir(1)-O(1)	2.1177(16)	O(1)-Ir(1)-O(2)	85.94(5)
Ir(1)-O(2)	2.1270(12)	O(1)-Ir(1)-Cl(1)	86.10(4)
Ir(1)-Cl(1)	2.4412(6)	O(2)-Ir(1)-Cl(1)	87.34(4)
Ir(1)-Cg(1)	1.7711(10)	Cg(1)-Ir(1)-O(1)	125.31(5)
		Cg(1)-Ir(1)-O(2)	129.07(5)
		Cg(1)-Ir(1)-Cl(1)	128.69(3)

The packing diagram show the molecules pack in pairs with intermolecular interactions holding the molecules together and when viewed along both the *a* and *c* axes the molecules have a herringbone arrangement, with intermolecular C-H...Cl interactions holding pairs of molecules together. The intramolecular interaction and packing diagrams are presented in **Figure 5.10**, with D...A distances and torsion angles stated in **Table 5.10**.



Intramolecular C(20)-H(20)...O(2)

Packing along the *a* axisPacking along the *c* axis**Figure 5.10** Intramolecular interactions and packing diagrams for **19****Table 5.10** Bond angles and torsion angles for **19**

Interaction	Atoms	Bond Lengths and Angles
Intramolecular	C(20)-H(20)...O(2)	2.729(2) Å
Intermolecular	Ir(1)-Cl(1)...Cg(1)	1.7711 Å
	C(18)-H(18)...Cl(1)	3.707(2) Å
Torsion	Centre-Cg(2)	4.49°

5.7 Cytotoxic Evaluation

After the success of the complexes stated in Chapter 4, this small library of complexes has been synthesised and their cytotoxic potential evaluated. The complexes were assessed using the MTT assay used previously and were again incubated using the same 5-day incubation period at 37°C under a 5.0% CO₂ concentration (see protocol in Chapter 9). The IC₅₀ values are stated in **Table 5.11** and have also been summarised as a bar-chart in **Figure 5.11**. When considering complex **14** it appears to be essential to have the β -ketoiminate ligand bound, as this aniline bound complex is completely inactive. The cytotoxic values were obtained against HT-29 and A2780 and due to having IC₅₀ values > 100 μ M, this complex was not tested against the other cell lines. Also when considering **15**, this has a β -ketoiminate ligand bound to the ruthenium but the aniline ring has been eliminated and instead bound by the N-H. It can be seen from **Table 5.11** this complex has a two-fold increase in activity when compared to complex **14**, however it still remains relatively inactive and is not within the same magnitude as the previous complexes seen in Chapter 4.

When changing the ruthenium *p*-cymene (complex **1**) for an iridium Cp* (**18**), the activity of the complex remains high against all four cell lines and like its ruthenium analogue, complex **18** shows the highest cytotoxic values against MCF-7. Complexes **16** and **19** were synthesised to allow comparisons to be made using a different mode of binding, and these complexes incorporate a β -diketonate (*O,O*) ligands. The ruthenium complex **17** is only moderately active against all four cell lines, where the iridium complex **19** is completely inactive. When comparing the same metals using the β -ketoiminate (*N,O*) ligands, complex **1** (*N,O*) is more active than complex **16** (*O,O*), with up to a 9-fold increase in IC₅₀ value against MCF-7 and **18** (*N,O*) is more active than complex **19** (*O,O*), with up to a 18-fold increase in IC₅₀ value against HT-29. In addition, complex **17** was synthesised to assess the importance of the *p*-cymene ligand, this complex is analogous to complex **16** but contains a phenyl arene ligand instead of the *p*-cymene. This complex was tested against both HT-29 and MCF-7 and it can be seen that the activity decreases further, with complex **17** being completely inactive against both lines.

Table 5.11 IC₅₀ values for cisplatin and the complexes synthesised within this chapter, against HT-29, MCF-7, A2780 and A2780cis cell lines

Complex	HT-29		MCF-7		A2780		A2780cis	
	IC ₅₀ (μM)	± SD	IC ₅₀ (μM)	± SD	IC ₅₀ (μM)	± SD	IC ₅₀ (μM)	± SD
Cisplatin	2.4	0.1	1.09	0.08	0.94	0.04	10.5	0.2
14	128	4	-	-	147	8	-	-
15	53	1	-	-	56	2	-	-
1	3.5	0.3	1.9	0.1	2.60	0.08	3.13	0.09
16	18	2	18.4	0.8	19.4	0.8	24.3	0.5
17	68	3	-	-	71	2	-	-
18	5.1	0.3	3.4	0.2	5.7	0.1	5.8	0.5
19	93	7	51	4	35	1	51	1

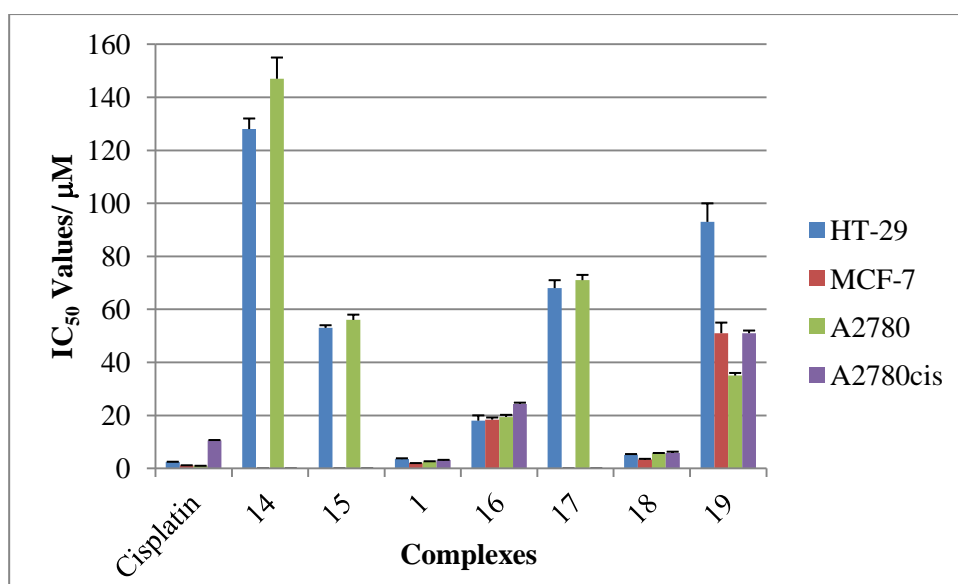


Figure 5.11 Bar-chart of IC_{50} values against HT-29, MCF-7, A2780 and A2780cis

5.8 Conclusion

A small library of complexes have been synthesised in an attempted to understand the key features of the complex which are needed for high *in vitro* activity. The results show that not only is a β -ketoiminate (N,O) ligand essential for high *in vitro* activity, but the ligand must be bound to an aniline substituent. On elimination of this ring or changing the binding mode of the ligand the activity of the complex decreases. The most noticeable results are seen for the iridium complexes where the (N,O) complex **18** has up to a 18-fold increase in activity when compared to the (O,O) complex **19**. These initial results show the β -ketoiminate complexes **1** and **18** are again the most active against all four cell lines tested, showing that high *in vitro* results can be seen with different metals, therefore suggesting the ligand is essential for activity. This library must be extended further to gain more extensive and conclusive structure activity relationships and to understand the key features required to tune the complexes activity.

5.9 Reference

1. P. Govindaswamy and M. R. Kollipara, *J. Coord. Chem.*, 2006, **59**, 131-136.
2. S. J. Lucas, University of Leeds, 2013.
3. S. J. Lucas, R. M. Lord, R. L. Wilson, R. M. Phillips, V. Sridharana and P. C. McGowan, *Dalton Trans.*, 2012, **41**, 13800-13802.

Chapter 6

Cytotoxicity Studies under Hypoxic Conditions

6 Cytotoxicity under Hypoxic Conditions

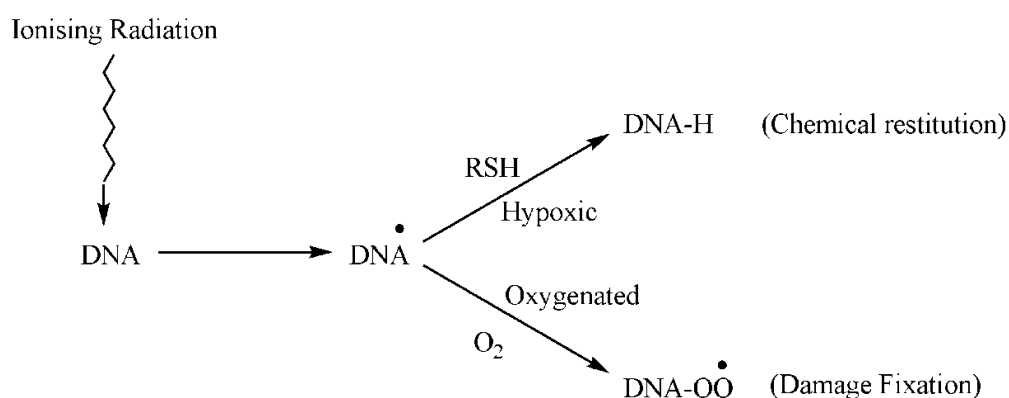
6.1 Hypoxia

Molecular O₂ is essential for aerobic metabolism and to maintain intracellular processes. Hypoxia is defined as an environment of reduced O₂ concentration and occurs in pathological conditions such as strokes, inflammation and growth of solid tumours. The ambient air is 21% O₂, with most mammalian tissues existing between 2-9% O₂. However, hypoxia is defined as $\leq 2\%$ O₂, where severe hypoxia (anoxia) is at $\leq 0.02\%$ O₂.^{1, 2} Early demonstrations of tumour hypoxia were observed in 1955 by Thomlinson and Gray, in which they studied the histology of sections of human tumours and observed that cells grow in cords, having a necrotic core surrounded by a region of viable cells, and proposed the necrosis was due to an insufficient supply of O₂ and nutrients.³ The effects and direct measurements of O₂ in tissues is still poorly understood, due to the lack of methods which are non-invasive, precise and quantitative.⁴ However, many researchers have attempted to study hypoxia by; (i) studying the oxyhaemoglobin of tumours by polarographic electrodes, gaining insight into the regional oxygen environment of the tumour,⁵ (ii) ³¹P NMR spectroscopy studies to monitor metabolism of misonidazole, which selectively binds hypoxic cells⁶⁻⁹ and (iii) using a DNA-binding stain to label cells based on their proximity to the blood supply.¹⁰ The latter was able to differentiate between diffusion-limited (chronic) hypoxia and acute hypoxia, and that cells adjacent to the blood supply may become hypoxic during treatment, concluding that the two types of hypoxia may have different effects on treatment response.

6.2 Effects of Hypoxia on Cancer

The decrease in O₂ concentration has been confirmed to inhibit tumour growth, and even as early as 1909 it was noted that normal cells irradiated under hypoxic/anoxic conditions were less sensitive than those irradiated in the presence of O₂.¹¹ The first studies showing a correlation were using vegetable seeds,¹² but in the 1950s this was quantified in mice studies, both *in vitro* and *in vivo*. Using human embryo liver cells, *in vitro* studies under anoxic conditions exhibited ~2.5 fold greater colony growth after irradiation, when compared to those cultured in air.¹³ More recently it has been proposed that hypoxic cells can be directly targeted using hypoxia-specific cytotoxins. Alongside radiation, this combination has the

potential of destroying the entire tumour population.¹⁴ It was known that exposing cancer cells to hypoxic conditions causes a reduced response to radiotherapy treatment, however it was shown that exposure to oxygen immediately after radiation has no effect on this response.¹⁵ The mechanism of radio-sensitivity is known to be a competition between the oxidation and reduction of the DNA following radiation.¹⁶ A DNA radical is formed, and under normal conditions the DNA is oxidised making the damage permanent. Under hypoxic conditions the DNA is repaired through reduction by a thiol containing protein, as shown in **Scheme 6.1**.



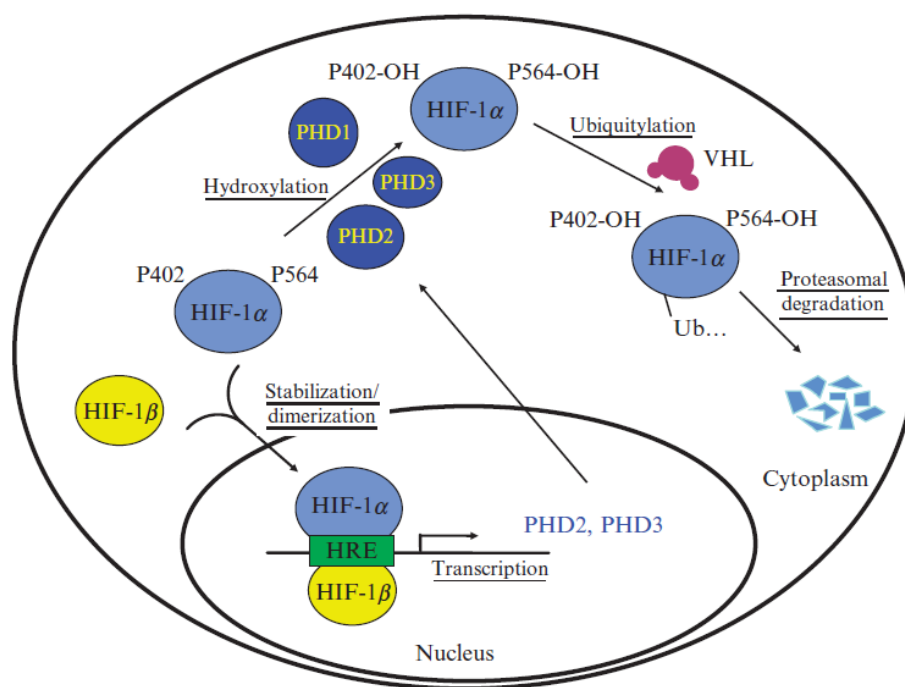
Scheme 6.1 Mechanism of hypoxia-induced resistance of a tumour cell to radiation

Tumours typically contain irregular networks of leaky micro-vessels with heterogeneous blood flow and large inter-vessel distances.¹⁷ Along with the lack of lymphatic drainage and high interstitial pressure, diffusion of nutrients and drugs dominates.¹⁸ The cancer cells are a greater distance from the capillary blood supply, meaning poor tissue penetration of drugs is a large limiting factor in cancer therapy. It has also been found that cell proliferation decreases further from the blood supply, meaning the reduction in division will lead to a decrease in drug activity.^{19, 20}

6.3 Hypoxia-Inducible Factor (HIF)

The hypoxia-inducible factor (HIF) is a transcription factor that responds to changes in available O₂ in cellular environments, in particular decreases in O₂ concentration. HIF-1 is heterodimeric and consists of two subunits; an oxygen-sensitive HIF-1 α and the oxygen-insensitive HIF-1 β . The α subunit is subject to enzymatic modifications by a hydroxylase enzyme and is a target for degradation

in the presence of oxygen. Hypoxia inhibits this activity of the enzyme and leads to accumulation of the α subunit and formation of the active HIF-1.²¹ The HIF-1 α subunit contains two proline residues, which are hydroxylated under normoxic conditions by a family of 4-prolyl hydroxylases. The hydroxylated HIF-1 α can be recognised by the von Hippel-Lindau (VHL) tumour suppressor gene, which further alters the subunit marking it for degradation by the proteasome.²²⁻²⁶ Under hypoxic conditions the hydroxylation of HIF-1 α is inhibited; the subunit is not degraded and instead stabilised by dimerisation with the HIF-1 β . This dimer binds to genes and activates the transcription of products which are involved in tumour survival and proliferation.²⁷⁻³⁰ An overview of HIF-1 regulation is shown in **Scheme 6.2**.

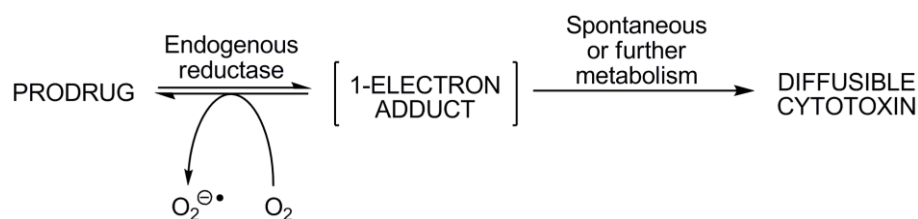


Scheme 6.2 Mechanism of HIF-1 α regulation within the cell³¹

6.4 Hypoxia Targeting Drugs

There has been much interest in the design of tumour-activated prodrugs (TAPs), which are administered as prodrugs and converted to their active form under hypoxic conditions (**Scheme 6.3**). These hypoxia-selective cytotoxins are required to undergo a one-electron reduction from a relatively non-toxic prodrug to a radical which becomes a substrate for re-oxidation by O_2 and reforms the original compound. These compounds are classified as bioreducible and the ability to

bioreduce is an essential feature for a successful hypoxic-selective drugs.³² Some compounds known as hypoxia-activated prodrugs of diffusible cytotoxins (HPDC) have been designed to target the hypoxia region of a tumour and also have the ability to diffuse into surrounding normoxic cells, thereby increasing the overall efficacy of the compounds.³³



Scheme 6.3 Mechanism of pro-drug activation by hypoxia³⁴

6.4.1 Organic Hypoxia-activated Drugs

- **Quinones**

The bioreductive agent mitomycin C (MMC) (**Figure 6.1**) was in clinical use but only in the 1980s it was recognised that the hypoxic environment could facilitate the bioreduction and activate MMC. *In vitro* results were compared to normoxic values and generally a five-fold increase in activity was seen.³⁵⁻³⁸ The one electron reduction produces a semi-quinone radical anion that covalently cross-links with DNA, then in the presence of oxygen is oxidised back to the quinone.^{35, 39, 40} Further investigation into these molecules has led to a methylated analogue known as porfiromycin^{41, 42} and a series of indolequinones,^{43, 44} which have all shown to be superior and when combined with radiotherapy gave promising pre-clinical data in tumour models.⁴⁵

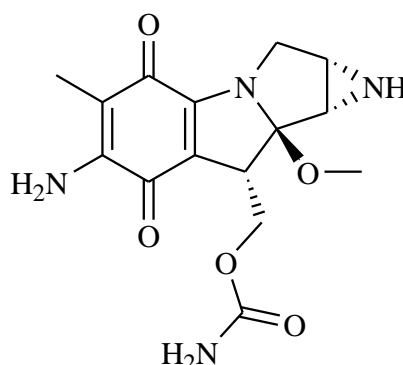


Figure 6.1 Structure of mitomycin C (MMC)

- **Nitroaromatics**

This work initially focused on a hypoxic cell radio-sensitiser misonidazole (**Figure**

6.2) after results showed promising selectivity towards hypoxic cells. These nitroaromatics are bio-reduced *via* stepwise addition of up to six electrons. Misonidazole was found to have a similar or higher hypoxic cytotoxic ratio (HCR) than MMC⁴⁶ and could enhance radiotherapeutic outcome.⁴⁷ A range of compounds including, 2-nitroimidazole,^{48, 49} bis-bioreductive agents (two reducible centre)⁵⁰ and dinitrobenzamide mustards⁵¹ have shown promising results, however, the lead compound PR-104 (Proacta) has been identified and commenced phase I clinical trials in solid tumours.⁵²

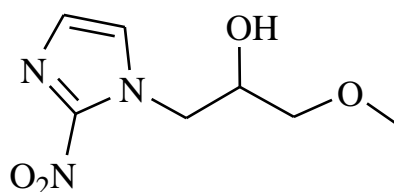


Figure 6.2 Structure of misonidazole

- **Aliphatic N-oxides**

The lead compound in this series is a *bis* N-oxide banoxantrone (AQ4N) (**Figure 6.3**) and is reduced under hypoxic conditions to the cytotoxic AQ4. This compound has high binding affinity for DNA and acts as a topoisomerase II inhibitor and causes cell death.⁵³ Hypoxic selectivity was observed when cultured cells were incubated with NADPH-supplemented microsomes.⁵⁴ When tested *in vivo*, AQ4 had limited effects on tumour growth, however when combined with methods to increase hypoxia, a substantial growth delay was observed.^{55, 56} The data were supported by human tumour xenograph studies with radio- or chemotherapy, showing that the addition of AQ4 gave more persistent damage than with just radiation alone.⁵⁷ Along with other promising results, AQ4 has since entered clinical trials, where phase I combinational studies with cisplatin and phase II studies with radiotherapy are still ongoing in Europe.⁵⁸

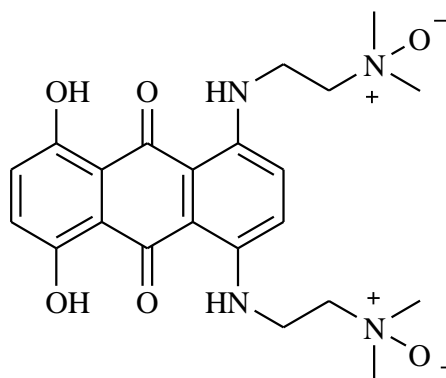
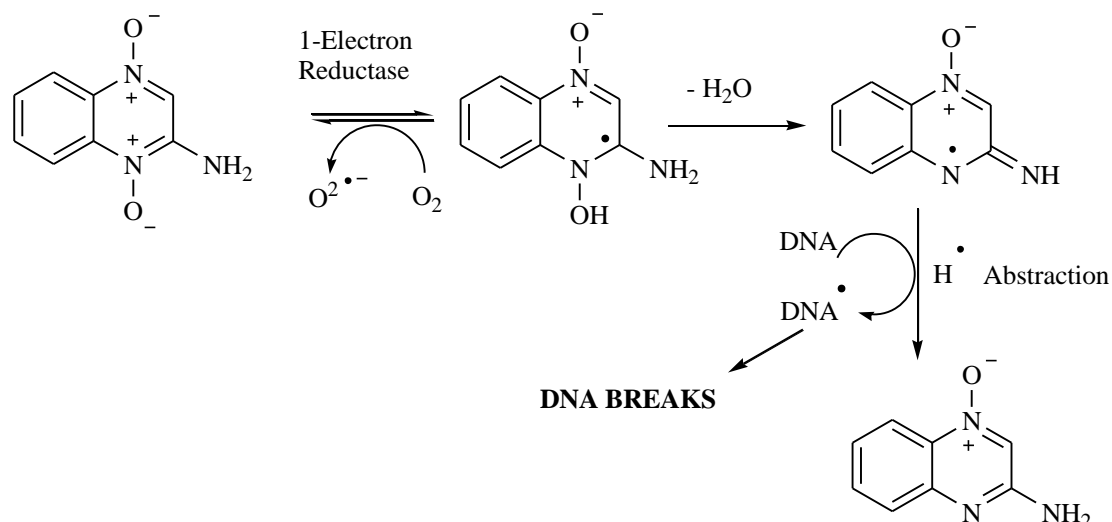


Figure 6.3 Structure of AQ4N

- **Heteroaromatic N-oxides**

The current lead compound of the heteroaromatics, is tirapazamine (TPZ), which was first understood as a hypoxia-selective cytotoxin in the 1980s.⁵⁹ This compound first entered clinical trial in 1994,⁶⁰ and since then there has been nine phase I trials and 15 phase II/III trials. TPZ has shown to be an excellent substrate for one-electron reductases, cytochrome P450 and P450R⁶¹⁻⁶⁵ and NOS.^{66, 67} In the absence of oxygen the nitroxide radical undergoes a rearrangement by the loss of water to form an oxidising radical which causes DNA damage through abstraction of a hydrogen atom.⁶⁸ TPZ has been shown to become increasingly cytotoxic as oxygen levels decrease,⁶⁹ meaning that it can target cells at intermediate oxygen tension but is not sufficiently hypoxic for targeting with other bioreductive drugs.⁷⁰ The most widely used range for TPZ is 260-330 mg/m², with neutropenia reported but in a tolerated range. The most frequent non-haematological toxicities reported are nausea, vomiting, diarrhoea and skin rashes, with the highest dosages showing grade 3-4 toxicities.^{60, 71-74}



Scheme 6.4 Mechanism of hypoxia-activation for tirapazamine

6.4.2 Transition Metal Complexes for Hypoxia

The first TAP compounds based around transition metals utilised DNA-alkylating nitrogen mustard ligands attached to Co(III) centres. These were hoped to stabilise the Co(III) centre and enable reduction to a labile Co(II) under hypoxic conditions, allowing the cytotoxic ligand to dissociate and target the tumour cells (**Figure 6.4**).⁷⁵⁻⁷⁷

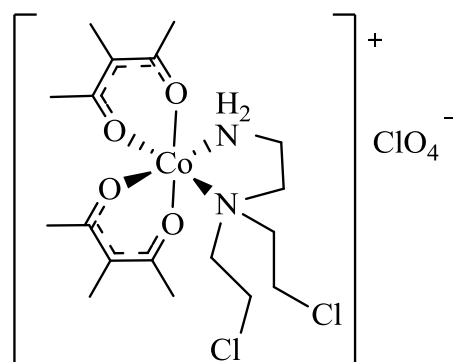


Figure 6.4 Cobalt(III) complex containing bidentate nitrogen mustard ligand

Tetradentate Cu(II) complexes have been synthesised by Parker *et al.* (**Figure 6.5**) which exhibited much greater selectivity than the previous Co(III) complexes. This drug is activated by reduction from Cu(II) to Cu(I). In the presence of oxygen, this process is reversed, the tetradentate ligand stabilises the complexes to avoid dissociation before oxidation back to Cu(II). Under hypoxic conditions the Cu(I) complex is hydrolysed to $[Cu(H_2O)_n]^+$ and the free mustard ligand.⁷⁸

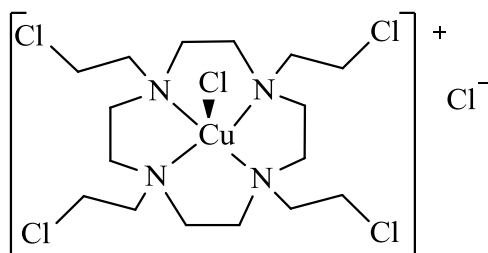


Figure 6.5 Copper(II) complex containing tetradentate nitrogen mustard ligand

Cobalt complexes containing a tetraazamacrocycle and 8-hydroxyquinoline have been studied by Ahn *et al.* (**Figure 6.6**)⁷⁹ and are activated through reduction by ionising radiation. This has advantages over enzyme activation, one being the ability to control precisely where the pro-drug is activated by specific radiation targeting.⁸⁰ Addition of a 8-hydroxyquinoline to the Co(III) reduced the compounds activity by >1000-fold. The cytotoxic ligand is released selectively under hypoxic conditions, when treated with ionising radiation, demonstrating the feasibility of the radiation-activated approach to hypoxia-selective drug design.⁸¹

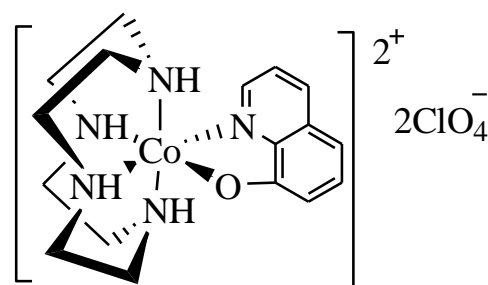


Figure 6.6 Cobalt(III) complex containing 8-hydroxyquinoline

6.5 Conducting the MTT Assay Under Hypoxic Conditions ($\leq 1\% \text{ O}_2$)

This assay was carried out as previously discussed in Chapter 4, with incubation periods carried out in a Don Whitley Scientific H35 Hypoxystation. This was kept at 37°C with an O₂ concentration of either 1.0% or 0.1%. The compounds were made up to an initial concentration of 25 mM using DMSO. Ten different dilutions were made using cell medium, ranging from 250-0.49 μM . The assays uses a 24-hour incubation of the cells within the well plate, followed by addition of the drug dilutions on day two and then a 5-day incubation period. After the 5-day incubation, MTT solution (5 mg/ mL) was added to the plates, incubated for a further 3 hours and then absorbance measured at 540 nm, using a Thermo Scientific Multiskan EX microplate photometer. All IC₅₀ values were taken from

an average of three different assays with good repeatability, any measurements not correlating we repeated until they were within an approximate 10% error. The protocols for this procedure are stated within Chapter 9.

6.6 Results and Discussion

The ruthenium and iridium complexes **1**, **16**, **18** and **19** (**Figure 6.7**) were tested for their cytotoxic potential under hypoxic conditions, at either 1.0% or 0.1% O₂ concentration. These were selected as they showed the largest differences in activity (Chapter 5). These complexes were tested under both O₂ concentrations, as they showed the largest differences in their normoxic values.

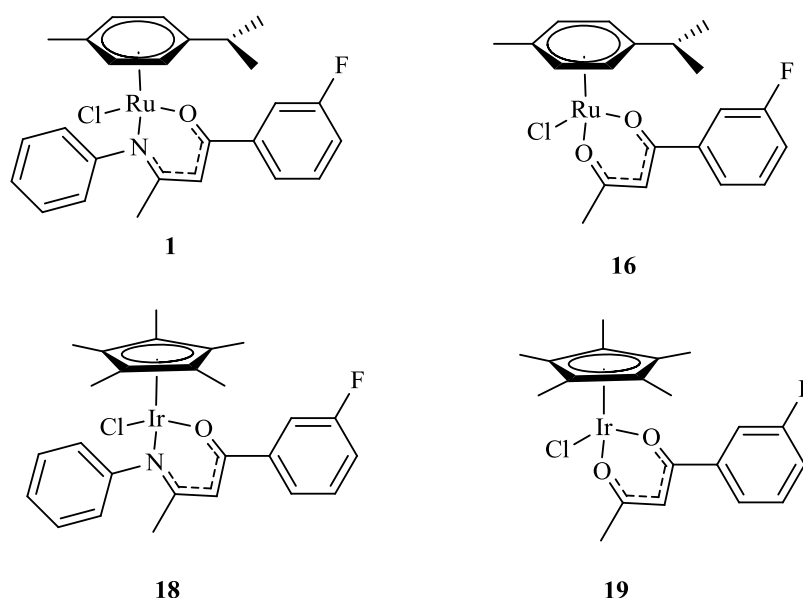


Figure 6.7 List of *meta*-fluoro complexes tested under hypoxic conditions

In addition to these, complexes **2**, **3**, **8**, **9** and **11** were chosen as they have a functional group in the *para* position and the modified complexes **14** and **15** were also tested (**Figure 6.8**). As previously discussed, tirapazamine is a well known hypoxic sensitive compound and was tested under hypoxic conditions to act as a positive control and cisplatin was also tested for completion.

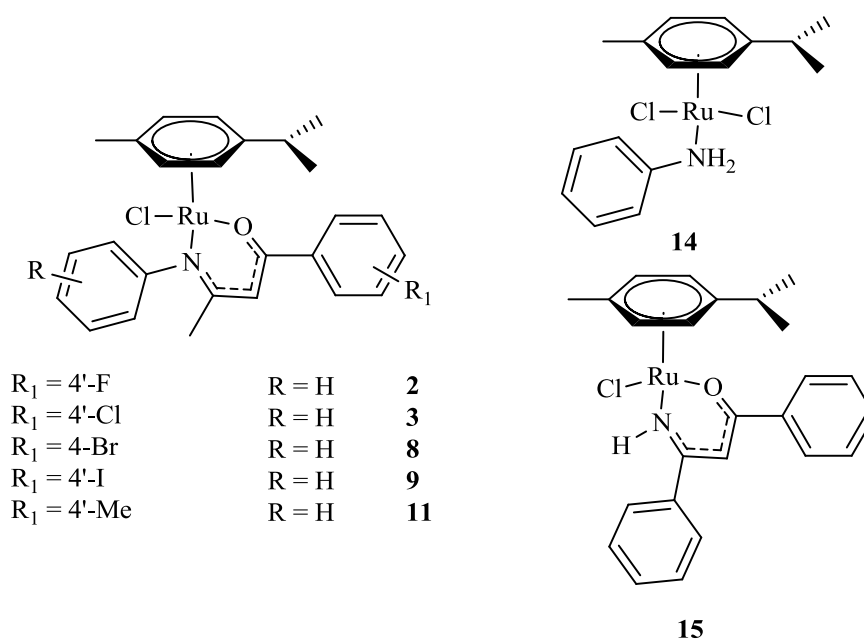


Figure 6.8 List of complexes tested under hypoxic conditions

The results in **Table 6.1** (**Figure 6.9**) show the cytotoxic results for the ruthenium complexes incorporating a β -ketoiminato ligand (**1**) and the β -diketonate ligand (**16**). The table also shows the results for the iridium analogues **18** and **19**. The hypoxic sensitive positive control tirapazamine was tested and as expected its activity increases on a decrease in O_2 concentration. A surprising result was seen for the ruthenium (N,O) complex **1**, which remains highly active even under very low O_2 concentrations. Comparing this to the (O,O) complex **16**, there is a 5-fold decrease in activity on decreasing the O_2 concentration from 21% to 0.1%. The iridium (N,O) complex **18** still remains moderately active even under very low O_2 concentration, but again the (O,O) complex **19** decreases under low O_2 concentrations and becomes completely inactive.

The results in **Table 6.2** (**Figure 6.10**) show the activity of the *para* substituted β -ketoiminato ruthenium complexes synthesised in Chapter 3; their activities all increase on a decrease in O_2 concentration, with up to a 1.8-fold increase in activity seen for complex **2**. This is a very promising result as it shows these complexes are hypoxic sensitive, which is a key feature that researchers strive to achieve with anti-cancer compounds, as the hypoxic environment gives a more realistic idea of the cytotoxic potential. The modified complexes **14** and **15** show only minor differences in IC_{50} on changing the O_2 concentration and these complexes are still

inactive under hypoxic conditions. The results presented both here and in Chapter 4 show that the library of ruthenium β -ketoiminate complexes synthesised in Chapter 3 are not only cytotoxic but activities are further increased under low O₂ concentrations, showing these complexes have the potential for future *in vivo* studies.

Table 6.1 IC₅₀ values for TPZ, cisplatin and complexes **1**, **16**, **18** and **19** in 21%, 1.0% and 0.1% O₂ concentrations

Complexes	21.0% O ₂		1.0% O ₂		0.1% O ₂	
	IC ₅₀ (μM)	± SD	IC ₅₀ (μM)	± SD	IC ₅₀ (μM)	± SD
TPZ	31	3	3.2	0.5	2.4	0.4
Cisplatin	2.4	0.1	3.5	0.2	2.8	0.4
1	3.5	0.3	6.4	0.2	5.7	0.2
16	18	2	62.9	0.3	95	4
18	5.1	0.3	10.6	0.2	20	2
19	93	7	109	2	121	3

Table 6.2 IC₅₀ values for TPZ, cisplatin and complexes **2**, **3**, **8**, **9**, **11**, **14** and **15** in 21% and 0.1% O₂ concentrations

Complexes	21% O ₂		0.1% O ₂	
	IC ₅₀ (μM)	± SD	IC ₅₀ (μM)	± SD
TPZ	31	3	2.4	0.4
Cisplatin	2.4	0.1	2.8	0.4
2	10.5	0.4	5.7	0.2
3	5.40	0.09	4.6	0.3
8	10.3	0.6	5.76	0.09
9	11.8	0.8	7.0	0.1
11	10.21	0.09	6.3	0.3
14	128	4	109	3
15	53	1	57.3	0.7

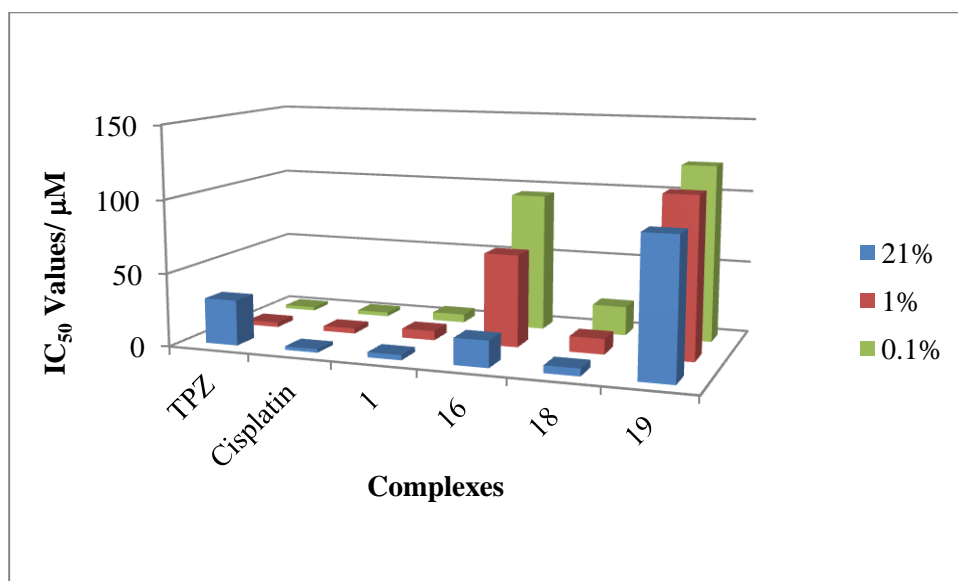


Figure 6.9 Bar-chart of IC₅₀ at differing O₂ concentrations for TPZ, cisplatin, **1**, **16**, **18** and **19**

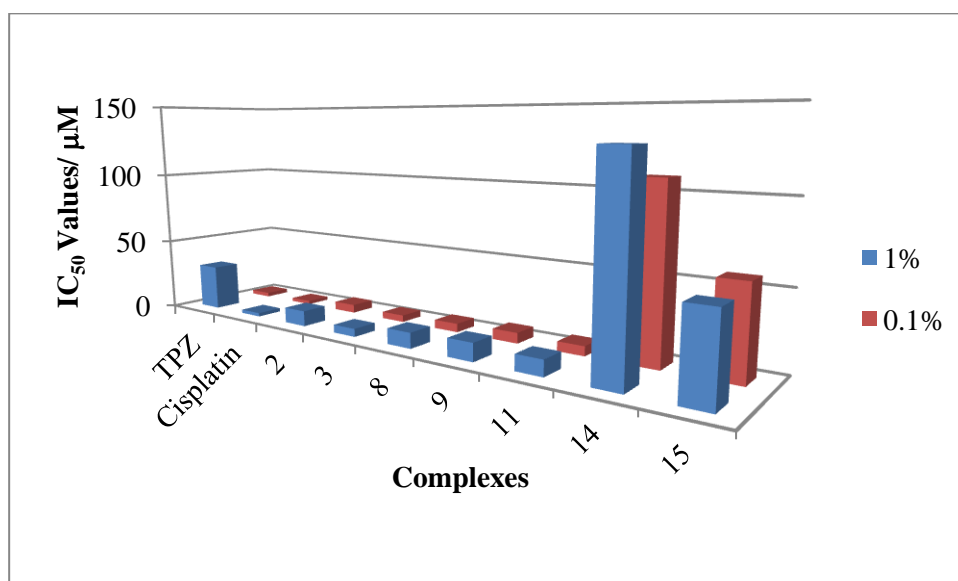


Figure 6.10 Bar-chart of IC₅₀ at differing O₂ concentrations for TPZ, cisplatin, **2**, **3**, **8**, **9**, **11**, **14** and **15**

6.7 Conclusions

This chapter presents *in vitro* cytotoxic values under hypoxic conditions for a small library of complexes synthesised in Chapters 3 and 5. The results for the comparisons between β -ketoiminate and β -diketonate ruthenium complexes (**1** and **16** respectively), shows that **1** remains active even under very low O₂ concentrations, whereas **16** decreases in activity under lower O₂ concentrations. Similar results were seen for the iridium β -ketoiminate and β -diketonate analogues, **18** and **19** respectively. Complex **18** only decreases slightly in activity and is still considered active, whereas **19** becomes completely inactive at 0.1% O₂. These results confirm that the complexes containing a β -ketoiminate ligand are promising candidates for further cell investigations.

Due to the success of **1** and to confirm the results stated above, a second small library of ruthenium β -ketoiminate complexes were tested under a 0.1% O₂ concentration. These consisted of a *para*-substituted ligand to allow comparisons to be made. It could be seen that all of the complexes increased in activity on decreasing the O₂ concentration, with the *para*-fluoro (**2**) giving the most promising result, with up to a 1.8-fold increase in activity. These were tested to prove the need for a β -ketoiminate ligand and show that the library synthesised within Chapter 3 all have the potential for future *in vivo* work, as they are all hypoxia-sensitive, a key feature required for the design of novel anti-cancer drugs.

6.8 References

1. J. A. Bertout, S. A. Patel and M. C. Simon, *Nat Rev Cancer*, 2008, **8**, 967-975.
2. L. H. Gray, A. D. Conger, M. Ebert, S. Hornsey and O. C. A. Scott, *Br. J. Radiol.*, 1953, **26**, 638-648.
3. R. H. Thomlinson and L. H. Gray, *Br. J. Cancer*, 1955, **9**, 539-549.
4. P. Okunieff, B. Fenton and Y. Chen, *Adv. Exp. Med. Biol.*, 2005, **566**, 213-222.
5. P. Veupel, K. Schlenger and M. Hoeckel, *Adv. Exp. Med. Biol.*, 1992, **317**, 139-151.
6. R. C. Urtasun, J. D. Chapman, J. A. Raleigh, A. J. Franko and C. J. Koch, *Int. J. Radiat. Oncol. Biol. Phys.*, 1986, **12**, 1263-1267.
7. R. C. Urtasun, C. J. Koch, A. J. Franko, J. A. Raleigh and J. D. Chapman, *Br. J. Cancer*, 1986, **S4**, 453-457.
8. J. D. Chapman, *Radiother. Oncol.*, 1991, **20**, 13-19.
9. G. Helmlinger, F. Yuan, M. Dellian and R. K. Jain, *Nat. Med.*, 1997, **3**, 177-182.
10. D. J. Chaplin, R. E. Durand and P. L. Olive, *Int. J. Radiat. Oncol. Biol. Phys.*, 1986, **12**, 1279-1282.
11. I. Churchill-Davidson, C. Sanger and R. H. Thomlinson, *Lancet*, 1955, **268**, 1091-1095.
12. E. J. Hall and A. Giaccia, *Radiobiol. Radiolog.*, 2006.
13. D. L. Dewey, *Nature*, 1960, **186**, 780-782.
14. J. M. Brown and A. J. Giaccia, *Int. J. Radiat. Biol.*, 1994, **65**, 95-102.
15. R. J. Hodgkiss, I. J. Roberts, M. E. Watts and M. Woodcock, *Int. J. Radiat. Rel. Studies Phys. Chem. Med.*, 1987, **52**, 735.
16. J. M. Brown, *Nat. Rev. Cancer*, 2004, **4**, 437.
17. K. I. Wijffels, J. H. Kaanders, P. F. Rijken, J. Bussink, F. J. van den Hoogen and H. A. Marres, *Br. J. Cancer*, 2000, **83**, 674-683.
18. R. K. Jain, *Adv. Drug Del. Rev.*, 2001, **46**, 149-168.
19. R. K. Jain, *Nat. Med.*, 1998, **4**, 655-657.
20. I. F. Tannock, *Lancet*, 1998, **351**, 9-16.
21. G. L. Semenza, *Physiology*, 2004, **19**, 176-182.
22. D. A. Chan, *Mol. Cell Biol.*, 2005, **25**, 6415.

23. M. Ivan, K. Kondo, H. Yang, W. Kim, J. Valiando, M. Ohh, A. Salic, J. M. Asara, L. W. S. and W. G. K. Jr, *Science*, 2001, **292**, 464-468.
24. P. Jaakkola, D. R. Mole, Y.-M. Tian, M. I. Wilson, J. Gielbert, S. J. Gaskell, A. v. Kriegsheim, H. F. Hebestreit, M. Mukherji, C. J. Schofield, P. H. Maxwell, C. W. Pugh and P. J. Ratcliffe, *Science*, 2001, **292**, 468-472.
25. N. Masson, C. Willam, P. H. Maxwell, C. W. Pugh and P. J. Ratcliffe, *EMBO*, 2001, **20**, 5197-5206.
26. F. Yu, S. B. White, Q. Zhao and F. L. Lee, *Proc. Natl. Acad. Sci. U.S.A.*, 2001, **98**, 9630-9635.
27. B. Krishnamachary, S. Berg-Dixon, B. Kelly, F. Agani, D. Feldser, G. Ferreira, N. Iyer, J. LaRusch, B. Pak, P. Taghavi and G. L. Semenza, *Cancer Res.*, 2003, **63**, 1138-1143.
28. S. Pennacchietti, P. Michieli, M. Galluzzo, M. Mazzone, S. Giordano and P. M. Comoglio, *Cancer Cell*, 2003, **3**, 347-361.
29. G. L. Semenza, *Intern. Med.*, 2001, **41**, 79-83.
30. C. C. Wykoff, C. W. Pugh, P. H. Maxwell, A. L. Harris and P. J. Ratcliffe, *Oncogene*, 2000, **19**, 6297-6305.
31. D. A. Chan, A. J. Krieg, S. Turcotte and A. J. Giaccia, *Meth. Enzymol.*, 2007, **435**, 323-345.
32. J. M. Brown and W. R. Wilson, *Nat Rev Cancer*, 2004, **4**, 437-447.
33. W. A. Denny and W. R. Wilson, *Cancer Metast. Rev.*, 1993, **12**, 135-151.
34. W. A. Denny, *Eur. J. Med. Chem.*, 2001, **36**, 577-595.
35. R. L. Cowen, A. V. Patterson and B. A. Telfer, *Mol. Cancer Ther.*, 2003, **2**, 901-909.
36. K. A. Kennedy, B. A. Teicher, S. Rockwell and A. C. Sartorello, *Biochem. Pharmacol.*, 1980, **29**, 1-8.
37. S. Rockwell, *Int. J. Cancer*, 1986, **38**, 229-235.
38. I. J. Stratford and M. A. Stephens, *Int. J. Radiat. Oncol. Biol. Phys.*, 1989, **16**, 973-976.
39. Y. Gan, Y. Mo, J. E. Kalns, J. Lu, K. Danenberg, P. Danenberg and M. A. Guill Wientjes, J. L-S, *Clin. Cancer Rev.*, 2001, **7**, 1313-1319.
40. R. D. Traver, T. Horikoshi, K. D. Danenberg, T. H. W. Stadlbauer, P. V. Danenberg, D. Ross and N. W. Gibson, *Cancer Res.*, 1992, **52**, 797-802.

41. P. M. Fracasso and A. C. Sartorello, *Cancer Res.*, 1986, **46**, 3939-3944.
42. S. R. Keyes, S. Rockwell and A. C. Sartorello, *Cancer Res.*, 1987, **47**, 5654-5657.
43. N. Robertson, A. Haigh, G. E. Adams and I. J. Stratford, *Eur. J. Cancer*, 1994, **30A**.
44. S. M. P., M. Jaffar, A. V. Patterson, Nolan J, M. A. Naylor, R. M. Phillips, A. L. Harris and I. J. Stratford, *Biochem. Pharmacol.*, 2000, **59**, 993-996.
45. I. J. Stratford, K. J. Williams, R. L. Cowen and M. Jaffar, *Sem. Radiat. Oncol.*, 2003, **13**, 42-52.
46. Y. C. Taylor and A. M. Rauth, *Br. J. Cancer*, 1980, **41**, 892-900.
47. J. Overgaard and M. R. Horsman, *Overcoming hypoxic cell radio-resistance, 2nd Edition*, Arnold Press, London, 1997.
48. I. J. Stratford, P. O'Neill, P. W. Sneldon, A. R. Silver, J. M. Walling and G. E. Adams, *Biochem. Pharmacol.*, 1986, **35**, 105-109.
49. I. J. Stratford, G. E. Adams, J. Godden and N. Howells, *Int. J. Radiat. Biol.*, 1989, **55**, 411-422.
50. M. V. Papadopoulou and W. D. Bloomer, *Clin. Cancer Rev.*, 2003, **9**, 5714-5720.
51. W. R. Wilson, S. M. Pullen, A. Degenkolbe, D. M. Ferry, N. A. Helsby, K. O. Hicks, G. J. Atwell, S. Yang, W. A. Denny and A. V. Patterson, *Eur. J. Cancer*, 2004, **Suppl. 2**.
52. www.clinicaltrials.gov, *Clinical Trials*, Accessed 10.11.2013.
53. L. H. Patterson and S. R. McKeown, *Br. J. Cancer*, 2000, **83**, 1589-1593.
54. L. H. Patterson, S. R. McKeown, T. Robson, R. Gallagher, S. M. Raleigh and S. Orr, *Anticancer Drug Des.*, 1999, **14**, 473-486.
55. S. R. McKeown, M. V. Hejmadi, I. A. McIntrye, J. J. McAleer and L. H. Patterson, *Br. J. Cancer*, 1995, **72**, 76-81.
56. L. H. Patterson, S. R. McKeown, K. Ruparelia, J. A. Double, M. C. Bibby, S. Cole and I. J. Stratford, *Br. J. Cancer*, 2000, **82**, 1984-1990.
57. M. V. Hejmadi, S. R. McKeown, O. P. Friery, I. A. McIntrye, L. H. Patterson and D. G. Hirst, *Br. J. Cancer*, 1996, **73**, 499-505.
58. S. R. McKeown, R. L. Cowen and K. J. Williams, *Clin. Oncol.*, 2007, **19**, 427-442.

59. E. M. Zeman, J. M. Brown, M. J. Lemmon, V. K. Hirst and W. W. Lee, *Int. J. Radiat. Oncol. Biol. Phys.*, 1986, **12**, 1239-1242.
60. N. Doherty, S. L. Hancock, S. Kaye, C. N. Coleman, L. Shulman, C. Marquez, C. Mariscal, R. Rampling, S. Senan and R. V. Roemeling, *Int. J. Radiat. Oncol. Biol. Phys.*, 1994, **29**, 379-382.
61. A. V. Patterson, H. M. Barham, E. C. Chinje, G. E. Adams, A. L. Harris and I. J. Stratford, *Br. J. Cancer*, 1995, **72**, 1144-1150.
62. A. V. Patterson, M. P. Saunders, E. C. Chinje, L. H. Patterson and I. J. Stratford, *Br. J. Cancer*, 1997, **76**, 1338-1347.
63. A. V. Patterson, M. P. Saunders, E. C. Chinje, L. H. Patterson and I. J. Stratford, *Anticancer Drug Des.*, 1998, **13**, 541-573.
64. M. P. Saunders, A. V. Patterson, E. C. Chinje, A. L. Harris and I. J. Stratford, *Br. J. Cancer*, 2000, **82**, 651-656.
65. S. A. Fitzsimmons, A. D. Lewis, R. J. Riley and P. Workman, *Carcinogenesis*, 1994, **15**, 1503-1510.
66. A. P. Garner, M. J. I. Paine, I. Rodriguez-Crespo, E. C. Chinje, P. R. Ortiz de Montellano, I. J. Stratford, D. G. Tew and C. R. Wolf, *Cancer Res.*, 1999, **59**, 1929-1934.
67. E. C. Chinje, R. L. Cowen, J. Feng, S. P. Sharma, N. S. Wind, A. L. Harris and I. J. Stratford, *Mol. Pharmacol.*, 2003, **63**, 1248-1255.
68. W. A. Denny, *Aus. J. Chem.*, 2004, **57**, 821-828.
69. C. J. Koch, *Cancer Res.*, 1993, **53**, 3992-3997.
70. S. J. Lunt, B. A. Telfer, R. J. Fitzmaurice, I. J. Stratford and K. J. Williams, *Clin. Cancer Res.*, 2005, **11**, 4212-4216.
71. D. J. Lee, A. Trotti, S. Spencer, R. Rostock, C. Fisher, R. von Roemeling, E. Harvey and E. Groves, *Int. J. Radiat. Oncol. Biol. Phys.*, 1998, **42**, 811-815.
72. V. A. Miller, K. K. Ng, S. C. Grant, H. Kindler, B. Pizzo, R. T. Heelan, R. von Roemeling and M. G. Kris, *Ann. Oncol.*, 1997, **8**, 1269-1271.
73. A. Y. Bedikian, S. S. Legha, O. Eton, A. C. Buzaid, N. Papadopoulos, S. Coates, T. Simmons, J. Neefe and R. von Roemeling, *Ann. Oncol.*, 1997, **8**, 363-367.

74. S. Senan, R. Rampling, M. A. Graham, P. Wilson, H. Robin Jr, N. Eckardt, N. Lawson, A. McDonald, R. von Roemeling, P. Workman and S. B. Kaye, *Clin. Cancer Res.*, 1997, **3**, 31-38.
75. D. C. Ware, *J. Med. Chem.*, 1993, **36**, 1839-1846.
76. M. Simic and J. Lillie, *J. Am. Chem. Soc.*, 1974, **96**, 291-292.
77. R. F. Anderson, W. A. Denny, D. C. Ware and W. R. Wilson, *Br. J. Cancer*, 1996, **74**, S48-S51.
78. L. L. Parker, S. M. Lacy, L. J. Farrugia, C. Evans, D. J. Robins, C. C. O'Hare, J. A. Hartley, M. Jaffar and I. J. Stratford, *J. Med. Chem.*, 2004, **47**, 5683-5689.
79. G.-O. Ahn, D. C. Ware, W. A. Denny and W. R. Wilson, *Radiat. Res.*, 2004, **162**, 315-325.
80. W. R. Wilson, M. Tercel, R. F. Anderson and W. A. Denny, *Anticancer Drug Des.*, 1998, **13**, 663-685.
81. W. A. Denny, *Expert Opin. Ther. Pat.*, 2005, **15**, 635-646.

Chapter 7

Mechanistic Studies and Biological Relevance

7 Biological Relevance

7.1 Introduction

This chapter discuss further biological testing to distinguish the potential of the ruthenium and iridium complexes discussed in Chapters 3 and 5 for future *in vivo* testing. Initial results have been obtained for the hydrolysis and hydrophobicity of the complexes, as a means to assess the complexes potential to enter a cell membrane. These types of organometallic ruthenium(II) arene complexes (Chapter 1) have shown to interact with DNA¹ and so using this as a possible target, studies have included Comet assays to measure the degree of DNA damage and melting curve analysis to determine the specific base interactions with these complexes. Apoptosis studies have been measured to assess if the activities seen in Chapters 4 and 5 are due to cell death or cell inhibition, and as we have previously shown these types of complexes cause thioredoxin reductase inhibition, this has been analysed for several complexes.²

7.2 Hydrolysis

As stated in Chapter 1, for cisplatin and titanocene dichloride hydrolysis is the proposed mechanism of action. Therefore, experiments have been carried out using either one equivalent of water or an excess of water. ¹H NMR spectra were recorded over a 5 day period as to mimic the 5-day MTT assay. To date, results have been inconclusive and no changes have been observed in the NMR spectra after a period of 5-days, suggesting that these complexes do not undergo hydrolysis or hydrolysis is too fast to measure. Attempts have been made to increase the concentration of water added to the samples, however this causes them to precipitate and neither NMR nor UV-*vis* spectrometry could be conducted.

7.3 Hydrophobicity (Log *P*)

This is a test of lipophilicity and can help determine if a drug is capable of entry into a cell membrane. One of Lipinski's rule of five (RO5) states that the octanol-water partition coefficient (Log *P*) must not exceed 5 if the drug is to be administrated orally.³⁻⁵ In an attempted to improve the predictions of drug likeness, the rules were extended to the Log *P* range -0.4 - +5.6⁶ and then later extended to the rule of three (RO3), which takes into consideration the molecular weight of the

compound. The compound should have a molecular weight of less than 300 dalton and a Log P of less than 3.⁷

7.3.1 Conducting Hydrophobicity

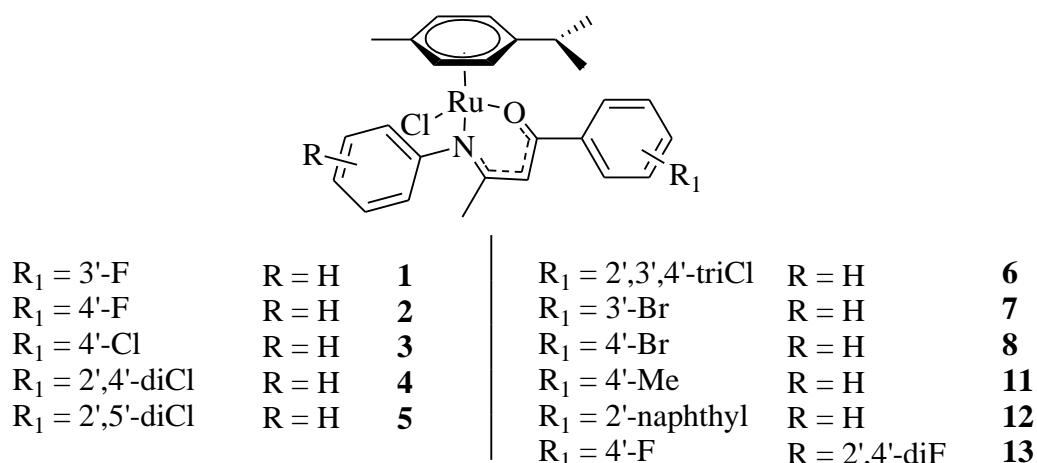
Complexes from Chapters 3 and 5 were tested to determine their effect partition coefficient (Log P) on changing the electronics features of the complex. Firstly, equal volumes of octanol and water (NaCl saturated) were stirred overnight at room temperature and then separated to give octanol-saturated water and water-saturated octanol. Most experiments use the octanol-saturated water layer to carry out the measurements due to cost efficiency; however, all compounds were insoluble in octanol-saturated water. Therefore, accurate amounts of the compound were dissolved in water-saturated octanol (25 mL), a volume of this was layered with an equal volume of octanol-saturated water and placed in a vibrax machine for 4 hours at 1000 gmin⁻¹, a minimum of six repeats were analysed. The layers were separated and the water-saturated octanol layer retained for analysis by UV-*vis* spectroscopy. Using the maximum absorbance of each compound, the average of the six runs was calculated and rearrangement of individual calibration graph gave the $[C]_{org}$ final. **Equation 7.1** and **Equation 7.2** were used to determine the partition coefficient and hence determine if the compound is predominantly hydrophilic or hydrophobic.^{5, 8-10}

$$\text{Log } p = \frac{[C]_{org}}{[C]_{aq}} \times 100 \quad \text{Equation 7.1}$$

$$[C]_{aq} = \frac{[C]_{org} \text{ final}}{[C]_{org} \text{ initial} - [C]_{org} \text{ final}} \quad \text{Equation 7.2}$$

7.3.2 Results and Discussion

Complexes **1-13** (**Figure 7.1**) were tested using the previously discussed experimental, in order to assess their lipophilicity. The results are summarised in **Table 7.1** and it can be seen that complexes range from slightly hydrophilic to slightly hydrophobic, -0.87-1.5, both cisplatin and $[p\text{-cymRuCl}_2]_2$ were tested as comparisons.

**Figure 7.1** List of complexes tested for lipophilicity**Table 7.1** Log *P* values for cisplatin, [*p*-cymRuCl₂]₂ and complexes **1-8, 11-13**

Complex	Log <i>p</i>	± SD
Cisplatin	-2.36	0.01
[<i>p</i> -cymRuCl ₂] ₂	-0.67	0.03
1	-0.87	0.04
2	-0.17	0.02
3	0.12	0.04
4	1.1	0.2
5	0.07	0.04
6	0.27	0.03
7	0.11	0.05
8	0.41	0.03
11	0.53	0.05
12	1.5	0.2
13	0.46	0.06

The results show that complexes **1** and **2** are both hydrophilic possibly due to the electronegative fluorine atoms within the molecules, which make strong hydrogen bonds with the H₂O. As cisplatin is also hydrophilic, it was thought that the hydrophilic nature is key for the complexes activity; however this contradicts Lipinski's rules. Cisplatin is highly activity and has a Log P value (-2.4) lower than the stated threshold for a drug candidate, this can also be seen for **1** which is highly active against most cell lines and again is outside the considered threshold. It can be seen that [*p*-cymRuCl₂]₂ is also hydrophilic and is completely inactive against

all cell lines. This shows that the Log P values calculated have no correlation with the activities seen. The remaining complexes are all hydrophobic and fall with the required range for a likely drug candidate. These results are summarised as a bar-chart in **Figure 7.2**.

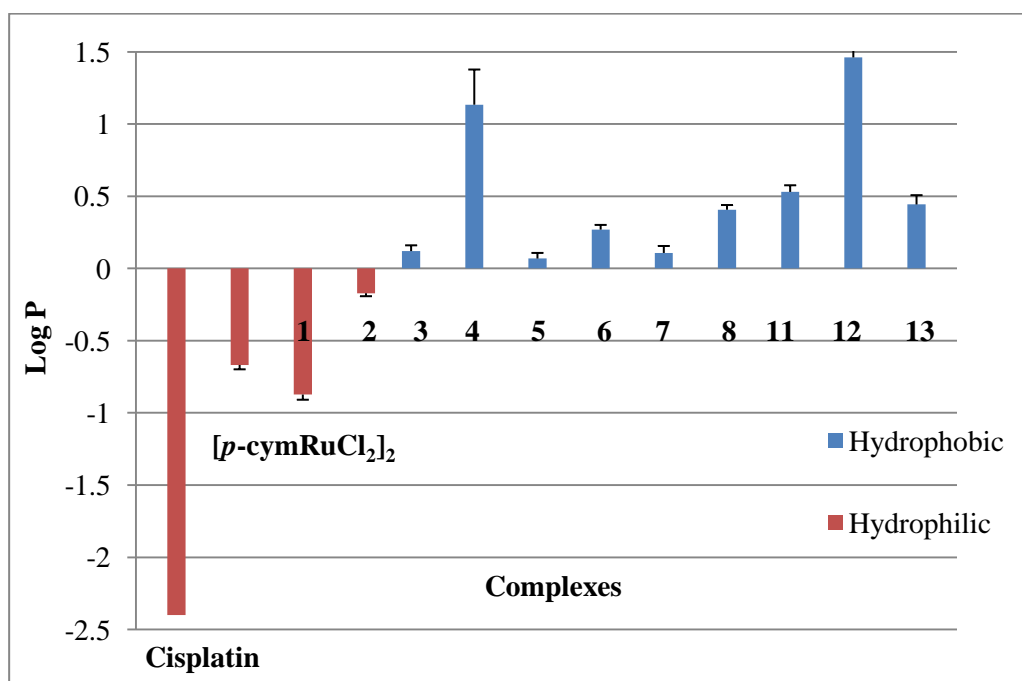


Figure 7.2 Bar-chart to show the Log P values for cisplatin, [*p*-cymRuCl₂]₂, complexes 1-8 and 11-13

It was seen in Chapter 5 that on changing the ligands from a β -ketoiminate to a β -diketonate produced a large difference in activity (**Figure 7.3**). Whereby, both of the ruthenium β -ketoiminate **1** and the iridium β -ketoiminate **18** gave IC₅₀ values much higher than their β -diketonate analogues. Therefore, their Log P values were analysed to evaluate if there was a correlation between hydrophobicity and activity. The results are shown in **Table 7.2** and summarised as a bar-chart in **Figure 7.4**. It can be seen that the more activity complexes are in fact opposite in their lipophilic nature, the ruthenium (**1**) is hydrophilic and the iridium (**18**) is hydrophobic. When assessing the β -diketonate analogues the opposite trend is seen and the ruthenium (**16**) is now hydrophobic and the iridium (**19**) is hydrophilic. These results confirm those previously, showing there is no correlation seen between IC₅₀ values obtained and lipophilic nature of the complex. This means that passive diffusion into the cell is unlikely and these complexes probably enter the cell through a cell-mediated response.

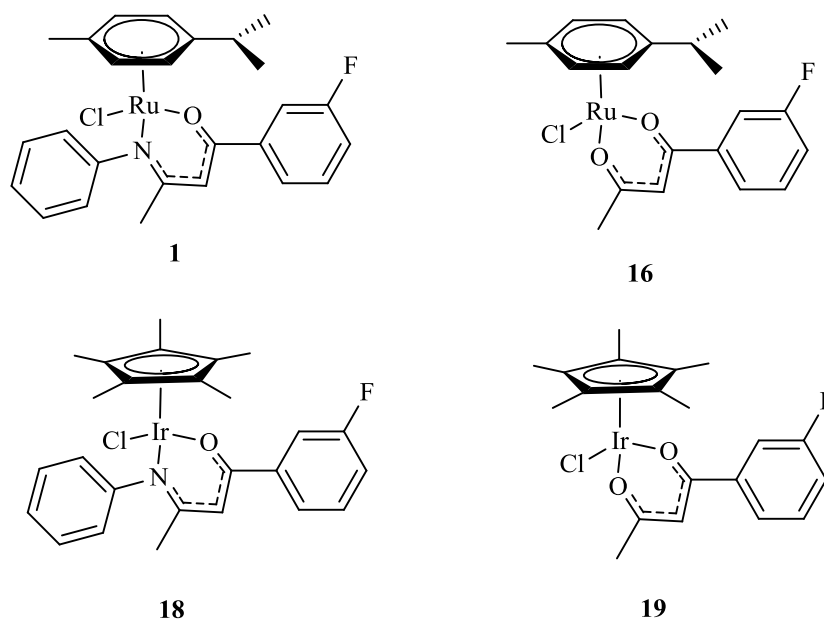


Figure 7.3 List of complexes from Chapter 5 tested for their Log P

Table 7.2 Log P values for complexes **1**, **16**, **18** and **19**

Complex	Log p	\pm SD
1	-0.87	0.04
16	0.11	0.06
18	0.63	0.06
19	-0.28	0.09

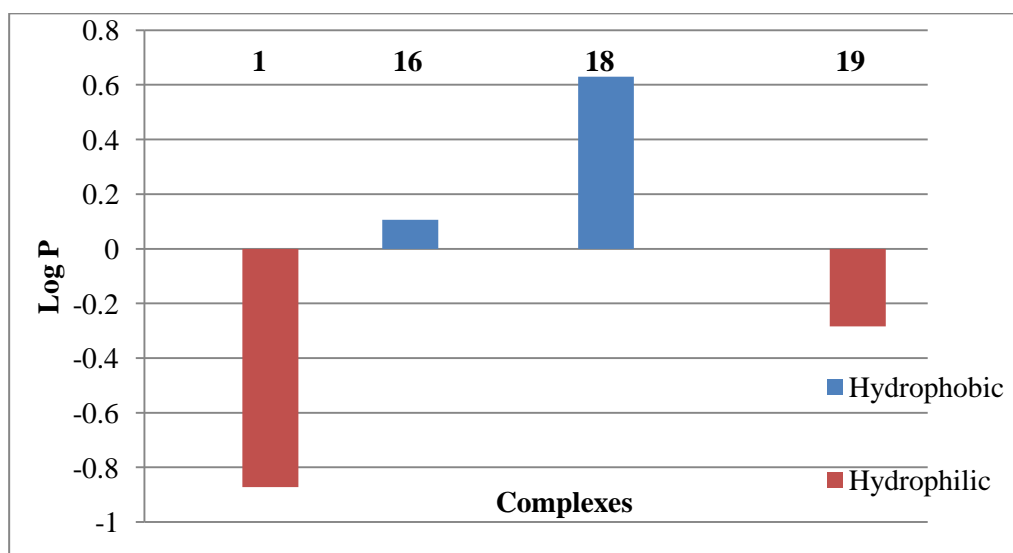


Figure 7.4 Bar-chart to show Log P values for **1**, **16**, **18** and **19**

As hydrolysis and hydrophobicity studies are inconclusive to the mode of entry of these complexes, it is essential that these are tested for protein and enzyme interactions as a means of determining cell uptake. Once inside the cell, a common target for these types of half-sandwich “piano-stool” complexes is DNA. Researchers have shown that these types of complexes bind selectively to either adenosine or guanine residues.¹ Therefore the next sections discuss DNA as a potential target for the activity of these complexes.

7.4 Comet Assay

Comet assay is a microelectrophoresis study first developed by Ostling and Johanson in 1984¹¹ and was later modified by Singh *et al.* in 1988.¹² It is a method used to analyse DNA breakage in single eukaryotic cells by gel electrophoresis. The cells are embedded into a layer of low melting point agarose, a lysis buffer solution is added to remove the membrane, proteins and histones, which diffuse into the agarose. Due to the high molecular weight of DNA, it uncoils and remains in the cell cavity within the agarose. Electrophoresis is then carried out at neutral, mildly alkaline or strongly alkaline conditions. The DNA is negatively charged and therefore when an electric field is applied the relaxed DNA is pulled towards the anode. DNA which remains coiled within the nucleoid forms the ‘head’ of the comet, whilst the relaxed loops of damaged DNA which are pulled towards the anode will form the ‘tail’. These comets can be seen when a SYBR™ Gold solution is added to the slides and they are studied using a microscope. DNA damaged is scored and the comet tail lengths recorded for 50 different comets. The % DNA in the tail is proportional to the amount of DNA damage and therefore the comets with the longest tails have the largest amount of DNA damage. This technique is a quantitative measurement of DNA damage.

7.4.1 Conducting the Comet Assay

HT-29 cells were used as they show the largest range of IC₅₀ values (Chapter 4 and 5), other cell lines showed no significant correlation and gave similar IC₅₀ values for most compounds. The HT-29 cells were incubated with the compounds at an initial concentration of 20 μM and four further concentrations were made each ranging from 20-1.25 μM. After incubation with the drugs, the cell suspensions were diluted in low melting point agarose and added to the previously prepared

slides containing an agarose layer. A neutral or alkaline lysis buffer was added to the slides and then placed into an electrophoresis tank where an electric field was applied for 25 minutes, after washing the slides were left to dry overnight. The SYBR™ Gold staining solution was added and the cells scored under a microscope and using the Comet assay III software.

Double Strand Breakage (DSB)

This assay uses a neutral lysis buffer containing 2% sarkosyl, 0.5 M Na₂EDTA, 0.5 mg/ mL proteinase K and adjusted to pH 8.0. The slides are incubated in the lysis buffer for one hour at 37°C, then submerged in the electrophoresis buffer for a period of thirty minutes and repeated three times. Finally, the slides are submerged in the electrophoresis tank with the buffer and a 24 V electric field applied. Once washed and dried overnight, the fluorescence dye is applied and comets scored. At neutral pH the double helices remain intact and any comet tails seen are representative of double strand damage.

Single Strand Breakage (SSB)

This assay uses an alkaline lysis buffer containing 2.5 M NaCl, 100 mM EDTA and 10 mM Trizma base. The slides are incubated at 4°C for 1 hour prior to the electrophoresis. The electrophoresis tank is then filled with alkaline buffer (pH < 13) and a 24V electric field applied for 25 minutes. The slides are then washed with a neutralisation buffer, and then repeatedly washed with deionised water and finally 100% ice cold ethanol. Once the slides are left to dry overnight, the Comet assay scoring can be continued when convenient.

7.4.2 Results and Discussion

Complexes **1**, **16**, **18**, **19** (**Figure 7.3**) and cisplatin were tested for both DSB and SSB, the compounds were incubated with HT-29 cells before harvesting and conducting the electrophoresis. It can be seen in Chapter 5 that complex **1** has a large difference in cytotoxicity when compared to complex **16** and the same trend is seen for the iridium Cp* complexes (**18** and **19**). The comet assays were conducted to distinguish if the IC₅₀ values seen correlated to the extent of DNA damaged measured. However, this assay required a positive control and a compound such as Camptothecin CAMP (**Figure 7.5**) which inhibits the DNA enzyme topoisomerase I (topo I) inducing apoptosis.^{13, 14}

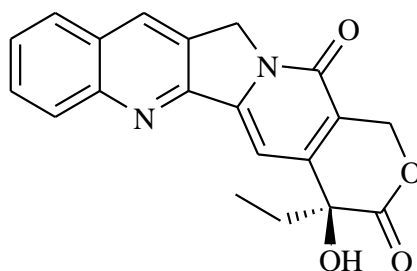
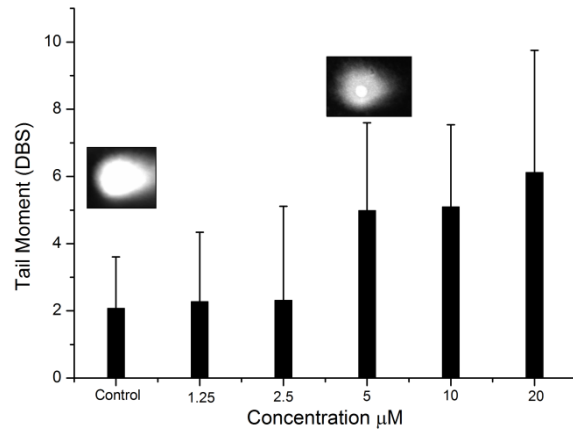


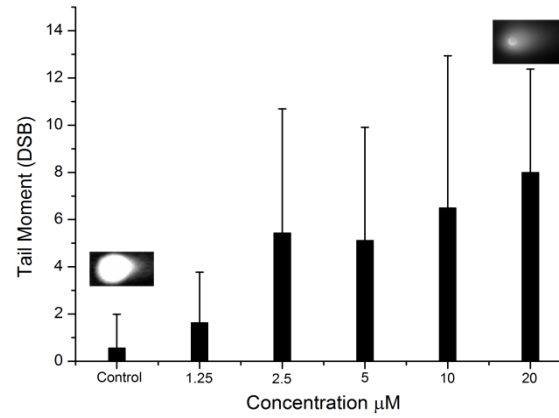
Figure 7.5 Camptothecin (CAMP)

The results are shown as bar-charts in **Figure 7.6** and show both DSB and SSB for cisplatin and complexes **1**, **16**, **18** and **19**. Results show that like cisplatin, both ruthenium complexes show no significant double strand breakage and have tail moments comparable to that of cisplatin. When considering the SSB assay, cisplatin shows moderate single strand damage and at a concentration of 20 μM has a tail moment of approximately 20. Complex **1** shows a larger degree of single strand damage when compared to cisplatin and at the same concentration it shows a tail moment of approximately 65, whereas complex **16** does not show any single strand breakage.

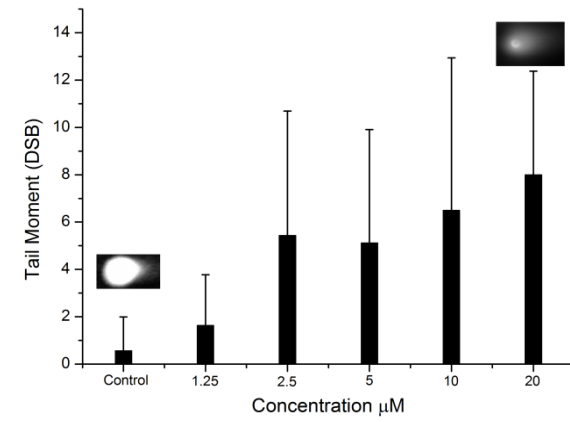
The same assays were conducted for the iridium analogues **18** and **19** and the results are shown as bar-charts in **Figure 7.7**. They do not show the same degree of damage as their ruthenium analogues, but still have the same general trend, with the complex **18** having preferential single strand breakage and complex **19** showing neither double or single strand damage. This preferential single strand breakage for the β -ketoiminate complexes could be the reason for their increase in IC_{50} values, as a direct trend is seen between cytotoxicity of the complex and the degree of DNA damage measured. This assay is quantitative, but only shows that the DNA is disrupted but does not quantify any cross-linking that may be present.



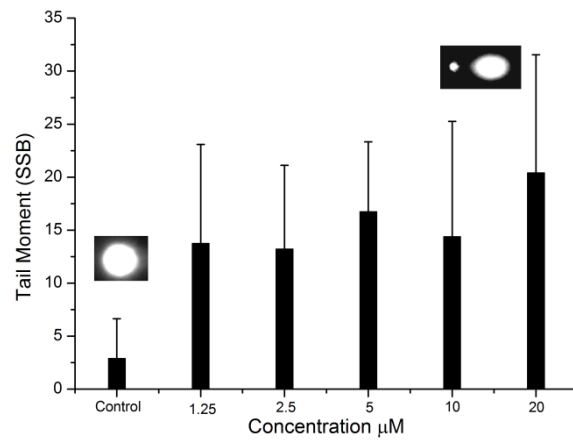
Cisplatin DSB



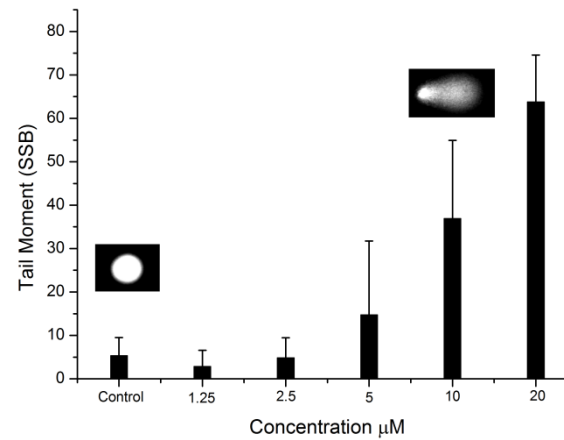
Complex 1 DSB



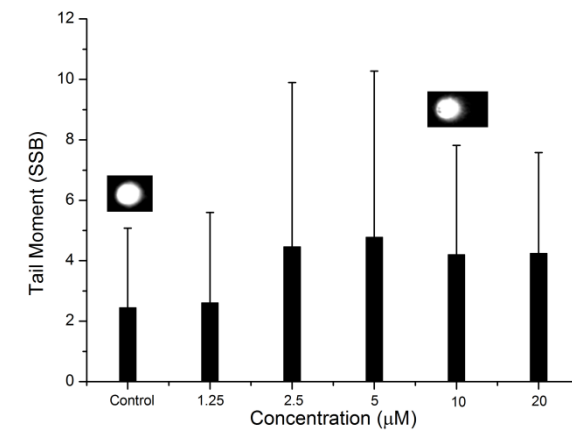
Complex 16 DSB



Cisplatin SSB

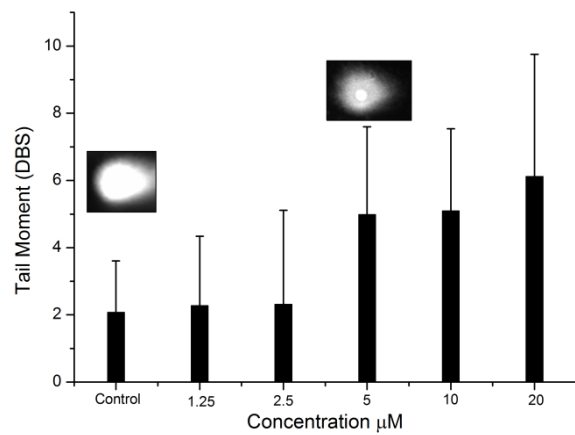


Complex 16 SSB

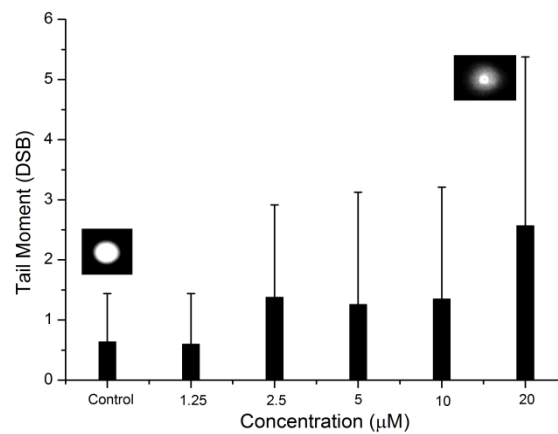


Complex 16 SSB

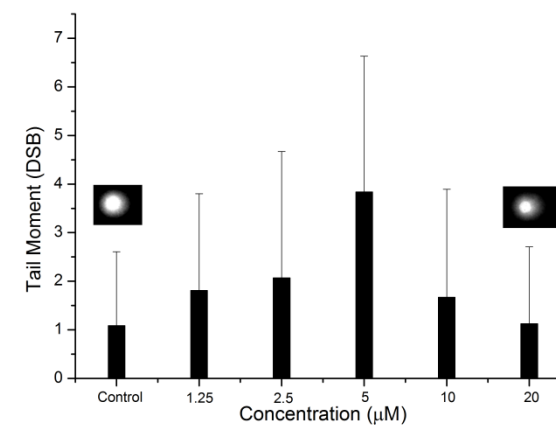
Figure 7.6 DSB and SSB Comet assay results for cisplatin, 1 and 16



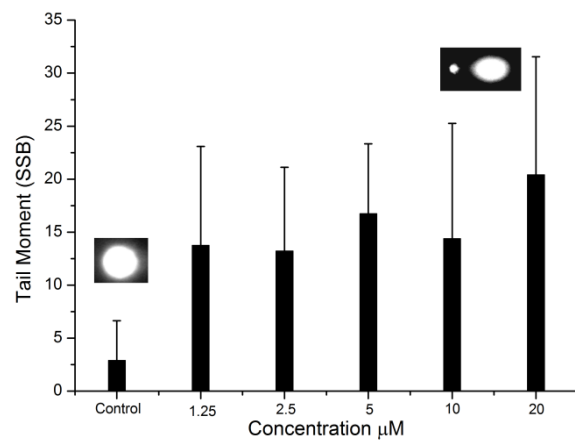
Cisplatin DSB



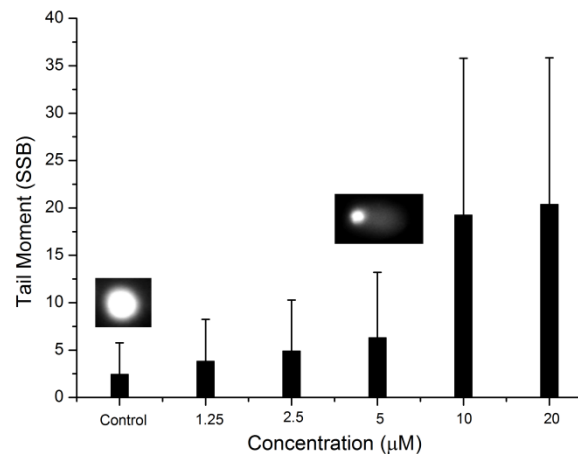
Compound 18 DSB



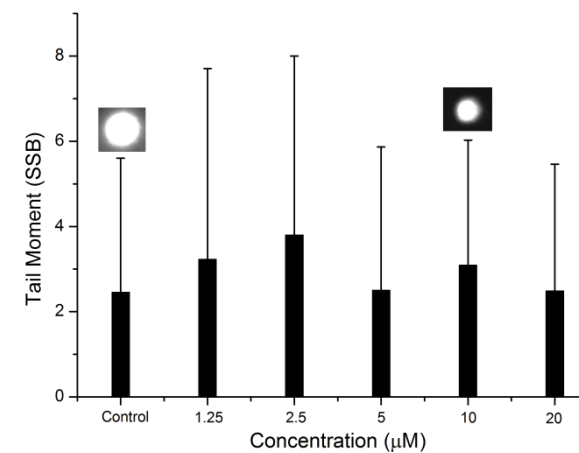
Compound 19 DSB



Cisplatin SSB



Compound 18 SSB



Compound 19 SSB

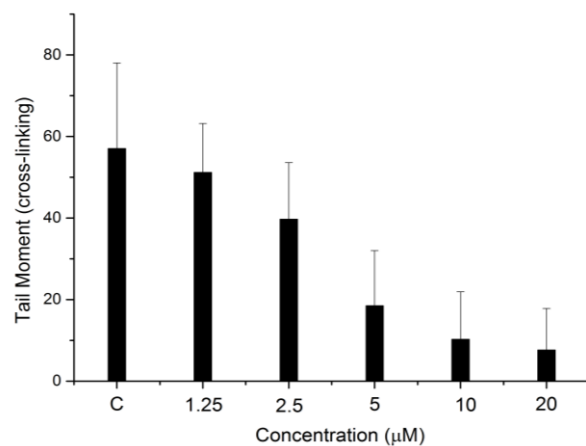
Figure 7.7 DSB and SSB Comet assay results for cisplatin, 18 and 19

Cross-Linking Comet Assay

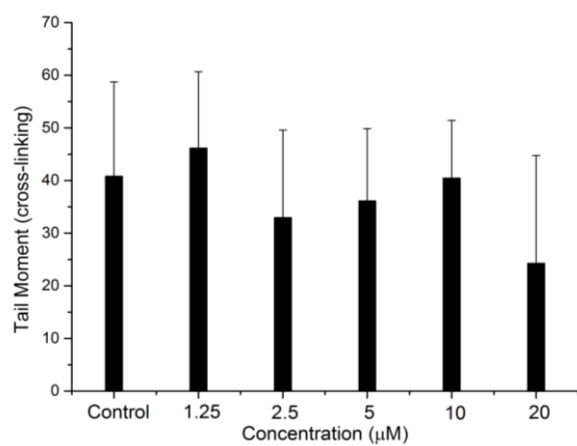
The previous section discusses the results from the double and single strand Comet assays, but as stated it does not provide any information for the possibility of cross-linking within the complexes mode of action. This assay follows the same experimental as the single strand breakage assay, but requires 20 minutes exposed with hydrogen peroxide after the incubation with the complexes. This is added to disrupt the DNA and produce the Comets usually seen; a measurement is then taken of percentage tail decrease. If the complexes are forming cross-links there should be a decrease in tail moment.

7.4.3 Results and Discussion

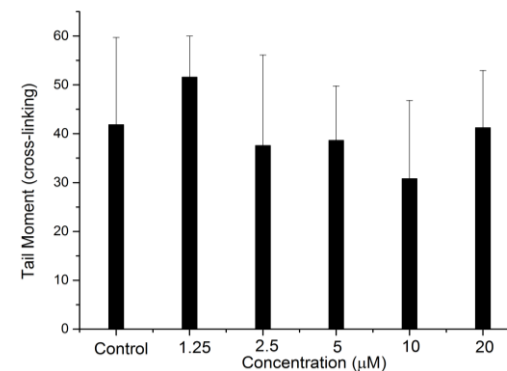
Complexes **1**, **16**, **18** and **19** (**Figure 7.3**) were tested using this cross-linking assay to distinguish if the preferential single strand breakage seen for complexes **1** and **18** is due to a cross-linking interaction. Cisplatin was tested as a positive control for this assay as it is a well know cross-linking complex.^{15, 16} The results are shown as bar-charts in **Figure 7.8** and show that cisplatin does cross-link with a % tail moment decrease of 17% when comparing the control and 20 μM . As expected, complexes **16** and **19**, which showed no double or single strand breakage, also show no cross-linking. When assessing complexes **1** and **18**, which do show single strand breakage, it can be seen that neither show a significant tail moment decrease. However, these values were taken from an average score of 50 comets, and in fact under the microscope a large proportion of the comets had significant tail decrease and this can account for the large standard deviations seen. This shows that at 20 μM there is some cross-linking present, however a higher concentration would have to be analysed in the hope to maximise the degree of cross-linking.



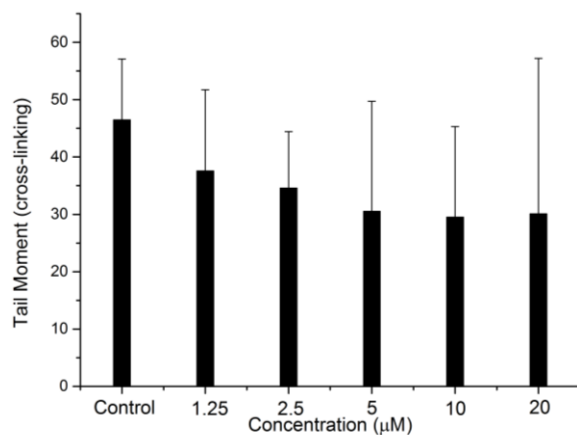
Cross-linking for Cisplatin



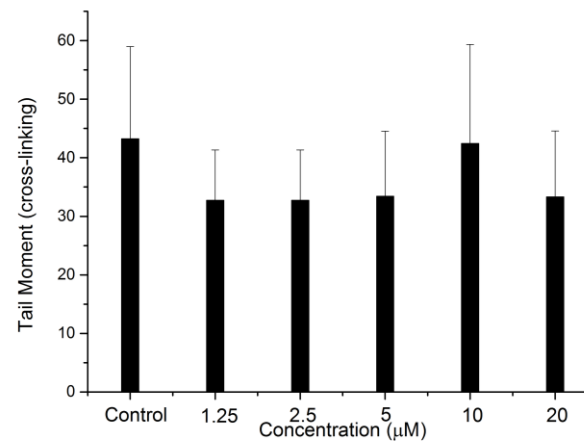
Cross-linking for 1



Cross-linking for 16



Cross-linking for 18



Cross-linking for 19

Figure 7.8 Cross-linking Comet assay results for cisplatin and complexes 1, 16, 18 and 19

7.5 Apoptosis

In the early stages of apoptosis, changes can occur at the cell membrane¹⁷⁻¹⁹ and one of these alterations is the translocation of the phosphatidylserine (PS). It is a phospholipid component that is usually found on the inner-leaflet of the membrane. In apoptotic cells, this can move from the inner to the outer part of the membrane, in which the PS then becomes exposed on the surface of the cell.²⁰ Fadok *et al.* showed that macrophages specifically recognise the exposed PS during the development of apoptosis.¹⁸ This recognition and phagocytosis of apoptotic cells protects the cellular compounds leading to inflammation and usually accompanies necrosis. The analysis of PS on apoptotic cell membranes is performed using Annexin-V-Fluorescein, and also Propidium Iodide (PI) for the differentiation from necrotic cells.

Annexin V is a Ca^{2+} dependent phospholipid-binding protein with a high affinity for PS.²⁰ Therefore this protein can be used as a sensitive probe for PS exposure on the outer-leaflet of the membrane and is able to detect apoptotic cells.²⁰⁻²³ The necrotic cells also expose PS due to the loss of membrane integrity, and so to distinguish these from apoptotic cells a DNA stain (PI) is used as a necrotic cell would uptake both stains and give a positive result for both.

7.5.1 Conducting the Annexin-V assay

The complexes shown in **Figure 7.3** were incubated with either HT-29 or A2780 for a period of 48 hours. These were then harvested according to the protocol in Chapter 9 and flow cytometry was used to analyse a minimum of 10,000 cells. The flow cytometer uses a 488 nm excitation and a 515 nm band-pass filter for fluorescein detection (Annexin-V) and a filter > 600 nm for PI detection. Electronic compensation of the instrument is required to exclude overlapping of the two emission spectra. **Figure 7.9** shows a general graph seen for the dual parameter FL1 = Annexin-V-FLUOS versus FL2 = Propidium Iodide.

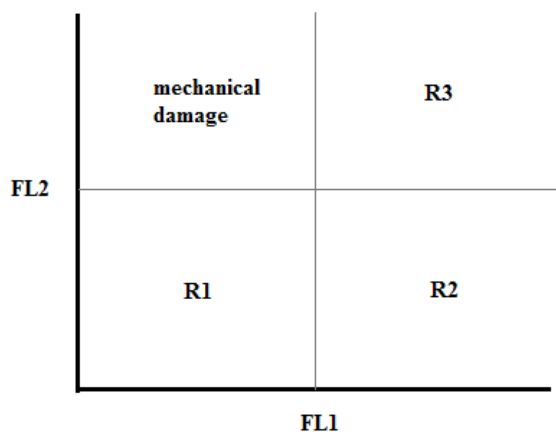


Figure 7.9 General graph seen for the quadrants seen using dual parameters

R1 = living cells – membranes are intact and therefore are not stained by either of the two dyes.

R2 = apoptotic cells – in which the Annexin-V binds to the negatively charged phospholipid surfaces but not the PI dye (excitation = 488 nm, emission = 518 nm)

R3 = necrotic cells – again this has the PS exposed and binds to the Annexin-V, but necrotic cells are ‘leaky’ and the PI stains the exposed DNA (excitation = 518 nm, emission = 617 nm)

7.5.2 Results and Discussion

The results for this assay are stated in **Table 7.3** and when considering incubation with the HT-29 cells (**Figure 7.10**), it can be seen that at a drug concentration of 20 μM , the active β -ketonate ruthenium complex (**1**) induces late apoptosis or necrosis of up to 72.25%, confirming that the IC_{50} values obtained are due to cell death. Also the active β -ketoiminate iridium complex (**18**) shows induced apoptosis, with 31.67% early apoptotic cells and 49.94% late apoptotic or necrotic cells. When considering the β -diketonate analogues, **17** and **19** respectively, it can be seen that even at the highest drug concentration of 20 μM , there are still over 84% of the cells living. Showing a clear correlation with the IC_{50} results seen for these complexes, in which the more active the complex the higher degree of cell death is induced.

When considering the incubations with A2780 cells (**Figure 7.11**), the same trend is seen, where at a drug concentration of 20 μM , both **1** and **18** have over 60% of the cells in the late apoptotic or necrotic stages. However, there is a difference seen in the early apoptotic stages in which **1** has a higher degree of living cells, showing it

induces later apoptosis only. Again, at the same drug concentration, the inactive **17** and **19** show over 82% of living cells. These results show that even against two different cells lines; these types of β -ketoiminate complexes are able to induce a high degree of late apoptosis or necrosis in cells. It also suggests that the cytotoxicities of these complexes seen in Chapters 4 and 5 are due to cell death and not to cell inhibition, therefore it was not necessary to undertake any cell cycling experiments.

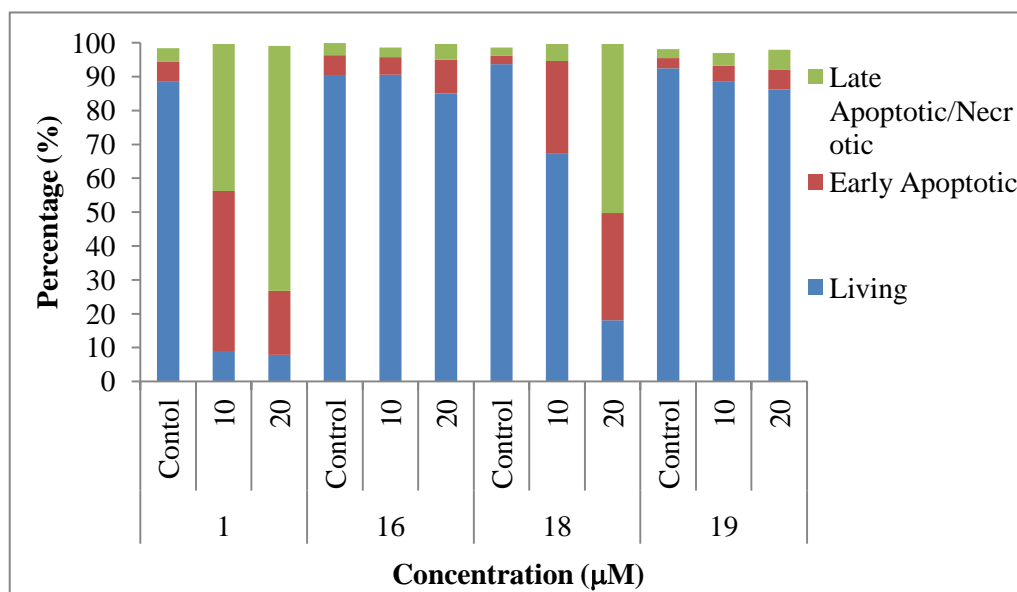


Figure 7.10 Bar-chart showing late apoptotic/necrotic, early apoptotic and living percentage for complexes **1**, **16**, **18** and **19**, against HT-29

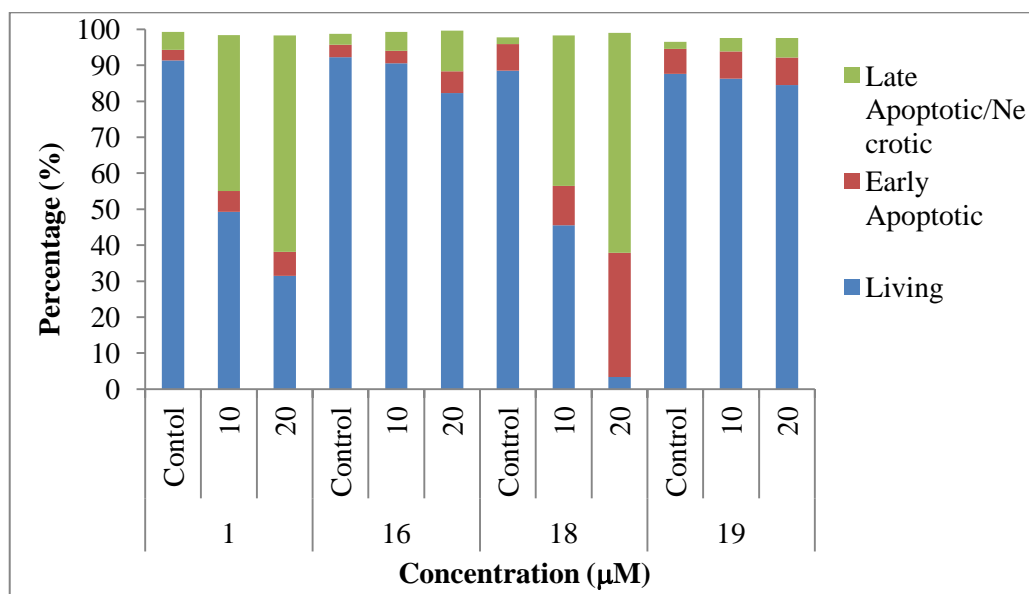


Figure 7.11 Bar-chart showing late apoptotic/necrotic, early apoptotic and living percentage for complexes **1**, **16**, **18** and **19**, against A2780

Table 7.3 Apoptosis results for complexes **1**, **16**, **18** and **19**, showing % of living, early apoptotic and late apoptotic/necrotic cells

Complexes	Concentration (μ M)	HT-29			A2780		
		Live (%)	Early Apoptotic (%)	Late Apoptotic/ Necrotic (%)	Live (%)	Early Apoptotic (%)	Late Apoptotic/ Necrotic (%)
1	0	88.67	5.70	4.07	91.37	2.91	4.95
	10	9.03	47.19	43.45	49.31	5.76	43.28
	20	7.86	18.95	72.25	31.52	6.63	60.13
16	0	90.43	5.94	3.57	92.25	3.45	2.99
	10	90.54	5.21	2.88	90.54	3.48	5.21
	20	84.96	10.07	4.62	82.29	5.99	11.38
18	0	93.68	2.52	2.40	88.52	7.39	1.81
	10	67.18	27.49	5.01	45.55	10.92	41.83
	20	18.03	31.67	49.94	3.34	34.57	61.09
19	0	92.42	3.04	2.65	87.60	6.91	2.01
	10	88.49	4.73	3.74	86.25	7.60	3.75
	20	86.26	5.73	5.98	84.52	7.63	5.41

7.6 Thioredoxin Reductase

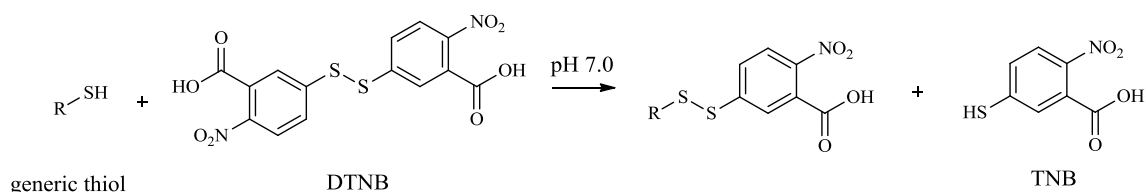
The thioredoxin (Trx) system is a thiol redox system that plays a key role in the cells survival and proliferation.^{24, 25} The thioredoxin reductase (TrxR) has two main forms; a cytosolic (TrxR1)²⁶ and a mitochondrial one (TrxR2),²⁷ it is the only known enzyme to catalyse the NADPH-dependent reduction of the active disulfide (Cys32 and Cys35) of oxidised Trx.²⁸ The electrons which are taken from NADPH *via* TrxR are transferred to the active site of Trx.²⁹ The Trx system performs in many biological functions, such as;^{23, 24, 29, 30}

1. Protection of cellular proteins against oxidation by reducing protein disulfides.
2. An antioxidant acting as an electron donor to peroxide scavengers.
3. Redox control of transcription factors, including the hypoxia-inducible factor HIF-1 α
4. An electron donor for enzyme ribonucleotide reductase (RNR) which is involved in DNA synthesis.

In cancer, the biological effects of the Trx system have been shown to contribute to tumour growth and progression.³⁰ However, over-expression of the Trx has been reported in several tumour cancers and therefore targeting the inhibition of this has been key in current drug research.³¹⁻³³ The increase of Trx expression has since been associated with the resistance to docetaxel in primary breast cancer³⁴ and decreased survival in colorectal cancer patients.³⁵ Therefore the TrxR in tumorigenesis has been studied in mouse models, in which tumour growth and metastasis were largely reduced.³⁶ The active site of the Trx is a selenoate group, which after reduction allows the site to react with “soft” metal ions, making the TrxR a likely target for metallodrugs and is potentially the reasons that gold(I) and platinum(II) compounds have been previously reported for their inhibition of mammalian TrxR.³⁷⁻⁴⁰ It was thought that ruthenium compounds, due to their “soft” nature, would have the potential of inhibiting TrxR. The first results were published on this in 2007 by Mura *et al.* in which they show that ruthenium(III) compounds in fact have selectivity towards the cytosolic TrxR1 and is reminiscent to that seen for calcium ions. In which the TrxR1 is also extremely sensitive to Ca²⁺ inhibition and exerts only a weak inhibitory action on the mitochondrial TrxR2.⁴¹

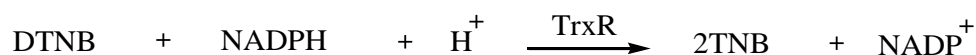
7.6.1 Conducting the Thioredoxin Reductase Assay

This assay is based on a modified assay by Chew *et al.*,⁴² in which the substrate DTNB also known as Ellman's reagent (5,5'-dithiobis-(2-nitrobenzoic acid)) is used to quantify the concentration of thiol groups in a sample, as thiols react with this compound and cleave the disulfide bond giving TNB (Scheme 7.1).⁴³



Scheme 7.1 Cleaving of a disulfide bond by DTNB to give TNB

The inhibition of TrxR is measured by addition of DTNB, NADPH and TrxR, and then differing concentrations of drug samples to gain the concentration needed to inhibit 50% (IC_{50}). The production of TNB is then measured at 412 nm and the IC_{50} calculated by plotting graphs of % absorption versus inhibition concentration [I]. This assay was carried out using complexes stated in **Figure 7.3** at varying concentrations, up to a maximum of 10 μM . The TrxR in buffer solutions were allowed to react with the drug samples for 30 seconds and then UV-vis spectroscopy was measured for 1 minute at 412 nm. An initial spectrum was recorded for the TrxR only and any decrease in absorbance seen indicated inhibition (**Scheme 7.2**).

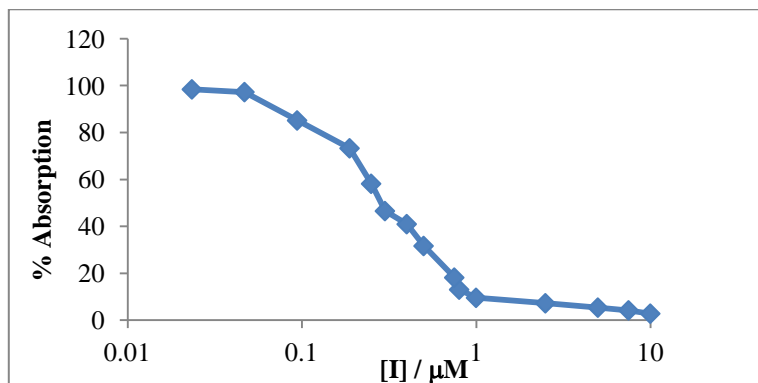
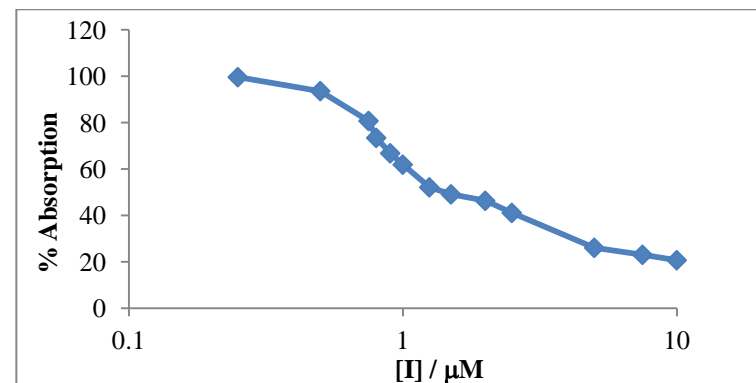
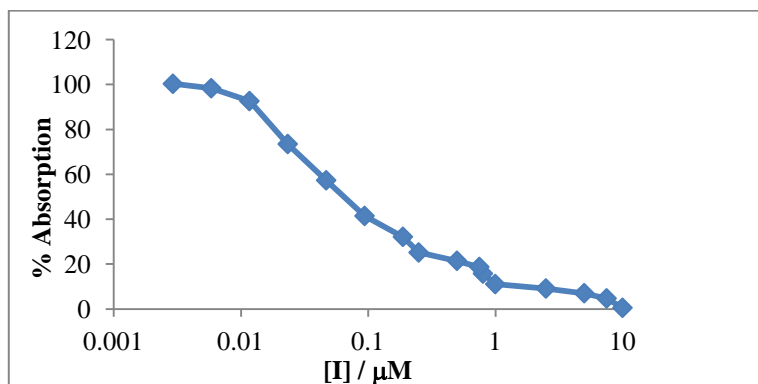
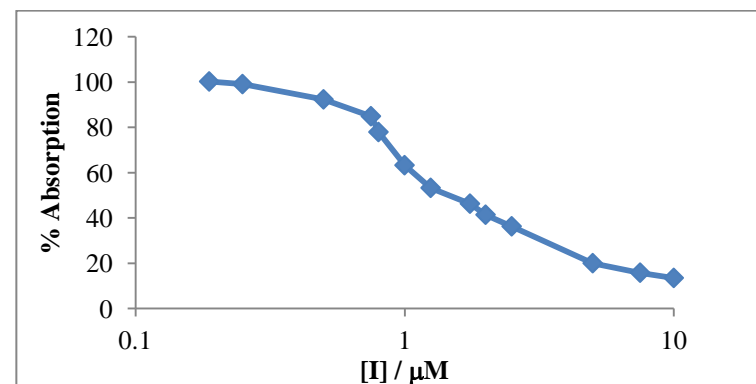


Scheme 7.2 The reaction of DTNB with NADPH with TrxR

7.6.2 Results and Discussion

The results for this assay are stated in **Figure 7.12** and show graphs of % absorption versus [I], straight line graphs were plotted for 50% region and from the line of best fit, IC_{50} values were calculated. It can be seen that the active β -ketonate ruthenium complex **1** is also good inhibitors of TrxR with a [I] of 285 nM and the inactive β -diketonate ruthenium complex **16** has a [I] of only 1.42 μM . A similar trend is seen for the iridium complexes, whereby the inactive β -diketonate iridium **19** only inhibits in the micromolar range and the iridium β -ketoiminate complex **18** has a [I] of 68.5 nM. These results show there is some

selectivity towards the complexes, with a trend seen in the IC_{50} inhibition and the cytotoxicity values. These results are similar to those obtained within the McGowan group, in which the iridium picolinamide complexes were the more active than their ruthenium analogues, with IC_{50} values in the nanomolar range. The results show that the ruthenium complexes were completely inactive and here the ruthenium complexes are as high as the nanomolar range, this could mean the β -ketoiminate ligands may play a role in the activity of these complexes.²

Complex **1** – $\text{IC}_{50} = 285 \text{ nM}$ Complex **16** – $\text{IC}_{50} = 1.42 \mu\text{M}$ Complex **18** – $\text{IC}_{50} = 68.5 \text{ nM}$ Complex **19** – $\text{IC}_{50} = 1.48 \mu\text{M}$ **Figure 7.12** Graphs showing the % Absorption versus [I] and IC_{50} values for complexes **1**, **16**, **18** and **19**

7.7 Conclusion

This chapter presents a range of biological experiments and assays on complexes **1**, **16**, **18** and **19**; to determine the activities of these complexes and to assess their potential for further *in vivo* testing. The initial hydrolysis and hydrophobicity studies were inconclusive as to the mode of action into the cell and future work needs to be carried out on the possible entry into a cell.

As previous research had stated such compounds to interact with DNA, single cell gel electrophoresis was conducted to assess interactions with complexes on double strand (DSB), single strand (SSB) and cross-linking samples. It was found that the active β -ketoiminate complexes **1** and **18** show preferential single strand damage but no double strand or cross-linking, whereas the inactive β -diketonate complexes show no interactions with DNA.

Assays were carried out to assess the nature of the cytotoxicity values measure in Chapters 4 and 5, to determine if these IC₅₀ values were due to cell death or cell inhibition. Firstly, apoptosis studies were carried out and showed the same trends seen in other assays, in which the β -ketoiminate complexes are able to induce cell death in both HT-29 and A2780 cells. Therefore, no cell cycling studies were required and the cytotoxicity values obtained were considered to be due to cell death and not inhibition.

As thioredoxin reductase is known to be over expressed in cancers, studies were carried out to assess the potential of these complexes to inhibit this enzyme. Results show that indeed the active β -ketoiminate complexes inhibit this enzyme well, with IC₅₀ values in the nanomolar range, and the most promising activity seen for the iridium complex **18**. As thought, the inactive β -diketonate complexes do not inhibit the TrxR enzyme to the same extent and are only active in the micromolar range.

7.8 References

1. R. Fernandez, M. Melchart, A. Habtemariam, S. Parsons and P. J. Sadler, *Chem. Eur. J.*, 2004, **10**, 5173-5179.
2. Z. Almodares, S. J. Lucas, B. D. Crossley, A. M. Basri, C. M. Pask, A. J. Hebden, R. M. Phillips and P. C. McGowan, *Inorg. Chem.*, 2014, *Accepted for Publication*.
3. C. A. Lipinski, F. Lombardo, B. W. Dominy and P. J. Feeney, *Adv. Drug Del. Rev.*, 2001, **46**, 3-26.
4. C. A. Lipinski, *Drug Discovery Today: Technologies*, 2004, **1**, 337-341.
5. A. Leo, C. Hansch and D. Elkins, *Chem. Rev.*, 1971, **71**, 525-616.
6. A. K. Ghose, V. N. Viswanadhan and J. J. Wendoloski, *J. Combin. Chem.*, 1999, **1**, 55-68.
7. M. Congreve, R. Carr, C. Murray and H. Jhoti, *Drug Dis. Today*, 2003, **8**, 876-877.
8. J. Sangster, *Octanol-Water Partition Coefficients: Fundamentals and Physical Chemistry*, John Wiley & Sons Ltd, Chichester, 1997.
9. M. P. Edwards and D. A. Price, *Annu. Rep. Med. Chem.*, 2010, **45**, 381-391.
10. P. D. Leeson and B. Springthorpe, *Nat. Rev. Drug Dis.*, 2007, **6**, 881-890.
11. O. Ostling and K. J. Johanson, *Biochem. Biophys. Res. Commun.*, 1984, **123**, 291-298.
12. N. P. Singh, M. T. McCoy, R. R. Tice and E. L. Schneider, *Exp. Cell Res.*, 1988, **175**, 184-191.
13. H. Ulukan and P. W. Swaan, *Drugs*, 2002, **62**, 2039-2057.
14. A. J. Lu, Z. S. Zhang, M. Y. Zheng, H. J. Zou, X. M. Luo and H. L. Jiang, *Acta Pharmacol. Sin.*, 2007, **28**, 307-314.
15. N. Poklar, D. S. Pilch, S. J. Lippard, E. A. Redding, S. U. Dunham and K. J. Breslauer, *Proc. Natl. Acad. Sci. U.S.A.*, 1996, **93**, 7606-7610.
16. G. N. Rudd, J. A. Hartley and R. L. Souhami, *Cancer Chemot. Pharm.*, 1995, **35**, 323-326.
17. H. A. Andree, C. P. Reutelingsperger, R. Hauptmann, H. C. Hemker, W. T. Hermens and G. M. Willems, *J. Biol. Chem.*, 1990, **265**, 4923-4928.
18. V. A. Fadok, D. R. Voelker, P. A. Campbell, J. J. Cohen, D. L. Bratton and P. M. Henson, *J. Immunol.*, 1992, **148**, 2207-2216.
19. C. E. Creutz, *Science*, 1992, **258**, 924-931.

20. I. Vermes, C. Haanen, H. Steffens-Nakken and C. Reutelingsperger, *J. Immunol. Meth.*, 1995, **184**, 39-51.
21. G. Koopman, C. P. Reutelingsperger, G. A. Kuijten, R. M. Keehnen, S. T. Pals and M. H. van Oers, *Blood*, 1994, **84**, 1415-1420.
22. C. H. Homburg, M. de Haas, A. E. von dem Borne, A. J. Verhoeven, C. P. Reutelingsperger and D. Roos, *Blood*, 1995, **85**, 532-540.
23. S. R. A. Verhoven B., Williamson P. (1995) *J. Exp. Med.* 182:1597–1601, *J. Exp. Meth.*, 1995, **182**, 1597-1601.
24. E. S. Arner and A. Holmgren, *Eur. J. Chem.*, 2000, **267**, 6102-6109.
25. S. Gromer, S. Urig and K. Becker, *Med. Res. Rev.*, 2004, **24**, 40-89.
26. P. Y. Gasdaska, J. R. Gasdaska, S. Cochran and G. Powis, *FEBS Letters*, 1995, **373**, 5-9.
27. A. Miranda-Vizuete, A. E. Damdimopoulos, J. R. Pedrajas, G. J. A. and G. Spyrou, *Eur. J. Biochem.*, 1999, **261**, 405-412.
28. D. Mustacich and G. Powis, *Biochem. J.*, 2000, **346 (Pt 1)**, 1-8.
29. A. Holmgren and L. Jun, *Biochem. Biophys. Res. Commun.*, 2010, **396**, 120-124.
30. E. S. Arner and A. Holmgren, *Sem. Cancer Biol.*, 2006, **16**, 420-426.
31. M. Berggren, A. Gallegos, J. R. Gasdaska, P. Y. Gasdaska, J. Warneke and G. Powis, *Anticancer Res.*, 1996, **16**, 3459-3466.
32. Y. Soini, K. Kahlos, U. Napankangas, R. Kaarteenaho-Wiik, M. Saily, P. Koistinen, P. Paaakko, A. Holmgren and V. L. Kinnula, *Clin. Cancer Res.*, 2001, **7**, 1750-1757.
33. K. Kahlos, Y. Soini, M. Saily, P. Koistinen, S. Kakko, P. Paakko, A. Holmgren and V. L. Kinnula, *Int. J. Cancer*, 2001, **95**, 198-204.
34. S. J. Kim, Y. Miyoshi, T. Taguchi, Y. Tamaki, H. Nakamura, J. Yodoi, K. Kato and S. Noguchi, *Clin. Cancer Res.*, 2005, **11**, 8425-8430.
35. J. Raffel, A. K. Bhattacharyya, A. Gallegos, H. Cui, J. G. Einspahr, D. S. Alberts and G. Powis, *J. Lab. Clin. Med.*, 2003, **142**, 46-51.
36. M. H. Yoo, X. M. Xu, B. A. Carlson, V. N. Gladyshev and D. L. Hatfield, *J. Biol. Chem.*, 2006, **281**, 13005-13008.
37. A. B. Witte, K. Anestal, E. Jerremalm, H. Ehrsson and E. S. Arner, *Free Radical Biol. Med.*, 2005, **39**, 696-703.

38. M. Coronello, E. Mini, B. Caciagli, M. A. Cinellu, A. Bindoli, C. Gabbiani and L. Messori, *J. Med. Chem.*, 2005, **48**, 6761-6765.
39. Y. Omata, M. Folan, M. Shaw, R. L. Messer, P. E. Lockwood, D. Hobbs, S. Bouillaguet, H. Sano, J. B. Lewis and J. C. Wataha, *Toxicol. in vitro*, 2006, **6**, 882-890.
40. C. Marzano, V. Gandin, A. Folda, G. Scutari, A. Bindoli and M. P. Rigobello, *Free Radical Biol. Med.*, 2007, **6**, 872-881.
41. M. P. Rigobello, F. Vianello, A. Folda, C. Roman, G. Scutari and A. Bindoli, *Biochem. Biophys. Res. Commun.*, 2006, **343**, 873-878.
42. E.-H. Chew, J. Lu, T. D. Bradshaw and A. Holmgren, *FASEB*, 2008, **22**, 2072-2083.
43. G. L. Ellman, *Arch. Biochem. Biophys.*, 1959, **82**, 70-77.

Chapter 8

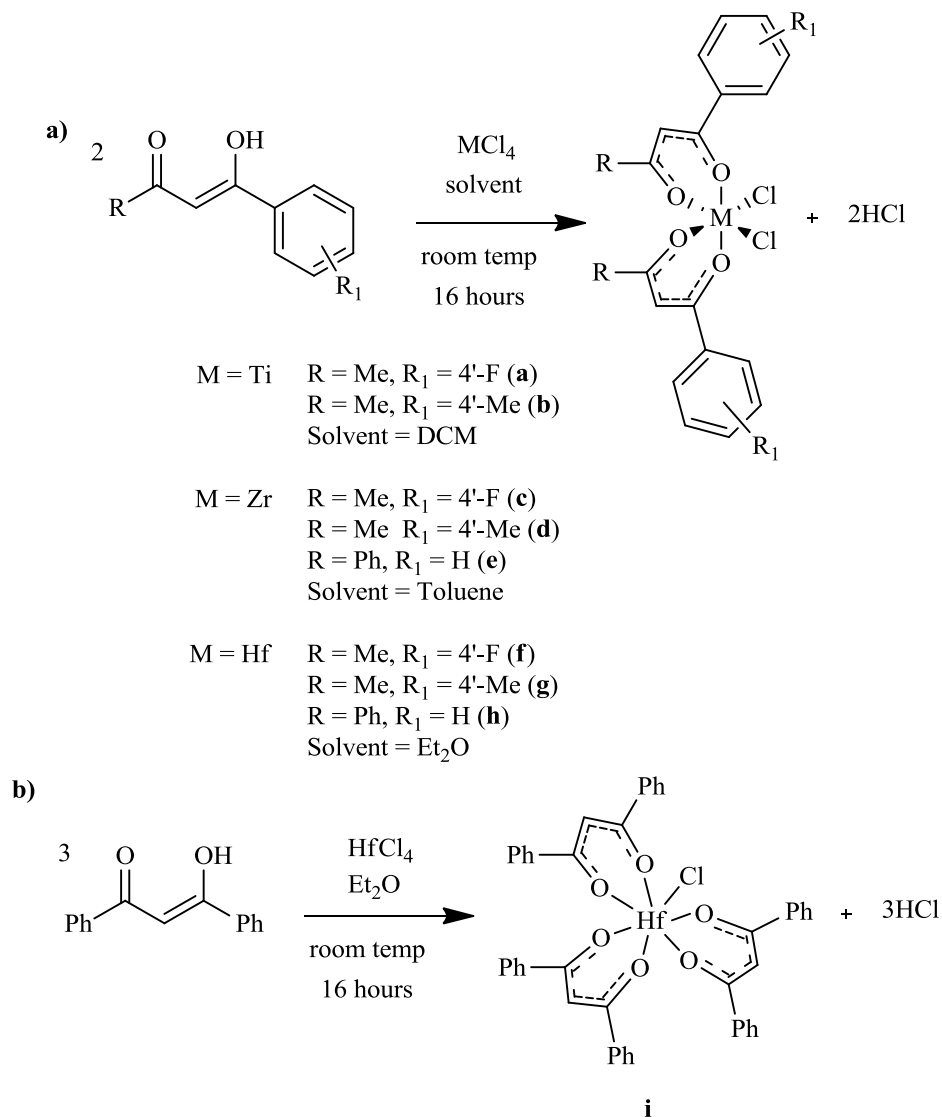
Synthesis and Characterisation of β -Diketonate and β - Ketoiminate Group IV Chloride Complexes

8 Synthesis and Characterisation of β -Diketonate and β -Ketoiminate Group IV Chloride Complexes

After the success of budotitane described in Chapter 1, modified analogues have been synthesised within the McGowan group.¹⁻³ Attempts have been made to synthesise novel group IV chloride complexes with incorporation of both the novel β -diketonate and β -ketoiminate ligands described in Chapter 2. ^1H and $^{13}\text{C}\{^1\text{H}\}$ NMR spectroscopy, mass spectrometry and X-ray crystallographic analysis have been described where possible. Due to the air sensitive nature of these complexes bulk purification has not been possible to date.

8.1 Mechanistic and Cytotoxicity Evaluation for β -Diketonate Group IV Chloride Complexes

A range of complexes have previously been reported within the McGowan group, where a small range was selected and tested for their cytotoxic potential. The titanium, zirconium and hafnium complexes were synthesised according to **Scheme 8.1 (1a)**. The *para*-fluoro and *para*-methyl β -diketonate complexes were selected for each metal, allowing comparisons to be made between the electronic effects and the cytotoxic behaviour down the group. Two symmetrical complexes (**e** and **h**), were also synthesised in order to limit the possible isomers. In addition a symmetrical *tris* β -diketonate hafnium complex (**i**) was synthesised according to **Scheme 8.1 (1b)**, in order to assess the need for the *cis*-chlorides and to increase the sterics of the complex.⁴



Scheme 8.1 Synthetic pathway for Ti, Zr and Hf (IV) β -diketonate complexes

Budotitane contains two asymmetric β -diketonate ligands and it has been postulated that different isomers of budotitane may exhibit different *in vitro* activities.^{5,6} It has been shown within the McGowan research group that complexes which contain asymmetric functionalised β -diketonates, show ^1H NMR spectra comprised of a series of broad peaks at room temperature (**Figure 8.1**). ^1H NMR spectra were recorded by Dr. James Mannion and upon cooling the samples from 333 K to 233 K, the broad signals separate into multiple peaks which were assigned as the three *cis* isomers.¹ This phenomenon is similar to that observed for the budotitane series of complexes in which they see the same three *cis* isomers.⁷

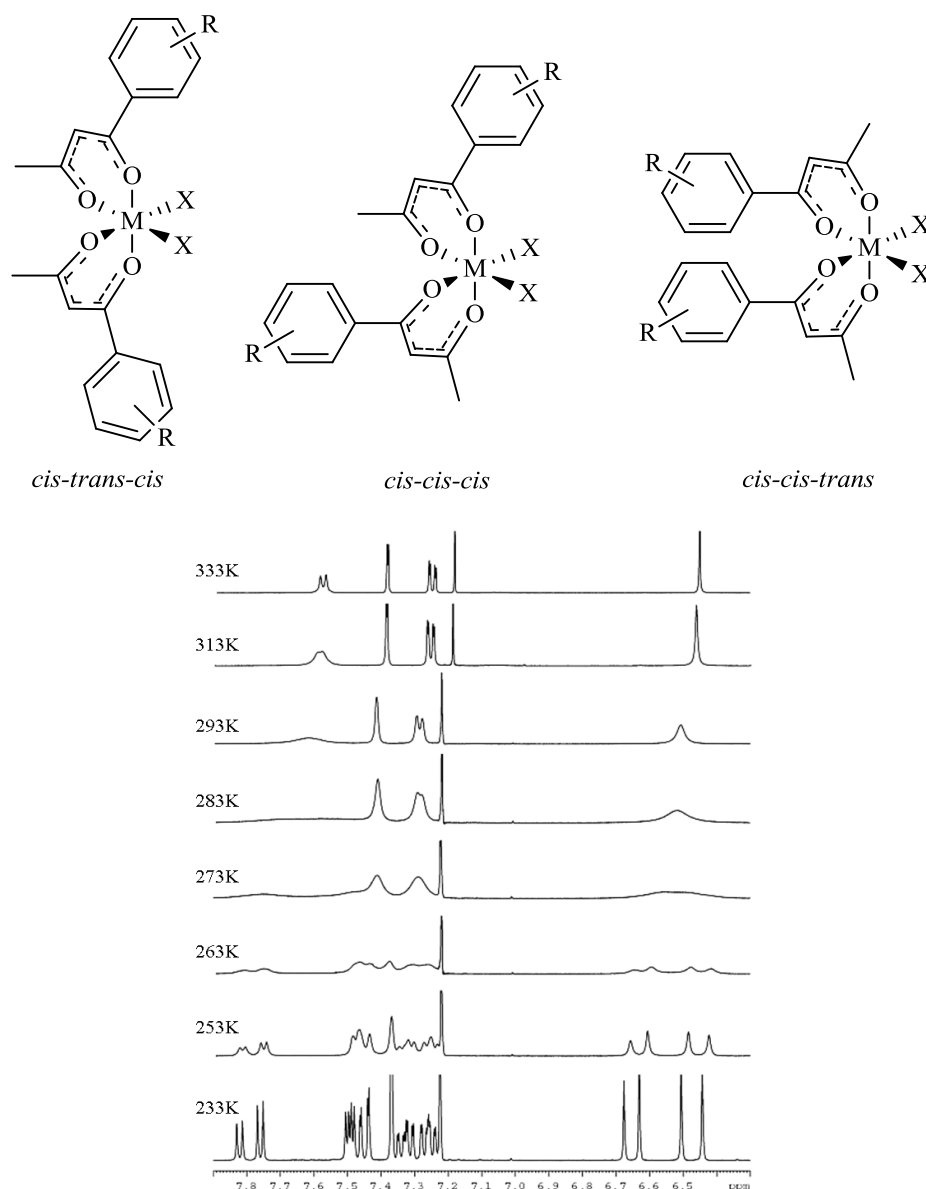
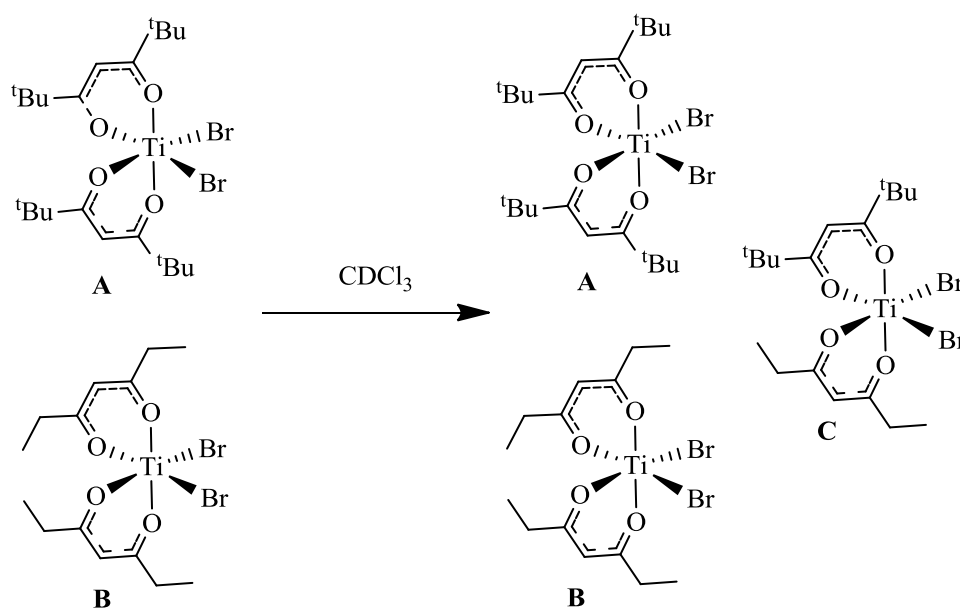


Figure 8.1 Possible *cis* isomers for the structure L_2TiX_2 ($L = \beta$ -diketonate, $X =$ halide) and the 1H NMR spectra from 333 K-233 K ($CDCl_3$, 300 MHz)

In order to restrict the number of isomers, the symmetrical titanium β -diketonate complexes **A** and **B** were synthesised to evaluate the nature of the exchange/fluxional process. These were both synthesised and the 1H NMR spectra recorded by Dr. Andrew Hebden. Approximately equal molar amounts of **A** and **B** were dissolved in deuterated chloroform and an initial proton spectrum was recorded at 300K. This showed two distinct sharp signals at 6.16 ppm and 6.01 ppm respectively, corresponding to the β -diketonate methine protons of both species. Another 1H NMR spectrum at 300K was recorded after eight hours and showed four separate signals in the same region. Two signals can be identified as

the original molecules **A** and **B** and the additional peaks for the ligand exchange product **C** (**Scheme 8.2**). The same experiment was carried out with complex **B** and free heptane-3,5-dione ligand, when followed using ^1H NMR the same exchange species was observed. It has been previously reported that zirconium compounds with higher coordination numbers of β -diketonate ligand also show an exchange process.⁸ The hexa coordinate β -diketonate complexes have shown fluxionality but we report that these group IV complexes show an exchange process.²



Scheme 8.2 Ligand exchange for symmetrical β -diketonate titanium (IV) compounds

The complexes **a-i** shown in **Scheme 8.1** and cisplatin were tested using the MTT assay stated in Chapter 4, using a 5-day incubation period at 37°C in a 5.0% CO_2 at atmosphere. The IC_{50} (μM) \pm SD values are shown in **Table 8.1** and also summarised as a bar-chart in **Figure 8.2**, complexes were tested against both HT-29 (human colon adenocarcinoma) and MCF-7 (human breast adenocarcinoma). Against HT-29 there is general trend seen in the cytotoxicity of the asymmetric complexes, with $\text{Hf} > \text{Zr} > \text{Ti}$. However, against MCF-7 asymmetric complexes of Ti and Zr do not show a particular trend, with the asymmetric Hf compounds all showing an increase in cytotoxicity when compared to both Ti and Zr. Symmetrical complexes **e**, **h** and **i** are comparable with cisplatin against both cell lines showing these symmetrical complexes to have superior cytotoxicity when compared to the asymmetric. An interesting result was seen for the symmetrical zirconium complex

e which has up to a 35-fold increase in its cytotoxicity when compared to **c**, against MCF-7. The *tris* diphenyl β -diketonate hafnium complex **i** is the most promising drug candidate of this library with high cytotoxicity values against both cell lines, with an IC_{50} value of $4.9 \pm 0.9 \mu\text{M}$ (cisplatin, $2.4 \pm 0.1 \mu\text{M}$) against the HT-29 cell line and $3.2 \pm 0.3 \mu\text{M}$ (cisplatin $1.1 \pm 0.08 \mu\text{M}$) against MCF-7. These results are in contrast to the *in vivo* results reported for the seven coordinate Hf complexes measured previously, which are only active in higher doses compared to the six coordinate counterparts.⁹ Our work also shows it is not essential to have two labile chloride ancillary ligands to gain high *in vitro* activity, suggesting these complexes may act *via* a different *in vitro* pathway to that of cisplatin.

Table 8.1 IC_{50} values for cisplatin and complexes **a-i** against HT-29 and MCF-7

Complexes	HT-29		MCF-7	
	IC_{50} (μM)	$\pm\text{SD}$	IC_{50} (μM)	$\pm\text{SD}$
Cisplatin	2.4	0.1	1.09	0.08
a	58	2	47	3
b	47	3	35	2
c	74	4	109	2
d	84	4	57	2
e	12.2	0.1	3.1	0.2
f	30.2	0.8	28.9	0.4
g	12	2	27	1
h	7.4	0.5	3.3	0.1
i	4.9	0.9	3.2	0.3

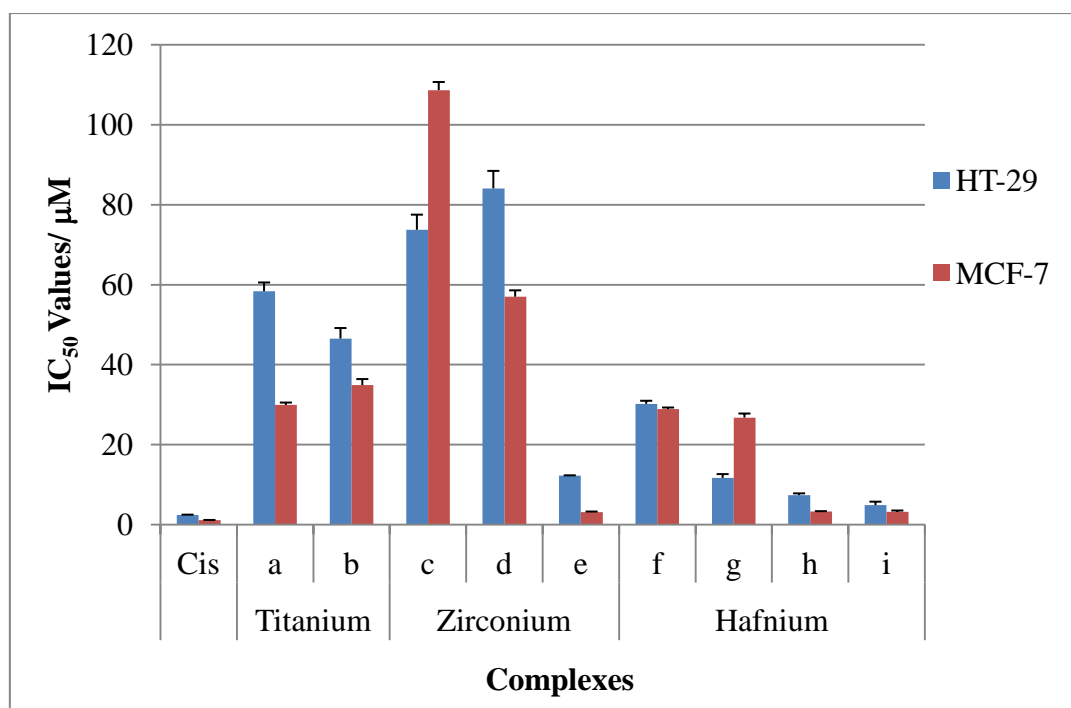
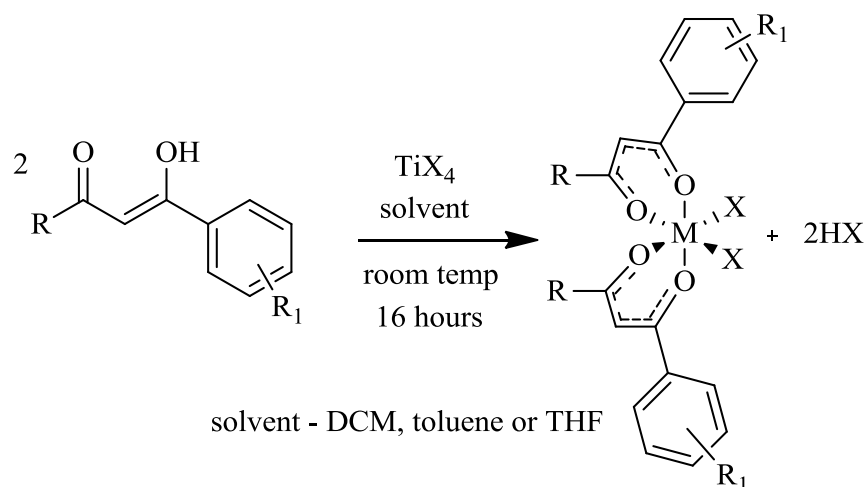


Figure 8.2 IC₅₀ values for cisplatin and complexes **a-i** against HT-29 and MCF-7

8.2 Attempted Synthesis of β -Diketonate Titanium (IV) Halide Complexes

Complexes were attempted to extend the library of complexes synthesised previously within the group. Synthesis was carried out according to **Scheme 8.3**, where two equivalents of the substituted β -diketonate ligand was added to one equivalent of titanium tetrahalide and stirred at room temperature in a relevant solvent.

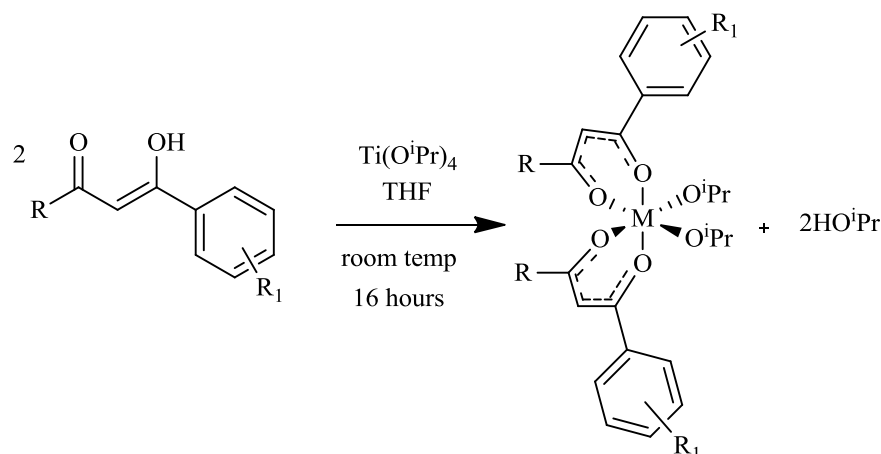


Scheme 8.3 Synthetic Pathway of β -Diketonate Titanium(IV) Complexes

Complexations have been attempted with the ligands **L1-L10**, however only crude ^1H NMR data has been obtained. Several of the NMR spectra show a shift in peaks for the methine CH, which suggests complexation. However, further analysis and bulk purification has proven unsuccessful for this library and further attempts to synthesise would include the use of a base in the hope to drive the reaction to completion.

8.3 β -Diketonate Titanium(IV) Isopropoxide Complexes

The synthesis of these complexes were attempted according to **Scheme 8.4**, where two equivalents of the substituted β -diketonate was added to one equivalent of titanium isopropoxide and stirred at room temperature in tetrahydrofuran.



Scheme 8.4 Synthetic pathway for titanium (IV) isopropoxide β -diketonate complexes

Complexations were attempting using ligands **L1-L10**, however only one product was obtained from this reaction, this complex was quickly oxidised and X-ray data shows a solvent bridged dimer. Re-synthesis of this complex and similar modifications has since proven unsuccessful.

8.3.1 ^1H NMR Data for $\text{Ti}_2(\text{C}_{28}\text{H}_{20}\text{N}_2\text{O}_4)(\text{OCH}_3)_6$ (**20**)

The crude ^1H NMR data were obtained for complex **20** (**Figure 8.3**), shows the complex with free ligand **L5** and clear shifts can be seen in ppm values and notable new peaks seen for the bridging methanol groups at approximately 1.0 ppm (**Figure 8.4**). However, the crystals disintegrated upon analyses before bulk purification was obtained.

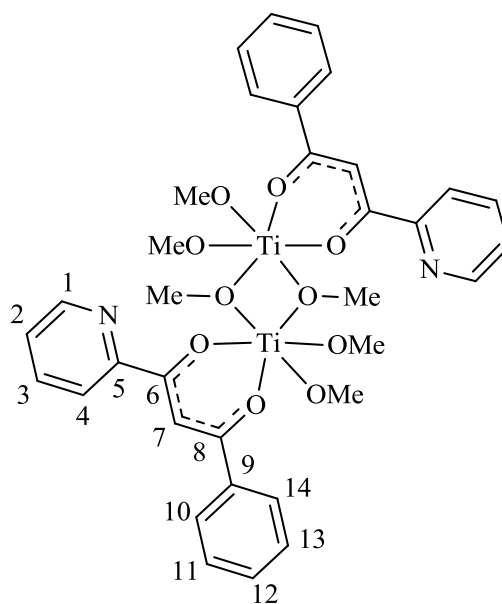


Figure 8.3 Structure of complex **20**

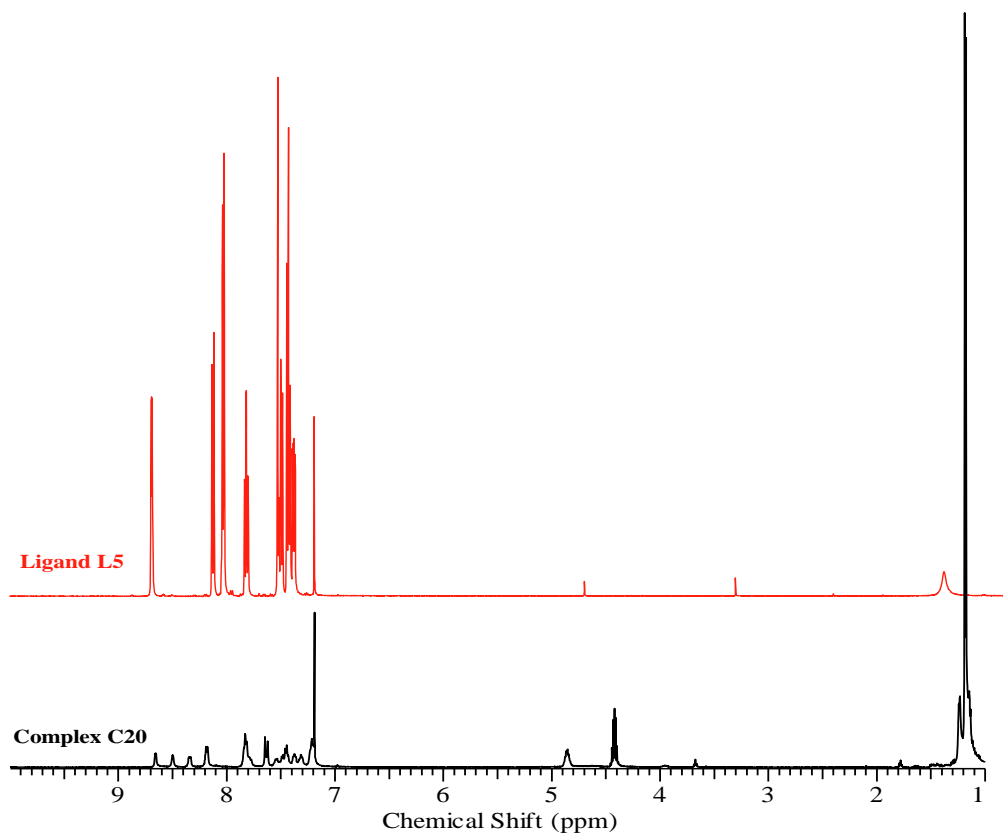


Figure 8.4 ^1H NMR data for complex **20** and unreacted ligand **L5** (CDCl_3 , 300 MHz, 300K)

8.3.2 X-ray Crystallography of $\text{Ti}_2(\text{C}_{28}\text{H}_{20}\text{N}_2\text{O}_4)(\text{OCH}_3)_6$ (**20**)

Yellow crystals of **20** suitable for X-ray crystallographic analysis were obtained from methanol at -20°C , over a period of 2 weeks. The molecular structure is given in **Figure 8.5**, selected bond lengths and angles are stated in **Table 8.2**. This compound crystallised in a monoclinic cell and structural solution was performed in the space group $P2_1/c$, with half a molecule in the asymmetric unit.

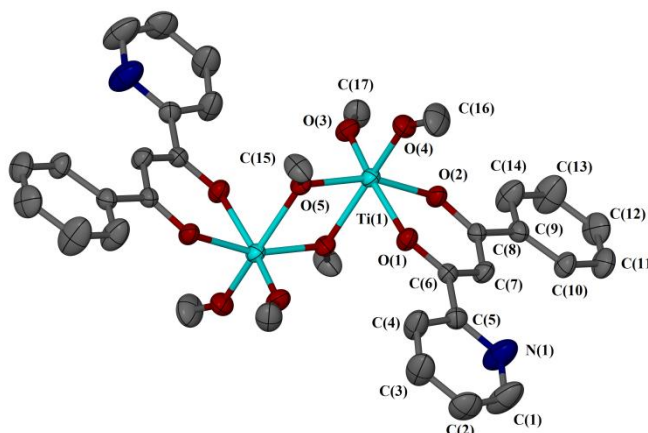


Figure 8.5 Molecular structure of **20**. Displacement ellipsoids are at the 50% probability level and hydrogen atoms are omitted for clarity.

Table 8.2 Selected bond lengths and angles for **20**

Bond	Distance (Å)	Bond	Angle (°)
Ti(1)-O(1)	2.0389(11)	O(1)-Ti(1)-O(2)	82.12(5)
Ti(1)-O(2)	2.0695(12)	O(1)-Ti(1)-O(3)	167.65(5)
Ti(1)-O(3)	1.8077(13)	O(1)-Ti(1)-O(4)	87.08(6)
Ti(1)-O(4)	1.8114(13)	O(1)-Ti(1)-O(5)	88.18(5)
Ti(1)-O(5)	1.9906(11)	O(2)-Ti(1)-O(3)	86.01(5)
O(1)-C(6)	1.2726(19)	O(2)-Ti(1)-O(4)	99.42(6)
C(6)-C(7)	1.411(2)	O(2)-Ti(1)-O(5)	90.11(5)
C(7)-C(8)	1.392(2)	O(3)-Ti(1)-O(4)	98.28(6)
C(8)-O(2)	1.2887(19)	O(3)-Ti(1)-O(5)	102.33(5)
		O(4)-Ti(1)-O(5)	95.13(5)
		Ti(1)-O(5)-Ti(1) ^(a)	106.31(5)
		O(5)-Ti(1)-O(5) ^(a)	73.69(5)

Symmetry related atoms (a) 1-x, -y, 1-z

The packing diagrams of **20** when viewed along the *c* axis shows the molecules pack in pairs of molecules with C-H...Cg interactions between each plane. Intramolecular interactions are seen between C(7)-H(7)...N(1), C(15)-C(15B)...O(1) and C(16)-C(16A)...O(2), and two intermolecular interactions between C(11)-H(11)...O(4) and C(16)-H(16C)...Cg(2). The packing diagrams are shown in **Figure 8.6**, with D...A distances and torsion angles stated in **Table 8.3**. A similar complex was obtained within the McGowan research group when reacting Ti(iOPr)₄ with two equivalents of a picolinamide ligand.¹⁰ These structures are similar to those by Johnson *et al.*, which were used for heterogeneous titanium-centred epoxidation catalysts.¹¹

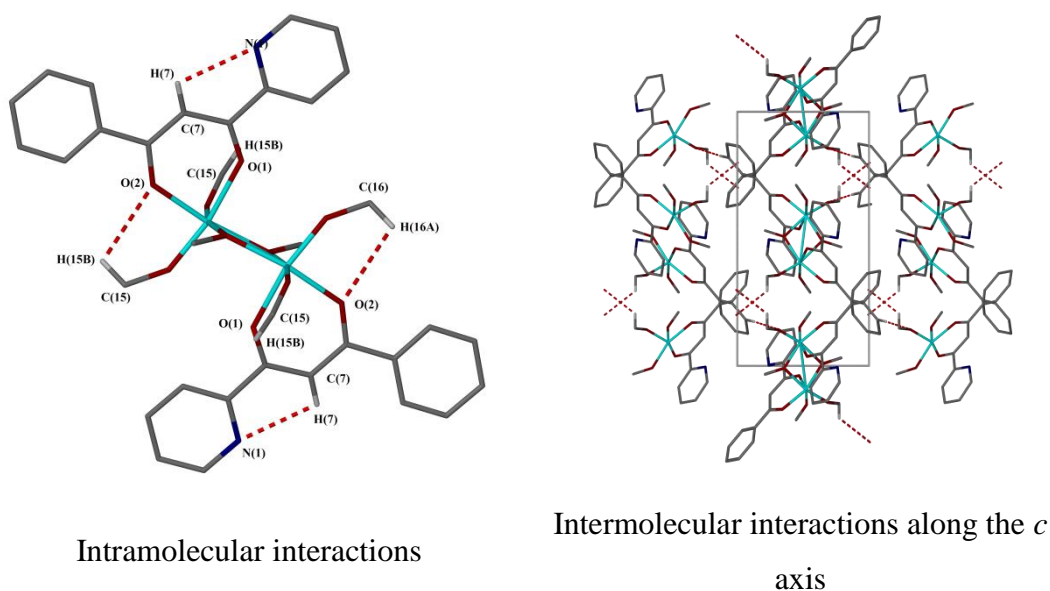


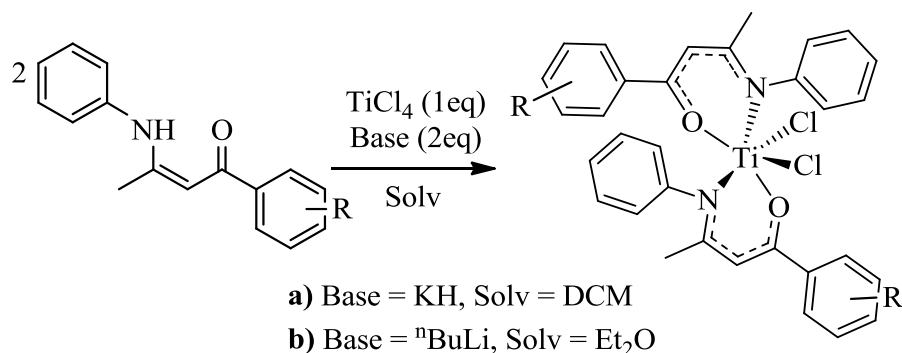
Figure 8.6 Packing diagram of **20** when viewed along the *c* axis

Table 8.3 Bond lengths and torsion angles for **20**

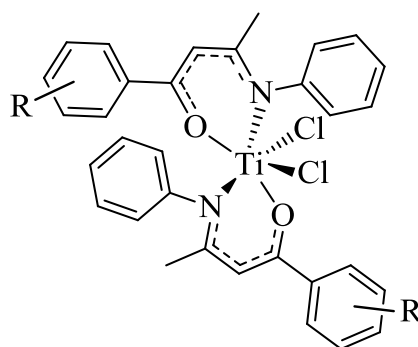
Interaction	Atoms	Bond Lengths and Angles
Intramolecular	C(7)-H(7)...N(1)	2.871(3) Å
	C(15)-C(15B)...O(1)	3.155(3) Å
	C(16)-H(16A)...O(2)	3.104(3) Å
Intermolecular	Cg(2)...Cg(4)	2.9723 Å
	C(11)-H(11)...O(4)	3.348(3) Å
	C(16)-H(16C)...Cg(3)	3.683 Å
Torsion	Cg(1)...Cg(2)	10.03°
	Cg(2)...Cg(3)	5.81°

8.4 β -Ketoiminate Titanium(IV) Chloride Complexes

The β -ketoiminate titanium (IV) chloride complexes were synthesised according to **Scheme 8.5**, where two equivalents of the substituted β -ketoiminate ligand and two equivalents of base were added to one equivalent of titanium tetrachloride and stirred at room temperature in a relevant solvent.



Scheme 8.5 Synthetic Route for β -Ketoiminate Titanium(IV) Chloride Complexes



R = 3'-F	21	R = 4'-Me	24
4'-Cl	22	4'-Et	25
4'-F	23	2',5'-diCl	26

Figure 8.7 List of β -ketoiminate titanium (IV) complexes synthesised in this chapter

Complexes **21-26** (**Figure 8.7**) were synthesised and characterised by the author, with full experimental data is described in Chapter 9. Limited analysis has been obtained for these complexes due to their extreme air sensitivity, however where possible complexes have been characterised by ¹H NMR, ¹H-¹H COSY, ¹³C{¹H}NMR, ¹H-¹³C{¹H} HMQC spectroscopy and mass spectrometry. In addition X-ray crystallographic data have been obtained for complexes **21-25**.

8.5 NMR Data for Titanium(IV) Chloride Complexes

The ^1H NMR has been obtained for complexes **22** and **24-27** using either deuterated chloroform or acetonitrile. A general structure is shown in **Figure 8.8** and an example for complex **25** shown in **Figure 8.9**. All spectra show a shift in proton peak for the methine CH **g** at approximately 6.0 ppm. The aromatic protons **b-d** and **j-l** all appear in the same region between 6.5-8.0 ppm and the methyl protons **e** between 1.5-2.0 ppm. The NH from the free β -ketoiminate is usually seen at approximately 12-13 ppm disappears upon complexation.

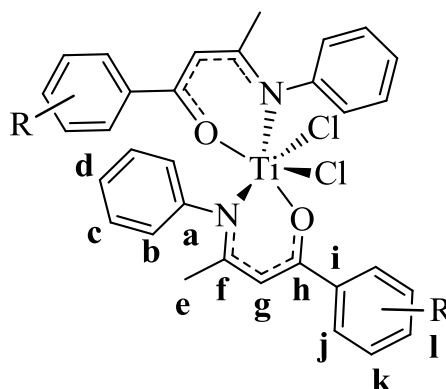


Figure 8.8 General structure of a β -ketoiminate titanium chloride complex

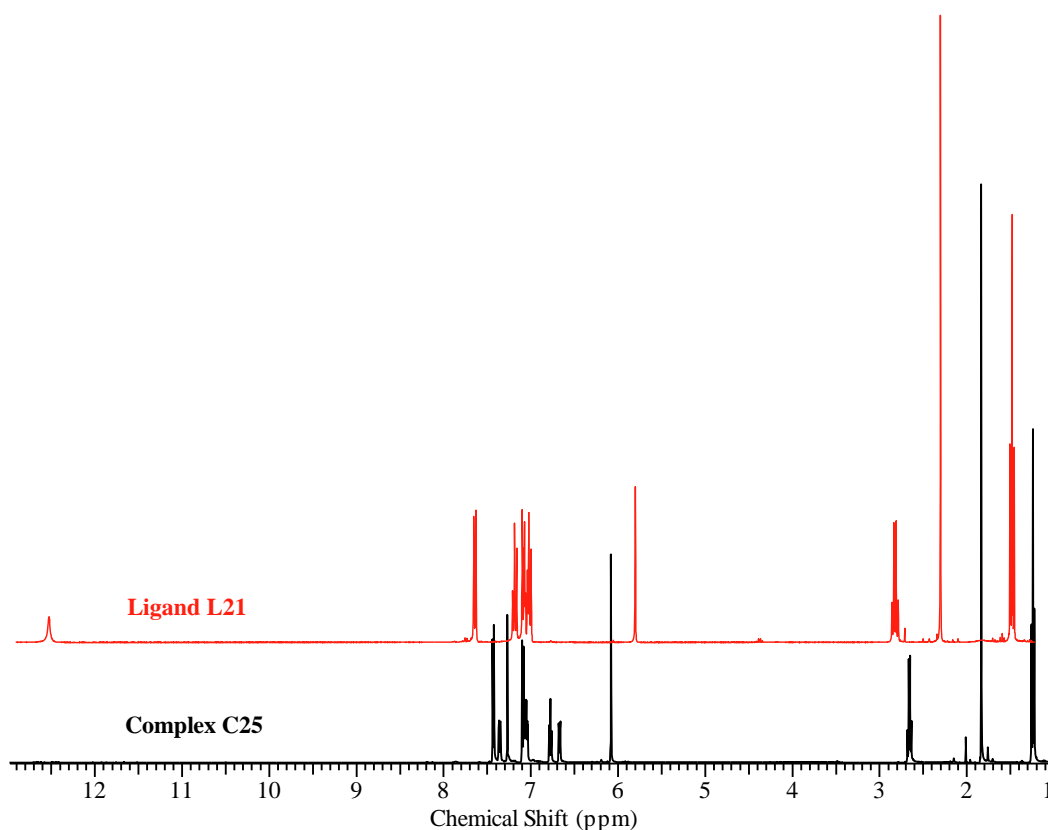


Figure 8.9 ^1H NMR spectra for complex **25** and free ligand **L21** (CDCl_3 , 300 MHz, 300K)

When analysing the $^{13}\text{C}\{^1\text{H}\}$ NMR spectra for the β -ketoiminate titanium complexes, they have similar trends with the highest shifts seen for the quaternary carbons **f** and **h** which are typically in the range 170-190 ppm. All of the CH peaks for the β -ketoiminate ligand are in the range 100-150 ppm. The methine CH **g** from the β -ketoiminate ligand is typically seen at 93-95 ppm and the lowest chemical shifts between 18-31 ppm for the methyl carbon **e**.

8.6 X-ray Crystallography for Titanium(IV) Chloride Complexes

Crystals were obtained from either acetonitrile or dichloromethane solutions stored at -20°C , appearing as yellow-red single crystals. X-ray crystallographic data was analysed for complexes **21-25**. Solutions were performed in either a monoclinic (**21**, **22**, **24** and **25**) or a trigonal (**23**) space groups. All of the angles around the metal centre show the geometry expected for an octahedral compound which is common for these *bis* chelating ligand structures. The angles between the N-Ti-O, N-Ti-Cl and O-Ti-Cl are expected to be 90° and complexes here show angles ranging between $85-97^\circ$. The smaller angles can be explained due to the restrictions caused by the bidentate ligand. The other coordination sites are occupied by the chloride ligands and have a Cl-Ti-Cl angle of $94-97^\circ$ and it appears that these complexes prefer a *cis-trans-cis* geometry, with the chlorides in a *cis* arrangement.

8.6.1 X-Ray Characterisation for $\text{Ti}(\text{C}_{32}\text{H}_{26}\text{F}_2\text{N}_2\text{O}_2)\text{Cl}_2$ (**21**)

Yellow crystals of **21** suitable for X-ray crystallographic analysis were obtained from DCM at room temperature, over a period of 3 days. The molecular structure is given in **Figure 8.10** with selected bond lengths and angles are stated in **Table 8.4**. Complex **20** crystallised in a monoclinic cell and structural solution was performed in the space group $C2/c$, with half a molecule in the asymmetric unit and has a *cis-trans-cis* geometry.

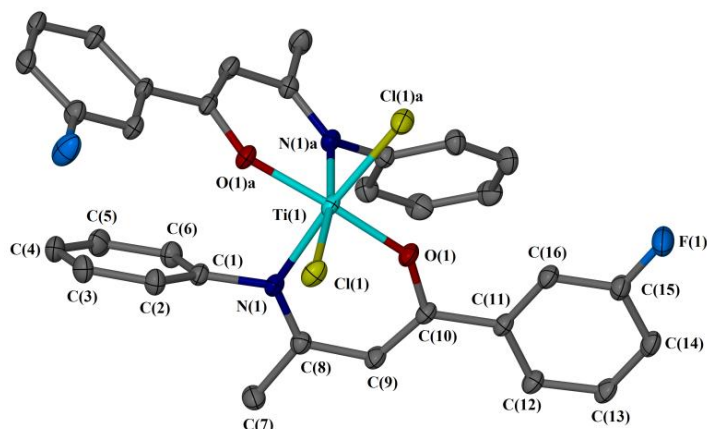


Figure 8.10 Molecular structure of **21**, displacement ellipsoids are at the 50% probability level and hydrogen atoms are omitted for clarity.

Table 8.4 Selected bond lengths and bond angles for **21**

Bond	Distance (Å)	Bond	Angle (°)
Ti(1)-Cl(1)	2.3385(4)	Cl(1)-Ti(1)-N(1)	88.67(3)
Ti(1)-N(1)	2.2090(10)	Cl(1)-Ti(1)-O(1)	95.84(3)
Ti(1)-O(1)	1.8824(8)	N(1)-Ti(1)-O(1)	81.54(4)
C(1)-N(1)	1.4561(14)	Cl(1)-Ti(1)-Cl(1) ^(a)	96.01(2)
N(1)-C(8)	1.3330(15)	Ti(1)-N(1)-C(1)	115.55(7)
C(7)-C(8)	1.5303(18)	Ti(1)-N(1)-C(8)	127.47(8)
C(8)-C(9)	1.4502(16)	C(1)-N(1)-C(8)	116.93(10)
C(9)-C(10)	1.3772(17)	N(1)-C(8)-C(9)	122.88(11)
O(1)-C(10)	1.3259(13)	C(8)-C(9)-C(10)	124.37(11)
C(10)-C(11)	1.4987(15)	C(9)-C(10)-O(1)	120.46(10)
		Ti(1)-O(1)-C(10)	142.06(8)
		O(1)-C(10)-C(11)	114.10(10)

Symmetry related atoms (a) $-x, +y, 1/2-z$

The packing diagrams show that when viewed in the b - c and a - b planes shows the molecules packing in pairs with a slight herringbone arrangement. There is an intramolecular hydrogen bonding interactions between C(16)-H(16)...O(1), and a suggested π - π stacking interaction between Cg(3)-Cg(3) of 3.5412(9) Å. The

interactions and packing diagrams are presented in **Figure 8.11**, with D...A distances and torsion angles stated in **Table 8.5**.

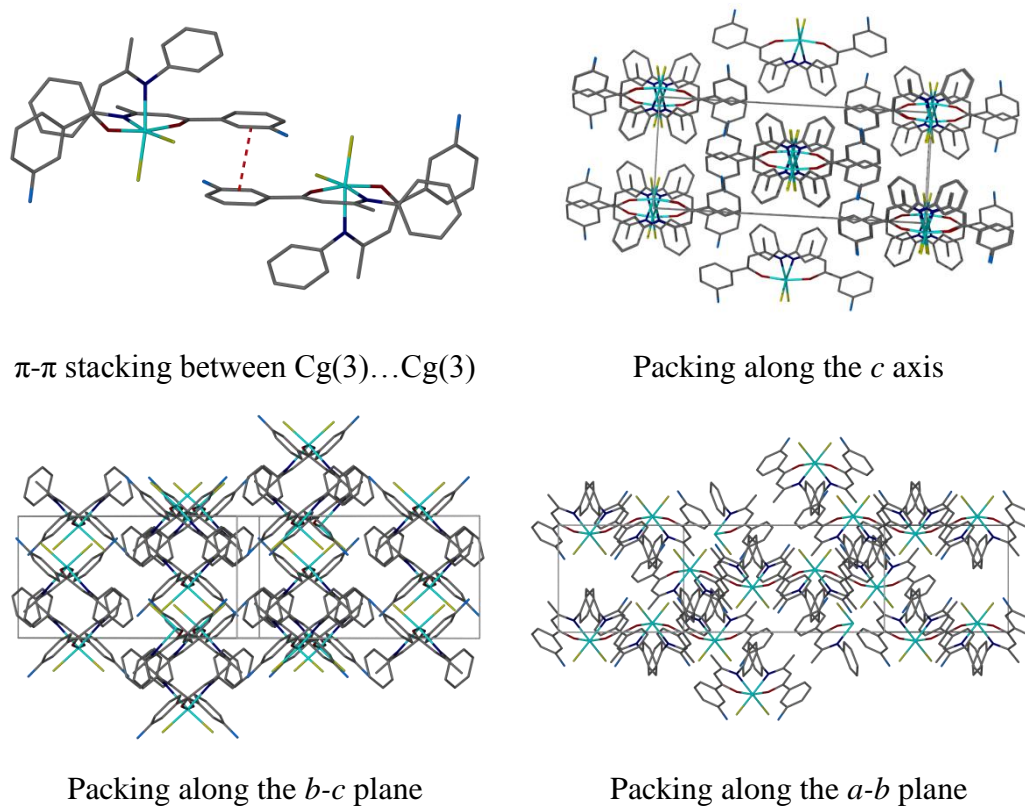


Figure 8.11 Interactions and packing diagrams for **21**

Table 8.5 Bond lengths and torsion angles for **21**

Interaction	Atoms	Bond Lengths and Angles
Intramolecular	C(16)-H(16)...O(1)	2.7011(16) Å
Intermolecular	Cg(3)...Cg(3)	3.5412 Å
Torsion	Cg(1)...Cg(2)	71.81°
	Cg(2)...Cg(3)	1.83°

8.6.2 X-Ray Characterisation for $\text{Ti}(\text{C}_{32}\text{H}_{26}\text{Cl}_2\text{N}_2\text{O}_2)\text{Cl}_2$ (**22**)

Yellow crystals of **22** suitable for X-ray crystallographic analysis were obtained from DCM at room temperature, over a period of several days. The molecular structure is given in **Figure 8.10**, selected bond lengths and angles are stated in **Table 8.4**. Complex **22** crystallised in a monoclinic cell and structural solution was performed in the space group $P2_1/n$, with one molecule in the asymmetric unit and two molecules of acetonitrile, and a *cis-trans-cis* geometry.

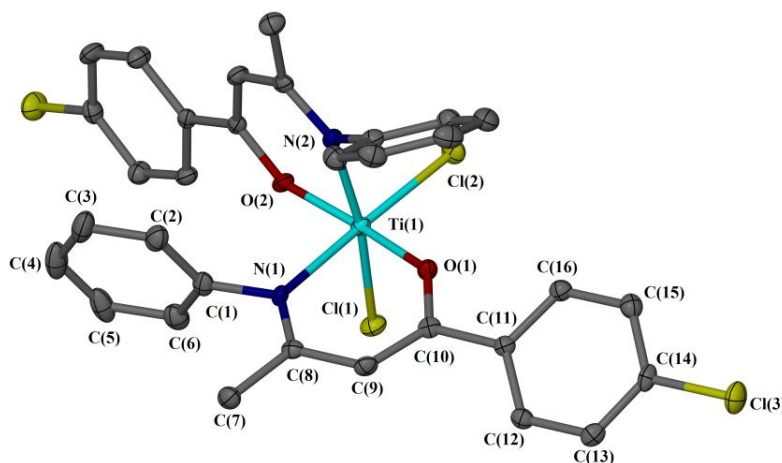
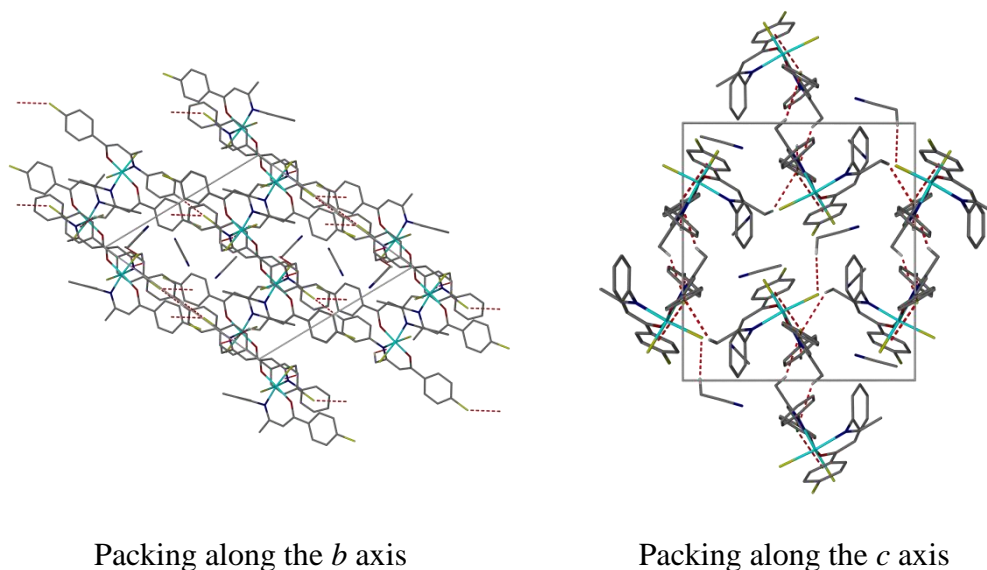


Figure 8.12 Molecular structure of **22**, displacement ellipsoids are at the 50% probability level and hydrogen atoms and solvent molecules are omitted for clarity

Table 8.6 Selected bond lengths and angles for **22**

Bond	Distance (Å)	Bond	Angle (°)
Ti(1)-Cl(1)	2.3364(8)	Cl(1)-Ti(1)-Cl(2)	95.93(3)
Ti(1)-Cl(2)	2.3161(8)	Cl(1)-Ti(1)-N(1)	87.13(6)
Ti(1)-N(1)	2.153(2)	Cl(1)-Ti(1)-O(1)	93.55(6)
Ti(1)-N(2)	2.149(2)	Cl(1)-Ti(1)-N(2)	172.01(6)
Ti(1)-O(1)	1.8881(17)	Cl(1)-Ti(1)-O(2)	92.18(6)
Ti(1)-O(2)	1.8698(17)	Cl(2)-Ti(1)-N(1)	174.39(6)
N(1)-C(8)	1.317(3)	Cl(2)-Ti(1)-O(1)	92.63(6)
C(8)-C(9)	1.423(4)	Cl(2)-Ti(1)-N(2)	90.63(6)
C(9)-C(10)	1.363(4)	Cl(2)-Ti(1)-O(2)	94.54(6)
C(10)-O(1)	1.316(3)	O(1)-Ti(1)-O(2)	170.31(8)
N(2)-C(28)	1.324(3)	O(1)-Ti(1)-N(1)	82.47(8)
C(28)-C(29)	1.424(4)	O(1)-Ti(1)-N(2)	90.68(8)
C(29)-C(30)	1.362(4)	O(2)-Ti(1)-N(1)	90.03(8)
C(30)-O(2)	1.320(3)	O(2)-Ti(1)-O(1)	82.74(8)
C(14)-Cl(3)	1.732(3)	N(1)-Ti(1)-N(2)	86.72(8)
C(34)-Cl(4)	1.739(3)		

When viewed along the *c* axis the molecules pack in a head-tail...tail-head arrangement with a slight herringbone structure. There is one intramolecular hydrogen bonding interaction between C(36)-H(36)...O(2) and several intermolecular interactions contributing to the packing of these molecules. The interactions and packing diagrams are presented in **Figure 8.13**, with D...A distances and torsion angles stated in **Table 8.7**.

**Figure 8.13** Packing diagram for **22****Table 8.7** Bond lengths and torsion angles for **22**

Interaction	Atoms	Bond Lengths and Angles
Intramolecular	C(36)-H(36)...O(2)	3.471(3) Å
Intermolecular	Cg(1)...Cg(5)	3.6996 Å
	C(7)-H(7A)...Cg(3)	3.463 Å
	C(27)-H(27C)...Cg(3)	3.573 Å
	C(14)-Cl(3)...Cg(6)	5.174 Å
	C(4)-H(4)...Cl(3)	3.471(3) Å
	C(39)-H(39B)...Cl(1)	3.554(3) Å
Torsion	Cg(1)...Cg(2)	82.97°
	Cg(2)...Cg(3)	27.61°
	Cg(4)...Cg(5)	70.41°
	Cg(5)...Cg(6)	7.15°

8.6.3 X-ray Crystallography for $\text{Ti}(\text{C}_{32}\text{H}_{26}\text{F}_2\text{N}_2\text{O}_2)\text{Cl}_2$ (**23**)

Orange crystals of **23** suitable for X-ray crystallographic analysis were obtained from DCM at -20°C , over a period of several weeks. The molecular structure is given in **Figure 8.14**, selected bond lengths and angles are stated in **Table 8.8**. This compound crystallised in a trigonal cell and structural solution was performed in the space group R-3, with a third molecule in the asymmetric unit. This complex oxidised on exposure to air and is an oxygen bridged trimer (**Figure 8.15**), instead of the expected *cis*-chloride monomer.

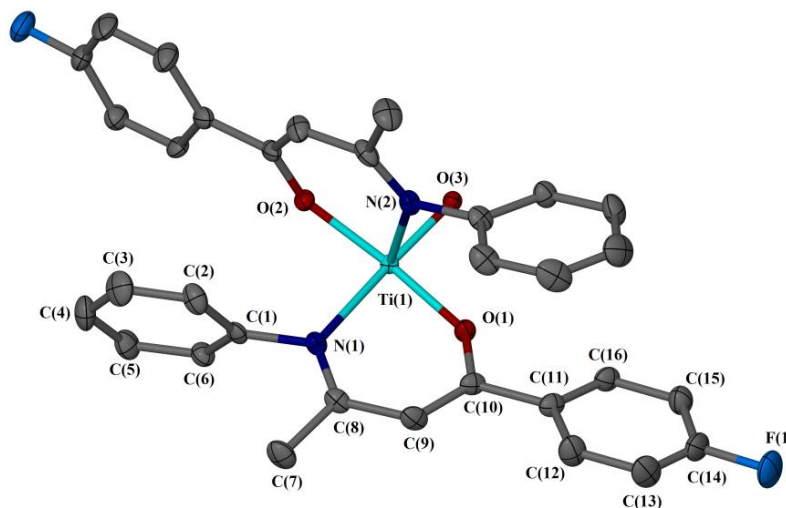


Figure 8.14 Asymmetric unit of **23**, displacement ellipsoids are at the 50% probability level and hydrogen atoms and other molecules are omitted for clarity

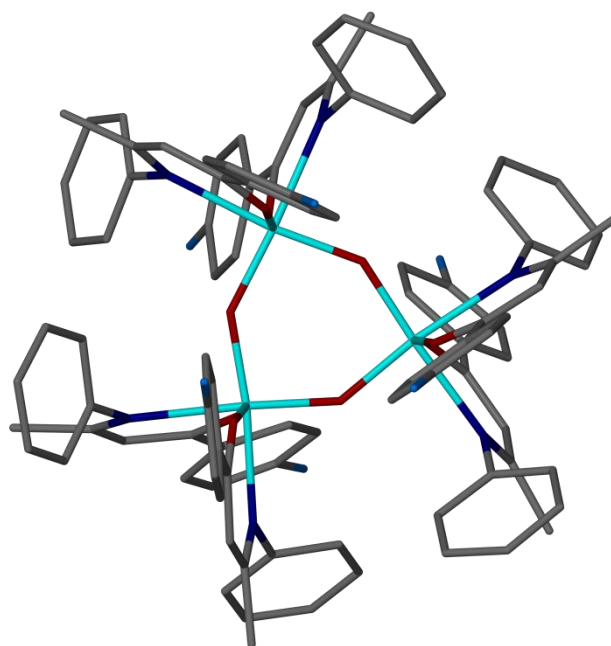


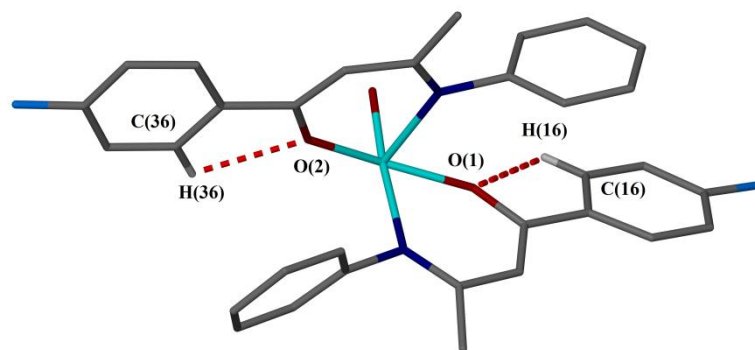
Figure 8.15 Molecular structure of the oxygen bridged trimer, ellipsoids and hydrogens omitted for clarity.

Table 8.8 Selected bond lengths and angles for **23**

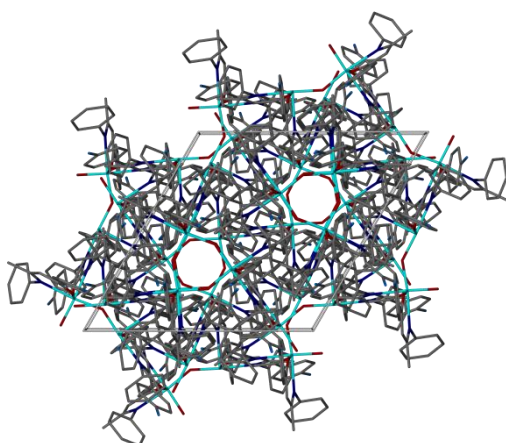
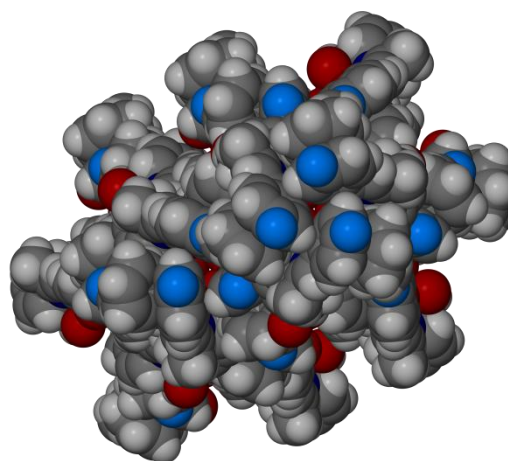
Bond	Distance (Å)	Bond	Angle (°)
Ti(1)-O(3)	1.833(2)	O(3)-Ti(1)-O(1)	96.18(9)
Ti(1)-O(3) ^(a)	1.854(3)	O(3)-Ti(1)-O(2)	96.70(9)
Ti(1)-N(1)	2.310(3)	O(3)-Ti(1)-N(1)	175.60(10)
Ti(1)-O(1)	1.949(2)	O(3)-Ti(1)-N(2)	89.60(10)
Ti(1)-N(2)	2.308(3)	O(3)-Ti(1)-O(3) ^(a)	96.87(11)
Ti(1)-O(2)	1.938(2)	O(1)-Ti(1)-O(2)	160.34(12)
N(1)-C(8)	1.322(5)	O(1)-Ti(1)-N(1)	80.71(9)
C(8)-C(9)	1.444(5)	O(1)-Ti(1)-N(2)	84.25(10)
C(9)-C(10)	1.380(6)	O(1)-Ti(1)-O(3) ^(a)	96.30(9)
C(10)-O(1)	1.316(5)	O(2)-Ti(1)-N(1)	85.54(9)
N(2)-C(28)	1.469(4)	O(2)-Ti(1)-N(2)	81.04(10)
C(28)-C(29)	1.443(5)	O(2)-Ti(1)-O(3) ^(a)	96.84(9)
C(29)-C(30)	1.388(6)	N(1)-Ti(1)-N(2)	87.00(10)
C(30)-O(2)	1.315(5)	N(1)-Ti(1)-O(3) ^(a)	86.60(11)
C(14)-F(1)	1.391(4)	N(2)-Ti(1)-O(3) ^(a)	173.40(11)
C(34)-F(2)	1.382(4)		

Symmetry related atoms (a) 1-y, x-y, z

The packing diagram when viewed along the c axis shows the molecules pack in a circular arrangement with the symmetry generated oxygen atom forming a cavity in the centre. A space filling diagram is shown along this axis and shows that this space is not large enough to be a void. Intramolecular interactions are seen between C-H...O of both β -ketoiminate ligands and several intermolecular π - π and X...Cg interactions which contribute to the packing of these molecules. The interactions and packing diagrams are presented in **Figure 8.16**, with D...A distances and torsion angles stated in **Table 8.9**. These types of oxygen bridged complexes have been shown within the McGowan group when reacting TiCl₄ with two equivalents of a picolinamide ligand.¹⁰



Intramolecular interactions

Packing along the *c* axis

Space filling diagram

Figure 8.16 Intramolecular interactions and packing diagrams of **23****Table 8.9** Bond lengths and torsion angles for **23**

Interaction	Atoms	Bond Lengths and Angles
Intramolecular	C(16)-H(16)...O(1)	2.741(4) Å
	C(36)-H(36)...O(2)	2.728(4) Å
Intermolecular	Cg(2)...Cg(5)	3.3429 Å
	Cg(3)...Cg(4)	3.936 Å
	C(15)-H(15)-Cg(3)	3.583 Å
Torsion	Cg(1)...Cg(2)	76.01°
	Cg(2)...Cg(3)	16.40°
	Cg(4)...Cg(5)	70.82°
	Cg(5)...Cg(6)	7.52°

8.6.4 X-ray Crystallography for $\text{Ti}(\text{C}_{34}\text{H}_{32}\text{N}_2\text{O}_2)\text{Cl}_2$ (24**)**

Orange crystals of **24** suitable for X-ray crystallographic analysis were obtained from acetonitrile at -20°C , over a period of several weeks. The molecular structure is given in **Figure 8.17**, selected bond lengths and angles are stated in **Table 8.10**. This compound crystallised in a monoclinic cell and structural solution was performed in the space group $P2_1/n$, with a one molecule and two molecules of acetonitrile in the asymmetric unit, and a *cis-trans-cis* geometry.

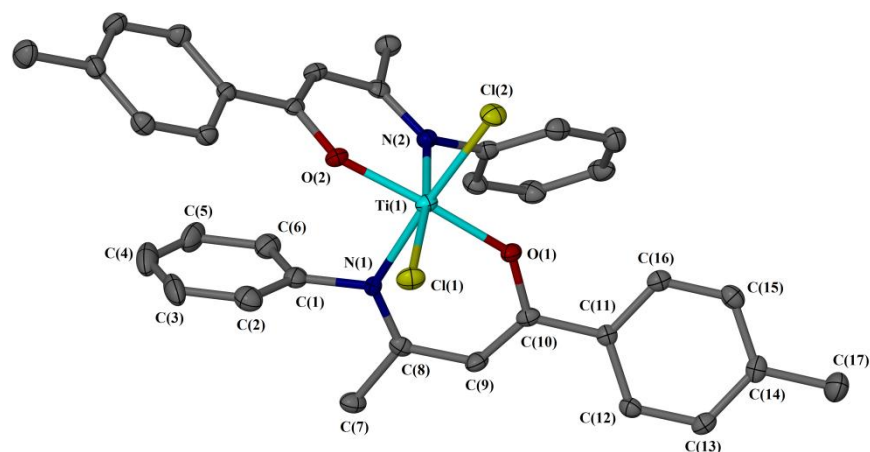


Figure 8.17 Molecular structure of **24**, displacement ellipsoids are at the 50% probability level and hydrogen atoms and other molecules are omitted for clarity.

Table 8.10 Selected bond lengths and angles for **24**

Bond	Distance (Å)	Bond	Angle (°)
Ti(1)-Cl(1)	2.3447(7)	Cl(1)-Ti(1)-Cl(2)	95.28(3)
Ti(1)-Cl(2)	2.3251(8)	Cl(1)-Ti(1)-N(1)	87.20(5)
Ti(1)-N(1)	2.1450(18)	Cl(1)-Ti(1)-O(1)	93.39(5)
Ti(1)-N(2)	2.1543(18)	Cl(1)-Ti(1)-N(2)	172.62(5)
Ti(1)-O(1)	1.8904(13)	Cl(1)-Ti(1)-O(2)	92.52(5)
Ti(1)-O(2)	1.8695(13)	Cl(2)-Ti(1)-N(1)	175.09(5)
N(1)-C(8)	1.327(3)	Cl(2)-Ti(1)-O(1)	92.88(5)
C(8)-C(9)	1.423(3)	Cl(2)-Ti(1)-N(2)	90.72(5)
C(9)-C(10)	1.355(3)	Cl(2)-Ti(1)-O(2)	94.35(5)
C(10)-O(1)	1.325(3)	O(1)-Ti(1)-O(2)	170.20(7)
N(2)-C(28)	1.325(2)	O(1)-Ti(1)-N(1)	82.73(6)
C(28)-C(29)	1.425(3)	O(1)-Ti(1)-N(2)	90.59(6)
C(29)-C(30)	1.366(3)	O(2)-Ti(1)-N(1)	89.76(6)
C(30)-O(2)	1.323(2)	O(2)-Ti(1)-O(1)	82.72(6)
C(14)-C(17)	1.503(3)	N(1)-Ti(1)-N(2)	87.14(7)
C(34)-Cl(37)	1.505(3)		

When viewed along the *c* axis, the molecules pack in pairs with C-H...Cg interactions between each pair. There are also X...C-H interactions seen with the acetonitrile solvent molecules. Unlike complex **23**, this molecule shows a C-H...O hydrogen bonding in just one β -ketoiminate ligands as the other ligand has a larger torsion angle between the planar centre and the aromatic ring. There are several intermolecular interactions contributing to the packing of these molecules. The interactions and packing diagrams are presented in **Figure 8.18**, with D...A distances and torsion angles stated in **Table 8.11**.

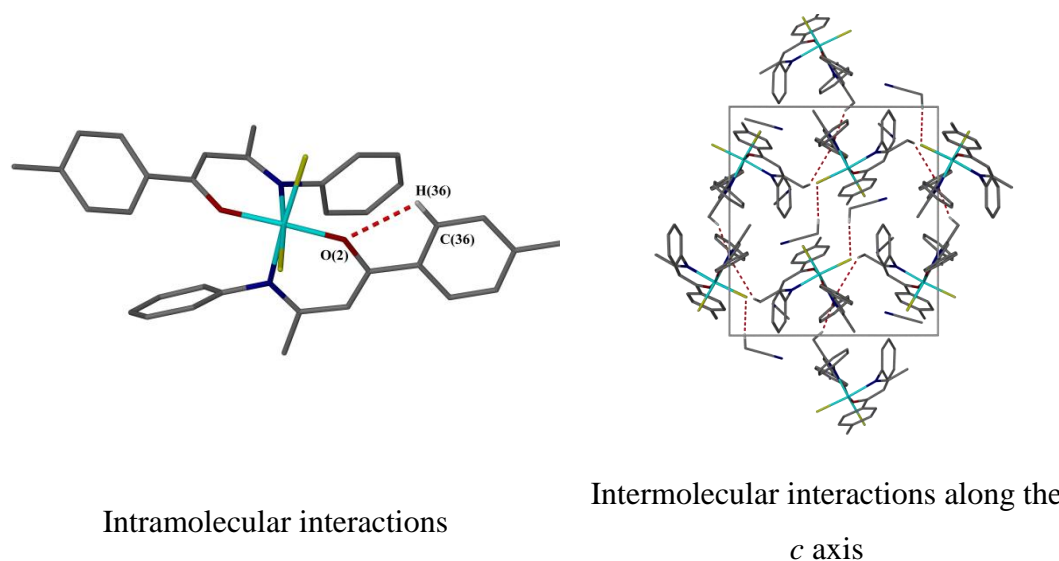


Figure 8.18 Intramolecular interaction and packing diagram for **24**

Table 8.11 Bond lengths and torsion angles for **24**

Interaction	Atoms	Bond Lengths and Angles
Intramolecular	C(36)-H(36)-O(2)	2.749(2) Å
Intermolecular	Cg(1)...Cg(5)	3.7132 Å
	C(7)-H(7C)-Cg(3)	3.429 Å
	C(27)-H(27A)-Cg(3)	3.547 Å
	C(41)-H(41B)-Cl(1)	3.588(3) Å
Torsion	Cg(1)...Cg(2)	84.58°
	Cg(2)...Cg(3)	28.39°
	Cg(4)...Cg(5)	69.26°
	Cg(5)...Cg(6)	7.67°

8.6.5 X-ray Crystallography for $\text{Ti}(\text{C}_{36}\text{H}_{36}\text{N}_2\text{O}_2)\text{Cl}_2$ (**25**)

Orange crystals of **25** suitable for X-ray crystallographic analysis were obtained from acetonitrile at -20°C , over a period of several weeks. The molecular structure is given in **Figure 8.19**, selected bond lengths and angles are stated in **Table 8.12**. This compound crystallised in a monoclinic cell and structural solution was performed in the space group $C2/c$, with a half a molecule in the asymmetric unit, and a *cis-trans-cis* geometry.

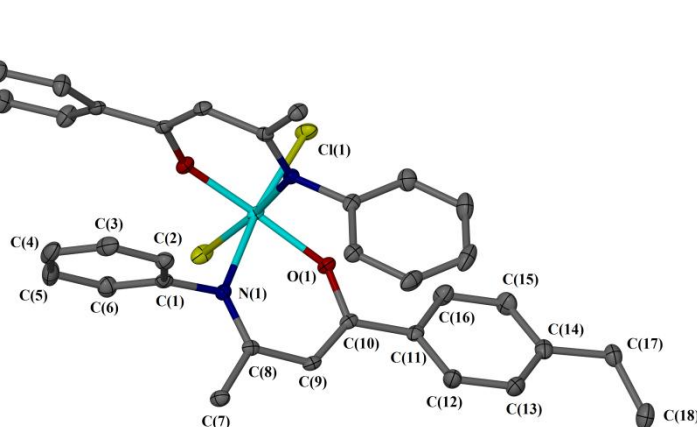


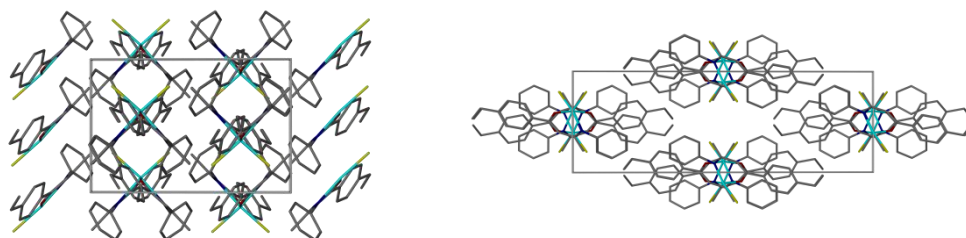
Figure 8.19 Molecular structure of **25**, displacement ellipsoids are at the 50% probability level and hydrogen atoms are omitted for clarity

Table 8.12 Selected bond lengths and angles for **25**

Bond	Distance (Å)	Bond	Angle (°)
Ti(1)-Cl(1)	2.3238(7)	Cl(1)-Ti(1)-Cl(1) ^(a)	96.42(4)
Ti(1)-N(1)	2.1710(15)	Cl(1)-Ti(1)-N(1)	170.63(6)
Ti(1)-O(1)	1.8673(18)	Cl(1)-Ti(1)-O(1)	91.15(5)
N(1)-C(8)	1.319(3)	Cl(1)-Ti(1)-N(1) ^(a)	90.23(5)
C(8)-C(9)	1.437(3)	Cl(1)-Ti(1)-O(1) ^(a)	95.58(5)
C(9)-C(10)	1.362(2)	Cl(1) ^(a) -Ti(1)-N(1)	90.23(5)
C(10)-O(1)	1.319(3)	Cl(1) ^(a) -Ti(1)-O(1)	95.58(5)
C(14)-C(17)	1.512(3)	Cl(1) ^(a) -Ti(1)-N(1) ^(a)	170.63(6)
		Cl(1) ^(a) -Ti(1)-O(1) ^(a)	91.15(5)
		O(1)-Ti(1)-O(1) ^(a)	169.91(6)
		O(1)-Ti(1)-N(1)	81.61(7)
		O(1)-Ti(1)-N(1) ^(a)	90.87(7)
		O(1) ^(a) -Ti(1)-N(1)	90.87(7)
		O(1) ^(a) -Ti(1)-N(1) ^(a)	81.61(7)
		N(1)-Ti(1)-N(1) ^(a)	83.97(6)

Symmetry related atoms (a) 1-x, y, 1/2-z

When viewed along the a axis the molecules pack head-tail and then alternate in the next row, giving a herringbone arrangement. When viewed along the c axis the molecules pack in pairs, with the two *cis*-chloride ligands pointing away from the metal centre, allowing the aromatic groups to pack in close proximity. However, distances between these aromatics are too large to be considered as π - π stacking interactions. The packing diagrams are shown in **Figure 8.20**, with D...A distances and torsion angles stated in **Table 8.13**.

Packing diagram along the a axisPacking diagram along the c axis**Figure 8.20** Packing diagrams along the a and c axes for **25****Table 8.13** Bond lengths and torsion angles for **25**

Interaction	Atoms	Bond Lengths and Angles
Intermolecular	Cg(1)-Cg(3)	3.6228 Å
Torsion	Cg(3)-Cg(1)	81.83°
	Cg(1)-Cg(4)	19.87°

8.7 Conclusions and Future Work

This chapter presents the mechanistic and cytotoxicity results for a library of group IV complexes. These results have been obtained as part of the McGowan research group, in which the author obtained the cytotoxicity results.⁴ Secondly, this chapter presents the initial synthesis of both β -diketonate and β -ketoiminate titanium complexes, where X-ray crystallographic data have been obtained for complexes **21-25**. Bond angles for these complexes show an octahedral geometry, with a preference for the *cis-trans-cis* geometry. Initial results have been obtained, however full analysis has not been possible due to issues with air sensitivity and the samples were easily oxidised.

Future work for this chapter would be work on bulk purification and attempts to optimise the reaction by trying a wider range of solvents and bases. These complexes would also be tested for their mechanistic and cytotoxic potential in order to compare with the previously synthesised β -diketonate complexes. It was hoped that like the ruthenium complexes stated in Chapter 3, these complexes incorporating a β -ketoiminate ligand could help to increase the cytotoxic potential of the group IV metals. However, these complexes have shown to be extremely air sensitive and change oxidation state and structure on contact with air, restricting the cytotoxic studies that can be achieved. However, these types of redox active d^0 complexes have been used extensively in the literature for olefin polymerisation, giving these complexes a potential application for future work.

8.8 References

1. J. J. Mannion, Ph.D Thesis, University of Leeds, 2008.
2. A. J. Hebden, Ph.D Thesis, University of Leeds, 2010.
3. B. D. Crossley, Ph.D Thesis, University of Leeds, 2011.
4. R. M. Lord, J. J. Mannion, A. J. Hebden, A. E. Nako, B. D. Crossley, M. W. McMullon, F. D. Janeway, R. M. Phillips and P. C. McGowan, *Chem. Commun.*, 2013.
5. B. K. Keppler and M. Hartmann, *Metal-Based Drugs*, 1994, **1**, 169.
6. B. K. Keppler, *Metal Complexes in Cancer Chemotherapy*, VCH, Weinheim, Germany, 1993.
7. P. Comba, H. Jakob, B. Nuber and B. K. Keppler, *Inorg. Chem.*, 1994, **33**, 3396-3400.
8. T. J. Pinnavaia and R. C. Fay, *Inorg. Chem.*, 1966, **5**, 233-239.
9. B. K. Keppler and K. Michels, *Arzneim. Forsch. (Drug Res.)*, 1985, **35(II)**, 1837-1839.
10. S. M. Lord, Ph. D Thesis, University of Leeds, 2007.
11. T. Maschmeyer, M. C. Klunduk, C. M. Martin, D. S. Shephard, J. M. Thomas and B. F. G. Johnson, *Chem. Commun.*, 1997, **1847**.

Chapter 9

Experimental Data and Protocols

9 Experimental

9.1 General Experimental Procedures

All novel titanium complexes were synthesised using standard Schlenk line techniques, under an atmosphere of dry dinitrogen with a dual vacuum/dinitrogen line to perform the synthesis. All ruthenium complexes were synthesised under aerobic conditions.

All chemicals were supplied by Sigma-Aldrich Chemical Co., Acros Organics, Strem Chemical Co. and BOC gases. Functionalised β -diketonate and β -ketoiminate ligands were prepared by adaptations of literature methods.^{1, 2} Deuterated NMR solvents were supplied by Sigma-Aldrich Chemical Co. or Acros Organics.

9.2 Instrumentation

All NMR spectra were recorded by either the author or Mr Simon Barrett on a Bruker DPX 300 or a Bruker DPX 500 spectrometer. Microanalyses were recorded by Mr. Ian Blakeley or Ms Tanya Marinko-Covell at the University of Leeds Microanalytical Service. Mass Spectra were recorded by Ms. Tanya Marinko-Covell or Dr. Stuart Warriner on a Micromass ZMD spectrometer with electrospray ionisation and photoiodide array analyser at the University of Leeds Mass Spectrometry Service.

9.3 X-Ray Crystallography

X-ray diffraction data were collected by either the author, Dr. Stephanie Lucas, Dr. Andrea Rodríguez Bárzano, Mr. Felix Janeway, Dr. Andrew Hebden or Dr. Helena Shephard (University of Leeds, X-ray service). A suitable single crystal was selected and immersed in an inert oil. The crystal was then mounted on a glass capillary and attached to a goniometer head on a Bruker X8 Apex or an Agilent Supernova diffractometer using graphite monochromated Mo-K α radiation ($\lambda = 0.71073 \text{ \AA}$) using 1.0° ϕ -rotation frames. The crystal was cooled to 100 K by an Oxford Cryostream low temperature device.³ The full data set was recorded and the images processed using DENZO and SCALEPACK programs.⁴ The structures were solved by either the author or Dr. Helena Shephard.

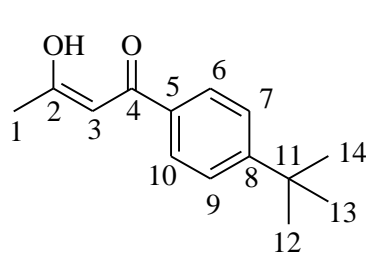
Structure solution by direct methods was achieved through the use of SHELXS86,⁵ SIR92⁶ or SIR97⁷ programs, and the structural model refined by full matrix least squares on F^2 using SHELX97.⁵ Molecular graphics were plotted using POV-Ray⁸ via the XSeed program. Editing of CIFs and construction of tables of bond lengths and angles were achieved using WC⁹ and PLATON.¹⁰ Unless otherwise stated, hydrogen atoms were placed using idealised geometric positions (with free rotation for methyl groups), allowed to move in a “riding model” along with the atoms to which they were attached, and refined isotropically.

9.4 Syntheses of Functionalised β -Diketonate Ligands

Ligands **L1-L4** have been synthesised according to a literature method¹¹ and ligands **L5-L10** were synthesised using a modified version of the synthetic route published by Levine *et al.*¹

9.4.1 Preparation of $C_{14}H_{18}O_2$ (**L1**)

Sodium ethoxide (0.60 g, 8.79 mmol) was added to ethyl acetate (40 mL) and 4-*tert*-butylacetophenone (1.55 g, 8.79 mmol). The mixture was stirred and heated under reflux for 4 hours, then allowed to cool to room temperature. The solvent was removed under reduced pressure and washed with petrol (60-80°C) (3 x 10 mL). The suspension was dissolved in ice cold water (40 mL) and ice cold sulfuric acid was added until just acidic to litmus. The crude product was extracted into diethyl ether (3 x 10 mL) and dried over Na_2SO_4 . The solvent was removed under reduced pressure, yielding **L1** as a pure yellow oil (0.94 g, 4.31 mmol, 49%).

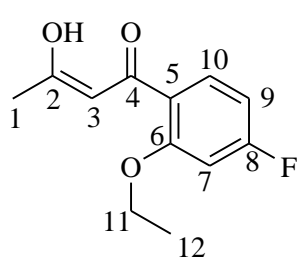


1H NMR ($CDCl_3$, 300.13 MHz, 293.6K) δ 16.23 (br. s, 1H, C-OH), 7.83 (dd, 2H, H_6 and H_{10} , $^3J(^1H-^1H) = 8.7$ Hz and $^4J(^1H-^1H) = 4.1$ Hz), 7.47 (dd, 2H, H_7 and H_9 , $^3J(^1H-^1H) = 8.7$ Hz and $^4J(^1H-^1H) = 4.0$ Hz), 6.17 (s, 1H, H_3), 2.20 (s, 3H, H_1), 1.35 (s, 9H, H_{12-14})

$^{13}C\{^1H\}$ NMR ($CDCl_3$, 75.5 MHz, 295.4 K) δ 193.3 (quaternary C-O, C_2 or C_4), 183.5 (quaternary C-O, C_2 or C_4), 156.0 (aromatic quaternary C, C_5), 132.0 (aromatic quaternary C, C_8), 126.9 (aromatic CH, C_6 and C_{10}), 125.6 (aromatic CH, C_7 and C_9), 96.4 (acac CH, C_3), 35.1 (quaternary *tert*-butyl C, C_{11}), 31.1 (*t*-butyl $C(CH_3)_3$, C_{12-14}), 25.8 (aliphatic CH_3 , C_1) **Analysis Calculated:** C 77.03, H 8.31% **Analysis Found:** C 77.05, H 8.35% **ES MS (+):** m/z 219.14 [MH^+]

9.4.2 Preparation of C₁₂H₁₃FO₃ (L2)

Sodium ethoxide (4.34 g, 64.0 mmol) was added to ethyl acetate (60 mL) and 2,4-difluoroacetophenone (5.04 g, 25.5 mmol). The mixture was stirred and heated under reflux for 3 hours and allowed to cool to room temperature. The suspension was dissolved in ice cold water (30 mL) and ice cold sulfuric acid was added until just acidic to litmus. The crude product was extracted into diethyl ether (3 x 10 mL) and dried over MgSO₄. The solvent was removed under reduced and recrystallised from hot ethanol (20 mL), filtered through glass wool and stored at -20°C, yielding pale yellow crystals of **L2** (4.01g, 17.9 mmol, 56%). The expected 2,4-difluoro- β -diketonate ligand was not obtained and instead the ethoxide substitutes the *para*-fluoro substituent.

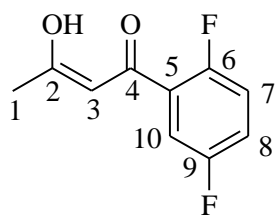


¹H NMR (CDCl₃, 300.13 MHz, 300.0K) δ 16.23 (br. s, 1H, C-OH), 7.94 (dd, 1H, H₁₀, ³J(¹H-¹H) = 8.7 and ⁴J(¹H-¹⁹F) = 7.0 Hz), 6.73 (ddd, 1H, H₉, ³J(¹H-¹H) = 8.9 Hz, ³J(¹H-¹⁹F) = 7.7 Hz and ⁴J(¹H-¹H) = 2.5 Hz), 6.65 (dd, 1H, H₇, ³J(¹H-¹⁹F) = 11.0 Hz and ⁴J(¹H-¹H) = 2.3 Hz), 6.52 (br. s, 1H, H₃), 4.12 (q, 2H, H₁₁, ³J(¹H-¹H) = 7.0 Hz), 2.18 (s, 3H, H₁), 1.52 (t, 3H, H₁₂, ³J(¹H-¹H) = 7.0 Hz) ¹³C{¹H} NMR (CDCl₃, 125.9 MHz, 300.0 K) δ 194.2 (quaternary C-O, C₂ or C₄), 180.3 (quaternary C-O, C₂ or C₄), 166.6 (d, aromatic quaternary C-F, C₈, ¹J(¹³C-¹⁹F) = 250.5 Hz), 159.5 (d, aromatic quaternary C, C₆, ³J(¹³C-¹⁹F) = 10.3 Hz), 132.1 (d, aromatic CH, C₁₀, ³J(¹³C-¹⁹F) = 11.3 Hz), 120.3 (d, aromatic quaternary C, C₅, ⁵J(¹³C-¹⁹F) = 3.1 Hz), 107.6 (d, aromatic CH, C₉, ²J(¹³C-¹⁹F) = 21.7 Hz), 101.5 (acac CH, C₃), 100.3 (d, aromatic CH, C₇, ²J(¹³C-¹⁹F) = 103.1 Hz), 64.7 (CH₂, C₁₁), 26.0 (CH₃, C₁), 14.5 (CH₃, C₁₂) **Analysis Calculated:** C 64.28, H 5.84% **Analysis Found:** C 64.30, H 5.90% **ES MS (+):** *m/z* 247.10 [MNa⁺]

9.4.3 Preparation of C₁₀H₈F₂O₂ (L3)

Sodium ethoxide (1.09 g, 16.0 mmol) was added to ethyl acetate (40 mL) and 2,5-difluoroacetophenone (2.02 mL, 16.0 mmol). These were stirred and heated under reflux for 3 hours, then allowed to cool to room temperature. The solvent was removed under reduced pressure and washed with petrol (60-80°C) (3 x 10 mL). The suspension was dissolved in ice cold water (40 mL) and ice cold sulfuric acid was added until just acidic to litmus. The crude product was extracted into diethyl

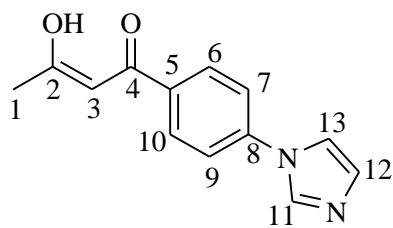
ether (3 x 10 mL) and dried over MgSO₄. Solvent was removed under reduced pressure and the residue recrystallised from hot EtOH (10 mL), yielding **L3** as pure pale yellow crystals (1.90 g, 0.96 mmol, 60%).



¹H NMR (CDCl₃, 500.23 MHz, 299.9 K) δ 7.64 (ddd, 1H, H₇ or H₈, ³*J* (¹H-¹H) = 8.9 Hz ³*J* (¹H-¹⁹F) = 5.7 Hz and ⁴*J* (¹H-¹⁹F) = 3.2 Hz), 7.18-7.13 (m, 1H, H₇ or H₈), 7.13-7.08 (m, 1H, H₁₀), 6.30 (vd, 1H, H₃, ⁵*J* (¹H-¹⁹F) = 1.4 Hz), 2.23 (br. s, 3H, H₁ CH₃) **¹³C{¹H} NMR** (CDCl₃, 125.9 MHz, 300.0 K) δ 195.5 (quaternary C=O, C₂ or C₄), 177.0 (d, quaternary C=O, C₅, ³*J* (¹³C-¹⁹F) = 4.1 Hz), 158.8 (dd, aromatic quaternary C-F, C₆ or C₉, ¹*J* (¹³C-¹⁹F) = 202.1 Hz and ⁴*J* (¹³C-¹⁹F) = 2.1 Hz), 156.9 (dd, aromatic quaternary C-F, C₆ or C₉, ¹*J* (¹³C-¹⁹F) = 210.3 Hz and ⁴*J* (¹³C-¹⁹F) = 2.1 Hz), 124.4 (dd, aromatic quaternary C, C₅, ²*J* (¹³C-¹⁹F) = 12.4 Hz and ³*J* (¹³C-¹⁹F) = 7.2 Hz), 119.9 (dd, aromatic CH, C₇ or C₈, ²*J* (¹³C-¹⁹F) = 24.7 Hz and ³*J* (¹³C-¹⁹F) = 9.3 Hz), 117.8 (dd, aromatic CH C₇ or C₈, ²*J* (¹³C-¹⁹F) = 26.8 Hz and ³*J* (¹³C-¹⁹F) = 8.3 Hz), 116.2 (dd, aromatic CH, C₁₀, ²*J* (¹³C-¹⁹F) = 25.8 Hz and ³*J* (¹³C-¹⁹F) = 3.1 Hz), 101.5 (d, acac CH, C₃, ⁴*J* (¹³C-¹⁹F) = 13.4 Hz), 26.1 (CH₃, C₁) **Analysis Calculated:** C 60.61, H 4.07% **Analysis Found:** C 60.55, H 4.00% **ES MS (+):** *m/z* 221.09 [MNa⁺]

9.4.4 Preparation of C₉H₉NO₂ (**L4**)

Sodium ethoxide (1.74 g, 25.5 mmol) was added to ethyl acetate (40 mL) and 4'-(imidazol-1-yl) acetophenone (5.04 g, 25.5 mmol). These were stirred and heated under reflux for 3 hours, then allowed to cool to room temperature. The suspension was dissolved in ice cold water (30 mL) and the aqueous layer collected then washed with diethyl ether (3 x 20 mL). Ice cold sulfuric acid was added until neutral to litmus. The crude product was extracted into diethyl ether (10 mL) and solid precipitated out on the first wash. This was filtered under reduced pressure and recrystallised by vapour diffusion in dichloromethane/pentane, yielding **L4** as yellow crystals (3.77 g, 16.5 mmol, 62%).

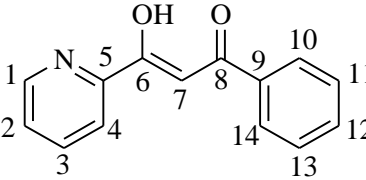


¹H NMR (CDCl₃, 500.23 MHz, 300.0 K) δ 8.02 (dt, 2H, H₇ and H₉, ³*J* (¹H-¹H) = 8.7 Hz and ⁴*J* (¹H-¹H) = 2.4 Hz), 7.98 (br. s, 1H, H₁₁), 7.50 (dt, 2H, H₆ and H₁₀, ³*J* (¹H-¹H) = 8.7 Hz and ⁴*J* (¹H-¹H) = 2.4 Hz), 7.36 (br. s, 1H, H₁₂ or H₁₃, ³*J* (¹H-¹H) =

1.6 Hz), 7.26 (br. s, 1H, H₁₂ or H₁₃), 6.20 (s, 1H, H₃), 2.24 (s, 3H, H₁) ¹³C{¹H} NMR (CDCl₃, 125.8 MHz, 300.0 K) δ 193.9 (quaternary C-O, C₂ or C₄), 181.9 (quaternary C-O, C₂ or C₄), 140.2 (quaternary aromatic C, C₈), 135.4 (imidazole CH, C₁₁), 133.9 (quaternary aromatic C, C₅), 131.10 (imidazole CH, C₁₂ or C₁₃), 128.9 (aromatic CH, C₆ and C₁₀), 120.9 (aromatic CH, C₇ and C₉), 117.8 (imidazole CH, C₁₂ or C₁₃), 96.8 (acac CH, C₃), 25.9 (aliphatic CH₃, C₁) **Analysis Calculated:** C 68.41, H 5.30, N 12.27% **Analysis Found:** C 68.20, H 5.25, N 12.15% **ES MS (+):** *m/z* 229.10 [MH⁺]

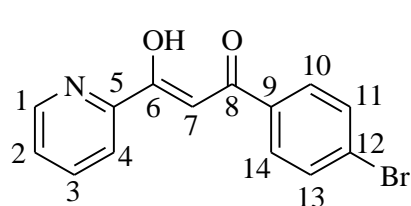
9.4.5 Preparation of C₁₄H₁₁NO₂ (L5)

Sodium ethoxide (1.42 g, 20.8 mmol) was added to diethyl ether (40 mL), ethyl 2-picolinate (2.81 mL, 20.8 mmol) and acetophenone (4.86 mL, 41.6 mmol). These were stirred and heated to reflux for 48 hours, then allowed to cool to room temperature. The suspension was stirred whilst adding acetic acid (1.19 mL, 20.8 mmol) and water (20 mL). The crude product was extracted into diethyl ether (3 x 20 mL) and dried over Na₂SO₄. The solvent was removed under reduced pressure and the residue recrystallised from hot methanol (20 mL), yielding **L5** as colourless crystals (2.54 g, 11.3 mmol, 54%)

 ¹H NMR (CDCl₃, 500.23 MHz, 300.0 K) δ 8.66-8.62 (m, 1H, H₁), 8.10 (br. d, 1H, H₄, ³J (¹H-¹H) = 7.9 Hz), 8.02-7.98 (br. dd, 2H, H₁₀ and H₁₄, ³J (¹H-¹H) = 7.2 Hz and ⁴J (¹H-¹H) = 1.2 Hz), 7.80 (td, 1H, H₃, ³J (¹H-¹H) = 7.6 Hz and ⁴J (¹H-¹H) = 1.6 Hz), 7.52 (s, 1H, H₇), 7.50-7.46 (br. tt, 1H, H₂, ³J (¹H-¹H) = 7.2 Hz and ⁴J (¹H-¹H) = 1.2 Hz), 7.44-7.40 (br. dd, 2H, H₁₁ and H₁₃, ³J (¹H-¹H) = 7.6 Hz and ⁴J (¹H-¹H) = 1.5 Hz), 7.37 (ddd, 1H, H₁₂, ³J (¹H-¹H) = 7.6 Hz and ⁴J (¹H-¹H) = 4.8 Hz) ¹³C{¹H} NMR (CDCl₃, 125.8 MHz, 300.0 K) δ 186.3 (quaternary C-O, C₆ or C₈), 183.7 (quaternary C-O, C₆ or C₈), 152.6 (pyridine quaternary C, C₅), 149.3 (pyridine CH, C₁), 137.1 (pyridine CH, C₃), 135.3 (aromatic quaternary C, C₉), 132.7 (pyridine CH, C₂), 128.7 (aromatic CH, C₁₀ and C₁₄), 127.5 (aromatic CH, C₁₁ and C₁₃), 126.4 (pyridine CH, C₄), 122.2 (aromatic CH, C₁₂), 93.6 (acac CH, C₇) **Analysis Calculated:** C 74.65, H 4.92, N 6.22% **Analysis Found:** C 74.80, H 4.85, N 6.05% **ES MS (+):** *m/z* 226.10 [MH⁺]

9.4.6 Preparation of C₁₄H₁₀BrNO₂ (L6)

Sodium ethoxide (1.08 g, 15.9 mmol) was added to diethyl ether (40 mL), ethyl 2-picolinate (2.15 mL, 15.9 mmol) and 4-bromoacetophenone (6.31 g, 31.8 mmol). These were stirred and heated to reflux for 48 hours, then allowed to cool to room temperature. The suspension was stirred whilst adding acetic acid (0.91 mL, 15.9 mmol) and water (40 mL). The crude product was extracted into diethyl ether (10 mL) and product obtained from the aqueous layer. This was filtered under reduced pressure and washed with hexane, yielding **L6** as a pure white precipitate (1.97 g, 7.59 mmol, 48%).

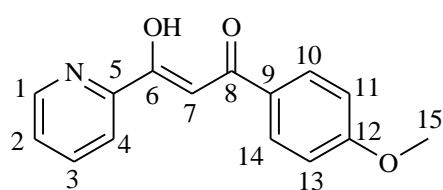


¹H NMR (CDCl₃, 500.23 MHz, 300.0 K) δ 8.73-8.70 (m, 1H, H₁), 8.17 (d, 1H, H₄, ³J (¹H-¹H) = 8.0 Hz), 7.94 (br. d, 2H, H₁₀ and H₁₄, ³J (¹H-¹H) = 8.8 Hz), 7.88 (td, 1H, H₃, ³J (¹H-¹H) = 8.0 Hz and ⁴J (¹H-¹H) = 2.0 Hz), 7.65-7.61 (br. dt, 2H, H₁₁ and H₁₃, ³J (¹H-¹H) = 8.3 Hz and ⁴J (¹H-¹H) = 2.4 Hz), 7.55 (s, 1H, H₇ [enolate tautomer]), 7.46 (br. dd, 1H, H₂, ³J (¹H-¹H) = 7.6 Hz and ⁴J (¹H-¹H) = 1.5 Hz), 4.79 (s, acac CH₂, H₇ [diketonate tautomer])
¹³C{¹H} NMR (CDCl₃, 125.8 MHz, 300.2 K) δ 206.9 (quaternary C=O [diketonate tautomer], C₆ or C₈), 184.9 (quaternary C-O [enolate tautomer], C₆ or C₈), 184.0 (quaternary C-O [enolate tautomer], C₆ or C₈), 152.4 (pyridine quaternary C [both tautomers] C₅), 149.3 (pyridine CH [both tautomers], C₁), 137.1 (pyridine CH [both tautomers], C₃), 134.2 (aromatic quaternary C [both tautomers], C₉), 132.0 (aromatic CH [both tautomers], C₁₀ and C₁₄), 129.0 (aromatic CH, [both tautomers], C₁₁ and C₁₃), 127.6 (aromatic quaternary C [both tautomers], C₁₂), 126.5 (pyridine CH [both tautomers], C₄), 93.5 (acac CH [enolate tautomer], C₇), 30.9 (acac CH₂ [diketonate tautomer], C₇) **Analysis Calculated:** C 55.29, H 3.31, N 4.61% **Analysis Found:** C 55.50, H 3.15, N 4.35% **ES MS (+):** *m/z* 304.0 [MH⁺]

9.4.7 Preparation of C₁₅H₁₃NO₃ (L7)

Sodium ethoxide (1.01 g, 14.8 mmol) was added to diethyl ether (40 mL), ethyl 2-picolinate (2.0 mL, 14.8 mmol) and 4-methoxy acetophenone (4.45 g, 29.6 mmol). These were stirred and heated to reflux for 48 hours, then allowed to cool to room temperature. The suspension was stirred whilst adding acetic acid (0.85 mL, 14.8 mmol) and water (40 mL). The product did not dissolve and was filtered under

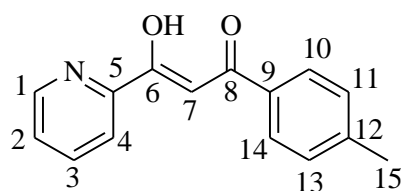
reduced pressure and washed with methanol (10 mL), yielding **L7** as a pure yellow precipitate (2.34 g, 9.17 mmol, 62%).



$^1\text{H NMR}$ (CDCl_3 , 500.23 MHz, 300.0 K) δ 8.72-8.69 (m, 1H, H_1), 8.15 (d, 1H, H_4 , 3J (^1H - ^1H) = 7.4 Hz), 8.09-8.05 (br. dt, 2H, H_{10} and H_{14} , 3J (^1H - ^1H) = 8.7 Hz and 4J (^1H - ^1H) = 2.7 Hz), 7.86 (td, 1H, H_3 , 3J (^1H - ^1H) = 7.8 Hz and 4J (^1H - ^1H) = 2.0 Hz), 7.51 (s, 1H, [enolate tautomer], H_7), 7.45-7.41 (m, 1H, H_2), 7.00-6.96 (br. dt, 2H, H_{11} and H_{13} , 3J (^1H - ^1H) = 9.1 Hz and 4J (^1H - ^1H) = 2.7 Hz), 4.81 (s, acac CH_2 [diketonate tautomer], H_7), 3.89 (s, 3H, H_{15}) $^{13}\text{C}\{^1\text{H}\}$ NMR (CDCl_3 , 125.8 MHz, 300.0 K) δ 206.9 (quaternary $\text{C}=\text{O}$ [diketonate tautomer], C_6 or C_8), 187.0 (quaternary $\text{C}-\text{O}$ [enolate tautomer], C_6 or C_8), 181.6 (quaternary $\text{C}-\text{O}$ [enolate tautomer], C_6 or C_8), 163.5 (pyridine quaternary C [both tautomers], C_5), 152.7 (aromatic quaternary C [both tautomers], C_9), 149.3 (pyridine CH [both tautomers], C_1), 137.0 (pyridine CH [both tautomers], C_3), 129.7 (aromatic CH [both tautomers], C_{10} and C_{14}), 128.1 (aromatic quaternary C [both tautomers], C_{12}), 126.1 (pyridine CH [both tautomers], C_2), 122.0 (pyridine CH [both tautomers], C_4), 114.0 (aromatic CH [both tautomers], C_{11} and C_{13}), 92.9 (acac CH [enolate tautomer], C_7), 55.5 (acac CH_2 [diketonate tautomer], C_7), 30.9 (methoxy OCH_3 [both tautomers], C_{15}) **Analysis Calculated:** C 70.58, H 5.13, N 5.49% **Analysis Found:** C 70.15, H 5.10, N 5.35 **ES MS (+):** m/z 256.10 [MH^+]

9.4.8 Preparation of $\text{C}_{15}\text{H}_{13}\text{NO}_2$ (**L8**)

Sodium ethoxide (0.76 g, 11.2 mmol) was added to diethyl ether (40 mL), ethyl 2-picolinate (1.51 mL, 11.2 mmol) and 4-methylacetophenone (2.99 mL, 22.4 mmol). These were stirred and heated to reflux for 48 hours, then allowed to cool to room temperature. The suspension was stirred whilst adding acetic acid (0.64 mL, 11.2 mmol) and water (40 mL). The product was extracted into diethyl ether (10 mL) and product was obtained from the aqueous layer. This was filtered under reduced pressure and recrystallised from methanol (10 mL), yielding **L8** as a pale yellow precipitate (1.72 g, 7.19 mmol, 61%).

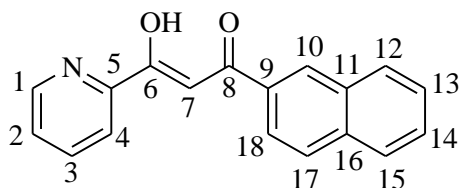


$^1\text{H NMR}$ (CDCl_3 , 500.23 MHz, 300.3 K) δ 8.71 (dd, 1H, H_1 , 3J (^1H - ^1H) = 4.8 Hz and 4J (^1H - ^1H) = 0.8 Hz), 8.16 (d, 1H, H_4 , 3J (^1H - ^1H) = 7.5 Hz),

7.98 (br. d, 2H, H₁₀ and H₁₄, $^3J(^1\text{H}-^1\text{H}) = 8.3$ Hz), 7.89-7.83 (m, 1H, H₁), 7.56 (s, 1H, H₇), 7.46-7.41 (m, 1H, H₂), 7.29 (d, 2H, H₁₁ and H₁₃, $^3J(^1\text{H}-^1\text{H}) = 8.3$ Hz), 2.43 (s, 3H, methyl CH_3) $^{13}\text{C}\{^1\text{H}\}$ NMR (CDCl₃, 125.8 MHz, 297.4 K) δ 186.8 (quaternary $\text{C}-\text{O}$, C₆ or C₈), 183.0 (quaternary $\text{C}-\text{O}$, C₆ or C₈), 152.6 (quaternary pyridine C, C₅), 149.3 (pyridine CH , C₁), 143.6 (quaternary aromatic C, C₉), 137.1 (pyridine CH , C₃), 132.7 (quaternary aromatic C, C₁₂), 129.4 (aromatic CH , C₁₁ and C₁₃), 127.6 (aromatic CH , C₁₀ and C₁₄), 126.4 (pyridine CH , C₂), 122.1 (pyridine CH , C₄), 93.3 (acac CH , C₇). 21.7 (methyl CH_3 , C₁₅) **Analysis Calculated:** C 75.30, H 5.48, N 5.85% **Analysis Found:** C 75.65, H 5.40, N 5.70% **ES MS (+):** m/z 240.10 [MH⁺]

9.4.9 Preparation of C₁₈H₁₃NO₂ (L9)

Sodium ethoxide (0.40 g, 5.88 mmol) was added to diethyl ether (40 mL), ethyl 2-picolinate (0.79 mL, 5.88 mmol) and 2-acetonaphthone (2.01 g, 11.8 mmol). These were stirred and heated to reflux for 48 hours, then allowed to cool to room temperature. The suspension was stirred whilst adding acetic acid (0.34 mL, 5.88 mmol) and water (40 mL). The crude product was separated with ether (3 x 20 mL) and dried over Na₂SO₄. The crude product was recrystallised from methanol (10 mL) and stored at -20°C. This was filtered under reduced pressure and washed with diethyl ether, yielding **L9** as a yellow precipitate (0.98 g, 3.56 mmol, 61%)

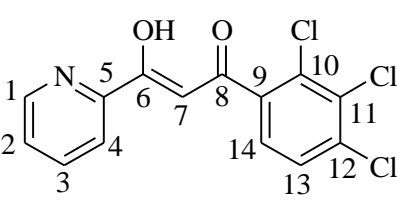


^1H NMR (CDCl₃, 500.23 MHz, 300.3 K) δ 8.78-8.75 (m, 1H, H₁), 8.65 (s, 1H, H₁₀), 8.21 (d, 1H, H₄, $^3J(^1\text{H}-^1\text{H}) = 7.9$ Hz), 8.12 (dd, 1H, naphthyl CH , $^3J(^1\text{H}-^1\text{H}) = 8.5$ Hz and $^4J(^1\text{H}-^1\text{H}) = 1.8$ Hz), 8.01 (d, 1H, naphthyl CH , $^3J(^1\text{H}-^1\text{H}) = 7.9$ Hz), 7.94 (d, 1H, H₃, $^3J(^1\text{H}-^1\text{H}) = 8.7$ Hz), 7.92-7.88 (m, 2H, naphthyl CH), 7.74 (s, 1H, H₇), 7.63-7.55 (m, 2H, naphthyl CH), 7.47 (ddd, 1H, H₂, $^3J(^1\text{H}-^1\text{H}) = 7.6$ Hz, $^3J(^1\text{H}-^1\text{H}) = 4.8$ Hz and $^4J(^1\text{H}-^1\text{H}) = 1.2$ Hz) $^{13}\text{C}\{^1\text{H}\}$ NMR (CDCl₃, 75.5 MHz, 300.1 K) δ 186.2 (quaternary $\text{C}-\text{O}$, C₆ or C₈), 183.55 (quaternary $\text{C}-\text{O}$, C₆ or C₈), 152.6 (quaternary pyridine C, C₅), 149.3 (pyridine CH , C₁), 137.1 (pyridine CH , C₃), 135.5 (quaternary naphthyl C, C₉), 132.6 (quaternary naphthyl C, C₁₁ and C₁₆), 129.5 (naphthyl CH), 128.8 (naphthyl CH), 128.4 (pyridine CH , C₂), 128.2 (naphthyl CH), 127.8 (naphthyl CH), 126.8 (naphthyl CH), 126.4 (naphthyl CH), 123.47 (naphthyl CH), 122.2 (pyridine CH , C₄), 93.9 (acac CH , C₇) **Analysis Calculated:**

C 78.53, H 4.76, N 5.09% **Analysis Found:** C 78.35, H 4.70, N 4.90% **ES MS (+):** m/z 276.10 [MH⁺]

9.4.10 Preparation of C₁₄H₈Cl₃NO₂ (L10)

Sodium ethoxide (0.47 g, 6.85 mmol) was added to diethyl ether (40 mL), ethyl 2-picolinate (0.92 mL, 6.85 mmol) and 2,3,4-trichloro acetophenone (3.06 g, 13.7 mmol). These were stirred and heated to reflux for 48 hours, then allowed to cool to room temperature. The suspension was stirred whilst adding acetic acid (0.39 mL, 6.85 mmol) and water (40 mL). The crude product was extracted with ether (3 x 20 mL) and dried over Na₂SO₄. The solvent was removed under reduced pressure and washed with diethyl ether (10 mL), yielding **L10** as a cream precipitate (1.06 g, 3.23 mmol, 47%).



¹H NMR (CDCl₃, 500.23 MHz, 300.0 K) δ 8.66 (d, 1H, H₁, ³J (¹H-¹H) = 4.0 Hz), 8.13 (d, 1H, H₄, ³J (¹H-¹H) = 7.9 Hz), 7.85 (td, 1H, H₃, ³J (¹H-¹H) = 7.7 Hz and ⁴J (¹H-¹H) = 1.6 Hz), 7.46 (d, 2H, H₁₃ and H₁₄, ³J (¹H-¹H) = 1.6 Hz), 7.45-7.41 (m, 1H, H₂), 7.24 (s, 1H, H₇) **¹³C{¹H} NMR** (CDCl₃, 125.8 MHz, 300.2 K) δ 186.98 (quaternary C=O, C₆ or C₈), 182.46 (quaternary C=O, C₆ or C₈), 151.66 (quaternary pyridine C, C₅), 149.54 (pyridine CH, C₁), 137.13 (pyridine CH, C₃), 136.80 (quaternary aromatic C, C₉), 136.48 (aromatic C-Cl, C₁₀₋₁₂), 133.23 (aromatic C-Cl, C₁₀₋₁₂), 132.13 (aromatic C-Cl, C₁₀₋₁₂), 128.48 (pyridine CH, C₂), 127.82 (aromatic CH, C₁₃), 126.70 (aromatic CH, C₁₄), 122.40 (pyridine CH, C₄), 98.74 (acac CH, C₇) **Analysis Calculated:** C 51.18, H 2.45, Cl 32.37 N 4.26% **Analysis Found:** C 51.25, H 2.30, Cl 32.50 N 4.00% **ES MS (+):** m/z 327.97 [M⁺]

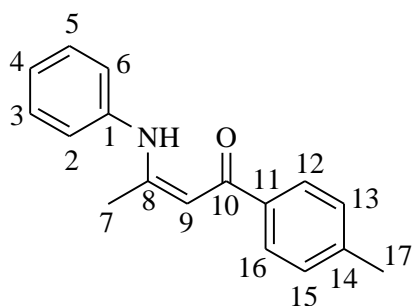
9.5 Syntheses of Functionalised β -Ketoiminate Ligands

Ligands **L11-28** were synthesised using a modified synthetic route based on work by Tang *et al.*²

9.5.1 Preparation of C₁₇H₁₇NO (L11)

4²-Methyl- β -diketonate (0.50 g, 2.84 mmol) was dissolved in toluene (10 mL), aniline (1 mL) and HCl (0.5 mL). This was stirred for 16 hours, the precipitate was filtered and the solvent was removed under reduced pressure. The crude product

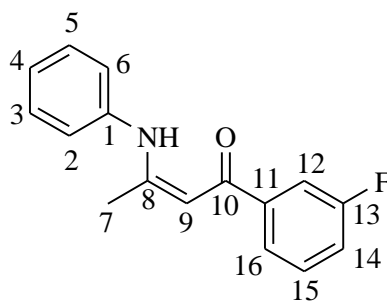
was recrystallised from hot ethanol (20 mL), yielding **L11** as a yellow crystals (0.42 g, 1.67 mmol, 59%). This ligand has previously been prepared,¹² although the X-ray crystal structure has been reported in Chapter 2, ¹H NMR has been reported here to prove synthesis.



¹H NMR (CDCl₃, 500.23 MHz, 300.0 K) δ 13.08 (br. d, 1H, NH), 7.86-7.86 (m, 2H, aromatic CH, H₁₃ and H₁₅), 7.41-7.34 (m, 2H, aniline CH, H₃ and H₅), 7.26-7.22 (m, 3H, aniline CH, H₂, H₄ and H₆), 7.21-7.17 (m, 2H, aromatic CH, H₁₃ and H₁₅), 5.89 (s, 1H, acnac CH, H₉), 2.41 (s, 3H, *para* methyl CH₃, H₁₇), 2.15 (s, 3H, aliphatic CH₃, H₇)

9.5.2 Preparation of C₁₆H₁₄FNO (L12)

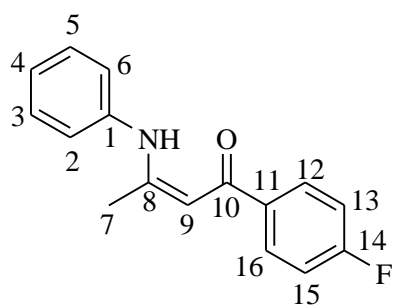
3'-Fluoro-β-diketonate (0.52 g, 2.89 mmol) was dissolved in toluene (10 mL), aniline (1 mL) and HCl (0.5 mL). This was stirred for 16 hours, the precipitate was filtered and the remove solvent was under reduced pressure. The crude product recrystallised was from hot ethanol (10 mL), yielding yellow crystals of **L12** (0.61 g, 2.39 mmol, 83%)



¹H NMR (CDCl₃, 300 MHz, 300 K) δ 13.09 (br. s, 1H, NH), 7.70 (br. d, 1H, aromatic CH, H₁₆, ³J(¹H-¹H) = 7.9 Hz), 7.65-7.59 (m, 1H, aromatic CH, H₁₂), 7.44-7.36 (m, 3H, aniline CH, H₃ and H₅ and aromatic H₁₅), 7.28-7.24 (m, 1H, aniline CH, H₄), 7.23-7.18 (m, 2H, aniline CH, H₂ and H₆), 7.18-7.12 (m, 1H, aromatic CH, H₁₄), 5.85 (s, 1H, acnac CH, H₉), 2.16 (s, 3H, aliphatic CH₃, H₇) ¹³C{¹H} NMR (CDCl₃, 75 MHz, 300 K) δ 186.9 (quaternary C-O, C₁₀), 163.9 (quaternary C, C₁ or C₈), 157.5 (quaternary C, C₁ or C₈), 137.0 (d, quaternary C-F, C₁₃, ¹J(¹³C-¹⁹F) = 217.5 Hz), 129.8 (d, quaternary C *meta* to C-F, C₁₁, ³J(¹³C-¹⁹F) = 7.5 Hz), 129.2 (aniline or aromatic CH, C₃, C₅ and C₁₅), 126.1 (aniline CH, C₄), 124.9 (aniline CH, C₂ and C₆), 122.6 (d, aromatic CH, C₁₆, ⁴J(¹³C-¹⁹F) = 3.0 Hz), 117.6 (d, aromatic CH, C₁₄, ²J(¹³C-¹⁹F) = 21 Hz), 114.0 (d, aromatic CH, C₁₂, ²J(¹³C-¹⁹F) = 21 Hz), 94.1 (acnac CH, C₉), 20.4 (aliphatic CH₃, C₇) **Analysis Calculated:** C 75.30 H 5.53, N 5.49% **Analysis Found:** C 74.90, H 5.20, N 5.16% **ES MS (+):** *m/z* 255.4 [M⁺]

9.5.3 Preparation of C₁₆H₁₄FNO (L13)

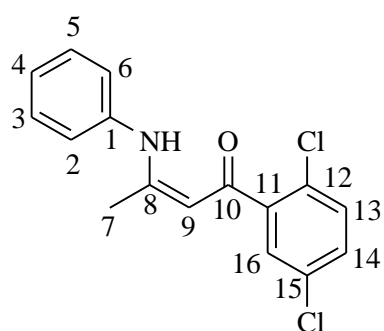
4'-Fluoro- β -diketonate (0.51 g, 2.83 mmol) was dissolved in toluene (10 mL), aniline (1 mL) and HCl (0.5 mL). This was stirred for 16 hours, the precipitate was filtered and the solvent was removed under reduced pressure. The crude product was recrystallised from hot ethanol (10 mL), yielding **L13** as green crystals (0.63 g, 2.47 mmol, 87%)



¹H NMR (CDCl₃, 300 MHz, 300 K) δ 13.05 (s, 1H, NH), 7.94 (v. dd, 2H, aromatic CH, H₁₂ and H₁₆, ³J(¹H-¹H) = 9.2 Hz and ³J(¹H-¹⁹F) = 2.3 Hz), 7.39 (br. t, 2H, aniline CH, H₃ and H₅, ³J(¹H-¹H) = 7.9 Hz), 7.24 (br. t, 1H, aniline CH, H₄, ³J(¹H-¹H) = 7.6 Hz), 7.19 (br. d, 2H, aromatic CH, H₂ and H₆, ³J(¹H-¹H) = 7.2 Hz), 7.11 (v. t, 2H, aromatic CH, H₁₂ and H₁₆, ³J(¹H-¹H) = 8.7 Hz and ⁴J(¹H-¹⁹F) = 1.9 Hz), 5.85 (s, 1H, acnac CH, H₉), 2.15 (s, 1H, aliphatic CH₃, H₇) ¹³C{¹H} NMR (CDCl₃, 75MHz, 300K) δ 187.2 (quaternary C-O, C₁₀), 164.5 (d, quaternary C-F, C₁₄, ¹J(¹³C-¹⁹F) = 249.7 Hz), 162.4 (quaternary aromatic C, C₁₁), 138.5 (quaternary aromatic C, C₁ and C₈), 129.3 (d, aromatic CH, C₁₃ and C₁₅, ²J(¹³C-¹⁹F) = 8.7 Hz), 129.2 (aniline CH, C₃ and C₅), 125.9 (aniline CH, C₄), 124.8 (aniline CH, C₂ and C₆), 115.2 (d, aromatic CH, C₁₂ and C₁₆, ³J(¹³C-¹⁹F) = 21.0 Hz), 93.8 (acnac CH, C₉), 20.38 (aliphatic CH₃, C₇) **Analysis Calculated:** C 74.30 H 5.53, N 5.49% **Analysis Found:** C 74.35, H 5.40, N 5.25% **ES MS (+):** *m/z* 255.6 [M⁺]

9.5.4 Preparation of C₁₆H₁₃Cl₂NO (L14)

2',5'-Dichloro- β -diketonate (0.51 g, 2.21 mmol) was dissolved in toluene (10 mL), aniline (1 mL) and HCl (0.5 mL). This was stirred for 16 hours, the precipitate filtered and solvent was removed under reduced pressure. The crude product was recrystallised from hot ethanol (10 mL), yielding **L14** as colourless crystals (0.46 g, 2.20 mmol, 68%)

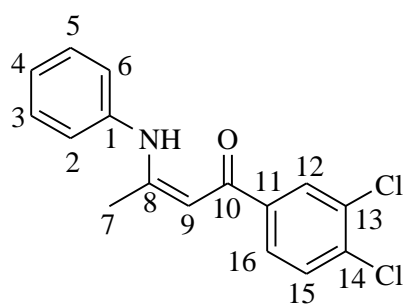


$^1\text{H NMR}$ (CDCl_3 , 300 MHz, 300 K) δ 12.71 (s, 1H, NH), 7.43 (m, 1H, aniline CH , H_4), 7.33 (br. t, 2H, aniline CH , H_3 and H_5 , $^3J(^1\text{H}-^1\text{H}) = 7.5$ Hz), 7.24 (br. s, 1H, aromatic CH , H_{16}), 7.21-7.16 (m, 2H, aromatic CH , H_{13} and H_{14}), 7.13(d, 2H, aniline CH , H_2 and H_6 , $^3J(^1\text{H}-^1\text{H}) = 7.5$ Hz), 5.43 (s, 1H, acnac CH , H_9), 2.03 (s, 3H, aliphatic CH_3 , H_7)

$^{13}\text{C}\{^1\text{H}\}$ NMR (CDCl_3 , 75 MHz, 300 K) δ 187.8 (quaternary $\text{C}=\text{O}$, C_{10}), 163.2 (quaternary C , C_{11}), 142.4 (quaternary C , C_1), 138.1 (quaternary C , C_8), 132.6 (quaternary $\text{C}-\text{Cl}$, C_{12} and C_{15}), 131.3 (aromatic CH , C_{13} or C_{14}), 130.0 (aromatic CH , C_{13} or C_{14}), 129.3 (aniline CH , C_3 and C_5), 126.4 (aniline CH , C_4), 125.1 (aniline CH , C_2 and C_6), 97.9 (acnac CH , C_9), 20.2 (aliphatic CH_3 , C_7) **Analysis Calculated:** C 62.67, H 4.29, N 4.58, Cl 23.15% **Analysis Found:** C 62.65, H 4.20, N 4.45, Cl 23.30 **ES MS (+):** m/z 306.2 [M^+]

9.5.5 Preparation of $\text{C}_{16}\text{H}_{13}\text{Cl}_2\text{NO}$ (**L15**)

3',4'-Dichloro- β -diketonate (0.62 g, 2.60 mmol) was dissolved in toluene (10 mL), aniline (1 mL) and HCl (0.5 mL). This was stirred for 16 hours, the precipitate filtered and the solvent was removed under reduced pressure. The crude product was recrystallised from hot ethanol (10 mL), yielding **L15** as yellow crystals (0.54 g, 1.77 mmol, 68%)



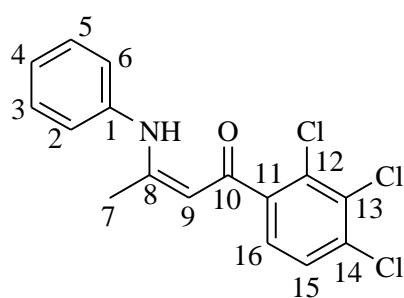
$^1\text{H NMR}$ (CDCl_3 , 300.13 MHz, 300.1 K) δ 13.07 (br. s, 1H, NH), 8.01 (d, 1H, H_{12} , $^4J(^1\text{H}-^1\text{H}) = 1.9$ Hz), 7.55 (dd, 1H, H_{16} , $^3J(^1\text{H}-^1\text{H}) = 8.5$ Hz, $^4J(^1\text{H}-^1\text{H}) = 2.1$ Hz), 7.51 (d, 1H, H_{15} , $^3J(^1\text{H}-^1\text{H}) = 8.7$ Hz), 7.40 (br. t, 2H, H_3 and H_5 , $^3J(^1\text{H}-^1\text{H}) = 7.9$ Hz), 7.26 (br. t, 1H, H_4 , $^3J(^1\text{H}-^1\text{H}) = 7.6$ Hz),

7.19 (d, 2H, H_2 and H_6 , $^3J(^1\text{H}-^1\text{H}) = 7.6$ Hz), 5.85 (s, 1H, H_9), 2.16 (s, 3H, H_7) $^{13}\text{C}\{^1\text{H}\}$ NMR (CDCl_3 , 75.0 MHz, 300.0 K) δ 185.5 (quaternary $\text{C}=\text{O}$, C_{10}), 163.5 (quaternary aromatic C , C_{11}), 139.9 (quaternary aniline C , C_1), 138.3 (quaternary $\text{C}-\text{NH}$, C_8), 135.0 (quaternary aromatic $\text{C}-\text{Cl}$, C_{13} or C_{14}), 132.7 (quaternary aromatic $\text{C}-\text{Cl}$, C_{13} or C_{14}), 130.3 (aromatic CH , C_{15}). 129.3 (aniline CH , C_3 and C_5), 129.2 (aromatic CH , C_{12}), 126.3 (aniline/aromatic CH , C_4 and C_{16}), 124.9 (aniline CH , C_2 and C_6), 93.7 (acnac CH , C_9), 20.4 (aliphatic CH_3 , C_7) **Analysis**

Calculated: C 62.76, H 4.28, N 4.57, Cl 23.16% **Analysis Found:** C 62.50, H 4.30, N 5.00, Cl 23.20% **ES MS (+):** m/z 306.1 [M^+]

9.5.6 Preparation of $C_{16}H_{12}Cl_3NO$ (L16)

2',3',4'-Trichloro- β -diketonate (0.14 g, 0.53 mmol) was dissolved in toluene (10 mL), aniline (1 mL) and HCl (0.5 mL). This was stirred for 16 hours, the precipitate was filtered and solvent was removed under reduced pressure. The crude product was recrystallised from hot ethanol (10 mL), yielding **L16** as a gold crystalline solid (0.10 g, 0.29 mmol, 55%)

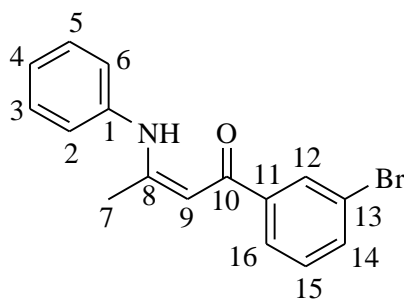


1H NMR ($CDCl_3$, 500.23 MHz, 300.1 K) δ 12.75 (br. s, 1H, NH), 7.43-7.39 (m, 3H, H₃-H₅), 7.33 (d, 1H, H₁₆, $^3J(^1H-^1H) = 8.2$ Hz), 7.29 (br. d, 1H, H₁₅, $^3J(^1H-^1H) = 7.3$ Hz), 7.22 (br. d, 2H, H₂ and H₆, $^3J(^1H-^1H) = 7.6$ Hz), 5.45 (s, 1H, H₉), 2.11 (s, 3H, H₇) ^{13}C NMR ($CDCl_3$, 125.9 MHz, 300.0 K) δ

187.9 (quaternary C=O, C₁₀), 163.4 (quaternary aromatic C, C₁₁), 141.6 (quaternary aniline C, C₁), 138.0 (quaternary C-NH, C₈), 134.5 (quaternary aromatic C-Cl, C₁₂, C₁₃ or C₁₄), 132.4 (quaternary aromatic C-Cl, C₁₂, C₁₃ or C₁₄), 131.0 (quaternary aromatic C-Cl, C₁₂, C₁₃ or C₁₄). 129.3 (aniline CH, C₃ and C₅), 128.4 (aniline CH, C₄), 126.9 (aromatic CH, C₁₆), 126.4 (aromatic CH, C₁₅), 125.1 (aniline CH, C₂ and C₆), 97.8 (acnac CH, C₉), 20.2 (aliphatic CH₃, C₇) **Analysis Calculated:** C 56.42, H 3.55, Cl 31.22, N 4.11% **Analysis Found:** C 56.25, H 3.45, Cl 31.05, N 4.05% **ES MS (+):** m/z 340.0 [M^+]

9.5.7 Preparation of $C_{16}H_{14}BrNO$ (L17)

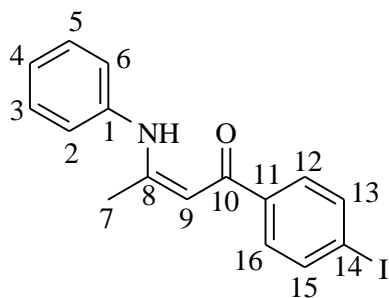
3'-Bromo- β -diketonate (0.52 g, 2.16 mmol) was dissolved in toluene (20 mL), aniline (2 mL) and HCl (1 mL). This was stirred for 16 hours, the product was filtered and solvent was removed under reduced pressure. The crude product was recrystallised from hot ethanol (10 mL), yielding **L17** as pale orange crystals (0.42 g, 1.33 mmol, 62%)



$^1\text{H NMR}$ (CDCl_3 , 300 MHz, 300 K) δ 13.08 (s, 1H, NH), 8.06 (t, 1H, aromatic CH , H_{12} , $^4J(^1\text{H}-^1\text{H}) = 1.7$ Hz), 7.84 (br. dt, 1H, aromatic CH , H_{14} , $^3J(^1\text{H}-^1\text{H}) = 8.0$ Hz and $^3J(^1\text{H}-^1\text{H}) = 1.5$ Hz), 7.59 (dq, 1H, aromatic CH , H_{16} , $^3J(^1\text{H}-^1\text{H}) = 7.9$ Hz and $^4J(^1\text{H}-^1\text{H}) = 0.9(\times 3)$ Hz), 7.40 (br. t, 2H, aniline CH , H_3 and H_5 , $^3J(^1\text{H}-^1\text{H}) = 8.1$ Hz) 7.31 (t, 1H, aromatic CH , H_{15} , $^3J(^1\text{H}-^1\text{H}) = 7.9$ Hz), 7.25 (br. t, 1H, aniline CH , H_4 , $^3J(^1\text{H}-^1\text{H}) = 7.2$ Hz), 7.20 (br. d, 2H, aniline CH , H_2 and H_6 , $^3J(^1\text{H}-^1\text{H}) = 7.5$ Hz), 5.83 (s, 1H, acnac CH , H_9), 2.16 (s, 3H, aliphatic CH_3 , H_7) $^{13}\text{C}\{^1\text{H}\}$ NMR (CDCl_3 , 75 MHz, 300 K) δ 186.7(quaternary $\text{C}-\text{O}$, C_{10}), 163.0 (quaternary aromatic C , C_{11}), 142.0 (quaternary $\text{C}-\text{NH}$, C_8 and quaternary aniline C , C_1), 138.4 (quaternary aromatic $\text{C}-\text{Br}$, C_{13}), 133.6 (aromatic CH , C_{16}), 130.2 (aromatic CH , C_{15}), 129.8 (aromatic CH , C_{12}), 129.2 (aniline CH , C_3 and C_5), 126.1 (aniline CH , C_4), 125.6 (aromatic CH , C_{14}), 124.9 (aromatic CH , C_2 and C_6), 94.0 (acnac CH , C_9), 20.4 (aliphatic CH_3 , C_7) **Analysis Calculated:** C 60.76, H 4.47, N 4.43% **Analysis Found:** C 60.80, H 4.45, N 4.43% **ES MS (+):** m/z 316.3 [M^+]

9.5.8 Preparation of $\text{C}_{16}\text{H}_{14}\text{INO}$ (**L18**)

4'-Iodo- β -diketonate (0.79 g, 2.74 mmol) was dissolved in toluene (20 mL), aniline (2 mL) and HCl (1 mL). This was stirred for 16 hours, the precipitate filtered and the solvent was removed under reduced pressure. The crude product was recrystallised from hot ethanol (10 mL), yielding **L18** as a gold crystalline solid (0.76 g, 2.09 mmol, 76%)

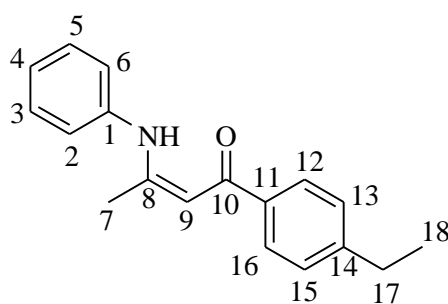


$^1\text{H NMR}$ (CDCl_3 , 500.23 MHz, 300.1 K) δ 13.09 (br. s, 1H, NH), 7.79 (d, 2H, H_{12} and H_{16} , $^3J(^1\text{H}-^1\text{H}) = 8.3$ Hz), 7.65 (d, 2H, H_{13} and H_{15} , $^3J(^1\text{H}-^1\text{H}) = 8.3$ Hz), 7.39 (br. t, 2H, H_3 and H_5 , $^3J(^1\text{H}-^1\text{H}) = 7.8$ Hz), 7.25 (br. t, 1H, H_4 , $^3J(^1\text{H}-^1\text{H}) = 7.3$ Hz), 7.19 (br. d, 2H, H_2 and H_6 , $^3J(^1\text{H}-^1\text{H}) = 7.3$ Hz), 5.84 (s, 1H, H_9), 2.15 (s, 3H, H_7) $^{13}\text{C}\{^1\text{H}\}$ NMR (CDCl_3 , 75 MHz, 300 K) δ 187.4 (quaternary $\text{C}-\text{O}$, C_{10}), 162.8 (quaternary aromatic C , C_{11}), 139.4 (quaternary $\text{C}-\text{NH}$, C_8 and quaternary aniline C , C_1), 138.4 (quaternary $\text{C}-\text{I}$, C_{14}), 137.5 (aromatic CH , C_{12} and C_{16}), 129.2 (aniline CH , C_3 and C_5), 128.7 (aromatic CH , C_{13} and C_{15}),

126.0 (aniline $\underline{\text{C}}\text{H}$, C₄), 124.9 (aniline $\underline{\text{C}}\text{H}$, C₂ and C₆), 93.8 (acnac $\underline{\text{C}}\text{H}$, C₉), 20.4 (aliphatic $\underline{\text{C}}\text{H}_3$, C₇) **Analysis Calculated:** C 52.91, H 3.89, I 34.94, N 3.86% **Analysis Found:** C 52.95, H 4.10, I 34.65, N 3.75% **ES MS (+):** m/z 364.0 [MH⁺]

9.5.9 Preparation of C₁₈H₁₉NO (L19)

4'-Ethyl- β -diketonate (1.03 g, 0.53 mmol) was dissolved in toluene (20 mL), aniline (2 mL) and HCl (1 mL). This was stirred for 16 hours, the precipitate filtered and the solvent removed under reduced pressure. The crude product was recrystallised from hot ethanol (20 mL), yielding **L19** as oily brown crystals (1.05 g, 3.96 mmol, 73%)

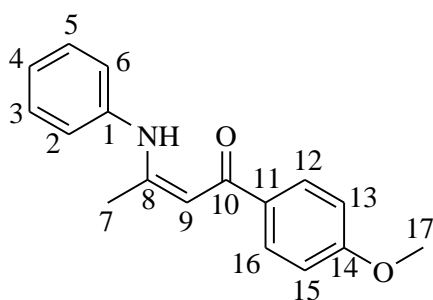


¹H NMR (CDCl₃, 300.13 MHz, 300.0 K) δ 13.09 (br. s, 1H, NH), 7.87 (d, 2H, H₁₂ and H₁₆, ³J (¹H-¹H) = 7.9 Hz), 7.38 (br. t, 2H, H₃ and H₅, ³J (¹H-¹H) = 7.9 Hz), 7.29-7.26 (m, 2H, H₂ and H₆), 7.25-7.22 (m, 1H, H₄), 7.19 (br. d, 2H, H₁₃ and H₁₅, ³J (¹H-¹H) = 7.2 Hz),

5.90 (s, 1H, H₉), 2.71 (q, 2H, H₁₇, ³J (¹H-¹H) = 8.0 Hz), 2.16 (s, 3H, H₇), 1.28 (t, 3H, H₁₈, ³J (¹H-¹H) = 7.6 Hz) ¹³C NMR (CDCl₃, 75.5 MHz, 300.0 K) δ 188.6 (quaternary $\underline{\text{C}}\text{-O}$, C₁₀), 161.8 (quaternary aromatic $\underline{\text{C}}$, C₁₁), 147.5 (quaternary aniline $\underline{\text{C}}$, C₁), 138.0 (quaternary $\underline{\text{C}}\text{-NH}$, C₈), 137.6 (quaternary aromatic $\underline{\text{C}}\text{-C}$, C₁₄), 129.1 (aniline $\underline{\text{C}}\text{H}$, C₃ and C₅), 127.8 (aniline $\underline{\text{C}}\text{H}$, C₂ and H₆), 127.2 (aromatic $\underline{\text{C}}\text{H}$, C₁₂ and C₁₆), 125.6 (aniline $\underline{\text{C}}\text{H}$, C₄), 124.7 (aromatic $\underline{\text{C}}\text{H}$, C₁₃ and C₁₅), 94.2 (acnac $\underline{\text{C}}\text{H}$, C₉), 28.8 (aliphatic $\underline{\text{C}}\text{H}_2$, C₁₇), 20.5 (aliphatic $\underline{\text{C}}\text{H}_3$, C₇), 15.3 (aliphatic $\underline{\text{C}}\text{H}_3$, C₁₈) **Analysis Calculated:** C 80.86, H 7.92, N 5.24% **Analysis Found:** C 80.85, H 7.15, N 5.05% **ES MS (+):** m/z 266.16 [MH⁺]

9.5.10 Preparation of C₁₇H₁₇NO₂ (L20)

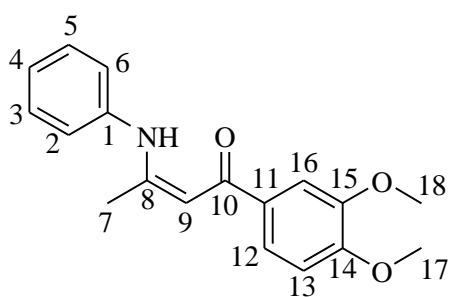
4'-Methoxy- β -diketonate (1.01 g, 5.25 mmol) was dissolved in toluene (20 mL), aniline (2 mL) and HCl (1 mL). This was stirred for 16 hours, the precipitate filtered and the solvent was removed under reduced pressure. The crude product washed with petrol (60-80°C) (10 mL) and recrystallised from hot ethanol (20 mL), yielding **L20** as a pale yellow crystalline precipitate (0.76 g, 2.84 mmol, 54%).



^1H NMR (CDCl_3 , 500.23 MHz, 300.0 K) δ 13.04 (br. s, 1H, NH), 7.92 (d, 2H, H_{12} and H_{16} , 3J (^1H - ^1H) = 8.9 Hz), 7.37 (br. t, 2H, H_3 and H_5 , 3J (^1H - ^1H) = 7.9 Hz), 7.24-7.20 (m, 1H, H_4), 7.18 (br. d, 2H, H_2 and H_6 , 3J (^1H - ^1H) = 7.3 Hz), 6.94 (br. d, 2H, H_{13} and H_{15} , 3J (^1H - ^1H) = 8.5 Hz), 5.87 (br. s, 1H, H_9), 3.87 (s, 3H, H_{17}), 2.15 (s, 3H, H_7) **$^{13}\text{C}\{^1\text{H}\}$ NMR** (CDCl_3 , 125.9 MHz, 300.0 K) δ 187.9 (quaternary $\text{C}=\text{O}$, C_{10}), 162.0 (quaternary aromatic C , C_{11}), 161.4 (quaternary aniline C , C_1), 138.9 (quaternary $\text{C}=\text{NH}$, C_8), 132.7 (quaternary aromatic C , C_{14}), 129.1 (aniline CH , C_3 and C_5), 129.0 (aromatic CH , C_{12} and C_{16}), 125.5 (aniline CH , C_4), 124.7 (aniline CH , C_2 and C_6), 113.5 (aromatic CH , C_{13} and C_{15}), 93.8 (acnac CH , C_9), 55.3 (methoxy OCH_3 C_{17}), 20.5 (aliphatic CH_3 , C_7) **Analysis Calculated:** C 76.38, H 6.41, N 5.24% **Analysis Found:** C 75.75, H 6.40, N 5.20% **ES MS (+):** m/z 268.13 [MH^+]

9.5.11 Preparation of $\text{C}_{18}\text{H}_{19}\text{NO}_3$ (L21)

3',4'-Dimethoxy- β -diketonate (0.76 g, 3.42 mmol) was dissolved in toluene (15 mL), aniline (1.5 mL) and HCl (1.2 mL). This was stirred for 16 hours, the precipitate filtered and the solvent was removed under reduced pressure. The crude product was recrystallised from hot ethanol (20 mL), yielding **L21** as a yellow crystalline precipitate (0.67 g, 2.26 mmol, 66%).

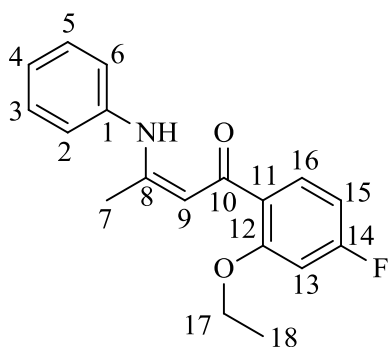


^1H NMR (CDCl_3 , 300.13 MHz, 295.7 K) δ 13.05 (br. s, 1H, NH), 7.57 (br. d, 1H, H_{12} , 4J (^1H - ^1H) = 1.7 Hz), 7.53 (br. dd, 1H, H_{15} , 3J (^1H - ^1H) = 8.3 Hz and 4J (^1H - ^1H) = 2.3 Hz), 7.41-7.35 (m, 2H, H_3 and H_5), 7.25-7.22 (m, 1H, H_4), 7.21-7.16 (m, 2H, H_2 and H_6), 6.90 (d, 1H, H_{16} , 3J (^1H - ^1H) = 8.3 Hz), 5.88 (br. s, 1H, H_9), 3.98 (s, 3H, H_{17}), 3.95 (s, 3H, H_{18}), 2.17 (s, 3H, H_7) **$^{13}\text{C}\{^1\text{H}\}$ NMR** (CDCl_3 , 75.5 MHz, 296.3 K) δ 187.7 (quaternary $\text{C}=\text{O}$, C_{10}), 161.5 (quaternary aromatic C , C_{11}), 151.5 (quaternary C , C_1 and C_8), 132.9 (quaternary aromatic C , C_{14} and C_{15}), 129.1 (aniline CH , C_3 and C_5), 125.6 (aniline CH , C_4), 124.6 (aniline CH , C_2 and C_6), 120.5 (aromatic CH , C_{15}), 110.1 (aromatic CH , C_{12}), 109.9 (aromatic CH , C_{16}), 93.7 (acnac CH , C_9), 56.0 (2C, methoxy OCH_3 , C_{17} and C_{18}), 20.5 (aliphatic CH_3 , C_7) **Analysis Calculated:**

C 72.71, H 6.44, N 4.71% **Analysis Found:** C 72.75, H 6.50, N 4.65% **ES MS (+):** m/z 320.13 [MNa⁺]

9.5.12 Preparation of C₁₈H₁₈FNO₂ (L22)

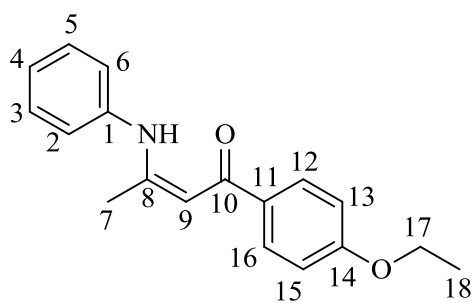
2'-Ethyl-4-fluoro- β -diketonate (0.41g, 1.83 mmol) was dissolved in toluene (10 mL), aniline (1 mL) and HCl (0.5 mL). This was stirred for 16 hours, the precipitate filtered and the solvent was removed under reduced pressure. The crude product was washed with petrol (60-80°C) (10 mL) and recrystallised from hot ethanol (20 mL), yielding **L22** as pale yellow crystals (0.25 g, 0.84 mmol, 46%).



¹H NMR (CDCl₃, 500.23 MHz, 294.7 K) δ 12.98 (br. s, 1H, NH), 7.78 (dd, 1H, H₁₆, ³ J (¹H-¹H) = 8.5 Hz and ⁴ J (¹H-¹⁹F) = 7.3 Hz), 7.40-7.35 (m, 2H, H₃ and H₅), 7.23 (br. d, 1H, H₄, ³ J (¹H-¹H) = 7.3 Hz), 7.21-7.18 (m, 2H, H₂ and H₆), 6.71 (td, 1H, H₁₅, ³ J (¹H-¹H) = 8.2 Hz and ³ J (¹H-¹⁹F) = 2.4 Hz), 6.64 (dd, 1H, H₁₃, ³ J (¹H-¹⁹F) = 11.1 Hz and ⁴ J (¹H-¹H) = 2.3 Hz), 6.02 (br. s, 1H, H₉), 4.12 (br. q, 2H, H₁₇, ³ J (¹H-¹H) = 7.0 Hz), 2.12 (s, 3H, H₇), 1.50 (br. t, 3H, H₁₈, ³ J (¹H-¹H) = 7.0 Hz) **¹³C NMR** (CDCl₃, 125.9 MHz, 300.0 K) δ 187.6 (quaternary C-O, C₁₀), 164.7 (quaternary aromatic C-F, C₁₄, ¹ J (¹³C-¹⁹F) = 248.4 Hz), 163.7 (quaternary aromatic C, C₁₁), 161.1 (quaternary C, C₁ or C₈), 158.2 (d, quaternary aromatic C, C₁₂, ³ J (¹³C-¹⁹F) = 10.3 Hz), 138.9 (quaternary C, C₁ or C₈), 131.9 (d, aromatic CH, C₁₆, ³ J (¹³C-¹⁹F) = 10.3 Hz), 129.1 (aniline CH, C₃ and C₅), 125.6 (aniline CH, C₄), 124.8 (aniline CH, C₂ and C₆), 107.2 (aromatic CH, C₁₅, ² J (¹³C-¹⁹F) = 20.6 Hz), 100.3 (aromatic CH, C₁₃, ² J (¹³C-¹⁹F) = 24.7 Hz), 99.2 (acnac CH, C₉), 64.5 (ethoxy CH₂, C₁₇), 20.2 (aliphatic CH₃, C₇), 14.6 (ethoxy CH₃, C₁₈) **Analysis Calculated:** C 72.22, H 6.06, N 4.68% **Analysis Found:** C 71.65, H 6.05, N 4.75% **ES MS (+):** m/z 300.14 [MH⁺]

9.5.13 Preparation of C₁₈H₁₉NO₂ (L23)

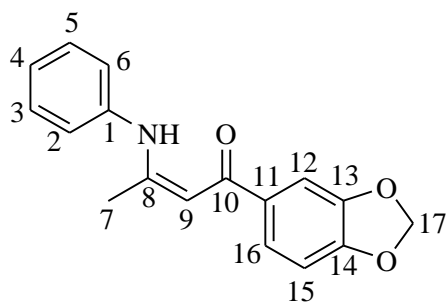
4'-Ethoxy- β -diketonate (0.77 g, 3.73 mmol) was dissolved in toluene (10 mL), aniline (1 mL) and HCl (0.5 mL). This was stirred for 16 hours, the precipitate filtered and the solvent was removed under reduced pressure. The crude product was recrystallised from hot ethanol (20 mL), yielding **L23** as yellow needle-like crystals (0.40 g, 1.42 mmol, 38%).



^1H NMR (CDCl_3 , 500.13 MHz, 319.2 K) δ 13.01 (br. s, 1H, NH), 7.91 (br. d, 2H, H_{12} and H_{16} , $^3J(^1\text{H}-^1\text{H}) = 8.8$ Hz), 7.39-7.34 (br. t, 2H, H_3 and H_5 , $^3J(^1\text{H}-^1\text{H}) = 7.3$ Hz) 7.23-7.20 (m, 1H, H_4), 7.18 (br. d, 2H, H_2 and H_6 , $^3J(^1\text{H}-^1\text{H}) = 8.8$ Hz), 5.86 (s, 1H, H_9), 4.11 (q, 2H, H_{17} , $^3J(^1\text{H}-^1\text{H}) = 6.7$ Hz), 2.14 (s, 3H, H_7), 1.45 (t, 3H, H_{18} , $^3J(^1\text{H}-^1\text{H}) = 6.7$ Hz) **$^{13}\text{C}\{^1\text{H}\}$ NMR** (CDCl_3 , 75.5 MHz, 300.0 K) δ 187.9 (quaternary $\text{C}=\text{O}$, C_{10}), 161.4 (quaternary aromatic C , C_{11}), 138.9 (quaternary aniline C , C_1 and C_8), 132.5 (quaternary aromatic C_{14}), 129.1 (aniline CH , C_3 and C_5), 129.0 (aromatic CH , C_{12} and C_{16}), 125.5 (aniline CH , C_4), 124.7 (aniline CH , C_2 and C_6), 114.0 (aromatic CH , C_{13} and C_{15}), 93.8 (acnac CH , C_9), 63.6 (ethoxy CH_2 , C_{17}), 20.5 (aliphatic CH_3 , C_7), 14.8 (ethoxy CH_3 , C_{18}) **Analysis Calculated:** C 75.23, H 5.65, N 13.85 **Analysis Found:** C 74.75, H 5.70, N 13.80 **ES MS (+):** m/z 282.15 [MH^+]

9.5.14 Preparation of $\text{C}_{17}\text{H}_{15}\text{NO}_3$ (L24)

3',4'-Methylene- β -diketonate (0.51 g, 2.47 mmol) was dissolved in toluene (10 mL), aniline (1 mL) and HCl (0.5 mL). This was stirred for 16 hours, the precipitate filtered and the solvent was removed under reduced pressure. The crude product was recrystallised from hot ethanol (20 mL), yielding **L24** as green crystals (0.33 g, 1.17 mmol, 47%).

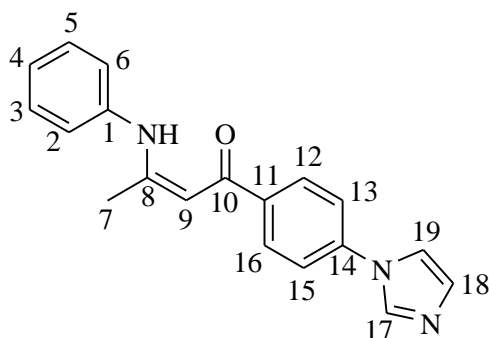


^1H NMR (CDCl_3 , 500.23 MHz, 300.0 K) δ 12.99 (br. s, 1H, NH), 7.51 (dd, 1H, H_{16} , $^3J(^1\text{H}-^1\text{H}) = 8.1$ Hz and $^4J(^1\text{H}-^1\text{H}) = 1.4$ Hz), 7.44 (d, 1H, H_{12} , $^4J(^1\text{H}-^1\text{H}) = 1.5$ Hz) 7.42-7.37 (m, 2H, H_2 and H_6), 7.27-7.23 (m, 1H, H_4), 7.20-7.17 (m, 2H, H_3 and H_5), 6.85 (d, 1H, H_{15} , $^3J(^1\text{H}-^1\text{H}) = 8.2$ Hz), 6.03 (s, 2H, H_{17}), 5.81 (s, 1H, H_9), 2.14 (s, 3H, H_7) **$^{13}\text{C}\{^1\text{H}\}$ NMR** (CDCl_3 , 125.8 MHz, 300.0 K) δ 161.7 (quaternary $\text{C}=\text{O}$, C_{10}), 150.0 (quaternary aromatic C , C_{13} or C_{14}), 147.9 (quaternary aromatic C , C_{13} or C_{14}), 138.7 (quaternary aromatic C , C_{11}), 130.7 (quaternary C , C_1 or C_8), 129.2 (aniline CH , C_2 and C_6), 129.2 (aniline CH , C_3 and C_5), 125.7 (aromatic CH , C_{12}), 124.8 (quaternary C , C_1 or C_8), 122.2 (aniline CH , C_4), 107.8 (aromatic CH , C_{16}), 107.5 (aromatic CH , C_{15}), 101.5 (methylene CH_2 , C_{17}), 98.2 (acnac CH , C_9), 20.5

(aliphatic $\underline{\text{C}}\text{H}_3$, C_7) **Analysis Calculated:** C 72.58, H 5.37, N 4.98% **Analysis Found:** C 72.25, H 5.35, N 4.95% **ES MS (+):** m/z 282.10 [M^+]

9.5.15 Preparation of $\text{C}_{17}\text{H}_{15}\text{NO}_3$ (L25)

4'-Imidazole- β -diketonate (**L4**) (0.12 g, 0.644 mmol) was dissolved in toluene (10 mL), aniline (1 mL) and HCl (0.5 mL). This was stirred for 16 hours, the precipitate filtered and the solvent was removed under reduced pressure. The crude product was recrystallised from hot ethanol (20 mL) and stored at -20°C , yielding **L25** as green crystals (0.34 g, 1.12 mmol, 49%).

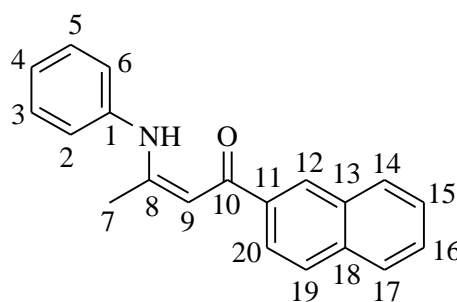


^1H NMR (CDCl_3 , 300.13 MHz, 300.0 K) δ 13.13 (br. s, 1H, $\underline{\text{N}}\underline{\text{H}}$), 8.05 (d, 2H, H_{12} and H_{16} , 3J (^1H - ^1H) = 8.5 Hz), 7.47 (d, 2H, H_{13} and H_{15} , 3J (^1H - ^1H) = 8.5 Hz), 7.45-7.36 (m, 3H, H_2 , H_4 and H_6), 7.29-7.26 (m, 2H, H_3 or H_5), 7.25-7.17 (m, 3H, H_{17-19}), 5.90 (s, 1H, H_9), 2.18 (s, 3H, H_7) $^{13}\text{C}\{^1\text{H}\}$

NMR (CDCl_3 , 75.5 MHz, 299.9 K) δ 186.7 (quaternary $\underline{\text{C}}\text{-O}$, C_{10}), 162.9 (quaternary aromatic $\underline{\text{C}}$, C_{11}), 139.0 (quaternary aromatic $\underline{\text{C}}$, C_{14}), 138.4 (quaternary $\underline{\text{C}}$, C_1 or C_8), 137.4 (quaternary $\underline{\text{C}}$, C_1 or C_8), 129.2 (aniline $\underline{\text{C}}\text{H}$, C_3 and C_5), 128.9 (aromatic $\underline{\text{C}}\text{H}$, C_{12} and C_{16}), 126.1 (aniline $\underline{\text{C}}\text{H}$, C_2 , C_4 and C_6), 124.9 (aromatic $\underline{\text{C}}\text{H}$, C_{13} and C_{15}), 120.8 (imidazole $\underline{\text{C}}\text{H}$, C_{17-19}), 93.9 (acnac $\underline{\text{C}}\text{H}$, C_9), 20.4 (aliphatic $\underline{\text{C}}\text{H}_3$, C_7) **Analysis Calculated:** C 75.23, H 5.65, N 13.85% **Analysis Found:** C 74.75, H 5.70, N 13.80% **ES MS (+):** m/z 304.14 [MH^+]

9.5.16 Preparation of $\text{C}_{20}\text{H}_{17}\text{NO}$ (L26)

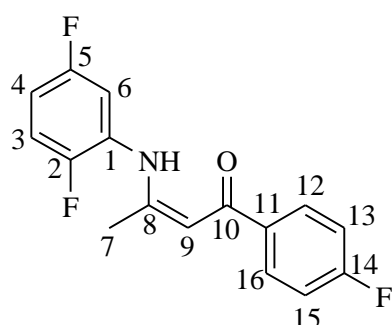
3'-Naphthyl- β -diketonate (0.59 g, 2.78 mmol) was dissolved in toluene (10 mL), aniline (1 mL) and HCl (0.5 mL). The suspension was stirred for 16 hours, the precipitate filtered and the solvent was removed under reduced pressure. The crude product was recrystallised from hot ethanol (20 mL), yielding **L26** as pale yellow crystals (0.65 g, 2.26 mmol, 81%)



$^1\text{H NMR}$ (CDCl_3 , 500 MHz, 300.0 K) δ 13.13 (br. s, 1H, NH), 8.51 (d, 2H, aniline CH , H_2 and H_6 , $^3J(^1\text{H}-^1\text{H}) = 8.3$ Hz), 7.89 (br. t, 2H, aniline CH , H_3 and C_5 , $^3J(^1\text{H}-^1\text{H}) = 8.3$ Hz), 7.70 (br. d, 1H, aromatic CH , H_{12} , $^4J(^1\text{H}-^1\text{H}) = 6.9$ Hz), 7.57-7.53 (m, 1H, aniline CH , H_4), 7.53-7.48 (m, 2H, aromatic CH , H_{19} and H_{20}), 7.42 (br. t, 2H, aromatic CH , H_{14-17} , $^3J(^1\text{H}-^1\text{H}) = 8.3$ Hz), 7.28-7.25 (m, 2H, aromatic CH , H_{14-17}), 5.70 (s, 1H, acnac CH , H_9), 2.16 (s, 3H, aliphatic CH_3 , H_7) $^{13}\text{C}\{^1\text{H}\}$ NMR (CDCl_3 , 125 MHz, 300 K) δ 193.0 (quaternary $\text{C}-\text{O}$, C_{10}), 162.0 (quaternary aromatic C , C_{11}), 143.2 (quaternary C , C_{13} or C_{18}), 140.1 (quaternary C , C_{13} or C_{18}), 138.6 (quaternary aromatic C , C_1 and C_8), 130.3 (aniline CH , C_3 or C_5), 129.9 (aniline CH , C_3 or C_5), 129.2 (naphthyl CH), 128.4 (naphthyl CH), 126.6 (naphthyl CH), 126.1 (naphthyl CH), 125.4 (naphthyl CH), 124.9 (naphthyl CH), 124.9 (naphthyl CH), 99.0 (acnac CH , C_9), 20.3 (aliphatic CH_3 , C_7) **Analysis Calculated:** C 83.59, H 5.96, N 4.87% **Analysis Found:** C 83.70, H 6.00, N 4.80% **ES MS (+):** m/z 288.14 [MH^+]

9.5.17 Preparation of $\text{C}_{16}\text{H}_{11}\text{F}_3\text{NO}$ (27)

4'-Fluoro- β -diketonate (0.54 g, 3.00 mmol) was dissolved in toluene (10 mL), 2,5-difluoroaniline (1 mL) and HCl (0.5 mL). This was stirred for 16 hours, the precipitate filtered and the solvent was removed under reduced pressure. The crude product was recrystallised from hot ethanol (20 mL), yielding **L27** as a pale brown crystalline precipitate (0.56 g, 1.92 mmol, 64%)

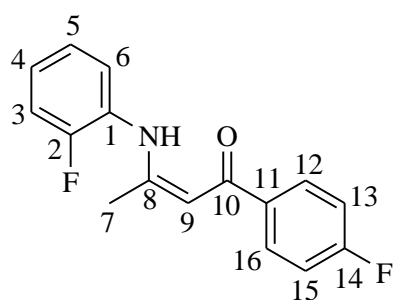


$^1\text{H NMR}$ (CDCl_3 , 300.13 MHz, 300.0 K) δ 12.90 (br. s, 1H, NH), 7.97-7.92 (m, 2H, H_{12} and H_{16}), 7.16-7.09 (m, 3H, H_3 , H_4 and H_6), 6.99 (ddd, 1H, H_{13} or H_{15} , $^3J(^1\text{H}-^1\text{H}) = 9.0$ Hz and $^3J(^1\text{H}-^{19}\text{F}) = 3.1$ and 2.0 Hz), 6.93-6.87 (m, 1H, H_{13} or H_{15}), 5.95 (s, 1H, H_9), 2.17 (s, 3H, H_7) $^{13}\text{C}\{^1\text{H}\}$ NMR (CDCl_3 , 125.9 MHz, 300.0 K) δ 188.1 (quaternary $\text{C}-\text{O}$, C_{10}), 164.8 (d, quaternary $\text{C}-\text{F}$, C_{14} , $^1J(^{13}\text{C}-^{19}\text{F}) = 250.5$ Hz), 161.5 (quaternary aromatic C , C_{11}), 158.3 (dd, quaternary aniline $\text{C}-\text{F}$, C_2 or C_5 , $^1J(^{13}\text{C}-^{19}\text{F}) = 242.3$ Hz and $^4J(^{13}\text{C}-^{19}\text{F}) = 3.1$ Hz), 152.7 (dd, quaternary aniline $\text{C}-\text{F}$, C_2 or C_5 , $^1J(^{13}\text{C}-^{19}\text{F}) = 242.3$ Hz and $^4J(^{13}\text{C}-^{19}\text{F}) = 3.1$ Hz), 135.7 (d, quaternary aromatic C , C_8 , $^4J(^{13}\text{C}-^{19}\text{F}) = 3.1$ Hz), 129.6 (d, 2C,

aromatic $\underline{\text{C}}\text{H}$, C_{12} and C_{16} , ${}^3J(^{13}\text{C}-^{19}\text{F}) = 8.3$ Hz). 127.9 (dd, quaternary aniline $\underline{\text{C}}$, C_1 , ${}^2J(^{13}\text{C}-^{19}\text{F}) = 24.7$ Hz and ${}^3J(^{13}\text{C}-^{19}\text{F}) = 4.1$ Hz), 115.3 (d, 3 $\underline{\text{C}}$, C_3 , C_4 and C_6 , ${}^3J(^{13}\text{C}-^{19}\text{F}) = 21.7$ Hz), 113.1 (d, aromatic $\underline{\text{C}}\text{H}$, C_{12} and C_{16} , ${}^3J(^{13}\text{C}-^{19}\text{F}) = 23.7$ Hz), 113.0 (d, aromatic $\underline{\text{C}}\text{H}$, C_{13} and C_{15} , ${}^2J(^{13}\text{C}-^{19}\text{F}) = 25.8$ Hz), 95.3 (acnac $\underline{\text{C}}\text{H}$, C_9), 20.3 (aliphatic $\underline{\text{C}}\text{H}_3$, C_7) **Analysis Calculated:** C 65.98, H 4.15, N 4.81% **Analysis Found:** C 65.35, H 4.35, N 4.70% **ES MS (+):** m/z 292.09 [MH^+]

9.5.18 Preparation of $\text{C}_{16}\text{H}_{13}\text{F}_2\text{NO}$ (L28)

4'-Fluoro- β -diketonate (0.63g, 2.84 mmol) was dissolved in toluene (10 mL), 2-fluoroaniline (1 mL) and HCl (0.5 mL). This was stirred for 16 hours, the precipitate filtered and the solvent was removed under reduced pressure. The crude product was recrystallised from hot ethanol (20 mL), yielding **L28** as a yellow crystalline precipitate (0.41 g, 1.50 mmol, 53%)

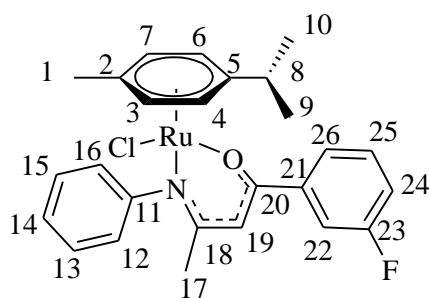


${}^1\text{H NMR}$ (CDCl_3 , 300.13 MHz, 300.1 K) δ 12.82 (br. s, 1H, $\underline{\text{N}}\text{H}$), 7.95 (ddd, 2H, H_{12} and H_{16} , ${}^3J(^1\text{H}-^1\text{H}) = 9.1$ Hz, ${}^4J(^1\text{H}-^1\text{H}) = 4.9$ Hz, ${}^4J(^1\text{H}-^{19}\text{F}) = 2.3$ Hz), 7.28-7.22 (m, 2H, H_3 - H_6), 7.21-7.15 (m, 2H, H_3 - H_6), 7.11 (ddd, 2H, H_{13} and H_{15} , ${}^3J(^1\text{H}-^1\text{H}) = 9.1$ Hz, ${}^4J(^1\text{H}-^1\text{H}) = 4.9$ Hz, ${}^3J(^1\text{H}-^{19}\text{F}) = 2.6$ Hz), 5.92 (s, 1H, H_9), 2.11 (s, 3H, H_7) ${}^{13}\text{C}\{^1\text{H}\}$ **NMR** (CDCl_3 , 75.5 MHz, 300.0 K) δ 187.7 (quaternary $\underline{\text{C}}-\text{O}$, C_{10}), 164.6 (d, quaternary $\underline{\text{C}}-\text{F}$, C_2 or C_{14} , ${}^1J(^{13}\text{C}-^{19}\text{F}) = 249.7$ Hz), 162.7 (quaternary aromatic $\underline{\text{C}}$, C_{11}), 156.7 (d, quaternary $\underline{\text{C}}-\text{F}$, C_2 or C_{14} , ${}^1J(^{13}\text{C}-^{19}\text{F}) = 247.2$ Hz), 136.0 (d, quaternary aniline $\underline{\text{C}}$, C_8 , ${}^4J(^{13}\text{C}-^{19}\text{F}) = 2.5$ Hz), 129.4 (d, aromatic $\underline{\text{C}}\text{H}$, C_{12} and C_{16} , ${}^3J(^{13}\text{C}-^{19}\text{F}) = 8.7$ Hz), 127.5 (d, aniline $\underline{\text{C}}\text{H}$, C_4 , ${}^3J(^{13}\text{C}-^{19}\text{F}) = 7.4$ Hz), 127.1 (aniline $\underline{\text{C}}\text{H}$, C_6), 126.7 (d, quaternary aromatic $\underline{\text{C}}$, C_1 , ${}^2J(^{13}\text{C}-^{19}\text{F}) = 12.4$ Hz). 124.4 (d, aniline $\underline{\text{C}}\text{H}$, C_5 , ${}^4J(^{13}\text{C}-^{19}\text{F}) = 3.7$ Hz), 116.4 (d, aniline $\underline{\text{C}}\text{H}$, C_3 , ${}^2J(^{13}\text{C}-^{19}\text{F}) = 19.8$ Hz), 115.2 (d, aromatic $\underline{\text{C}}\text{H}$, C_{13} and C_{15} , ${}^2J(^{13}\text{C}-^{19}\text{F}) = 21.0$ Hz), 94.3 (acnac $\underline{\text{C}}\text{H}$, C_9), 20.1 (d, aliphatic $\underline{\text{C}}\text{H}_3$, C_7 , ${}^5J(^{13}\text{C}-^{19}\text{F}) = 2.5$ Hz) **Analysis Calculated:** C 70.32, H 4.79, N 5.13% **Analysis Found:** C 69.60, H 4.80, N 4.90% **ES MS (+):** m/z 274.1 [M^+]

9.6 Synthesis of Ruthenium Chloride Complexes

9.6.1 Preparation of C₂₆H₂₇ClFNORu (1)

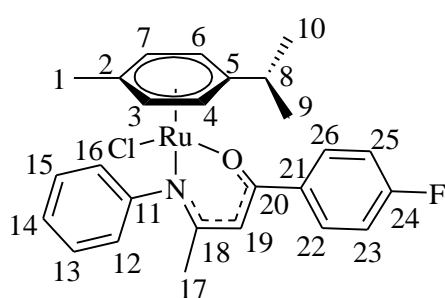
3-Fluoro- β -ketoiminate (**L12**) (0.10 g, 0.392 mmol) was dissolved in dichloromethane (30 mL) and whilst stirring triethylamine (0.05 mL, 0.39 mmol) and [*p*-cymRuCl₂]₂ (0.12 g, 0.200 mmol) were added. The mixture was stirred at room temperature for 16 hours and then the solvent was removed under reduced pressure. The crude product was recrystallised from methanol (10 mL) and stored at 4°C for 2 days, yielding red crystals of **1** (0.12 g, 0.227 mmol, 58%).



¹H NMR (CDCl₃, 500.23 MHz, 300.0 K) δ 7.75 (br. d, 1H, H₂₂, ³*J* (¹H-¹H) = 8.5 Hz), 7.61-7.56 (m, 2H, H₂₅ and H₂₆), 7.43 (br. tt, 2H, H₁₃ and H₁₅, ³*J* (¹H-¹H) = 6.9 Hz and ³*J* (¹H-¹H) = 1.6 Hz), 7.31-7.28 (m, 1H, H₁₄), 7.26-7.22 (m, 1H, H₁₂ or H₁₆), 7.10-7.07 (m, 1H, H₁₂ or H₁₆), 7.07-7.03 (m, 1H, H₂₄), 5.41 (s, 1H, H₁₉), 5.35 (br. d, 1H, H_{3,4,6,7}, ³*J* (¹H-¹H) = 6.0 Hz), 5.17 (br. d, 1H, H_{3,4,6,7}, ³*J* (¹H-¹H) = 6.4 Hz), 5.07 (br. d, 1H, H_{3,4,6,7}, ³*J* (¹H-¹H) = 5.6 Hz), 3.69 (br. d, H_{3,4,6,7}, ³*J* (¹H-¹H) = 6.0 Hz), 2.72-2.66 (br. sept, 1H, H₈, CH(CH₃)₂), 2.03 (s, 3H, H₁), 1.79 (s, 3H, H₁₇), 1.21 (br. d, 3H, H₉ or H₁₀, ³*J* (¹H-¹H) = 6.8 Hz), 1.20 (br. d, 3H, H₉ or H₁₀, ³*J* (¹H-¹H) = 7.3 Hz) **¹³C{¹H} NMR** (CDCl₃, 75.5 MHz, 300.0 K) δ 170.0 (d, quaternary C-O, C₂₀, ⁴*J* (¹³C-¹⁹F) = 2.1 Hz), 165.1 (quaternary C, C₁₁ or C₁₈), 162.7 (d, quaternary C-F, C₂₃, ¹*J* (¹³C-¹⁹F) = 243.3 Hz), 157.2 (quaternary C, C₁₁ or C₁₈), 142.0 (d, quaternary C, C₂₁ *ipso*, ³*J* (¹³C-¹⁹F) = 6.2 Hz), 129.7 (aniline CH, C₁₃ or C₁₅), 129.2 (d, aromatic CH, C₂₅, ³*J* (¹³C-¹⁹F) = 7.2 Hz), 127.8 (aniline CH, C₁₃ or C₁₅), 126.0 (aniline CH, C₁₄), 125.5 (aniline CH, C₁₂ or C₁₆), 123.3 (aniline CH, C₁₂ or C₁₆), 122.4 (d, aromatic CH, C₂₆, ⁴*J* (¹³C-¹⁹F) = 2.1 Hz), 116.1 (d, aromatic CH, C₂₄, ²*J* (¹³C-¹⁹F) = 20.6 Hz), 114.0 (d, aromatic CH, C₂₂, ²*J* (¹³C-¹⁹F) = 22.7 Hz), 101.0 (quaternary C, C₂ or C₅), 96.3 (quaternary C, C₂ or C₅), 94.8 (acnac CH, C₁₉), 87.1 (*p*-cymene CH, C_{3,4,6,7}), 84.6 (*p*-cymene CH, C_{3,4,6,7}), 84.5 (*p*-cymene CH, C_{3,4,6,7}), 79.6 (*p*-cymene CH, C_{3,4,6,7}), 30.5 (*p*-cymene CH, C₈), 24.7 (aliphatic CH₃, C₁₇), 23.4 (*p*-cymene CH₃, C₉ or C₁₀), 20.9 (*p*-cymene CH₃, C₉ or C₁₀), 18.4 (*p*-cymene CH₃, C₁) **Analysis Calculated:** C 59.48, H 5.18, N 2.67% **Analysis Found:** C 59.40, H 5.20, N 2.60% **ES MS (+):** *m/z* 490.11 [M⁺]-Cl

9.6.2 Preparation of C₂₆H₂₇ClFNORu (2)

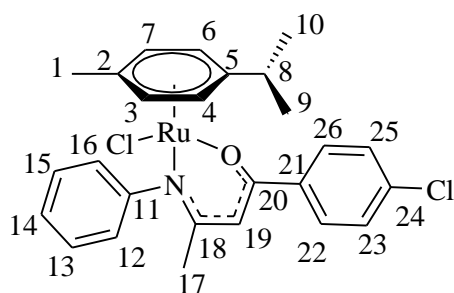
4-Fluoro- β -ketoiminate (**L13**) (0.13 g, 0.490 mmol) was dissolved in dichloromethane (30 mL), whilst stirring triethylamine (0.07 mL, 0.490 mmol) and [*p*-cymRuCl₂]₂ (0.15 g, 0.245 mmol) were added. The mixture was stirred for 16 hours at room temperature and then the solvent was removed under reduced pressure. The crude product was recrystallised from methanol (10 mL), the residue was filtered and the solution stored at 4°C for 5 days, yielding red crystals of **2** which were washed with THF (3 x 10 mL) (0.07 g, 0.133 mmol, 54%).



¹H NMR (CDCl₃, 500.57 MHz, 300.0 K) δ 7.84 (dd, 2H, H₂₂ and H₂₆, ³*J* (¹H-¹H)= 9.0 Hz and ⁴*J* (¹H-¹H)= 2.2 Hz), 7.75 (br. d, 1H, H₁₄, ³*J* (¹H-¹H)= 9.0 Hz), 7.43 (br. t, 2H, H₁₃ and H₁₅, ³*J* (¹H-¹H)= 7.7 Hz), 7.26-7.22 (br. dd, 1H, H₁₂ or H₁₆, ³*J* (¹H-¹H)= 6.2 Hz and ⁴*J* (¹H-¹H)= 2.1 Hz), 7.09 (br. d, 1H, H₁₂ or H₁₆, ³*J* (¹H-¹H)= 6.9 Hz), 7.03-6.99 (a. t (v. dd), 2H, H₂₃ and H₂₅, ³*J* (¹H-¹H) = 8.6 Hz and ⁴*J* (¹H-¹H) = 3.9 Hz), 5.37 (s, 1H, H₁₉), 5.35 (br. d, 1H, H_{3,4,6,7}, ³*J* (¹H-¹H) = 6.0 Hz), 5.16 (br. d, 1H, H_{3,4,6,7}, ³*J* (¹H-¹H) = 6.0 Hz), 5.06 (br. d, 1H, H_{3,4,6,7}, ³*J* (¹H-¹H) = 5.6 Hz), 3.68 (br. d, 1H, H_{3,4,6,7}, ³*J* (¹H-¹H) = 5.6 Hz), 2.67 (br. sept, 1H, H₈, ³*J* (¹H-¹H) = 6.9 Hz), 2.03 (s, 3H, H₁), 1.79 (s, 3H, H₁₇), 1.20 (a. t (v. dd), 6H, H₉ and H₁₀, ³*J* (¹H-¹H) = 7.5 Hz) **¹³C{¹H} NMR** (CDCl₃, 125.9 MHz, 300.0 K) δ 170.6 (quaternary C-O, C₂₀), 164.8 (quaternary C-N, C₂₁), 163.6 (quaternary C-F, C₂₄, ¹*J* (¹³C-¹⁹F) = 247.4 Hz), 157.2 (quaternary C, C₁₁ or C₁₈), 137.5 (quaternary C, C₁₁ or C₁₈), 129.6 (aniline CH, C₁₂ and C₁₆), 128.2 (aromatic CH, C₂₂ and C₂₆, ³*J* (¹³C-¹⁹F) = 7.3 Hz), 126.1 (aniline CH, C₁₄), 125.4 (aniline CH, C₁₃ or C₁₅), 123.9 (aniline CH, C₁₃ or C₁₅), 114.6 (aromatic CH, C₂₃ and C₂₅, ²*J* (¹³C-¹⁹F) = 21.7 Hz), 100.8 (quaternary C, C₂ or C₅), 96.2 (quaternary C, C₂ or C₅), 94.2 (acnac CH, C₁₉), 87.0 (*p*-cymene CH, C_{3,4,6,7}), 84.6 (*p*-cymene CH, C_{3,4,6,7}), 84.5 (*p*-cymene CH, C_{3,4,6,7}), 79.4 (*p*-cymene CH, C_{3,4,6,7}), 30.5 (*p*-cymene CH, C₈), 24.7 (acnac CH₃, C₁₇), 23.6 (*p*-cymene CH₃, C₉ or C₁₀), 20.9 (*p*-cymene CH₃, C₉ or C₁₀), 18.3 (*p*-cymene CH₃, C₁) **Analysis Calculated:** C 59.48, H 5.18, N 2.67% **Analysis Found:** C 59.25, H 5.20, N 2.75% **ES MS (+):** *m/z* 490.11 [M⁺]-Cl

9.6.3 Preparation of C₂₆H₂₇Cl₂NORu (3)

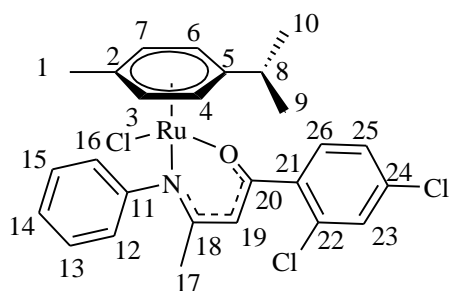
4'-Chloro- β -ketoiminate (0.05 g, 0.184 mmol) was dissolved in dichloromethane (30 mL) and whilst stirring triethylamine (0.03 mL, 0.184 mmol) and [*p*-cymRuCl₂]₂ (0.06 g, 0.092 mmol) were added. The mixture was stirred overnight at room temperature, and then the solvent removed under reduced pressure. The crude product was recrystallised from methanol (10 mL), and the residue filtered. The dark red solution was stored at 4°C for 2 days, yielding **3** as a red crystalline solid (0.06 g, 0.114 mmol, 62%).



¹H NMR (CDCl₃, 500.23 MHz, 299.9 K) δ 7.81–7.77 (br. dt, 2H, H₂₃ and H₂₅, ³*J* (¹H-¹H)= 8.7 Hz and ⁴*J* (¹H-¹H)= 1.8 Hz), 7.74 (br. d, 1H, H₁₃ or H₁₅, ³*J* (¹H-¹H)= 7.5 Hz), 7.43 (br. t, 2H, H₁₂ and H₁₆, ³*J* (¹H-¹H)= 8.3 Hz), 7.30 (br. dt, 2H, H₂₂ and H₂₆, ³*J* (¹H-¹H)= 8.7 Hz and ⁴*J* (¹H-¹H)= 2.0 Hz), 7.26–7.22 (br. t, 1H, H₁₃ or H₁₅, ³*J* (¹H-¹H)= 7.5 Hz), 7.09 (br. d, 1H, H₁₄, ³*J* (¹H-¹H) = 6.8 Hz), 5.39 (s, 1H, H₁₉), 5.35 (br. d, H_{3,4,6,7}, ³*J* (¹H-¹H) = 6.0 Hz), 5.16 (br. d, 1H, H_{3,4,6,7}, ³*J* (¹H-¹H) = 6.0 Hz), 5.06 (br. d, 1H, H_{3,4,6,7}, ³*J* (¹H-¹H) = 5.6 Hz), 3.68 (br. d, 1H, H_{3,4,6,7}, ³*J* (¹H-¹H) = 5.6 Hz), 2.67 (br. sept, 1H, H₈, ³*J* (¹H-¹H) = 7.0 Hz), 2.03 (s, 3H, H₁), 1.79 (s, 3H, H₁₇), 1.21 (d, 3H, CH₃, H₉ or H₁₀, ³*J* (¹H-¹H) = 9.9 Hz), 1.91 (d, 3H, CH₃, H₉ or H₁₀, ³*J* (¹H-¹H) = 9.9 Hz) **¹³C{¹H} NMR** (CDCl₃, 75.5 MHz, 300.1 K) δ 170.3 (quaternary C-O, C₂₀), 164.9 (quaternary C, C₂₁), 157.2 (quaternary C-Cl, C₂₄), 138.0 (quaternary C, C₁₁ or C₁₈), 135.2 (quaternary C, C₁₁ or C₁₈), 129.6 (aniline CH, C₁₂ and C₁₆), 128.2 (aromatic CH, C₂₃ or C₂₅), 128.0 (aromatic CH, C₂₃ or C₂₅), 127.8 (aromatic CH, C₂₂ and C₂₆), 126.0 (aniline CH, C₁₃ or C₁₅), 125.5 (aniline CH, C₁₃ or C₁₅), 123.3 (aniline CH, C₁₄), 104.4 (quaternary C, C₂ or C₅), 96.3 (quaternary C, C₂ or C₅), 94.5 (acnac CH, C₁₉), 87.1 (*p*-cymene CH, C_{3,4,6,7}), 84.7 (*p*-cymene CH, C_{3,4,6,7}), 84.6 (*p*-cymene CH, C_{3,4,6,7}), 79.5 (*p*-cymene CH, C_{3,4,6,7}), 30.5 (*p*-cymene CH, C₈), 24.7 (acnac CH₃, C₁₇), 23.6 (*p*-cymene CH₃, C₉ or C₁₀), 20.9 (*p*-cymene CH₃, C₉ or C₁₀), 18.4 (*p*-cymene CH₃, C₁) **Analysis Calculated:** C 57.67, H 5.03, N 2.59, Cl 13.09% **Analysis Found:** C 57.40, H 5.00, N 2.40, Cl 13.05% **ES MS (+):** *m/z* 506.08 [M⁺]-Cl

9.6.4 Preparation of C₂₆H₂₆Cl₃NORu (4)

2',4'-Dichloro- β -ketoiminate (0.16 g, 0.523 mmol) was dissolved in dichloromethane (30 mL) and whilst stirring triethylamine (0.07 mL, 0.523 mmol) and [*p*-cymRuCl₂]₂ (0.16 g, 0.261 mmol) were added. The mixture was stirred for 16 hours at room temperature, and then the solvent removed under reduced pressure. The crude product was recrystallised from methanol (10 mL) and after a period of 2 days yielded red crystals of **4**, which were further washed with petrol (40-60°) (3 x 5 mL) (0.19 g, 0.330 mmol, 63%).



¹H NMR (CDCl₃, 500.13 MHz, 240.2 K)

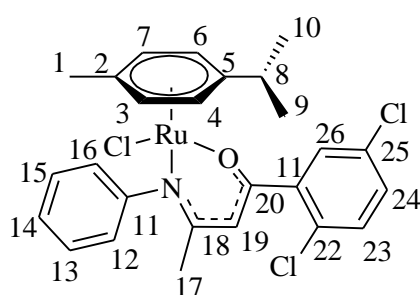
δ 7.72 (br. d, 1H, H₁₄, ³J (¹H-¹H) = 7.8 Hz), 7.45 (br. d, 2H, H₁₃ and H₁₅, ³J (¹H-¹H) = 6.2 Hz), 7.35 (br. d, 1H, H₂₅, ³J (¹H-¹H) = 5.9 Hz), 7.32 (br. d, 1H, H₂₆, ³J (¹H-¹H) = 8.2 Hz), 7.26-7.23 (m, 1H, H₁₂ or H₁₆), 7.20 (br. dd, 1H, H₂₃, ³J (¹H-¹H) = 8.2 Hz and ⁴J (¹H-¹H) = 1.9 Hz), 5.30 (br. d, 1H, H_{3,4,6,7}), 5.22 (br. d, 1H, H_{3,4,6,7}, ³J (¹H-¹H) = 6.0 Hz), 5.01 (br. d, 1H, H_{3,4,6,7}, ³J (¹H-¹H) = 5.2 Hz), 4.93 (s, 1H, H₁₉), 3.44 (br. d, 1H, H_{3,4,6,7}, ³J (¹H-¹H) = 5.1 Hz), 2.74 (br. sept, 1H, H₈, ³J (¹H-¹H) = 6.6 Hz), 2.05 (s, 3H, H₁), 1.74 (s, 3H, H₁₇), 1.27 (br. d, 3H, H₉ or H₁₀, ³J (¹H-¹H) = 6.7 Hz), 1.22 (br. d, 3H, H₉ or H₁₀, ³J (¹H-¹H) = 6.7 Hz)

¹³C{¹H} NMR (CDCl₃, 125.8 MHz, 240.2 K) δ 171.5 (quaternary C-O, C₂₀), 164.3 (quaternary C, C₂₁), 156.7 (quaternary C, C₁₈), 138.5 (quaternary C, C₁₁), 133.9 (quaternary C-Cl, C₂₂ or C₂₄), 131.4 (quaternary C-Cl, C₂₂ or C₂₄), 130.9 (aromatic CH, C₂₅ or C₂₆), 129.6 (aniline CH, C₁₃ or C₁₅), 129.1 (aromatic CH, C₂₃), 127.8 (aniline CH, C₁₃ or C₁₅), 126.7 (aromatic CH, C₂₅ or C₂₆), 125.2 (aniline CH, C₁₄), 99.6 (quaternary C, C₂ or C₅), 98.1 (acnac CH, C₁₉), 97.2 (quaternary C, C₂ or C₅), 87.8 (*p*-cymene CH, C_{3,4,6,7}), 83.4 (*p*-cymene CH, C_{3,4,6,7}), 83.2 (*p*-cymene CH, C_{3,4,6,7}), 79.9 (*p*-cymene CH, C_{3,4,6,7}), 30.1 (*p*-cymene CH, C₈), 24.6 (acnac CH₃, C₁₇), 23.8 (*p*-cymene CH₃, C₉ or C₁₀), 21.1 (*p*-cymene CH₃, C₉ or C₁₀), 18.8 (*p*-cymene CH₃, C₁)

Analysis Calculated: C 54.22, H 4.55, N 2.43, Cl 18.47% **Analysis Found:** C 54.05, H 4.65, N 2.35, Cl 18.45% **ES MS (+):** *m/z* 540.04 [M⁺]-Cl

9.6.5 Preparation of C₂₆H₂₆Cl₃NORu (5)

2',5'-Dichloro- β -ketoiminate (**L14**) (0.28 g, 0.912 mmol) was dissolved in dichloromethane (30 mL) and whilst stirring triethylamine (0.13 mL, 0.912 mmol) and [*p*-cymRuCl₂]₂ (0.28 g, 0.457 mmol) were added. The mixture was stirred for 16 hours at room temperature, and then the solvent removed under reduced pressure. The crude product was recrystallised from methanol (10 mL) and after a period of 2 days yielded red crystalline precipitate of **5** which was further washed with THF (3 x 5 mL) (0.32 g, 0.558 mmol, 61%)

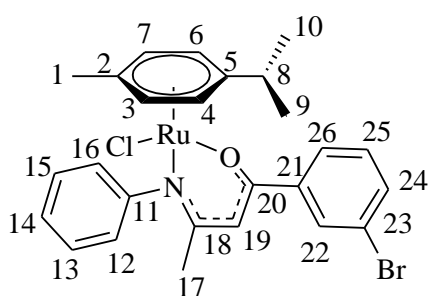


¹H NMR (CDCl₃, 300.13 MHz, 295.5 K) δ 7.78–7.73 (m, 1H, H₁₄), 7.47–7.43 (br. d, 2H, H₁₃ and H₁₅), 7.42 (m, 1H, H₂₃ or H₂₄), 7.25 (d, 2H, H₁₂ and H₁₆, ³J (¹H-¹H) = 7.0 Hz), 7.21–7.16 (m, 1H, H₂₆), 7.13–7.08 (m, 1H, H₂₃ or H₂₄), 5.28 (br. d, 1H, H_{3,4,6,7}, ³J (¹H-¹H) = 6.2 Hz),

5.14 (br. d, 1H, H_{3,4,6,7}, ³J (¹H-¹H) = 6.2 Hz), 5.02 (br. d, 1H, H_{3,4,6,7}, ³J (¹H-¹H) = 5.5 Hz), 4.94 (s, 1H, H₁₉), 3.64 (br. d, 1H, H_{3,4,6,7}, ³J (¹H-¹H) = 5.7 Hz), 2.76 (br. sept, 1H, H₈, ³J (¹H-¹H) = 7.0 Hz), 2.07 (s, 3H, H₁), 1.74 (s, 3H, H₁₇), 1.28 (br. d, 3H, CH₃, H₉ or H₁₀, ³J (¹H-¹H) = 6.8 Hz), 1.22 (br. d, 3H, CH₃, H₉ or H₁₀, ³J (¹H-¹H) = 7.0 Hz) ¹³C{¹H} NMR (CDCl₃, 75.5 MHz, 295.6 K) δ 171.4 (quaternary C=O, C₂₀), 164.9 (quaternary C, C₂₁), 156.9 (quaternary C-Cl, C₂₂ and C₂₅), 141.7 (aromatic quaternary C, C₁₁ or C₁₈), 132.3 (quaternary C, C₁₁ or C₁₈), 130.6 (aniline CH, C₁₃ or C₁₅), 130.2 (aromatic CH, C₂₃ or C₂₄), 129.0 (aromatic CH, C₂₆), 127.0 (aniline CH, C₁₃ or C₁₅), 125.8 (aniline CH, C₁₆ and C₁₆), 125.6 (aniline CH, C₁₄), 123.2 (aromatic CH, C₂₃ or C₂₄), 100.7 (quaternary C, C₂ or C₅), 98.5 (acnac CH, C₁₉), 97.2 (quaternary C, C₂ or C₅), 87.0 (*p*-cymene CH, C_{3,4,6,7}), 83.7 (*p*-cymene CH, C_{3,4,6,7}), 83.5 (*p*-cymene CH, C_{3,4,6,7}), 80.4 (*p*-cymene CH, C_{3,4,6,7}), 30.3 (*p*-cymene CH, C₈), 24.3 (acnac CH₃, C₁₇), 23.5 (*p*-cymene CH₃, C₉ or C₁₀), 21.4 (*p*-cymene CH₃, C₉ or C₁₀), 18.6 (*p*-cymene CH₃, C₁) **Analysis Calculated:** C 54.22, H 4.55, N 2.43, Cl 18.47% **Analysis Found:** C 53.95, H 4.50, N 2.35, Cl 18.70% **ES MS (+):** *m/z* 540.05 [M⁺]-Cl

9.6.7 Preparation of C₂₆H₂₇BrClRu (7)

3'-Bromo- β -ketoiminate (**L19**) (0.24 g, 0.759 mmol) was dissolved in dichloromethane (30 mL) and whilst stirring triethylamine (0.11 mL, 0.759 mmol) and [*p*-cymRuCl₂]₂ (0.23 g, 0.380 mmol) were added. The mixture was stirred for 16 hours at room temperature, and then the solvent removed under reduced pressure. The crude product was recrystallised from methanol (10 mL) and stored at 4°C for 2 days, yielding a red crystalline solid of **7**, which was further washed with THF (3 x 5mL) (0.31 g, 0.539 mmol, 71%).



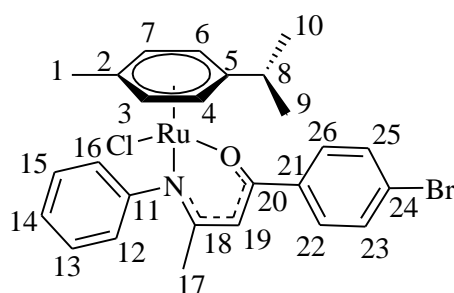
¹H NMR (CDCl₃, 500.23 MHz, 300.0 K)

δ 8.00 (br. t, 1H, H₂₂, ⁴J (¹H-¹H) = 1.6 Hz), 7.76-7.73 (br. d, 2H, H₁₂ and H₁₆, ³J (¹H-¹H) = 8.0 Hz), 7.48 (br. d, 1H, H₂₄, ³J (¹H-¹H) = 7.6 Hz), 7.43 (br. t, 2H, H₁₃ and H₁₅, ³J (¹H-¹H) = 7.5 Hz), 7.24 (br. t, 1H, ³J (¹H-¹H) = 7.6 Hz), 7.20 (t, 1H,

³J (¹H-¹H) = 7.9 Hz), 7.09 (d, 1H, H₂₅, ³J (¹H-¹H) = 6.4 Hz), 5.38 (s, 1H, H₁₉), 5.35 (br. d, 1H, H_{3,4,6,7}, ³J (¹H-¹H) = 6.4 Hz), 5.17 (br. d, 1H, H_{3,4,6,7}, ³J (¹H-¹H) = 6.0 Hz), 5.07 (br. d, 1H, *p*-cymene $\underline{\text{C}}\text{H}$, H_{3,4,6,7}, ³J (¹H-¹H) = 5.6 Hz), 3.69 (br. d, 1H, H_{3,4,6,7}, ³J (¹H-¹H) = 5.6 Hz), 2.67 (br. sept, 1H, H₈), 2.03 (s, 3H, H₁), 1.79 (s, 3H, H₁₇), 1.22 (d, 3H, H₉ or H₁₀, ³J (¹H-¹H) = 7.1 Hz), 1.20 (d, 3H, $\underline{\text{C}}\text{H}_3$, H₉ or H₁₀, ³J (¹H-¹H) = 7.1 Hz) ¹³C{¹H} NMR (CDCl₃, 125.9 MHz, 301.2 K) δ 169.9 (quaternary $\underline{\text{C}}\text{-O}$, C₂₀), 165.1 (quaternary $\underline{\text{C}}$, C₂₁), 157.1 (quaternary $\underline{\text{C}}\text{-Br}$, C₂₃), 141.7 (quaternary C, C₁₁ or C₁₈), 132.1 (aromatic $\underline{\text{C}}\text{H}$, C₂₄), 130.0 (aromatic $\underline{\text{C}}\text{H}$, C₂₂ and C₂₆), 129.7 (aniline $\underline{\text{C}}\text{H}$, C₁₃ or C₁₅), 129.3 (aniline $\underline{\text{C}}\text{H}$, C₁₄), 127.8 (aniline $\underline{\text{C}}\text{H}$, C₁₃ or C₁₅), 125.4 (aniline $\underline{\text{C}}\text{H}$, C₁₂ or C₁₆), 125.4 (aniline $\underline{\text{C}}\text{H}$, C₁₂ or C₁₆), 123.3 (aromatic $\underline{\text{C}}\text{H}$, C₂₅), 122.2 (quaternary C, C₂ or C₅), 101.0 (quaternary C, C₂ or C₅), 94.8 (acnac $\underline{\text{C}}\text{H}$, C₁₉), 87.1 (*p*-cymene $\underline{\text{C}}\text{H}$, C_{3,4,6,7}), 84.6 (*p*-cymene $\underline{\text{C}}\text{H}$, C_{3,4,6,7}), 84.4 (*p*-cymene $\underline{\text{C}}\text{H}$, C_{3,4,6,7}), 79.4 (*p*-cymene $\underline{\text{C}}\text{H}$, C_{3,4,6,7}), 30.5 (*p*-cymene $\underline{\text{C}}\text{H}$, C₈), 24.7 (acnac $\underline{\text{C}}\text{H}_3$, C₁₇), 23.3 (*p*-cymene $\underline{\text{C}}\text{H}_3$, C₉ or C₁₀), 21.0 (*p*-cymene $\underline{\text{C}}\text{H}_3$, C₉ or C₁₀), 18.4 (*p*-cymene $\underline{\text{C}}\text{H}_3$, C₁) **Analysis Calculated:** C 53.30, H 4.64, N 2.39% **Analysis Found:** C 52.90, H 4.60, N 2.35% **ES MS (+):** *m/z* 522.03 [M⁺]-Cl (⁷⁹Br)

9.6.8 Preparation of C₂₆H₂₇BrClNORu (8)

4'-Bromo- β -ketoiminate (0.15 g, 0.490 mmol) was dissolved in dichloromethane (30 mL) and whilst stirring triethylamine (0.07 mL, 0.490 mmol) and [*p*-cymRuCl₂]₂ (0.15 g, 0.245 mmol) were added. The mixture was stirred for 16 hours at room temperature, and then the solvent removed under reduced pressure. The crude product was recrystallised from methanol (10 mL) and stored at 4°C. for 2 days, yielding a red crystalline solid of **8**, which was further washed with THF (3 x 10 mL) (0.19 g, 0.324 mmol, 66%).

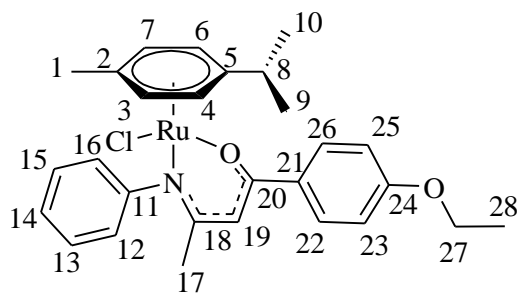


¹H NMR (CDCl₃, 300 MHz, 300 K) δ 7.76-7.70(m, 3H, H₂₂, H₂₆ and H₁₃ or H₁₅), 7.49-7.44 (m, 3H, H₂₃, H₂₅ and H₁₃ or H₁₅), 7.42 (br. d, 1H, H₁₂ or H₁₆, ³J (¹H-¹H)= 7.6 Hz), 7.23 (a. br. t, 1H, H₁₂ or H₁₆, ³J (¹H-¹H)= 7.4 Hz), 7.09 (br. d, 1H, H₁₄, ³J (¹H-¹H)= 6.4 Hz), 5.39 (s, 1H,

H₁₉), 5.35 (br. d, 1H, H_{3,4,6,7}, ³J (¹H-¹H) = 6.2 Hz), 5.16 (br. d, 1H, H_{3,4,6,7}, ³J (¹H-¹H) = 6.2 Hz), 5.07 (br. d, 1H, H_{3,4,6,7}, ³J (¹H-¹H) = 5.3 Hz), 3.68 (br. d, 1H, H_{3,4,6,7}, ³J (¹H-¹H) = 5.7 Hz), 2.66 (br. sept, 1H, H₈, ³J (¹H-¹H) = 6.9 Hz), 2.02 (s, 3H, H₁), 1.79 (s, 3H, H₁₇), 1.20 (a. t, 6H, H₉ and H₁₀, ³J (¹H-¹H) = 6.3 Hz) ¹³C{¹H} NMR (CDCl₃, 75 MHz, 300 K) δ 164.9 (quaternary C-O, C₂₀), 157.2 (quaternary C, C₂₁), 138.7(quaternary C-Br, C₂₄), 135.2 (quaternary C, C₁₁ or C₁₈), 130.9 (aromatic CH, C₂₃ and C₂₅), 129.6 (aniline CH, C₁₃ or C₁₅), 128.5 (aromatic CH, C₂₂ and C₂₆), 127.8 (aniline CH, C₁₂ or C₁₆), 126.0 (aniline CH, C₁₃ or C₁₅), 125.5 (aniline CH, C₁₂ or C₁₆), 123.3 (aniline CH, C₁₄), 100.9 (quaternary C, C₂ or C₅), 96.2 (quaternary C, C₂ or C₅), 94.4 (acnac CH, C₁₉), 87.1 (*p*-cymene CH, C_{3,4,6,7}), 84.6 (*p*-cymene CH, C_{3,4,6,7}), 84.5 (*p*-cymene CH, C_{3,4,6,7}), 79.4 (*p*-cymene CH, C_{3,4,6,7}), 30.5 (*p*-cymene CH, C₈), 24.7 (acnac CH₃, C₁₇), 23.3 (*p*-cymene CH₃, C₉ or C₁₀), 20.9 (*p*-cymene CH₃, C₉ or C₁₀), 18.4 (*p*-cymene CH₃, C₁) **Analysis Calculated:** C 53.30, H 4.64, N 2.39% **Analysis Found:** C 53.20, H 4.65, N 2.30% **ES MS (+):** *m/z* 552.03 [M⁺]-Cl (⁷⁹Br)

9.6.9 Preparation of C₂₆H₂₇ClINORu (9)

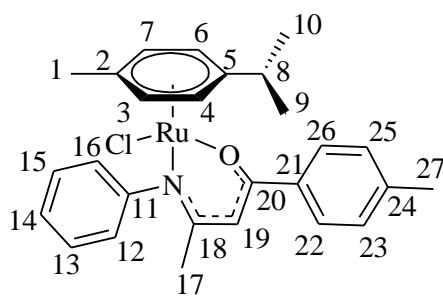
4'-Iodo- β -ketoiminate (**L20**) (0.13 g, 0.405 mmol) was dissolved in dichloromethane (30 mL) and whilst stirring triethylamine (0.06 mL, 0.405 mmol) and [*p*-cymRuCl₂]₂ (0.13 g, 0.205 mmol) were added. The mixture was stirred for



^1H NMR (CDCl_3 , 500.57 MHz, 300.7 K) δ 7.82 (br. d, 2H, H_{22} and H_{26} , $^3J(^1\text{H}-^1\text{H}) = 8.7$ Hz), 7.76 (br. d, 1H, H_{14} , $^3J(^1\text{H}-^1\text{H}) = 8.2$ Hz), 7.42 (br. t, 2H, H_{13} and H_{15} , $^3J(^1\text{H}-^1\text{H}) = 7.6$ Hz), 7.25-7.20 (m, 1H, H_{12} or H_{16}), 7.10 (br. d, 1H, H_{12} or H_{16} , $^3J(^1\text{H}-^1\text{H}) = 7.4$ Hz), 6.84 (br. d, 2H, H_{23} and H_{25} , $^3J(^1\text{H}-^1\text{H}) = 8.7$ Hz), 5.39 (s, 1H, H_{19}), 5.34 (br. d, 1H, $\text{H}_{3,4,6,7}$, $^3J(^1\text{H}-^1\text{H}) = 5.0$ Hz), 5.16 (br. d, 1H, $\text{H}_{3,4,6,7}$, $^3J(^1\text{H}-^1\text{H}) = 6.0$ Hz), 5.05 (br. d, 1H, $\text{H}_{3,4,6,7}$, $^3J(^1\text{H}-^1\text{H}) = 5.0$ Hz), 4.07 (q, 2H, H_{27} , $^3J(^1\text{H}-^1\text{H}) = 6.9$ Hz), 3.69 (br. d, 1H, $\text{H}_{3,4,6,7}$, $^3J(^1\text{H}-^1\text{H}) = 5.0$ Hz), 2.68 (br. sept, 1H, H_8 , $^3J(^1\text{H}-^1\text{H}) = 7.4$ Hz), 2.03 (s, 3H, H_1), 1.78 (s, 3H, H_{17}), 1.43 (t, 3H, H_{28} , $^3J(^1\text{H}-^1\text{H}) = 6.9$ Hz), 1.24-1.16 (br. t, 6H, H_9 and H_{10} , $^3J(^1\text{H}-^1\text{H}) = 6.9$ Hz) **$^{13}\text{C}\{^1\text{H}\}$ NMR** (CDCl_3 , 125.5 MHz, 300.7 K) δ 171.4 (quaternary $\text{C}-\text{O}$, C_{20}), 164.3 (quaternary C , C_{21}), 160.2 (quaternary $\text{C}-\text{O}$, C_{24}), 157.4 (quaternary C , C_{11} or C_{18}), 131. (quaternary C , C_{11} or C_{18}), 128.5 (aromatic CH , C_{22} and C_{26}), 127.7 (aniline CH , C_{13} and C_{15}), 126.3 (aniline CH , C_{14}), 125.3 (aniline CH , C_{12} or C_{16}), 123.7 (aniline CH , C_{12} or C_{16}), 113.6 (aromatic CH , C_{23} and C_{25}), 100.7 (quaternary C , C_2 or C_5), 96.1 (quaternary C , C_2 or C_5), 93.5 (acnac CH , C_{19}), 87.1 (*p*-cymene CH , $\text{C}_{3,4,6,7}$), 84.6 (*p*-cymene CH , $\text{C}_{3,4,6,7}$), 84.4 (*p*-cymene CH , $\text{C}_{3,4,6,7}$), 79.4 (*p*-cymene CH , $\text{C}_{3,4,6,7}$), 63.4 (ethoxy CH_2 , C_{27}), 30.5 (*p*-cymene CH , C_8), 24.7 (acnac CH_3 , C_{17}), 23.4 (*p*-cymene CH_3 , C_9 or C_{10}), 21.0 (*p*-cymene CH_3 , C_9 or C_{10}), 18.4 (*p*-cymene CH_3 , C_1), 14.8 (ethoxy CH_3 , C_{28}) **Analysis Calculated:** C 61.03, H 5.85, N 2.54, Cl 6.43% **Analysis Found:** C 59.65, H 5.85, N 2.55, Cl 6.43% **ES MS (+):** m/z 516.15 [M^+]-Cl

2.1.1 Preparation of $\text{C}_{27}\text{H}_{30}\text{ClNORu}$ (**11**)

4²-Methyl- β -ketoiminate (**L11**) (0.05 g, 0.187 mmol) was dissolved in dichloromethane (30 mL) and whilst stirring triethylamine (0.03 mL, 0.187 mmol) and [*p*-cymRuCl₂]₂ (0.06 g, 0.094 mmol) were added. The mixture was stirred for 16 hours at room temperature, and then the solvent removed under reduced pressure. The crude product was recrystallised from methanol (10 mL) and stored at 4°C for 2 days, yielding red crystals of **11** (0.06 g, 0.115 mmol, 62%)



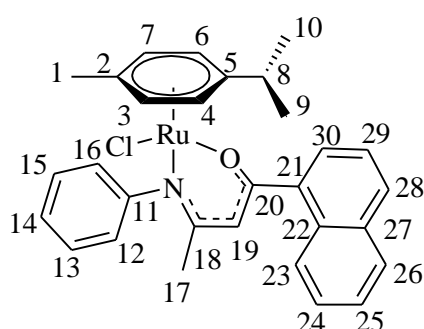
¹H NMR (CDCl₃, 300 MHz, 300 K) δ 7.76 (br. d, 2H, H₂₂ and H₂₆, ³J (¹H-¹H)= 8.3 Hz), 7.42 (br. t, 2H, H₁₃ and H₁₅, ³J (¹H-¹H)= 7.7 Hz), 7.25-7.20 (m, 2H, H₁₂ or H₁₆), 7.14 (br. d, 2H, H₂₃ or H₂₅, ³J (¹H-¹H)= 7.9 Hz), 7.09 (br. d, 1H, H₂₄, ³J (¹H-¹H)= 7.2 Hz), 5.42

(s, 1H, H₁₉), 5.35 (br. d, 1H, H_{3,4,6,7}, ³J (¹H-¹H) = 6.0 Hz), 5.17 (br. d, 1H, H_{3,4,6,7}, ³J (¹H-¹H) = 6.0 Hz), 5.06 (br. d, 1H, H_{3,4,6,7}, ³J (¹H-¹H) = 5.7 Hz), 3.69 (br. d, 1H, H_{3,4,6,7}, ³J (¹H-¹H) = 5.7 Hz), 2.68 (br. sept, 1H, H₈, ³J (¹H-¹H)= 6.9 Hz), 2.37 (s, 3H, methyl H₂₇), 2.03 (s, 3H, H₁), 1.79 (s, 3H, H₁₇), 1.24-1.16 (m, 6H, H₉ and H₁₀)

¹³C{¹H} NMR (CDCl₃, 75 MHz, 300 K) δ 171.7 (quaternary C-O, C₂₀), 164.5 (quaternary C, C₂₁), 157.4 (quaternary C, C₁₈), 139.4 (quaternary C, C₁₁), 136.8 (quaternary C, C₂₄), 128.5 (aromatic CH, C₂₃ and C₂₅), 127.6 (aniline CH, C₁₃ and C₁₅), 126.9 (aromatic CH, C₂₂ and C₂₆), 125.3 (aniline CH, C₁₂ or C₁₆), 123.5 (aniline CH, C₁₄), 100.7 (quaternary C, C₂ or C₅), 96.2 (quaternary C, C₂ or C₅), 94.0 (acnac CH, C₁₉), 87.2 (*p*-cymene CH, C_{3,4,6,7}), 84.6 (*p*-cymene CH, C_{3,4,6,7}), 84.4 (*p*-cymene CH, C_{3,4,6,7}), 79.4 (*p*-cymene CH, C_{3,4,6,7}), 30.4 (*p*-cymene CH, C₈), 24.7 (acnac CH₃, C₁₇), 23.4 (*p*-cymene CH₃, C₉ or C₁₀), 21.4 (methyl CH₃, C₂₇), 20.9 (*p*-cymene CH₃, C₉ or C₁₀), 18.4 (*p*-cymene CH₃, C₁) **Analysis Calculated:** C 62.24, H 5.80, N 2.69, Cl 6.80% **Analysis Found:** C 62.10, H 5.85, N 2.65, Cl 6.85% **ES MS (+):** *m/z* 486.14 [M⁺]-Cl

9.6.11 Preparation of C₃₀H₃₀ClNORu (12)

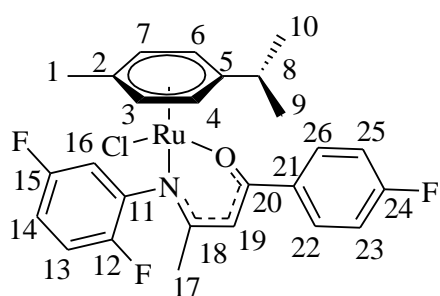
3'-Nathyl-β-ketoiminate (**L28**) (0.08 g, 0.281 mmol) was dissolved in dichloromethane (30 mL) and whilst stirring triethylamine (0.04 mL, 0.281 mmol) and [*p*-cymRuCl₂]₂ (0.09 g, 0.141 mmol) were added. The mixture was stirred for 16 hours at room temperature, and then the solvent removed under reduced pressure. The crude product was recrystallised from methanol (10 mL) and stored at 4°C for 2 days, yielding red crystals of **12** (0.10 g, 0.172 mmol, 61%)



^1H NMR (CDCl_3 , 300 MHz, 300 K)
 δ 7.85–7.78 (m, 3H, aromatic $\underline{\text{CH}}$), 7.53-7.36 (m, 9H, aromatic $\underline{\text{CH}}$), 5.60 (s, 1H, H_{19}), 5.56 (br. d, 1H, $\text{H}_{3,4,6,7}$, 3J ($^1\text{H}-^1\text{H}$) = 6.2 Hz), 5.49 (br. d, 1H, $\text{H}_{3,4,6,7}$, 3J ($^1\text{H}-^1\text{H}$) = 5.5 Hz), 5.27 (br. d, 2H, $\text{H}_{3,4,6,7}$, 3J ($^1\text{H}-^1\text{H}$) = 5.7 Hz), 3.00-2.90 (m, 1H, H_8), 2.13 (s, 3H, H_1), 1.57 (s, 3H, H_{17}), 1.35 (dd, 6H, H_9 and H_{10} , 3J ($^1\text{H}-^1\text{H}$) = 6.9 Hz and 3J ($^1\text{H}-^1\text{H}$) = 3.9Hz) **$^{13}\text{C}\{^1\text{H}\}$ NMR** (CDCl_3 , 75 MHz, 300 K)
 δ 162.4 (quaternary $\underline{\text{C}}-\text{O}$, C_{20}), 154.3 (quaternary $\underline{\text{C}}$, C_{21}), 148.3 (quaternary $\underline{\text{C}}$, C_{11} or C_{18}), 133.7 (quaternary $\underline{\text{C}}$, C_{11} or C_{18}), 126.7 (quaternary $\underline{\text{C}}$, C_{22} or C_{27}), 125.4 (quaternary $\underline{\text{C}}$, C_{22} or C_{27}), 129.8 (aromatic $\underline{\text{CH}}$), 127.8 (aromatic $\underline{\text{CH}}$), 126.4 (aromatic $\underline{\text{CH}}$), 126.0 (aromatic $\underline{\text{CH}}$), 125.0 (aromatic $\underline{\text{CH}}$), 124.6 (aromatic $\underline{\text{CH}}$), 100.8 (quaternary $\underline{\text{C}}$, C_2 or C_5), 99.8 (acnac $\underline{\text{CH}}$, C_{19}), 97.5 (quaternary $\underline{\text{C}}$, C_2 or C_5), 84.3 (*p*-cymene $\underline{\text{CH}}$, $\text{C}_{3,4,6,7}$), 82.5 (*p*-cymene $\underline{\text{CH}}$, $\text{C}_{3,4,6,7}$), 79.1 (*p*-cymene $\underline{\text{CH}}$, $\text{C}_{3,4,6,7}$), 79.0 (*p*-cymene $\underline{\text{CH}}$, $\text{C}_{3,4,6,7}$), 30.7 (*p*-cymene $\underline{\text{CH}}$, C_8), 27.9 (acnac $\underline{\text{CH}}_3$, C_{17}), 22.4 (*p*-cymene $\underline{\text{CH}}_3$, C_9 or C_{10}), 22.3 (*p*-cymene $\underline{\text{CH}}_3$, C_9 or C_{10}), 17.9 (*p*-cymene $\underline{\text{CH}}_3$, C_1) **Analysis Calculated:** C 64.68, H 5.43, N 2.51, Cl 6.36% **Analysis Found:** C 61.70, H 5.35, N 1.55, Cl 7.30% **ES MS (+):** m/z 522.1 [M^+]-Cl

9.6.12 Preparation of $\text{C}_{30}\text{H}_{30}\text{ClNORu}$ (**13**)

4'-Fluoro-2,4-difluoroaniline- β -ketoiminate (**L29**) (0.14 g, 0.512 mmol) was dissolved in dichloromethane (30 mL) and whilst stirring triethylamine (0.07 mL, 0.512 mmol) and [*p*-cymRuCl₂]₂ (0.16 g, 0.256 mmol) were added. The mixture was stirred for 16 hours at room temperature, and then the solvent removed under reduced pressure. The crude product was recrystallised from methanol (10 mL) and stored at 4°C for 2 days, yielding red crystals of **13**, which were further washed with petrol (40-60°) (3 x 5 mL) (0.18 g, 0.317 mmol, 62%).



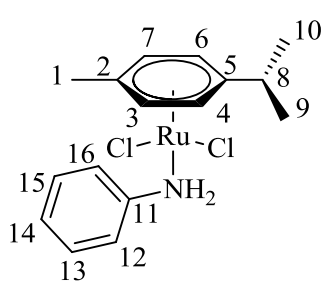
^1H NMR (CDCl_3 , 300.13 MHz, 300.0 K)
 δ 7.88-7.81 (m, 2H, H_{22} and H_{26}), 7.65 (ddd, 1H, H_{16} , 3J ($^1\text{H}-^{19}\text{F}$) = 9.3 Hz, 4J ($^1\text{H}-^{19}\text{F}$) = 6.2 Hz and 4J ($^1\text{H}-^1\text{H}$) = 3.2 Hz), 7.18 (td, 1H, H_{13} , 3J ($^1\text{H}-^{19}\text{F}$) = 9.1 Hz and 3J ($^1\text{H}-^1\text{H}$) = 4.8 Hz), 7.06-6.97 (m, 2H, H_{23} and H_{25}), 6.93 (ddt, 1H,

H_{14} , ${}^3J(^1H-^{19}F) = 9.1$ Hz, ${}^3J(^1H-^1H) = 7.2$ Hz and ${}^4J(^1H-^{19}F) = 3.5$ Hz), 5.43 (s, 1H, H_{19}), 5.41 (br. d, 1H, $H_{3,4,6,7}$, ${}^3J(^1H-^1H) = 5.7$ Hz), 5.24 (br. d, 1H, $H_{3,4,6,7}$, ${}^3J(^1H-^1H) = 5.7$ Hz), 5.18 (br. d, 1H, $H_{3,4,6,7}$, ${}^3J(^1H-^1H) = 6.2$ Hz), 3.86 (br. d, 1H, $H_{3,4,6,7}$, ${}^3J(^1H-^1H) = 5.5$ Hz), 2.65 (br. sept, 1H, H_8 , ${}^3J(^1H-^1H) = 7.0$ Hz), 2.05 (s, 3H, H_1), 1.82 (br. d, 3H, H_{17} , ${}^5J(^1H-^{19}F) = 0.8$ Hz), 1.18 (dd (vt), 6H, H_9 and H_{10} , ${}^3J(^1H-^1H) = 7.3$ Hz) **$^{13}C\{^1H\}$ NMR** ($CDCl_3$, 75.5 MHz, 300.1 K) δ 166.1 (quaternary $\underline{C-O}$, C_{20}), 163.8 (d, quaternary aromatic $\underline{C-F}$, C_{24} , ${}^1J(^{13}C-^{19}F) = 247.2$ Hz), 161.4 (quaternary \underline{C} , C_{21}), 155.0 (d, quaternary aniline $\underline{C-F}$, C_{12} or C_{15} , ${}^1J(^{13}C-^{19}F) = 213.9$ Hz), 152.6 (d, quaternary aniline $\underline{C-F}$, C_{12} or C_{15} , ${}^1J(^{13}C-^{19}F) = 225.0$ Hz), 135.4 (quaternary C, C_{18}), 131.3 (d, quaternary aromatic C, C_{11} , ${}^2J(^{13}C-^{19}F) = 119.9$ Hz) 128.9 (aromatic \underline{CH} , C_{22} and C_{26} , ${}^3J(^{13}C-^{19}F) = 8.7$ Hz), 115.8 (d, aniline \underline{CH} , C_{13} , C_{14} or C_{16} , ${}^2J(^{13}C-^{19}F) = 23.5$ Hz), 115.6 (d, aniline \underline{CH} , C_{13} , C_{14} or C_{16} , ${}^2J(^{13}C-^{19}F) = 23.5$ Hz), 114.7 (aromatic \underline{CH} , C_{23} and C_{25} , ${}^2J(^{13}C-^{19}F) = 22.3$ Hz), 113.3 (d, aniline \underline{CH} , C_{13} , C_{14} or C_{16} , ${}^2J(^{13}C-^{19}F) = 16.1$ Hz), 101.1 (quaternary C, C_2 or C_5), 96.1 (quaternary C, C_2 or C_5), 94.2 (acnac \underline{CH} , C_{19}), 86.9 (*p*-cymene \underline{CH} , $C_{3,4,6,7}$), 84.9 (*p*-cymene \underline{CH} , $C_{3,4,6,7}$), 84.3 (*p*-cymene \underline{CH} , $C_{3,4,6,7}$), 78.5 (*p*-cymene \underline{CH} , $C_{3,4,6,7}$), 30.6 (*p*-cymene \underline{CH} , C_8), 23.9 (*p*-cymene \underline{CH}_3 , C_9 or C_{10}), 23.2 (*p*-cymene \underline{CH}_3 , C_9 or C_{10}), 20.7 (acnac \underline{CH}_3 , C_{17}), 18.3 (*p*-cymene \underline{CH}_3 , C_1) **Analysis Calculated:** C 55.66, H 4.49, N 2.50% **Analysis Found:** C 55.45, H 4.50, N 2.45% **ES MS (+):** m/z 526.09 [M^+]-Cl

9.7 Ruthenium and Iridium Adaptations

9.7.1 Preparation of $RuC_{16}H_{21}Cl_2NO$ (**14**)

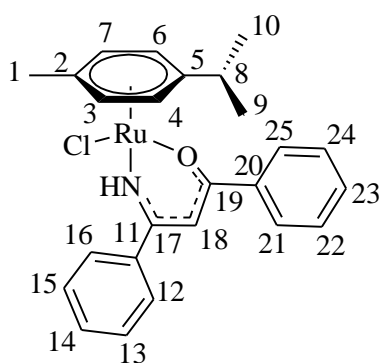
Aniline (0.03 mL, 0.355 mmol) was added to dichloromethane (30 mL) and whilst stirring Et_3N (0.05 mL, 0.356 mmol) and [*p*-cym $RuCl_2$] $_2$ (0.11g, 0.180 mmol) were added. The mixture was stirred for 16 hours and then the solvent removed under reduced pressure. The crude product was recrystallised from methanol (10 mL) and stored at 4°C for 3 days, yielding red crystals of **14**. These were filtered and excess precipitate washed with benzene (10 mL) (0.08 g, 0.210 mmol, 59%). This complex has previously been prepared,¹¹ although the X-ray crystal structure has been reported in Chapter 5, 1H NMR and microanalysis have been reported here to prove synthesis.



¹H NMR (CDCl₃, 500 MHz, 300.0 K) δ 7.41 (br. t, 2H, H₁₃ and H₁₅, ³*J* (¹H-¹H) = 7.3 Hz), 7.31 (br. d, 2H, H₁₂ and H₁₆, ³*J* (¹H-¹H) = 7.6 Hz), 7.26-7.23 (m, 1H, H₄), 5.03 (br. d, 2H, H₃ and H₇, ³*J* (¹H-¹H) = 5.8 Hz), 4.89 (br. d, 2H, H₄ and H₆, ³*J* (¹H-¹H) = 6.1 Hz), 4.75 (br. s, 2H, NH₂), 2.90 (br. sept, 1H, H₈, ³*J* (¹H-¹H) = 6.7 Hz), 2.16 (s, 3H, H₁), 1.26 (br. d, 6H, H₉ and H₁₀, ³*J* (¹H-¹H) = 7.0 Hz) **Analysis Calculated:** C 55.35, H 5.70, N 2.93, Cl 14.37% **Analysis Found:** C 54.85, H 5.50, N 3.10, Cl 13.00%

9.7.2 Preparation of RuC₂₅H₂₅ClNO (15)

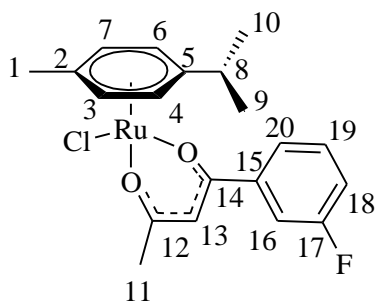
Diphenyl-β-ketoiminate (0.08 g, 0.360 mmol) was added to dichloromethane (30 mL), and whilst stirring Et₃N (0.05 mL, 0.360 mmol) and [*p*-cymRuCl₂]₂ (0.11g, 0.180 mmol) were added. The mixture was stirred for 16 hours and then the solvent removed until reduced pressure. The crude product was recrystallised from methanol (10 mL) and stored at 4°C and after a period of several days yielded red crystals of **15** (0.08g, 0.211 mmol).



¹H NMR (CDCl₃, 300 MHz, 300.0 K) δ 7.90-7.85 (m, 2H, H₁₂₋₁₆ or H₂₁₋₂₅), 7.61-7.56 (m, 2H, H₁₂₋₁₆ or H₂₁₋₂₅), 7.45-7.30 (m, 2H, H₁₂₋₁₆ or H₂₁₋₂₅), 5.72 (d, 1H, NH, ⁴*J* (¹H-¹H) = 2.3 Hz), 5.45 (br. s, 2H, H_{3,4,6,7}), 5.21 (m, 2H, H_{3,4,6,7}), 2.85 (br. sept, 1H, H₈, ³*J* (¹H-¹H) = 7.0 Hz), 2.30 (s, 3H, H₁), 1.32 (br. d, 6H, H₉ and H₁₀, ³*J* (¹H-¹H) = 6.8 Hz) **¹³C{¹H} NMR** (CDCl₃, 75 MHz, 300.0 K) δ 210.3 (quaternary C-O, C₁₉), 206.4 (quaternary C-O, C₂₀), 174.5 (quaternary C, C₁₇), 159.3 (quaternary C, C₁₁), 129.7 (aromatic CH, C₁₂₋₁₆ or C₂₁₋₂₅), 128.7 (aromatic CH, C₁₂₋₁₆ or C₂₁₋₂₅), 127.8 (aromatic CH, C₁₂₋₁₆ or C₂₁₋₂₅), 126.9 (aromatic CH, C₁₂₋₁₆ or C₂₁₋₂₅), 126.2 (aromatic CH, C₁₂₋₁₆ or C₂₁₋₂₅), 100.9 (quaternary *p*-cymene C, C₂ or C₅), 99.8 (quaternary *p*-cymene C, C₂ or C₅), 99.3 (acnac CH, C₁₈), 91.8 (*p*-cymene CH, C_{3,4,6,7}), 84.9 (*p*-cymene CH, C_{3,4,6,7}), 30.7 (*p*-cymene CH, C₈), 25.2 (*p*-cymene CH₃, C₉ or C₁₀), 18.3 (*p*-cymene CH₃, C₁) **Analysis Calculated:** C 60.91, H 5.32, N 2.84, Cl 7.19% **Analysis Found:** C 60.90, H 5.30, N 3.10, Cl 7.40% **ES MS (+):** *m/z* 456.33 [M⁺]-Cl

9.7.3 Preparation of RuC₂₀H₂₂ClFO₂ (16)

3'-Fluoro- β -diketonate (0.09 g, 0.49 mmol) dissolved in dichloromethane (30 mL) and whilst stirring triethylamine (0.07 mL, 0.49 mmol) and [*p*-cymRuCl₂]₂ (0.15 g, 0.245 mmol) were added. The mixture was stirred at room temperature for 16 hours, and then the solvent removed under reduced pressure. The crude product was recrystallised from methanol at 4°C for 2 days, yielded red crystals of **16** (0.18 g, 0.401 mmol, 82%).



¹H NMR (CDCl₃, 500.13 MHz, 299.2 K) δ 7.57 (br. d, 1H, H₂₀, ³J (¹H-¹H) = 7.8 Hz), 7.54 (br. dt, 1H, H₁₆, ³J (¹H-¹⁹F) = 9.3 Hz and ⁴J (¹H-¹H) = 2.6 Hz), 7.30 (dt, 1H, H₁₉, ³J (¹H-¹H) = 7.8 Hz and ³J (¹H-¹H) = 5.7 Hz), 7.11 (td, 1H, H₁₈, ³J (¹H-¹H) = 8.3 Hz, ³J (¹H-¹⁹F) = 2.6 Hz and ⁴J (¹H-¹H) = 1.0 Hz), 5.75 (s, 1H, H₁₃), 5.55 (br. d, 1H, H_{3,4,6,7}, ³J (¹H-¹H) = 6.4 Hz), 5.52 (br. d, 1H, H_{3,4,6,7}, ³J (¹H-¹H) = 6.2 Hz), 5.26 (m, 2H, H_{3,4,6,7}), 2.97 (m, 1H, H₈), 2.30 (br. s, 3H, H₁), 2.14 (br. s, 3H, H₁₁), 1.37 (br. d, 6H, H₉ and H₁₀, ³J (¹H-¹H) = 6.7 Hz)

¹³C{¹H} NMR (CDCl₃, 125.8 MHz, 299.2 K) δ 189.2 (quaternary C-O, C₁₂ or C₁₄), 177.9 (quaternary C-O, C₁₂ or C₁₄), 162.6 (d, quaternary C-F, C₁₇, ¹J (¹³C-¹⁹F) = 246.1 Hz), 140.8 (quaternary C, C₁₅), 129.5 (d, aromatic CH, C₁₉, ⁴J (¹³C-¹⁹F) = 8.6 Hz), 122.4 (d, aromatic CH, C₂₀, ⁵J (¹³C-¹⁹F) = 3.2 Hz), 117.6 (d, aromatic CH, C₁₈, ³J (¹³C-¹⁹F) = 21.5 Hz), 114.3 (d, aromatic CH, C₁₆, ³J (¹³C-¹⁹F) = 23.6 Hz), 99.8 (quaternary *p*-cymene C, C₂ or C₅), 97.5 (quaternary *p*-cymene C, C₂ or C₅), 96.1 (acac CH, C₁₃), 83.0 (*p*-cymene CH, C_{3,4,6,7}), 82.6 (*p*-cymene CH, C_{3,4,6,7}), 79.2 (*p*-cymene CH, C_{3,4,6,7}), 30.8 (*p*-cymene CH, C₈), 28.2 (acac CH₃, C₁₁), 22.4 (*p*-cymene CH₃, C₉ or C₁₀), 22.31 (*p*-cymene CH₃, C₉ or C₁₀), 18.03 (*p*-cymene CH₃, C₁)

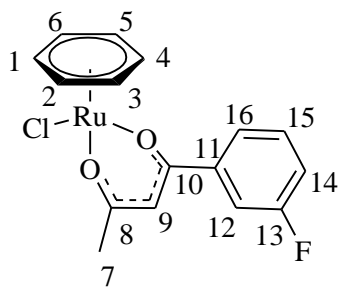
Analysis Calculated: C 53.39, H 4.93% **Analysis Found:** C 53.40, H, 4.90%

ES MS (+): *m/z* 415.07 [M⁺]-Cl

9.7.4 Preparation of C₁₆H₁₄ClFO₂Ru (17)

3'-Fluoro- β -diketonate (0.07 g, 0.383 mmol) dissolved in dichloromethane (30 mL) and whilst stirring triethylamine (0.05 mL, 0.383 mmol) and [*benzene*RuCl₂]₂ (0.10 g, 0.191 mmol) were added. The mixture was stirred at room temperature for 16 hours, and then the solvent removed under reduced pressure. The crude product

was recrystallised from methanol (10 mL) and stored at 4°C for 2 days, yielding red crystals of **17** (0.12 g, 0.288 mmol, 67%).



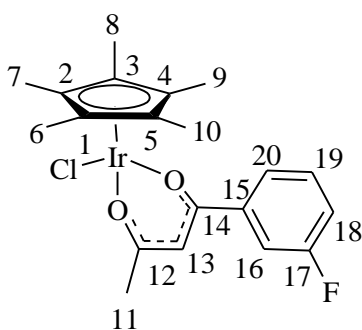
^1H NMR (CDCl_3 , 500 MHz, 300.0 K) δ 7.59 (br. d, 1H, H_{16} , $^3J(^1\text{H}-^1\text{H}) = 7.9$ Hz), 7.56 (m, 1H, H_{12}), 7.30 (br. d, 1H, H_{15} , $^3J(^1\text{H}-^1\text{H}) = 7.8$), 7.11 (m, 1H, H_{14}), 5.81 (s, 6H, C_6H_6), 5.77 (s, 1H, H_9), 2.15 (br. s, 3H, H_7)

$^{13}\text{C}\{^1\text{H}\}$ NMR (CDCl_3 , 75 MHz, 299.2 K) δ 188.3 (quaternary $\text{C}-\text{O}$, C_8 or C_{10}), 180.1 (quaternary $\text{C}-\text{O}$, C_8 or C_{10}), 163.0 (d, quaternary $\text{C}-\text{F}$, C_{13} , $^1J(^{13}\text{C}-^{19}\text{F}) = 245.1$ Hz), 142.2 (quaternary C , C_{11}), 129.6 (aromatic CH , C_{15}), 122.5 (d, aromatic CH , C_{16}), 117.8 (d, aromatic CH , C_{14} , $^3J(^{13}\text{C}-^{19}\text{F}) = 21.0$ Hz), 114.5 (d, aromatic CH , C_{12} , $^3J(^{13}\text{C}-^{19}\text{F}) = 23.9$ Hz), 98.5 (aromatic CH , C_6H_6), 96.5 (acac CH , C_9), 28.3 (acac CH_3 , C_7)

micro-analysis pending, **MS** (+): m/z 359.0 [M^+]-Cl

9.7.5 Preparation of $\text{C}_{20}\text{H}_{23}\text{ClF}\text{O}_2\text{Ir}$ (**19**)

3'-Fluoro- β -diketonate (0.04 g, 0.222 mmol) dissolved in dichloromethane (30 mL) and whilst stirring triethylamine (0.03 mL, 0.200 mmol) and $[\text{Cp}^*\text{IrCl}_2]_2$ (0.08 g, 0.100 mmol) were added. The mixture was stirred at room temperature for 16 hours, and then the solvent removed under reduced pressure. The crude product was recrystallised from methanol (10 mL) and stored at 4°C for several days yielded yellow crystals of **19** (0.07 g, 0.129 mmol, 58%).



^1H NMR (CDCl_3 , 300 MHz, 299.2 K) δ 7.66–7.61 (m, 1H, H_{19}), 7.61–7.54 (m, 1H, H_{20}), 7.35–7.28 (m, 1H, H_{18}), 7.19–7.10 (m, 1H, H_{16}), 5.85 (s, 1H, H_{13}), 2.08 (s, 3H, H_{11}), 1.66 (br. s, 15H, H_{6-10})

$^{13}\text{C}\{^1\text{H}\}$ NMR (CDCl_3 , 75 MHz, 300 K) δ 187.3 (quaternary $\text{C}-\text{O}$, C_{12} or C_{14}), 175.5 (quaternary $\text{C}-\text{O}$, C_{12} or C_{14}), 162.7 (d, quaternary $\text{C}-\text{F}$, C_{17} , $^1J(^{13}\text{C}-^{19}\text{F}) = 243.5$ Hz), 141.1 (quaternary C , C_{15}), 129.6 (d, aromatic CH , C_{19} , $^3J(^{13}\text{C}-^{19}\text{F}) = 8.7$ Hz), 122.6 (d, aromatic CH , C_{20} , $^4J(^{13}\text{C}-^{19}\text{F}) = 2.5$ Hz), 117.5 (d, aromatic CH , C_{18} , $^2J(^{13}\text{C}-^{19}\text{F}) = 21.0$ Hz), 113.9 (d, aromatic CH , C_{16} , $^2J(^{13}\text{C}-^{19}\text{F}) = 23.5$ Hz), 97.3 (acac CH , C_{13}), 83.7 (quaternary C , Cp^* CCH_3 , C_{1-5}), 28.2 (acac CH_3 , C_{11}), 8.7 (Cp^* CCH_3 , C_{6-10})

Analysis Calculated: C 44.31, H 4.28, Cl 6.54% **Analysis Found:** C 44.55, H 4.20, Cl I/m (re-send)% **ES MS** (+): m/z 507.0 [MH^+]-Cl

9.8 Syntheses of Titanium(IV) β -Diketonate Complexes

The following complexes were synthesised following a modification of previously established synthetic route from within the McGowan group.¹²

9.8.1 Preparation of $\text{Ti}_2(\text{C}_{28}\text{H}_{20}\text{N}_2\text{O}_4)(\text{OCH}_3)_6$ (**20**)

L5 (0.30 g, 1.33 mmol) dissolved with stirring in dry THF (20 mL) and added to a stirred solution of $\text{Ti}(\text{O}^i\text{Pr})_4$ (0.20 mL, 0.67 mmol) in dry THF (20 mL). The yellow solution was stirred for 4 hours and then the solvent removed *in vacuo*. The crude yellow product was washed with dry MeOH (20 mL) and filtered; the solution was stored at -20°C and yielded yellow crystals of **20** after a period of several days.

X-ray crystallographic analysis was obtained for complex **20**, but the crystals disintegrated after exposure to air and no further analytical data was obtained. Further synthesis has proven unsuccessful to date.

9.8.2 Preparation of $\text{Ti}(\text{C}_{32}\text{H}_{26}\text{F}_2\text{N}_2\text{O}_2)\text{Cl}_2$ (**21**)

3'-Fluoro- β -ketoiminate (**L12**) (0.66 g, 2.59 mmol) and KH (0.11 g, 2.74 mmol) were dissolved with stirring in dry dichloromethane (20 mL) and added to a stirred solution of TiCl_4 (0.14 mL, 1.29 mmol) in dry dichloromethane (20 mL). The dark red solution was stirred for approximately 16 hours and then the solvent filtered *in vacuo*. The solution was stored at -20°C , yielding yellow crystals of **21** after a period of several days.

X-ray crystallographic analysis was obtained for complex **21**, but the crystals disintegrated after exposure to air and no further analytical data was obtained. Further synthesis has proven unsuccessful to date.

9.8.3 Preparation of $\text{Ti}(\text{C}_{32}\text{H}_{26}\text{Cl}_2\text{N}_2\text{O}_2)\text{Cl}_2$ (**22**)

4'-Chloro- β -ketoiminate (0.13 g, 0.478 mmol) and KH (0.025 g, 0.623 mmol) were dissolved with stirring in dry dichloromethane (20 mL) and added to a stirred solution of TiCl_4 (0.03 mL, 0.239 mmol) in dry dichloromethane (20 mL). The dark red solution was stirred for approximately 16 hours and then the solvent removed *in vacuo*. The suspension was filtered and the solution was stored at -20°C , yielding yellow crystals of **22** after a period of several days.

X-ray crystallographic analysis was obtained for complex **22**, but the crystals disintegrated after exposure to air and no further analytical data was obtained. Further synthesis has proven unsuccessful to date.

9.8.4 Preparation of $\text{Ti}(\text{C}_{32}\text{H}_{26}\text{F}_2\text{N}_2\text{O}_2)\text{Cl}_2$ (**23**)

4-Fluoro- β -ketoiminate (**L13**) (0.39 g, 1.61 mmol) and KH (0.06 g, 1.61 mmol) were dissolved with stirring in dry dichloromethane (20 mL) and added to a stirred solution of TiCl_4 (0.03 mL, 0.239 mmol) in dry dichloromethane (20 mL). The dark red solution was stirred for approximately 16 hours the solution, turning green overnight. The solution was stored at -20°C and had returned to the dark red colour first seen. After a period of several weeks orange crystals of **23** were obtained.

X-ray crystallographic analysis was obtained for complex **23**, but the crystals disintegrated after exposure to air and no further analytical data was obtained. Further synthesis has since proven to be unsuccessful to date.

9.8.5 Preparation of $\text{Ti}(\text{C}_{34}\text{H}_{32}\text{N}_2\text{O}_2)\text{Cl}_2$ (**24**)

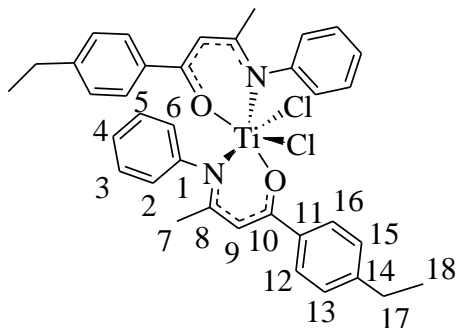
4-Methyl- β -ketoiminate (**L11**) (0.50 g, 1.99 mmol) in dry diethyl ether (20 mL) was stirred and cooled to -78°C , ${}^n\text{BuLi}$ 1.6M in hexane (1.24 mL, 1.99 mmol) was added and the suspension allowed to warm to room temperature. This was then filtered onto a stirred solution of TiCl_4 (0.11 mL, 0.995 mmol) in dry diethyl ether (20 mL) at -78°C . Once added the dark red solution was allowed to warm to room temperature and stirred for approximately 16 hours. The solvent was filtered *in vacuo* and the crude product recrystallised from acetonitrile (20 mL) and stored at -20°C , yielding yellow crystals of **24** after a period of several days.

X-ray crystallographic analysis was obtained for complex **24**, but the crystals disintegrated after exposure to air and no further analytical data was obtained. Further synthesis has proven unsuccessful to date

9.8.6 Preparation of $\text{Ti}(\text{C}_{36}\text{H}_{36}\text{N}_2\text{O}_2)\text{Cl}_2$ (**25**)

4-Methyl- β -ketoiminate (**L19**) (0.54 g, 2.04 mmol) in dry diethyl ether (20 mL) was stirred and cooled to -78°C , ${}^n\text{BuLi}$ 1.6M in hexane (1.27 mL, 2.04 mmol) was added and the suspension allowed to warm to room temperature. This was then filtered onto a stirred solution of TiCl_4 (0.11 mL, 1.02 mmol) in dry diethyl ether (20 mL) at -78°C . Once added the dark red solution was allowed to warm to room

temperature and stirred for approximately 16 hours. The solvent was filtered *in vacuo* and the crude product recrystallised from acetonitrile (20 mL) and stored at -20°C , yielding yellow crystals of **25** after a period of several days (0.71 g, 1.10 mmol, 54%).

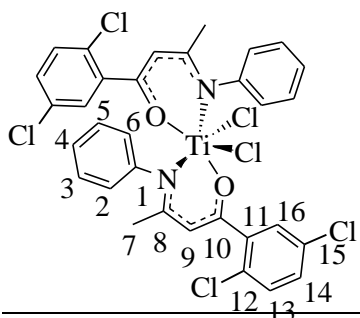


$^1\text{H NMR}$ (CDCl_3 , 500 MHz, 300 K) δ 7.43 (d, 4H, H_{12} and H_{16} , 3J ($^1\text{H}-^1\text{H}$) = 8.3 Hz), 7.37-7.34 (m, 2H, H_2 or H_6), 7.09 (d, 4H, H_{13} and H_{15} , 3J ($^1\text{H}-^1\text{H}$) = 8.3 Hz), 7.05 (dtd, 4H, H_3 and H_5 , 3J ($^1\text{H}-^1\text{H}$) = 7.7 Hz, 4J ($^1\text{H}-^1\text{H}$) = 3.95 (x 2) Hz and 4J ($^1\text{H}-^1\text{H}$) = 2.3 Hz), 6.78 (br. t, 2H, H_4 , 3J ($^1\text{H}-^1\text{H}$) = 7.6 Hz), 6.69-6.66 (m,

2H, H_2 or H_6), 6.08 (s, 2H, H_9), 2.66 (q, 4H, H_{17} , 3J ($^1\text{H}-^1\text{H}$) = 7.5 Hz), 1.83 (br. s, 6H, H_7), 1.24 (t, 6H, H_{18} , 3J ($^1\text{H}-^1\text{H}$) = 7.6 Hz) $^{13}\text{C NMR}$ (CDCl_3 , 75 MHz, 300 K) δ 170.3 (quaternary $\text{C}-\text{O}$, C_{10}), 169.9 (quaternary aromatic C , C_{11}), 151.1 (quaternary aniline C , C_1), 148.1 (quaternary $\text{C}-\text{N}$, C_8), 130.9 (quaternary aromatic C , C_{14}), 128.9 (aromatic CH , C_3 or C_5), 128.0 (aromatic CH , C_3 or C_5), 127.5 (aromatic CH , $\text{C}_{12,13,15}$ and 16), 125.6 (aromatic or aniline CH , $\text{C}_{2,4}$ or 6), 125.4 (aromatic or aniline CH , $\text{C}_{2,4}$ or 6), 121.8 (aniline CH , C_2 or 6), 105.6 (acnac CH , C_9), 28.9 (ethyl CH_2CH_3 , C_{17}), 25.1 (aliphatic CH_3 , C_7), 15.3 (ethyl CH_2CH_3 , C_{18})

9.8.7 Preparation of $\text{Ti}(\text{C}_{32}\text{H}_{24}\text{Cl}_4\text{N}_2\text{O}_2)\text{Cl}_2$ (**26**)

2',5'-Dichloro- β -ketoiminate (**L14**) (0.30 g, 0.979 mmol) in dry diethyl ether (20 mL) was stirred and cooled to -78°C , $n\text{BuLi}$ (0.61 mL, 0.979 mmol) was added and the suspension allowed to warm to room temperature. This was then filtered onto a stirred solution of TiCl_4 (0.05 mL, 0.490 mmol) in dry diethyl ether (20 mL) at -78°C . Once added the red solution was allowed to warm to room temperature and stirred for approximately 16 hours. The solvent was filtered *in vacuo* and the crude product recrystallised from acetonitrile (20 mL) and stored at -20°C , yielding an orange precipitate of **26** (0.40g, 0.548 mmol, 56%).



$^1\text{H NMR}$ (CDCl_3 , 500 MHz, 300 K) δ 7.34 (d, 2H, H_{16} , 4J ($^1\text{H}-^1\text{H}$) = 1.8 Hz), 7.32 (d, 2H, H_2 or H_6 , 3J ($^1\text{H}-^1\text{H}$) = 8.3 Hz), 7.28-7.26 (m, 2H, H_4), 7.25-7.22 (m, 2H, H_{13}), 7.18 (dd, 2H, H_{14} , 3J ($^1\text{H}-^1\text{H}$) = 8.3 Hz and 4J ($^1\text{H}-^1\text{H}$) = 1.8 Hz), 7.09 (td, 2H, H_3 or H_5 , 3J

(^1H - ^1H) = 7.7 Hz and 4J (^1H - ^1H) = 1.2 Hz), 7.00 (br. t, 2H, H₃ or H₅, 3J (^1H - ^1H) = 7.8 Hz), 6.70 (d, 2H, H₂ or H₆, 4J (^1H - ^1H) = 7.8 Hz), 6.38 (s, 2H, H₉), 1.86 (s, 6H, H₇) ^{13}C NMR (CDCl₃, 75 MHz, 300K) δ 171.2 (quaternary $\underline{\text{C}}$ -O, C₁₀), 165.4 (quaternary aromatic $\underline{\text{C}}$, C₁₁), 150.7 (quaternary aniline $\underline{\text{C}}$, C₁), 136.5 (quaternary $\underline{\text{C}}$ -N, C₈), 132.6 (aniline $\underline{\text{C}}\text{H}$, C₂ or C₆), 132.6 (quaternary $\underline{\text{C}}$ -Cl, C₁₂ or C₁₅), 131.3 (quaternary $\underline{\text{C}}$ -Cl, C₁₂ or C₁₅), 130.3 (aromatic $\underline{\text{C}}\text{H}$, C₁₆), 129.0 (aniline $\underline{\text{C}}\text{H}$, C₃ or C₅), 128.5 (aromatic $\underline{\text{C}}\text{H}$, C₁₃), 127.0 (aromatic $\underline{\text{C}}\text{H}$, C₁₄), 125.9 (aniline $\underline{\text{C}}\text{H}$, C₃ or C₅), 125.4 (aniline $\underline{\text{C}}\text{H}$, C₄), 121.6 (aniline $\underline{\text{C}}\text{H}$, C₂ or C₆), 111.4 (acnac $\underline{\text{C}}\text{H}$, C₉), 25.4 (aliphatic $\underline{\text{C}}\text{H}_3$, C₇)

9.9 Normoxic Cytotoxic Evaluation

9.9.1 General

Sterile techniques were used throughout this work. Chemicals were purchased from Sigma Aldrich and used as supplied. MCF-7 cells (human breast adenocarcinoma), HT-29 cells (human colon adenocarcinoma), A2780 cells (human ovarian carcinoma) and A2780cis cells (cisplatin resistant human ovarian carcinoma) were obtained from Dr. Roger Phillips (Reader in Cancer Pharmacology, University of Bradford UK). The stock cultures were grown in either T-25 or T-75 flasks containing RPMI-1640 complete medium (20 mL) and incubated at 37°C with 5.0% CO₂. The complete medium was prepared from RPMI-1640 incomplete medium (500 mL), sodium pyruvate (5 mL, 0.5 mmol), L-glutamine (5 mL, 1.0 mmol) and foetal bovine serum (50 mL). HANKS Balanced Salt Solution (HBSS) was used to wash cells before use, and 0.25% trypsin-EDTA solution was used to detach the cells from the flask. MTT stock solutions (5 mg/ mL) were prepared by dissolving MTT (250 µg) in distilled water (50 mL), then passing through a 0.2 µm sterile filter. RPMI-1640 incomplete medium, RPMI-1640 complete medium, sodium pyruvate, MTT and MTT stock solutions were all stored at 4°C. L-glutamine, foetal bovine serum and 0.25% trypsin-EDTA solution were all stored at -20°C. All chemicals except the MTT stock solution were incubated at 37°C prior to use.

9.9.2 Passaging Cells

Cell monolayer was washed with HANKS Balanced Salt Solution (3 x 10 mL), and then all HBSS was carefully removed. 0.25% trypsin-EDTA solution (5 mL) was added to the flasks and incubated at 37°C for 5 minutes. When the cells became detached from the flask wall, cell medium (10 mL) was added. Cells were split into new flasks and diluted with cell medium; the lids were loosened and placed into the incubator for future use.

9.9.3 Cell Counting

The cells were passaged to the point of suspension, as previously described. 10 µL of the cell suspension was transferred to each side of the glass haemocytometer and cells were counted under the microscope and an average was taken, with units of 10⁴ cells/ mL.

9.9.4 Conducting the 5-Day MTT Assay

After counting the cells, the cell suspension was diluted with RPMI-1640 complete medium to give a concentration of 2×10^4 cells/ mL. 96-well plates were used and 100 μ L of cell medium was added to lane one, to serve as a blank. 100 μ L of the diluted cell suspension was then added to lanes two to twelve, and the plates incubated overnight at 37°C with 5.0% CO₂.

The drugs to be tested were dissolved in DMSO to give concentrations of 25 mM. 40 μ L of this solution was added to 1960 μ L of RPMI-1640 complete media to give a total of 2 mL. This was mixed well and 1 mL taken and added to another 1 mL of RPMI-1640 complete media, further dilutions were carried out to give 10 different concentrations of the drug. 100 μ L of RPMI-1640 cell media was added to lanes 1 and 2 to serve a control and 100% cell respectively. 100 μ L of the least concentrated drug solution was added to lane 3, and subsequent concentrations were added until 100 μ L of the most concentrated drug solution was added to lane 12. The plates were incubated for 5 days at 37°C with 5.0% CO₂.

After 5 days incubation, MTT stock solution was prepared (5 mg/ mL) and 20 μ L added to each 96-well plate and incubated at 37°C in 5.0% CO₂ for a further 3 hours. The medium/MTT was removed *via* pipette and 150 μ L of DMSO added to each well. Solutions were mixed well and the absorbance measured at 540 nm, using a Thermo Scientific Multiskan EX microplate photometer.

9.9.5 Data Analysis

Averages were taken from the eight cells in each lane, and the % cell survival for each concentration was calculated using the following formula:

$$C = \frac{L_n - L_1}{L_2 - L_1} \times 100$$

Where C is the % cell survival for lane n and L_n is the mean absorbance at 540 nm for lane n. IC₅₀ values and standard deviations were calculated from a minimum of three repeats for each drug used.

9.10 Hypoxic Cytotoxic Evaluation

This assay was conducted according to the protocol stated previously for normoxic conditions. However, all the incubations periods, the addition of the drug dilutions and the addition of the MTT solution were carried out inside a Don Whitley Scientific H35 Hypoxystation which was set at 1.0 or 0.1% O₂.

9.11 Hydrophobicity

Firstly, equal volumes of octanol and NaCl saturated water were stirred overnight at room temperature then separated to give octanol-saturated water and water-saturated octanol. Accurate amounts of the complexes were dissolved in water-saturated octanol (25 mL). 2 mL of octanol-saturated water was placed in a centrifuge tube and 2 mL of water-saturated octanol complex samples layered on top. The samples were shaken for 4 hours using a vibrax machine at 1000 gmin⁻¹; a minimum of six repeats were analysed. The layers were separated and the water-saturated octanol layer retained for analysis by UV/*vis* spectroscopy. Using the maximum absorbance of each complex, the average of the six runs was calculated and rearrangement of individual calibration graphs gave the [C]_{org} final. The following equations were used to determine the partition coefficient and hence determining if the compound is predominantly hydrophilic or hydrophobic.

$$\text{Log } p = \frac{[C]_{org}}{[C]_{aq}} \times 100$$
$$[C]_{aq} = \frac{[C]_{org} \text{ final}}{[C]_{org} \text{ initial} - [C]_{org} \text{ final}}$$

9.12 DSB Comet Assay

9.12.1 Preparation of Comet assay slides:

1% normal melting point agarose (500 mg) in PBS (50 mL) was prepared and placed in the microwave for approximately 20 seconds until it had fully dissolved. This was poured into a 50 mL centrifuge tube and the glass slides were dipped into the agarose. The underside of the slide was wiped clean and these were left on the bench overnight to dry.

9.12.2 Reagents

- **Neutral Lysing Solution** (2% sarkosyl, 0.5 M Na₂EDTA, 0.5 mg/ mL proteinase K (pH 8.0))

Sarkosyl (2 g) and Na₂EDTA (18.61 g) were added to distilled water (80 mL) and the pH adjusted to 8.0 with 10M NaOH. Proteinase K (50 mg) was then added and made up to a final volume of 100 mL.

- **Electrophoresis Buffer** (90 mM Tris buffer, 90 mM boric acid, 2 mM Na₂EDTA (pH 8.0))

Tris base (32.707 g), boric acid (16.694 g) and Na₂EDTA (2.233 g) were added to distilled water (2.5 L). The pH was adjusted to 8.0 and the volume made up to 3 L with distilled water.

- **Staining Solution:**

SYBRTMGold solution (molecular probes inc, S-11494) (1 µL) was added to PBS 1(10 mL); this was made on the day of imaging.

- **Imaging and Analysis**

Staining solution (150 µL) was added to each slide and a cover slip placed on top. Excess solution was blotted away and the comets analysed using Comet assay III software. A minimum of 50 different comets were scored and the computer outputs an average on head and tail intensities and tail moments. Images were taken of the comets and the tail moments plotted against concentration of drug sample used.

9.12.3 Sample Preparation:

The cells were washed with PBS, trypsinised and counted (see previous, same as cytotoxicity assay). The cells were diluted with complete medium to a concentration of 1×10^6 cells/ mL, 2 mL of the cell suspension was placed in each well of a 6-well plate. The cells were incubated for 24 hours at 37°C in a 5.0% CO₂ atmosphere. Drug samples were prepared in the range 20-1.25 µM, the medium was removed from the wells, and 2 mL of drug sample added to each well. The plate was then incubated again for 24 hours in the drug solutions, at 37°C in a 5.0% CO₂ atmosphere. The drug samples were removed and added to centrifuge tubes, the wells each washed with PBS (1 mL), which was also placed into the centrifuge tube. The wells were then trypsinised (1 mL) for 5 minutes and then neutralised

with complete medium (1 mL), these were all added to the centrifuge tube and centrifuged at 1500 rpm for 3 minutes. The supernatant was removed and the pellet re-suspended in complete medium containing 10% DMSO. The tubes were wrapped in several sheets of tissue and stored at -80°C until required for the assay.

9.12.4 Conducting the Assay:

- **Preparation of sample slides** (conducted under low light conditions):

0.5% low melting agarose (LMPA) was prepared (250 mg/ 50 mL PBS) and placed in the microwave for approximately 20 seconds, until fully dissolved. This was placed into a water bath set at 37°C and the temperature allowed to equilibrate. The sample eppendorfs from **Section 9.12.3** were defrosted and centrifuged at 16.1 rcf for 20 seconds. The supernatant was removed and the pellet re-suspended in LMPA (150-1000 µL, depending on pellet size). The cell suspension (150 µL) was added to a previously coated glass slide and a cover slip placed over, these were placed on a cool tray and allowed to set (3-5 minutes). Once set the slip was removed and LMPA (150 µL) added to the slide and another slip placed on top. These were again transferred to a cool tray to set. The slip was again removed and all slides placed into a tray where freshly prepared neutral lysing solution was added and the slides incubate for 1 hour at 37°C in dark conditions.

- **Electrophoresis Conditions**

The lysing solution was gently poured off and the slides submerged in electrophoresis buffer for 30 minutes. The buffer was gently poured off and this step repeated two more times. The slides were then placed close together in an electrophoresis chamber and reservoirs were carefully filled with freshly prepared buffer (pH 8.0) and filled until the buffer just covered the slides. The chamber was adjusted to 24 V and the electrophoresis was run for 25 minutes. The slides were transferred to a clean tray and rinsed three times with distilled water and finally with 100% ice cold ethanol. They were then transferred to a slide rack and left to dry overnight before imaging could commence.

- **Imaging and Analysis**

Staining solution (150 mL) was added to each slide and a cover slip placed on top, excess solution was blotted away and the comets analysed using Comet assay III software. A minimum of 50 different comets were scored and the computer outputs

an average on head and tail intensities and tail moments. Images were taken of the comets and the tail moments plotted against concentration of drug sample used.

9.13 SSB and Cross-Linking Comet Assay

9.13.1 Preparation of Comet assay slides:

1% normal melting point agarose (500 mg) in PBS (50 mL) was prepared and placed in the microwave for approximately 20 seconds until it had fully dissolved. This was poured into a 50 mL centrifuge tube and the glass slides were dipped into the agarose. The underside of the slide was wiped clean and these were left on the bench overnight to dry.

9.13.2 Reagents

- **Alkaline Lysing Solution:**

2.5 M NaCl (146.1 g), 100 mM EDTA (37.2 g) and 10 mM Trizma base (1.2 g) were added to distilled water (700 mL). NaOH (8 g) was added and stirred until fully dissolved, once dissolved the pH was adjusted to pH 10.0 and made up to a final volume of 890 mL and stored at 4°C.

- **Final Lysing Solution:**

The previously made lysing solution (178 mL) was added to Triton-X-100 (2 mL) and DMSO (20 ml)

- **Electrophoresis Buffer** (300 mM NaOH/ 1mM EDTA)

10 M NaOH - 200 g/ 500 mL distilled water

200 mM EDTA - 14.89 g/ 200 mL distilled water at pH 10.0

10 M NaOH (90 mL) was added to 200 mM EDTA (15 mL) and made up to a total volume of 3 L using distilled water and adjusted to a pH > 13.0

- **Neutralisation Buffer:**

Tris base (48.5 g) was dissolved in distilled water (800 mL) and adjusted to pH 7.5 using concentrated HCl. This was then made up to 1 L using distilled water and stored at room temperature.

- **Staining Solution:**

The staining was carried out according to that stated previously in **Section 9.12.1**

9.13.3 Sample Preparation:

The samples were prepared following the same steps as the DBS assay, with elimination of the 10% DMSO in the final step.

9.13.4 Conducting the Assay:

- **Preparation of sample slides** (conducted under low light conditions):

0.5% low melting agarose (LMPA) was prepared (250 mg/ 50 mL PBS) and placed in the microwave for approximately 20 seconds, until fully dissolved. This was placed into a water bath set at 37°C and the temperature allowed to equilibrate. The sample eppendorfs were defrosted and centrifuged at 16.1 rcf for 20 seconds. The supernatant was removed and the pellet re-suspended in LMPA (150-1000 µL, depending on pellet size). The cell suspension (150 µL) was added to a previously coated glass slide and a cover slip placed over, these were placed on a cool tray and allowed to set (3-5 minutes). Once set the slip was removed and LMPA (150 µL) added to the slide and another slip placed on top. These were again transferred to a cool tray to set. The slip was again removed and all slides placed into a tray where freshly prepared ice cold lysing solution was added, these were left to incubate for 1 hour at 4°C.

- **Electrophoresis Conditions**

After the 1 hour incubation, the lysing solution was gently poured off and the slides placed close together in an electrophoresis chamber. The reservoirs were carefully filled with freshly prepared buffer (pH > 13.0) and filled until the buffer just covered the slides. The slides were incubated for 30 minutes and then the chamber adjusted to 24 V, the electrophoresis was run for 25 minutes and then the slides were removed. The slides were transferred to a clean tray and drop-wise neutralisation with the neutralisation buffer. The buffer was added to coat the slides and then these were incubated for 5 minutes. The buffer was removed and this step repeated twice more. Then slides were then rinsed three times with distilled water and finally with 100% ice cold ethanol. They were then transferred to a slide rack and left to dry overnight before imaging could commence.

- **Imaging and Analysis**

The imaging for the SSB and cross-linking assay was carried out according to that stated in the DSB assay.

9.14 Apoptosis

9.14.1 Cell counting

This assay was conducted using both HT-29 and A2780 cells, where the cells were counted using a haemocytometer and an average taken from the 10 quadrants. The cells were diluted with complete media to give concentrations of 2.5×10^4 cells/flask (0.5×10^4 cells/mL). The flasks were incubated for 24 hours at 37°C and an atmosphere of 5.0% CO₂. Initial stock solutions of the drugs were made at 1 mM, these were further diluted with complete media to give dilutions of 20 μM and 10 μM. The flasks were incubated in 5 mL of these drug solutions or media only (control), for a period of 48 hours at 37°C and an atmosphere of 5.0% CO₂.

9.14.2 Harvesting

The media/drug solution was removed from the flasks and placed into a 25 mL centrifuge tube, the flask is then washed with PBS (5 mL), which was also added to the centrifuge tube. Trypsin (1 mL/flask) was added and then incubated for 5 minutes until a single cell suspension was obtained. The trypsin was then neutralised with media (5 mL) and the whole contents of the flask is transferred to the same centrifuge tube. The tube was spun at 1000 rcf for 3-5 minutes, the supernatant was removed and the pellet re-suspended in PBS (1 mL). The 1 mL was transferred to an eppendorf and spun again at 1500 rpm for 5 minutes, the supernatant is removed and the pellet re-suspended in 16 μL PI, 16 μL AmV and 800 μL buffer solution (100 μL). The eppendorfs were incubated at room temperature for 10 minutes and kept in suspension; and then transferred to FACS tubes for analysis.

9.15 Data Analysis

Samples were run using flow cytometry and parameters adjusted depending on the sample tested. A cell count of 10,000 was necessary to conduct this experiment and gave results of PI versus AnV, each quadrant was analysed manually and a percentage taken from each quadrant of the plot.

9.16 Thioredoxin Reductase

Thioredoxin reductase was obtained from Sigma Aldrich and is sourced from rat liver. It is a buffered aqueous glycerol solution, ≥ 100 units/ mg protein. Solution in 50 mM Tris-HCl, pH 7.5, 300 mM NaCl, 1 mM EDTA, and 10% glycerol.

Stock solutions:

1 M K_2HPO_4 - 17.42 g in 100 mL distilled water

1 M KH_2PO_4 - 13.6 g in 100 mL distilled water

100 mM EDTA - 3.72 g in 100 mL distilled water at pH 7.0

9.16.1 Reaction Reagents:

- **Potassium phosphate buffer** (0.1 M at pH 7.0)

K_2HPO_4 (61.5 mL), KH_2PO_4 (38.5 mL), EDTA (10 mL) all made up to 1 L using distilled water and the pH was adjusted to 7.0.

- **Reaction Buffer A**

Potassium phosphate buffer (50 mL), NADPH (8.3 mg) and BSA (5.0 mg)

- **Reaction Buffer B**

Phosphate buffer (50 mL), NADPH (8.3 mg), BSA (5.0 mg) and DTNB (1.98 mg)

9.16.2 Conducting the assay

Buffer A (0.5 mL) was added to a 1 mL cuvette and to this TrxR (2 μ L) was added. The test compound or DMSO control (1 μ L) was added and the reaction left for approximately 30 seconds. Buffer B (0.5 mL) was added to the cuvette and using a pipette mixed well. The UV-*vis* absorbance was measure at 412 nm and the experiment was carried out using just the enzyme to get the initial absorbance; different dilutions of the test compound were tested using a maximum of 10 μ M.

9.16.3 Analysis of Results

The UV-*vis* was obtained for just the enzyme, hence giving the maximum absorbance. Using the maximum absorbance obtained from each run, a value was obtained for A and once plotted against [I], giving the % inhibition. The IC_{50} value is obtained at 50% enzyme inhibition.

9.17 References

1. R. Levine and J. K. Sneed, *J. Am. Chem. Soc.*, 1951, **73**, 5614-5616.
2. L.-M. Tang, Y.-Q. Duan, X.-F. Li and Y.-S. Li, *J. Organomet. Chem.*, 2006, **691**, 2023.
3. J. Cosier and A. M. Glazer, *J. Appl. Crystallogr.*, 1986, **19**, 105-107.
4. Z. Otwinowski and W. Minor, in '*DENZO and SCALEPACK programs*', 1995.
5. G. Sheldrick, in '*SHELXS86, Program for Crystal Structure Solution*', 1986.
6. A. Altomare, G. Cascarano, C. Giacovazzo and A. Guagliardi, *J. Appl. Crystallogr.*, 1993, **26**, 343-350.
7. A. Altomare, M. C. Burla, M. Camalli, G. L. Cascarano, C. Giacovazzo, A. Guagliardi, A. G. G. Moliterni, G. Polidori and R. Spagna, *J. Appl. Crystallogr.*, 1999, **32**, 115-119.
8. L. J. Barbour, in '*XSeed*', 1999.
9. M. Thornton-Pett, in '*WC-A Windows CIF Processor*', 2000.
10. A. L. Spek, *J. Appl. Crystallogr.*, 2003, **36**, 7-13.
11. P. Govindaswamy and M. R. Kollipara, *J. Coord. Chem.*, 2006, **59**, 131-136
12. J. J. Mannion, Ph. D Thesis, University of Leeds, 2008.
13. A. J. Hebden, Ph. D Thesis, University of Leeds, 2010.

Appendix

Appendix

Crystal data and structure refinement for ligand **L11**

Formula	$C_{17}H_{17}NO$	
Formula weight	251.32	
Size	0.27 x 0.24 x 0.21 mm	
Crystal morphology	Colourless Fragment	
Temperature	150(2) K	
Wavelength	0.71073 Å [Mo- K_{α}]	
Crystal system	Monoclinic	
Space group	$P2_1/n$	
Unit cell dimensions	$a = 7.3817(3)$ Å	$\alpha = 90^\circ$
	$b = 12.0369(4)$ Å	$\beta = 90.0110(10)^\circ$
	$c = 29.9551(11)$ Å	$\gamma = 90^\circ$
Volume	2661.59(17) Å ³	
Z	8	
Density (calculated)	1.254 Mg/m ³	
Absorption coefficient	0.078 mm ⁻¹	
$F(000)$	1072	
Data collection range	$2.17 \leq \theta \leq 33.92^\circ$	
Index ranges	$-9 \leq h \leq 11, -14 \leq k \leq 18, -42 \leq l \leq 46$	
Reflections collected	40768	
Independent reflections	10589 [$R(\text{int}) = 0.0513$]	
Observed reflections	6833 [$I > 2\sigma(I)$]	
Absorption correction	multi-scan	
Max. and min. transmission	0.9841 and 0.9797	
Refinement method	Full	
Data / restraints / parameters	10589 / 0 / 349	
Goodness of fit	1.016	
Final R indices [$I > 2\sigma(I)$]	$R_1 = 0.0517, wR_2 = 0.1322$	
R indices (all data)	$R_1 = 0.0889, wR_2 = 0.1532$	
Largest diff. peak and hole	0.419 and $-0.257 e.\text{Å}^{-3}$	

Crystal data and structure refinement for ligand **L12**

Formula	C ₁₆ H ₁₄ FNO
Formula weight	255.28
Size	0.54 x 0.28 x 0.11 mm
Crystal morphology	Yellow Plate
Temperature	150(2) K
Wavelength	0.71073 Å [Mo-K _α]
Crystal system	Monoclinic
Space group	<i>P</i> 2 ₁ / <i>c</i>
Unit cell dimensions	$a = 14.6120(14)$ Å $\alpha = 90^\circ$ $b = 7.0373(6)$ Å $\beta = 106.929(3)^\circ$ $c = 12.8634(10)$ Å $\gamma = 90^\circ$
Volume	1265.41(19) Å ³
Z	4
Density (calculated)	1.34 Mg/m ³
Absorption coefficient	0.094 mm ⁻¹
<i>F</i> (000)	536
Data collection range	2.91 ≤ θ ≤ 27.41°
Index ranges	-18 ≤ <i>h</i> ≤ 18, -9 ≤ <i>k</i> ≤ 8, -16 ≤ <i>l</i> ≤ 16
Reflections collected	9617
Independent reflections	2860 [<i>R</i> (int) = 0.0488]
Observed reflections	2598 [<i>I</i> > 2σ(<i>I</i>)]
Absorption correction	multi-scan
Max. and min. transmission	0.9898 and 0.9512
Refinement method	Full
Data / restraints / parameters	2860 / 0 / 174
Goodness of fit	1.055
Final <i>R</i> indices [<i>I</i> > 2σ(<i>I</i>)]	<i>R</i> ₁ = 0.0426, <i>wR</i> ₂ = 0.1139
<i>R</i> indices (all data)	<i>R</i> ₁ = 0.046, <i>wR</i> ₂ = 0.1175
Largest diff. peak and hole	0.37 and -0.266e.Å ⁻³

Crystal data and structure refinement for ligand **L14**

Formula	$C_{16}H_{13}Cl_2NO$	
Formula weight	306.17	
Size	0.22 x 0.18 x 0.05 mm	
Crystal morphology	Yellow plate	
Temperature	150(2) K	
Wavelength	0.71073 Å [Mo- K_{α}]	
Crystal system	Monoclinic	
Space group	$P2_1/n$	
Unit cell dimensions	$a = 12.3180(4)$ Å	$\alpha = 90^\circ$
	$b = 7.4714(2)$ Å	$\beta = 108.3020(10)^\circ$
	$c = 16.4245(5)$ Å	$\gamma = 90^\circ$
Volume	1435.13(7) Å ³	
Z	4	
Density (calculated)	1.417 Mg/m ³	
Absorption coefficient	0.446 mm ⁻¹	
$F(000)$	632	
Data collection range	$2.48 \leq \theta \leq 27.49^\circ$	
Index ranges	$-16 \leq h \leq 14$, $-6 \leq k \leq 9$, $-21 \leq l \leq 21$	
Reflections collected	12165	
Independent reflections	3264 [$R(\text{int}) = 0.0572$]	
Observed reflections	2944 [$I > 2\sigma(I)$]	
Absorption correction	multi-scan	
Max. and min. transmission	0.978 and 0.9083	
Refinement method	Full	
Data / restraints / parameters	3264 / 0 / 183	
Goodness of fit	1.025	
Final R indices [$I > 2\sigma(I)$]	$R_1 = 0.0344$, $wR_2 = 0.0938$	
R indices (all data)	$R_1 = 0.0381$, $wR_2 = 0.0986$	
Largest diff. peak and hole	0.337 and $-0.415 e \cdot \text{Å}^{-3}$	

Crystal data and structure refinement for ligand **L15**

Formula	C ₁₆ H ₁₃ Cl ₂ NO	
Formula weight	306.17	
Size	0.3655 x 0.1575 x 0.0861 mm	
Crystal morphology	Yellow Plate	
Temperature	100.00(10) K	
Wavelength	0.7107 Å [Mo -K _α]	
Crystal system		
Space group		
Unit cell dimensions	$a = 12.6921(14)$ Å	$\alpha = 90^\circ$
	$b = 8.4056(6)$ Å	$\beta = 90^\circ$
	$c = 26.694(2)$ Å	$\gamma = 90^\circ$
Volume	2847.9(4) Å ³	
Z	8	
Density (calculated)	1.428 Mg/m ³	
Absorption coefficient	0.45 mm ⁻¹	
$F(000)$	1264	
Data collection range	$2.21 \leq \theta \leq 29.9^\circ$	
Index ranges	$-10 \leq h \leq 15, -8 \leq k \leq 10, -37 \leq l \leq 23$	
Reflections collected	8100	
Independent reflections	3301 [$R(\text{int}) = 0.0533$]	
Observed reflections	2423 [$I > 2\sigma(I)$]	
Absorption correction	multi-scan	
Max. and min. transmission	1 and 0.82463	
Refinement method	Full	
Data / restraints / parameters	3301 / 0 / 182	
Goodness of fit	1.078	
Final R indices [$I > 2\sigma(I)$]	$R_1 = 0.0575, wR_2 = 0.1011$	
R indices (all data)	$R_1 = 0.0872, wR_2 = 0.1132$	
Largest diff. peak and hole	0.339 and -0.331 e.Å ⁻³	

Crystal data and structure refinement for ligand **L16**

Formula	C ₁₆ H ₁₂ Cl ₃ NO	
Formula weight	340.62	
Size	0.29 x 0.25 x 0.21 mm	
Crystal morphology	Yellow Fragment	
Temperature	173(2) K	
Wavelength	0.71073 Å [Mo-K _α]	
Crystal system	Monoclinic	
Space group	P2 ₁ /c	
Unit cell dimensions	$a = 11.4886(4)$ Å	$\alpha = 90^\circ$
	$b = 9.5459(3)$ Å	$\beta = 98.829(3)^\circ$
	$c = 13.6456(4)$ Å	$\gamma = 90^\circ$
Volume	1478.77(8) Å ³	
Z	4	
Density (calculated)	1.53 Mg/m ³	
Absorption coefficient	0.616 mm ⁻¹	
<i>F</i> (000)	696	
Data collection range	$1.79 \leq \theta \leq 29.72^\circ$	
Index ranges	$-15 \leq h \leq 15$, $-12 \leq k \leq 13$, $-18 \leq l \leq 11$	
Reflections collected	6404	
Independent reflections	3469 [<i>R</i> (int) = 0.0285]	
Observed reflections	2956 [<i>I</i> > 2σ(<i>I</i>)]	
Absorption correction	multi-scan	
Max. and min. transmission	1 and 0.8524	
Refinement method	Full	
Data / restraints / parameters	3469 / 0 / 191	
Goodness of fit	1.054	
Final <i>R</i> indices [<i>I</i> > 2σ(<i>I</i>)]	<i>R</i> ₁ = 0.0358, <i>wR</i> ₂ = 0.0765	
<i>R</i> indices (all data)	<i>R</i> ₁ = 0.0446, <i>wR</i> ₂ = 0.0831	
Largest diff. peak and hole	0.372 and -0.334 e.Å ⁻³	

Crystal data and structure refinement for ligand **L19**

Formula	$C_{36}H_{38}N_2O_2$
Formula weight	530.68
Size	0.4296 x 0.3789 x 0.1417 mm
Crystal morphology	Brown Fragment
Temperature	293(2) K
Wavelength	0.71073 Å [Mo- K_α]
Crystal system	Monoclinic
Space group	$P2_1/n$
Unit cell dimensions	$a = 7.7796(5)$ Å $\alpha = 90^\circ$ $b = 11.6210(7)$ Å $\beta = 91.400(5)^\circ$ $c = 31.457(2)$ Å $\gamma = 90^\circ$
Volume	$2843.1(3)$ Å ³
Z	4
Density (calculated)	1.24 Mg/m ³
Absorption coefficient	0.076 mm ⁻¹
$F(000)$	1136
Data collection range	$2.59 \leq \theta \leq 29.8^\circ$
Index ranges	$-9 \leq h \leq 10$, $-15 \leq k \leq 15$, $-26 \leq l \leq 43$
Reflections collected	12204
Independent reflections	6563 [$R(\text{int}) = 0.0343$]
Observed reflections	4869 [$I > 2\sigma(I)$]
Absorption correction	multi-scan
Max. and min. transmission	1 and 0.65501
Refinement method	Full
Data / restraints / parameters	6563 / 0 / 365
Goodness of fit	1.087
Final R indices [$I > 2\sigma(I)$]	$R_1 = 0.0623$, $wR_2 = 0.1231$
R indices (all data)	$R_1 = 0.0888$, $wR_2 = 0.1371$
Largest diff. peak and hole	0.277 and $-0.262 e.\text{Å}^{-3}$

Appendix

Crystal data and structure refinement for ligand **L21**

Formula	$C_{18}H_{19}NO_3$
Formula weight	297.34
Size	0.35 x 0.35 x 0.21 mm
Crystal morphology	Yellow Fragment
Temperature	150(2) K
Wavelength	0.71073 Å [Mo- K_α]
Crystal system	Triclinic
Space group	$P1$
Unit cell dimensions	$a = 6.6562(7)$ Å $\alpha = 89.870(5)^\circ$ $b = 8.6335(9)$ Å $\beta = 89.960(5)^\circ$ $c = 14.6783(14)$ Å $\gamma = 72.170(5)^\circ$
Volume	802.99(14) Å ³
Z	2
Density (calculated)	1.23 Mg/m ³
Absorption coefficient	0.084 mm ⁻¹
$F(000)$	316
Data collection range	$1.39 \leq \theta \leq 33.75^\circ$
Index ranges	$-10 \leq h \leq 9$, $-12 \leq k \leq 11$, $-22 \leq l \leq 19$
Reflections collected	9291
Independent reflections	7369 [$R(\text{int}) = 0.0524$]
Observed reflections	6256 [$I > 2\sigma(I)$]
Absorption correction	multi-scan
Max. and min. transmission	0.9829 and 0.971
Refinement method	Full
Data / restraints / parameters	7369 / 3 / 403
Goodness of fit	1.031
Final R indices [$I > 2\sigma(I)$]	$R_1 = 0.0747$, $wR_2 = 0.2011$
R indices (all data)	$R_1 = 0.0834$, $wR_2 = 0.214$
Largest diff. peak and hole	0.671 and $-0.646\text{e.}\text{\AA}^{-3}$
Absolute structure parameter	-0.5(11)

Crystal data and structure refinement for ligand **L22**

Formula	$C_{18}H_{17}FNO_2$
Formula weight	298.33
Size	0.41 x 0.23 x 0.12 mm
Crystal morphology	Yellow Plate
Temperature	150(2) K
Wavelength	0.71073 Å [Mo- K_α]
Crystal system	Triclinic
Space group	$P \bar{1}$
Unit cell dimensions	$a = 10.5457(16)$ Å $\alpha = 66.443(5)^\circ$ $b = 12.754(2)$ Å $\beta = 74.668(6)^\circ$ $c = 13.716(2)$ Å $\gamma = 70.382(5)^\circ$
Volume	1574.6(4) Å ³
Z	4
Density (calculated)	1.258 Mg/m ³
Absorption coefficient	0.09 mm ⁻¹
$F(000)$	628
Data collection range	$1.64 \leq \theta \leq 30.33^\circ$
Index ranges	$-13 \leq h \leq 14$, $-17 \leq k \leq 18$, $-19 \leq l \leq 16$
Reflections collected	22286
Independent reflections	8869 [$R(\text{int}) = 0.0865$]
Observed reflections	5069 [$I > 2\sigma(I)$]
Absorption correction	none
Max. and min. transmission	0.9893 and 0.9641
Refinement method	Full
Data / restraints / parameters	8869 / 0 / 401
Goodness of fit	1.126
Final R indices [$I > 2\sigma(I)$]	$R_1 = 0.1147$, $wR_2 = 0.3088$
R indices (all data)	$R_1 = 0.1664$, $wR_2 = 0.3501$
Largest diff. peak and hole	0.71 and -0.861 e.Å ⁻³

Crystal data and structure refinement for ligand **L24**

Formula	$C_{17}H_{15}NO_3$
Formula weight	281.3
Size	0.9 x 0.71 x 0.4 mm
Crystal morphology	Green Plate
Temperature	150(2) K
Wavelength	0.71073 Å [Mo- K_α]
Crystal system	Monoclinic
Space group	$P2_1$
Unit cell dimensions	$a = 3.9619(6)$ Å $\alpha = 90^\circ$ $b = 18.622(3)$ Å $\beta = 91.075(7)^\circ$ $c = 9.1110(15)$ Å $\gamma = 90^\circ$
Volume	672.07(19) Å ³
Z	2
Density (calculated)	1.39 Mg/m ³
Absorption coefficient	0.096 mm ⁻¹
$F(000)$	296
Data collection range	$2.19 \leq \theta \leq 33.72^\circ$
Index ranges	$-4 \leq h \leq 4$, $-29 \leq k \leq 29$, $-14 \leq l \leq 14$
Reflections collected	15456
Independent reflections	4004 [$R(\text{int}) = 0.0853$]
Observed reflections	3065 [$I > 2\sigma(I)$]
Absorption correction	none
Max. and min. transmission	0.9627 and 0.9187
Refinement method	Full
Data / restraints / parameters	4004 / 1 / 192
Goodness of fit	0.992
Final R indices [$I > 2\sigma(I)$]	$R_1 = 0.0581$, $wR_2 = 0.1391$
R indices (all data)	$R_1 = 0.0814$, $wR_2 = 0.1553$
Largest diff. peak and hole	0.392 and $-0.407 e \cdot \text{Å}^{-3}$
Absolute structure parameter	-0.8(12)

Crystal data and structure refinement for ligand **L25**

Formula	C ₁₉ H ₁₇ N ₃ O	
Formula weight	303.36	
Size	0.43 x 0.32 x 0.19 mm	
Crystal morphology	Green Plate	
Temperature	150(2) K	
Wavelength	0.71073 Å [Mo-K _α]	
Crystal system	Orthorhombic	
Space group	<i>Pbca</i>	
Unit cell dimensions	$a = 7.7635(8)$ Å	$\alpha = 90^\circ$
	$b = 11.0134(11)$ Å	$\beta = 90^\circ$
	$c = 36.431(4)$ Å	$\gamma = 90^\circ$
Volume	3114.9(6) Å ³	
Z	8	
Density (calculated)	1.294 Mg/m ³	
Absorption coefficient	0.082 mm ⁻¹	
<i>F</i> (000)	1280	
Data collection range	2.24 ≤ θ ≤ 30.17°	
Index ranges	-10 ≤ <i>h</i> ≤ 9, -15 ≤ <i>k</i> ≤ 15, -50 ≤ <i>l</i> ≤ 51	
Reflections collected	64849	
Independent reflections	4572 [<i>R</i> (int) = 0.0759]	
Observed reflections	3782 [<i>I</i> > 2σ(<i>I</i>)]	
Absorption correction	multi-scan	
Max. and min. transmission	0.9845 and 0.9655	
Refinement method	Full	
Data / restraints / parameters	4572 / 0 / 209	
Goodness of fit	1.036	
Final <i>R</i> indices [<i>I</i> > 2σ(<i>I</i>)]	<i>R</i> ₁ = 0.0478, <i>wR</i> ₂ = 0.1265	
<i>R</i> indices (all data)	<i>R</i> ₁ = 0.0588, <i>wR</i> ₂ = 0.1371	
Largest diff. peak and hole	0.408 and -0.249 e.Å ⁻³	

Crystal data and structure refinement for complex **1**

Formula	C ₂₆ H ₂₇ ClFNORu	
Formula weight	525.01	
Size	0.18 x 0.15 x 0.12 mm	
Crystal morphology	Red Fragment	
Temperature	173(2) K	
Wavelength	0.71073 Å [Mo-K _α]	
Crystal system	Triclinic	
Space group	<i>P</i> $\bar{1}$	
Unit cell dimensions	$a = 9.8410(5)$ Å	$\alpha = 100.643(2)^\circ$
	$b = 10.4805(6)$ Å	$\beta = 102.502(2)^\circ$
	$c = 12.3289(7)$ Å	$\gamma = 104.424(2)^\circ$
Volume	1163.39(11) Å ³	
Z	2	
Density (calculated)	1.499 Mg/m ³	
Absorption coefficient	0.814 mm ⁻¹	
<i>F</i> (000)	536	
Data collection range	3.14 ≤ θ ≤ 30.55°	
Index ranges	-14 ≤ <i>h</i> ≤ 12, -14 ≤ <i>k</i> ≤ 13, -17 ≤ <i>l</i> ≤ 17	
Reflections collected	19946	
Independent reflections	6817 [<i>R</i> (int) = 0.0326]	
Observed reflections	6190 [<i>I</i> > 2σ(<i>I</i>)]	
Absorption correction	multi-scan	
Max. and min. transmission	0.91 and 0.8693	
Refinement method	Full	
Data / restraints / parameters	6817 / 0 / 284	
Goodness of fit	1.036	
Final <i>R</i> indices [<i>I</i> > 2σ(<i>I</i>)]	<i>R</i> ₁ = 0.0286, <i>wR</i> ₂ = 0.0793	
<i>R</i> indices (all data)	<i>R</i> ₁ = 0.0326, <i>wR</i> ₂ = 0.0819	
Largest diff. peak and hole	2.243 and -0.636e.Å ⁻³	

Crystal data and structure refinement for complex **2**

Formula	C ₂₆ H ₂₇ ClFNORu	
Formula weight	525.01	
Size	0.2678 x 0.161 x 0.0985 mm	
Crystal morphology	Red Fragment	
Temperature	173(2) K	
Wavelength	0.71073 Å [Mo-K _α]	
Crystal system	Triclinic	
Space group	<i>P</i> $\bar{1}$	
Unit cell dimensions	<i>a</i> = 7.5924(8) Å	α = 101.176(8)°
	<i>b</i> = 10.2922(11) Å	β = 94.516(8)°
	<i>c</i> = 15.9991(15) Å	γ = 106.506(9)°
Volume	1164.0(2) Å ³	
Z	2	
Density (calculated)	1.498 Mg/m ³	
Absorption coefficient	0.814 mm ⁻¹	
<i>F</i> (000)	536	
Data collection range	2.62 ≤ θ ≤ 29.76°	
Index ranges	-9 ≤ <i>h</i> ≤ 9, -12 ≤ <i>k</i> ≤ 10, -15 ≤ <i>l</i> ≤ 21	
Reflections collected	8512	
Independent reflections	5315 [<i>R</i> (int) = 0.0583]	
Observed reflections	4083 [<i>I</i> > 2 σ (<i>I</i>)]	
Absorption correction	multi-scan	
Max. and min. transmission	1 and 0.2399	
Refinement method	Full	
Data / restraints / parameters	5315 / 0 / 284	
Goodness of fit	1.037	
Final <i>R</i> indices [<i>I</i> > 2 σ (<i>I</i>)]	<i>R</i> ₁ = 0.0555, <i>wR</i> ₂ = 0.1024	
<i>R</i> indices (all data)	<i>R</i> ₁ = 0.0767, <i>wR</i> ₂ = 0.1208	
Largest diff. peak and hole	1.222 and -1.296 e.Å ⁻³	

Crystal data and structure refinement for complex **3**

Formula	C ₂₆ H ₂₇ Cl ₂ NORu	
Formula weight	541.46	
Size	0.49 x 0.26 x 0.11 mm	
Crystal morphology	Red Fragment	
Temperature	150(2) K	
Wavelength	0.71073 Å [Mo-K _α]	
Crystal system	Triclinic	
Space group	<i>P</i> $\bar{1}$	
Unit cell dimensions	$a = 7.7826(7)$ Å	$\alpha = 68.270(3)^\circ$
	$b = 11.3982(10)$ Å	$\beta = 83.106(4)^\circ$
	$c = 15.2492(14)$ Å	$\gamma = 70.938(4)^\circ$
Volume	1187.69(18) Å ³	
Z	2	
Density (calculated)	1.514 Mg/m ³	
Absorption coefficient	0.903 mm ⁻¹	
<i>F</i> (000)	552	
Data collection range	1.44 ≤ θ ≤ 30.38°	
Index ranges	-11 ≤ <i>h</i> ≤ 11, -16 ≤ <i>k</i> ≤ 16, -21 ≤ <i>l</i> ≤ 18	
Reflections collected	9731	
Independent reflections	4330 [<i>R</i> (int) = 0.0475]	
Observed reflections	4113 [<i>I</i> > 2σ(<i>I</i>)]	
Absorption correction	none	
Max. and min. transmission	0.9072 and 0.6659	
Refinement method	Full	
Data / restraints / parameters	4330 / 0 / 284	
Goodness of fit	1.231	
Final <i>R</i> indices [<i>I</i> > 2σ(<i>I</i>)]	<i>R</i> ₁ = 0.0575, <i>wR</i> ₂ = 0.178	
<i>R</i> indices (all data)	<i>R</i> ₁ = 0.0593, <i>wR</i> ₂ = 0.1821	
Largest diff. peak and hole	1.515 and -1.469 e.Å ⁻³	

Crystal data and structure refinement for complex **4**

Formula	$C_{17.33}H_{17.33}Cl_2N_{0.67}O_{0.67}Ru_{0.67}$
Formula weight	383.94
Size	0.47 x 0.33 x 0.24 mm
Crystal morphology	Red Fragment
Temperature	150(2) K
Wavelength	0.71073 Å [Mo- K_α]
Crystal system	Triclinic
Space group	$P \bar{1}$
Unit cell dimensions	$a = 11.3992(12)$ Å $\alpha = 88.692(4)^\circ$ $b = 11.6491(11)$ Å $\beta = 87.058(4)^\circ$ $c = 19.5678(19)$ Å $\gamma = 80.287(4)^\circ$
Volume	$2557.5(4)$ Å ³
Z	6
Density (calculated)	1.496 Mg/m ³
Absorption coefficient	0.945 mm ⁻¹
$F(000)$	1168
Data collection range	$2.96 \leq \theta \leq 28.17^\circ$
Index ranges	$-15 \leq h \leq 15$, $-15 \leq k \leq 15$, $-25 \leq l \leq 25$
Reflections collected	47038
Independent reflections	12361 [$R(\text{int}) = 0.0504$]
Observed reflections	11047 [$I > 2\sigma(I)$]
Absorption correction	multi-scan
Max. and min. transmission	0.8078 and 0.6651
Refinement method	Full
Data / restraints / parameters	12361 / 0 / 585
Goodness of fit	1.043
Final R indices [$I > 2\sigma(I)$]	$R_1 = 0.0254$, $wR_2 = 0.0658$
R indices (all data)	$R_1 = 0.0298$, $wR_2 = 0.069$
Largest diff. peak and hole	0.799 and $-0.605e.$ Å ⁻³

Crystal data and structure refinement for complex **5**

Formula	C ₂₆ H ₂₆ Cl ₃ NORu	
Formula weight	575.9	
Size	0.1363 x 0.1102 x 0.0754 mm	
Crystal morphology	Red Plate	
Temperature	173(2) K	
Wavelength	0.71073 Å [Mo-K _α]	
Crystal system	Monoclinic	
Space group	Cc	
Unit cell dimensions	$a = 14.2172(6)$ Å	$\alpha = 90^\circ$
	$b = 14.3632(6)$ Å	$\beta = 90.373(4)^\circ$
	$c = 11.7497(4)$ Å	$\gamma = 90^\circ$
Volume	2399.29(16) Å ³	
Z	4	
Density (calculated)	1.594 Mg/m ³	
Absorption coefficient	1.007 mm ⁻¹	
<i>F</i> (000)	1168	
Data collection range	2.02 ≤ θ ≤ 29.66°	
Index ranges	-19 ≤ h ≤ 18, -18 ≤ k ≤ 19, -16 ≤ l ≤ 12	
Reflections collected	6519	
Independent reflections	4231 [$R(\text{int}) = 0.0417$]	
Observed reflections	3907 [$I > 2\sigma(I)$]	
Absorption correction	multi-scan	
Max. and min. transmission	1 and 0.8823	
Refinement method	Full	
Data / restraints / parameters	4231 / 2 / 293	
Goodness of fit	1.05	
Final <i>R</i> indices [$I > 2\sigma(I)$]	$R_1 = 0.0411$, $wR_2 = 0.0726$	
<i>R</i> indices (all data)	$R_1 = 0.0462$, $wR_2 = 0.0764$	
Largest diff. peak and hole	0.784 and -0.609 e.Å ⁻³	
Absolute structure parameter	-0.06(4)	

Crystal data and structure refinement for complex **6**

Formula	$\text{C}_{4.16}\text{H}_4\text{Cl}_{0.64}\text{N}_{0.16}\text{O}_{0.16}\text{Ru}_{0.16}$
Formula weight	97.65
Size	0.47 x 0.41 x 0.41 mm
Crystal morphology	Red Fragment
Temperature	150(2) K
Wavelength	0.71073 Å [Mo- K_α]
Crystal system	Triclinic
Space group	$P \bar{1}$
Unit cell dimensions	$a = 11.4864(13)$ Å $\alpha = 76.377(6)^\circ$ $b = 13.9138(16)$ Å $\beta = 86.339(6)^\circ$ $c = 18.324(2)$ Å $\gamma = 75.571(6)^\circ$
Volume	2756.4(5) Å ³
Z	25
Density (calculated)	1.471 Mg/m ³
Absorption coefficient	0.975 mm ⁻¹
$F(000)$	1232
Data collection range	$2.15 \leq \theta \leq 30.13^\circ$
Index ranges	$-16 \leq h \leq 16$, $-19 \leq k \leq 19$, $-25 \leq l \leq 25$
Reflections collected	135555
Independent reflections	16199 [$R(\text{int}) = 0.0753$]
Observed reflections	12965 [$I > 2\sigma(I)$]
Absorption correction	multi-scan
Max. and min. transmission	0.6889 and 0.6561
Refinement method	Full
Data / restraints / parameters	16199 / 0 / 598
Goodness of fit	1.045
Final R indices [$I > 2\sigma(I)$]	$R_1 = 0.0534$, $wR_2 = 0.1572$
R indices (all data)	$R_1 = 0.068$, $wR_2 = 0.1746$
Largest diff. peak and hole	3.802 and $-1.463\text{e.}\text{Å}^{-3}$

Appendix

Crystal data and structure refinement for complex **7**

Formula	C ₂₆ H ₂₇ BrClNORu	
Formula weight	585.92	
Size	0.22 x 0.17 x 0.13 mm	
Crystal morphology	Red Fragment	
Temperature	173(2) K	
Wavelength	0.71073 Å [Mo-K _α]	
Crystal system	Monoclinic	
Space group	<i>Cc</i>	
Unit cell dimensions	$a = 14.8418(5) \text{ \AA}$	$\alpha = 90^\circ$
	$b = 13.6395(5) \text{ \AA}$	$\beta = 90.581(3)^\circ$
	$c = 11.7988(4) \text{ \AA}$	$\gamma = 90^\circ$
Volume	2388.36(14) Å ³	
Z	4	
Density (calculated)	1.629 Mg/m ³	
Absorption coefficient	2.46 mm ⁻¹	
<i>F</i> (000)	1176	
Data collection range	2.03 ≤ θ ≤ 29.83°	
Index ranges	-20 ≤ h ≤ 19, -18 ≤ k ≤ 19, -16 ≤ l ≤ 16	
Reflections collected	17435	
Independent reflections	5760 [<i>R</i> (int) = 0.0451]	
Observed reflections	5536 [<i>I</i> > 2σ(<i>I</i>)]	
Absorption correction	multi-scan	
Max. and min. transmission	0.7324 and 0.6088	
Refinement method	Full	
Data / restraints / parameters	5760 / 2 / 284	
Goodness of fit	1.034	
Final <i>R</i> indices [<i>I</i> > 2σ(<i>I</i>)]	<i>R</i> ₁ = 0.0281, <i>wR</i> ₂ = 0.0524	
<i>R</i> indices (all data)	<i>R</i> ₁ = 0.0303, <i>wR</i> ₂ = 0.0537	
Largest diff. peak and hole	0.351 and -0.643 e.Å ⁻³	
Absolute structure parameter	0.004(5)	

Crystal data and structure refinement for complex **8**

Formula	C ₂₆ H ₂₇ BrClNORu	
Formula weight	585.92	
Size	0.1486 x 0.1419 x 0.113 mm	
Crystal morphology	Red Plate	
Temperature	173(2) K	
Wavelength	0.71073 Å [Mo-K _α]	
Crystal system	Triclinic	
Space group	<i>P</i> $\bar{1}$	
Unit cell dimensions	<i>a</i> = 7.7084(3) Å	α = 68.311(4)°
	<i>b</i> = 11.3524(5) Å	β = 82.804(4)°
	<i>c</i> = 15.1513(7) Å	γ = 70.580(4)°
Volume	1161.91(9) Å ³	
Z	2	
Density (calculated)	1.675 Mg/m ³	
Absorption coefficient	2.528 mm ⁻¹	
<i>F</i> (000)	588	
Data collection range	2.03 ≤ θ ≤ 29.76°	
Index ranges	-9 ≤ <i>h</i> ≤ 8, -15 ≤ <i>k</i> ≤ 12, -18 ≤ <i>l</i> ≤ 17	
Reflections collected	11871	
Independent reflections	5475 [<i>R</i> (int) = 0.041]	
Observed reflections	4847 [<i>I</i> > 2 σ (<i>I</i>)]	
Absorption correction	multi-scan	
Max. and min. transmission	1 and 0.90679	
Refinement method	Full	
Data / restraints / parameters	5475 / 0 / 284	
Goodness of fit	1.053	
Final <i>R</i> indices [<i>I</i> > 2 σ (<i>I</i>)]	<i>R</i> ₁ = 0.0328, <i>wR</i> ₂ = 0.0628	
<i>R</i> indices (all data)	<i>R</i> ₁ = 0.0392, <i>wR</i> ₂ = 0.0674	
Largest diff. peak and hole	0.537 and -0.597 e.Å ⁻³	

Crystal data and structure refinement for complex **9**

Formula	C ₂₆ H ₂₇ ClINORu	
Formula weight	632.91	
Size	0.2195 x 0.1161 x 0.0959 mm	
Crystal morphology	Orange Fragment	
Temperature	173(2) K	
Wavelength	0.71073 Å [Mo-K _α]	
Crystal system	Triclinic	
Space group	<i>P</i> $\bar{1}$	
Unit cell dimensions	$a = 7.7700(7)$ Å	$\alpha = 106.660(9)^\circ$
	$b = 11.5552(10)$ Å	$\beta = 97.552(8)^\circ$
	$c = 15.2078(15)$ Å	$\gamma = 109.544(8)^\circ$
Volume	1193.01(19) Å ³	
Z	2	
Density (calculated)	1.762 Mg/m ³	
Absorption coefficient	2.081 mm ⁻¹	
<i>F</i> (000)	624	
Data collection range	2 ≤ θ ≤ 29.82°	
Index ranges	-10 ≤ <i>h</i> ≤ 9, -11 ≤ <i>k</i> ≤ 15, -19 ≤ <i>l</i> ≤ 17	
Reflections collected	10248	
Independent reflections	5583 [<i>R</i> (int) = 0.038]	
Observed reflections	4481 [<i>I</i> > 2σ(<i>I</i>)]	
Absorption correction	multi-scan	
Max. and min. transmission	1 and 0.72236	
Refinement method	Full	
Data / restraints / parameters	5583 / 0 / 284	
Goodness of fit	1.02	
Final <i>R</i> indices [<i>I</i> > 2σ(<i>I</i>)]	<i>R</i> ₁ = 0.0429, <i>wR</i> ₂ = 0.0841	
<i>R</i> indices (all data)	<i>R</i> ₁ = 0.057, <i>wR</i> ₂ = 0.0929	
Largest diff. peak and hole	1.48 and -1.045e.Å ⁻³	

Crystal data and structure refinement for complex **10**

Formula	$C_{28}H_{32}ClNO_2Ru$	
Formula weight	551.07	
Size	0.21 x 0.1511 x 0.1103 mm	
Crystal morphology	Red Fragment	
Temperature	173(2) K	
Wavelength	0.71073 Å [Mo- K_α]	
Crystal system	Triclinic	
Space group	$P \bar{1}$	
Unit cell dimensions	$a = 9.5863(5) \text{ \AA}$	$\alpha = 106.161(4)^\circ$
	$b = 11.5806(5) \text{ \AA}$	$\beta = 102.739(4)^\circ$
	$c = 13.3596(6) \text{ \AA}$	$\gamma = 110.123(4)^\circ$
Volume	1252.61(10) Å ³	
Z	2	
Density (calculated)	1.461 Mg/m ³	
Absorption coefficient	0.758 mm ⁻¹	
$F(000)$	568	
Data collection range	$1.69 \leq \theta \leq 29.77^\circ$	
Index ranges	$-13 \leq h \leq 13, -16 \leq k \leq 15, -16 \leq l \leq 18$	
Reflections collected	23922	
Independent reflections	6323 [$R(\text{int}) = 0.0443$]	
Observed reflections	5807 [$I > 2\sigma(I)$]	
Absorption correction	multi-scan	
Max. and min. transmission	1 and 0.85957	
Refinement method	Full	
Data / restraints / parameters	6323 / 0 / 303	
Goodness of fit	1.067	
Final R indices [$I > 2\sigma(I)$]	$R_1 = 0.03, wR_2 = 0.0654$	
R indices (all data)	$R_1 = 0.0344, wR_2 = 0.0678$	
Largest diff. peak and hole	0.65 and -0.615 e.Å ⁻³	

Crystal data and structure refinement for complex **11**

Formula	C ₂₇ H ₃₀ ClNORu	
Formula weight	521.04	
Size	0.35 x 0.29 x 0.24 mm	
Crystal morphology	Red Fragment	
Temperature	173(2) K	
Wavelength	0.71073 Å [Mo-K _α]	
Crystal system	Triclinic	
Space group	<i>P</i> $\bar{1}$	
Unit cell dimensions	<i>a</i> = 7.7691(10) Å	α = 68.399(6)°
	<i>b</i> = 11.4508(14) Å	β = 83.185(6)°
	<i>c</i> = 15.4307(18) Å	γ = 71.461(6)°
Volume	1210.1(3) Å ³	
Z	2	
Density (calculated)	1.43 Mg/m ³	
Absorption coefficient	0.777 mm ⁻¹	
<i>F</i> (000)	536	
Data collection range	2.01 ≤ θ ≤ 32.23°	
Index ranges	-11 ≤ <i>h</i> ≤ 11, -17 ≤ <i>k</i> ≤ 17, -22 ≤ <i>l</i> ≤ 22	
Reflections collected	76647	
Independent reflections	8293 [<i>R</i> (int) = 0.0556]	
Observed reflections	7744 [<i>I</i> > 2 σ (<i>I</i>)]	
Absorption correction	multi-scan	
Max. and min. transmission	0.8379 and 0.7706	
Refinement method	Full	
Data / restraints / parameters	8293 / 0 / 285	
Goodness of fit	1.079	
Final <i>R</i> indices [<i>I</i> > 2 σ (<i>I</i>)]	<i>R</i> ₁ = 0.0322, <i>wR</i> ₂ = 0.0848	
<i>R</i> indices (all data)	<i>R</i> ₁ = 0.0344, <i>wR</i> ₂ = 0.0862	
Largest diff. peak and hole	1.191 and -1.848e.Å ⁻³	

Crystal data and structure refinement for complex **12**

Formula	$C_{59.72}H_{58.85}Cl_2N_2O_2Ru_2$	
Formula weight	1109.56	
Size	0.258 x 0.2103 x 0.1547 mm	
Crystal morphology	Red Fragment	
Temperature	173(2) K	
Wavelength	0.71073 Å [Mo- K_α]	
Crystal system	Triclinic	
Space group	$P \bar{1}$	
Unit cell dimensions	$a = 13.7807(7)$ Å	$\alpha = 90.868(4)^\circ$
	$b = 14.3381(6)$ Å	$\beta = 114.234(5)^\circ$
	$c = 14.7586(6)$ Å	$\gamma = 104.725(4)^\circ$
Volume	2548.1(2) Å ³	
Z	2	
Density (calculated)	1.446 Mg/m ³	
Absorption coefficient	0.743 mm ⁻¹	
$F(000)$	1138	
Data collection range	$1.69 \leq \theta \leq 25.03^\circ$	
Index ranges	$-14 \leq h \leq 16$, $-17 \leq k \leq 15$, $-17 \leq l \leq 16$	
Reflections collected	19216	
Independent reflections	9023 [$R(\text{int}) = 0.0589$]	
Observed reflections	7512 [$I > 2\sigma(I)$]	
Absorption correction	multi-scan	
Max. and min. transmission	0.8536 and 0.819	
Refinement method	Full	
Data / restraints / parameters	9023 / 0 / 632	
Goodness of fit	1.154	
Final R indices [$I > 2\sigma(I)$]	$R_1 = 0.0702$, $wR_2 = 0.1566$	
R indices (all data)	$R_1 = 0.0847$, $wR_2 = 0.1648$	
Largest diff. peak and hole	2.006 and $-0.813e. \text{Å}^{-3}$	

Crystal data and structure refinement for complex **13**

Formula	$C_{26}H_{25}ClF_3NORu$
Formula weight	560.99
Size	0.59 x 0.29 x 0.21 mm
Crystal morphology	Red Fragment
Temperature	150(2) K
Wavelength	0.71073 Å [Mo- K_{α}]
Crystal system	Monoclinic
Space group	Cc
Unit cell dimensions	$a = 14.0726(14)$ Å $\alpha = 90^{\circ}$ $b = 14.2648(14)$ Å $\beta = 90.643(5)^{\circ}$ $c = 12.2405(14)$ Å $\gamma = 90^{\circ}$
Volume	2457.0(4) Å ³
Z	4
Density (calculated)	1.517 Mg/m ³
Absorption coefficient	0.788 mm ⁻¹
$F(000)$	1136
Data collection range	$2.03 \leq \theta \leq 30.55^{\circ}$
Index ranges	$-19 \leq h \leq 19, -20 \leq k \leq 20, -17 \leq l \leq 17$
Reflections collected	39809
Independent reflections	7151 [$R(\text{int}) = 0.0606$]
Observed reflections	6998 [$I > 2\sigma(I)$]
Absorption correction	multi-scan
Max. and min. transmission	0.8539 and 0.6536
Refinement method	Full
Data / restraints / parameters	7151 / 2 / 302
Goodness of fit	1.085
Final R indices [$I > 2\sigma(I)$]	$R_1 = 0.0272, wR_2 = 0.0826$
R indices (all data)	$R_1 = 0.0285, wR_2 = 0.084$
Largest diff. peak and hole	0.96 and $-1.525 e \cdot \text{Å}^{-3}$
Absolute structure parameter	-0.01(2)

Appendix

Crystal data and structure refinement for complex **14**

Formula	C ₁₆ H ₂₁ Cl ₂ NRu	
Formula weight	399.31	
Size	0.26 x 0.22 x 0.19 mm	
Crystal morphology	Red Fragment	
Temperature	296(2) K	
Wavelength	0.71073 Å [Mo-K _α]	
Crystal system	Triclinic	
Space group	<i>P</i> $\bar{1}$	
Unit cell dimensions	<i>a</i> = 7.9068(7) Å	α = 87.914(3)°
	<i>b</i> = 9.0739(7) Å	β = 85.084(3)°
	<i>c</i> = 12.5987(10) Å	γ = 69.616(3)°
Volume	844.16(12) Å ³	
<i>Z</i>	2	
Density (calculated)	1.571 Mg/m ³	
Absorption coefficient	1.235 mm ⁻¹	
<i>F</i> (000)	404	
Data collection range	2.76 ≤ θ ≤ 26.29°	
Index ranges	-9 ≤ <i>h</i> ≤ 9, -11 ≤ <i>k</i> ≤ 11, -14 ≤ <i>l</i> ≤ 15	
Reflections collected	10049	
Independent reflections	3358 [<i>R</i> (int) = 0.0174]	
Observed reflections	3267 [<i>I</i> > 2σ(<i>I</i>)]	
Absorption correction	multi-scan	
Max. and min. transmission	0.745 and 0.65	
Refinement method	Full	
Data / restraints / parameters	3358 / 0 / 192	
Goodness of fit	1.121	
Final <i>R</i> indices [<i>I</i> > 2σ(<i>I</i>)]	<i>R</i> ₁ = 0.0163, <i>wR</i> ₂ = 0.0405	
<i>R</i> indices (all data)	<i>R</i> ₁ = 0.017, <i>wR</i> ₂ = 0.0408	
Largest diff. peak and hole	0.271 and -0.539e.Å ⁻³	

Appendix

Crystal data and structure refinement for complex **15**

Formula	C ₂₅ H ₂₆ ClNO ₂ Ru	
Formula weight	492.99	
Size	0.2645 x 0.2443 x 0.1851 mm	
Crystal morphology	Red Plate	
Temperature	173(2) K	
Wavelength	0.71073 Å [Mo-K _α]	
Crystal system	Monoclinic	
Space group	P2 ₁ /c	
Unit cell dimensions	$a = 9.4634(9) \text{ \AA}$	$\alpha = 90^\circ$
	$b = 25.1678(17) \text{ \AA}$	$\beta = 113.405(10)^\circ$
	$c = 9.9602(9) \text{ \AA}$	$\gamma = 90^\circ$
Volume	2177.1(3) Å ³	
Z	4	
Density (calculated)	1.504 Mg/m ³	
Absorption coefficient	0.859 mm ⁻¹	
<i>F</i> (000)	1008	
Data collection range	2.35 ≤ θ ≤ 29.74°	
Index ranges	-13 ≤ <i>h</i> ≤ 9, -34 ≤ <i>k</i> ≤ 33, -11 ≤ <i>l</i> ≤ 13	
Reflections collected	11633	
Independent reflections	5210 [<i>R</i> (int) = 0.0692]	
Observed reflections	4097 [<i>I</i> > 2σ(<i>I</i>)]	
Absorption correction	multi-scan	
Max. and min. transmission	1 and 0.78519	
Refinement method	Full	
Data / restraints / parameters	5210 / 0 / 265	
Goodness of fit	1.036	
Final <i>R</i> indices [<i>I</i> > 2σ(<i>I</i>)]	<i>R</i> ₁ = 0.0536, <i>wR</i> ₂ = 0.1058	
<i>R</i> indices (all data)	<i>R</i> ₁ = 0.0722, <i>wR</i> ₂ = 0.1157	
Largest diff. peak and hole	1.869 and -1.321 e.Å ⁻³	

Appendix

Crystal data and structure refinement for complex **16**

Formula	C ₂₀ H ₂₂ ClFO ₂ Ru	
Formula weight	449.9	
Size	0.77 x 0.71 x 0.68 mm	
Crystal morphology	Red Fragment	
Temperature	150(2) K	
Wavelength	0.71073 Å [Mo-K _α]	
Crystal system	Monoclinic	
Space group	P2 ₁ /c	
Unit cell dimensions	$a = 8.0542(10)$ Å	$\alpha = 90^\circ$
	$b = 12.4910(16)$ Å	$\beta = 100.154(6)^\circ$
	$c = 20.288(2)$ Å	$\gamma = 90^\circ$
Volume	2009.1(4) Å ³	
Z	4	
Density (calculated)	1.487 Mg/m ³	
Absorption coefficient	0.931 mm ⁻¹	
<i>F</i> (000)	912	
Data collection range	2.57 ≤ θ ≤ 36.8°	
Index ranges	-11 ≤ h ≤ 11, -17 ≤ k ≤ 17, -27 ≤ l ≤ 28	
Reflections collected	67057	
Independent reflections	6061 [$R(\text{int}) = 0.0638$]	
Observed reflections	5671 [$I > 2\sigma(I)$]	
Absorption correction	multi-scan	
Max. and min. transmission	0.57 and 0.5341	
Refinement method	Full	
Data / restraints / parameters	6061 / 0 / 230	
Goodness of fit	1.186	
Final <i>R</i> indices [$I > 2\sigma(I)$]	$R_1 = 0.0449$, $wR_2 = 0.1204$	
<i>R</i> indices (all data)	$R_1 = 0.0482$, $wR_2 = 0.1233$	
Largest diff. peak and hole	2.532 and -1.139e.Å ⁻³	

Crystal data and structure refinement for complex **17**

Formula	C ₆₄ H ₅₆ Cl ₄ F ₄ O ₈ Ru ₄	
Formula weight	1575.17	
Size	0.2384 x 0.1015 x 0.0463 mm	
Crystal morphology	Fragment Red	
Temperature	173(2) K	
Wavelength	0.71073 Å [Mo-K _α]	
Crystal system	Monoclinic	
Space group	P2 ₁ /c	
Unit cell dimensions	$a = 9.7211(3) \text{ \AA}$	$\alpha = 90^\circ$
	$b = 15.3371(5) \text{ \AA}$	$\beta = 104.656(3)^\circ$
	$c = 10.0487(4) \text{ \AA}$	$\gamma = 90^\circ$
Volume	1449.45(9) Å ³	
Z	1	
Density (calculated)	1.805 Mg/m ³	
Absorption coefficient	1.277 mm ⁻¹	
<i>F</i> (000)	784	
Data collection range	2.66 ≤ θ ≤ 29.8°	
Index ranges	-13 ≤ <i>h</i> ≤ 10, -13 ≤ <i>k</i> ≤ 20, -10 ≤ <i>l</i> ≤ 12	
Reflections collected	8123	
Independent reflections	3467 [<i>R</i> (int) = 0.0364]	
Observed reflections	3019 [<i>I</i> > 2σ(<i>I</i>)]	
Absorption correction	multi-scan	
Max. and min. transmission	1 and 0.46536	
Refinement method	Full	
Data / restraints / parameters	3467 / 0 / 191	
Goodness of fit	1.049	
Final <i>R</i> indices [<i>I</i> > 2σ(<i>I</i>)]	<i>R</i> ₁ = 0.0322, <i>wR</i> ₂ = 0.0722	
<i>R</i> indices (all data)	<i>R</i> ₁ = 0.0396, <i>wR</i> ₂ = 0.076	
Largest diff. peak and hole	0.753 and -0.73e.Å ⁻³	

Appendix

Crystal data and structure refinement for complex **19**

Formula	C ₂₀ H ₂₃ ClF ₃ IrO ₂	
Formula weight	542.03	
Size	0.21 x 0.18 x 0.12 mm	
Crystal morphology	Yellow Fragment	
Temperature	150(2) K	
Wavelength	0.71073 Å [Mo-K _α]	
Crystal system	Orthorhombic	
Space group	P2 ₁ 2 ₁ 2 ₁	
Unit cell dimensions	$a = 8.3447(9) \text{ \AA}$	$\alpha = 90^\circ$
	$b = 15.2720(18) \text{ \AA}$	$\beta = 90^\circ$
	$c = 15.4729(18) \text{ \AA}$	$\gamma = 90^\circ$
Volume	1971.9(4) Å ³	
Z	4	
Density (calculated)	1.826 Mg/m ³	
Absorption coefficient	6.925 mm ⁻¹	
$F(000)$	1048	
Data collection range	$2.63 \leq \theta \leq 31.9^\circ$	
Index ranges	$-10 \leq h \leq 12, -22 \leq k \leq 22, -22 \leq l \leq 22$	
Reflections collected	109495	
Independent reflections	6682 [$R(\text{int}) = 0.0492$]	
Observed reflections	6515 [$I > 2\sigma(I)$]	
Absorption correction	multi-scan	
Max. and min. transmission	0.4954 and 0.3282	
Refinement method	Full	
Data / restraints / parameters	6682 / 0 / 232	
Goodness of fit	1.038	
Final R indices [$I > 2\sigma(I)$]	$R_1 = 0.0144, wR_2 = 0.0323$	
R indices (all data)	$R_1 = 0.0154, wR_2 = 0.0327$	
Largest diff. peak and hole	0.84 and -1e.Å ⁻³	
Absolute structure parameter	0.010(4)	

Appendix

Crystal data and structure refinement for complex **20**

Formula	$C_{3.09}H_{3.45}N_{0.18}O_{0.91}Ti_{0.18}$	
Formula weight	66.4	
Size	0.33 x 0.29 x 0.28 mm	
Crystal morphology	Yellow Fragment	
Temperature	150(2) K	
Wavelength	0.71073 Å [Mo- K_{α}]	
Crystal system	Monoclinic	
Space group	$P2_1/c$	
Unit cell dimensions	$a = 8.6093(17)$ Å	$\alpha = 90^\circ$
	$b = 16.186(3)$ Å	$\beta = 102.517(9)^\circ$
	$c = 12.669(2)$ Å	$\gamma = 90^\circ$
Volume	1723.5(6) Å ³	
Z	22	
Density (calculated)	1.408 Mg/m ³	
Absorption coefficient	0.522 mm ⁻¹	
$F(000)$	760	
Data collection range	$2.07 \leq \theta \leq 33.11^\circ$	
Index ranges	$-13 \leq h \leq 8, -24 \leq k \leq 24, -16 \leq l \leq 19$	
Reflections collected	56323	
Independent reflections	6532 [$R(\text{int}) = 0.0599$]	
Observed reflections	5062 [$I > 2\sigma(I)$]	
Absorption correction	multi-scan	
Max. and min. transmission	0.8663 and 0.8487	
Refinement method	Full	
Data / restraints / parameters	6532 / 0 / 220	
Goodness of fit	1.047	
Final R indices [$I > 2\sigma(I)$]	$R_1 = 0.0504, wR_2 = 0.1367$	
R indices (all data)	$R_1 = 0.0671, wR_2 = 0.1506$	
Largest diff. peak and hole	0.814 and $-0.317 e \cdot \text{Å}^{-3}$	

Crystal data and structure refinement for complex **21**

Formula	$C_{16}H_{13}ClFNOTi_{0.50}$	
Formula weight	313.67	
Size	0.29 x 0.17 x 0.11 mm	
Crystal morphology	Yellow Fragment	
Temperature	150(2) K	
Wavelength	0.71073 Å [Mo- K_{α}]	
Crystal system	Monoclinic	
Space group	$C2/c$	
Unit cell dimensions	$a = 25.614(3)$ Å	$\alpha = 90^{\circ}$
	$b = 8.3638(9)$ Å	$\beta = 126.138(4)^{\circ}$
	$c = 16.6382(19)$ Å	$\gamma = 90^{\circ}$
Volume	$2878.6(6)$ Å ³	
Z	8	
Density (calculated)	1.448 Mg/m ³	
Absorption coefficient	0.529 mm ⁻¹	
$F(000)$	1288	
Data collection range	$1.97 \leq \theta \leq 34.46^{\circ}$	
Index ranges	$-39 \leq h \leq 40$, $-12 \leq k \leq 12$, $-25 \leq l \leq 26$	
Reflections collected	39322	
Independent reflections	5866 [$R(\text{int}) = 0.0528$]	
Observed reflections	4505 [$I > 2\sigma(I)$]	
Absorption correction	multi-scan	
Max. and min. transmission	0.9431 and 0.8595	
Refinement method	Full	
Data / restraints / parameters	5866 / 0 / 187	
Goodness of fit	1.03	
Final R indices [$I > 2\sigma(I)$]	$R_1 = 0.0378$, $wR_2 = 0.0943$	
R indices (all data)	$R_1 = 0.0568$, $wR_2 = 0.1042$	
Largest diff. peak and hole	0.58 and $-0.263 e \cdot \text{Å}^{-3}$	

Crystal data and structure refinement for complex **22**

Formula	$C_{36}H_{32}Cl_4N_4O_2Ti$	
Formula weight	742.36	
Size	0.47 x 0.18 x 0.09 mm	
Crystal morphology	Yellow Fragment	
Temperature	293(2) K	
Wavelength	0.71073 Å [Mo- K_α]	
Crystal system	Monoclinic	
Space group	$P2_1/n$	
Unit cell dimensions	$a = 15.1938(5)$ Å	$\alpha = 90^\circ$
	$b = 15.4956(5)$ Å	$\beta = 113.222(2)^\circ$
	$c = 16.0930(7)$ Å	$\gamma = 90^\circ$
Volume	3481.9(2) Å ³	
Z	4	
Density (calculated)	1.416 Mg/m ³	
Absorption coefficient	0.592 mm ⁻¹	
$F(000)$	1528	
Data collection range	$2.63 \leq \theta \leq 26.4^\circ$	
Index ranges	$-18 \leq h \leq 18, -16 \leq k \leq 19, -20 \leq l \leq 17$	
Reflections collected	18609	
Independent reflections	6914 [$R(\text{int}) = 0.0405$]	
Observed reflections	5178 [$I > 2\sigma(I)$]	
Absorption correction	multi-scan	
Max. and min. transmission	0.7454 and 0.6607	
Refinement method	Full	
Data / restraints / parameters	6914 / 0 / 428	
Goodness of fit	1.029	
Final R indices [$I > 2\sigma(I)$]	$R_1 = 0.0414, wR_2 = 0.0863$	
R indices (all data)	$R_1 = 0.065, wR_2 = 0.0959$	
Largest diff. peak and hole	0.502 and $-0.488e.\text{Å}^{-3}$	

Crystal data and structure refinement for complex **23**

Formula	$C_{32}H_{26}F_2N_2O_4Ti$	
Formula weight	588.45	
Size	0.31 x 0.27 x 0.17 mm	
Crystal morphology	Orange prism	
Temperature	120(2) K	
Wavelength	0.71073 Å [Mo- K_{α}]	
Crystal system		
Space group		
Unit cell dimensions	$a = 13.9627(13)$ Å	$\alpha = 90^{\circ}$
	$b = 13.9627(13)$ Å	$\beta = 90^{\circ}$
	$c = 77.719(7)$ Å	$\gamma = 120^{\circ}$
Volume	13122(2) Å ³	
Z	18	
Density (calculated)	1.34 Mg/m ³	
Absorption coefficient	0.345 mm ⁻¹	
$F(000)$	5472	
Data collection range	$2.13 \leq \theta \leq 25.02^{\circ}$	
Index ranges	$-16 \leq h \leq 16, -16 \leq k \leq 16, -92 \leq l \leq 91$	
Reflections collected	33971	
Independent reflections	5166 [$R(\text{int}) = 0.0487$]	
Observed reflections	4423 [$I > 2\sigma(I)$]	
Absorption correction	multi-scan	
Max. and min. transmission	0.7457 and 0.7016	
Refinement method	Full	
Data / restraints / parameters	5166 / 0 / 372	
Goodness of fit	1.144	
Final R indices [$I > 2\sigma(I)$]	$R_1 = 0.057, wR_2 = 0.1229$	
R indices (all data)	$R_1 = 0.0676, wR_2 = 0.1267$	
Largest diff. peak and hole	0.332 and $-0.464e.\text{Å}^{-3}$	

Crystal data and structure refinement for complex **24**

Formula	$C_{38}H_{38}Cl_2N_4O_2Ti$
Formula weight	701.52
Size	0.31 x 0.27 x 0.09 mm
Crystal morphology	Orange Fragment
Temperature	293(2) K
Wavelength	0.71073 Å [Mo- K_α]
Crystal system	Monoclinic
Space group	$P2_1/n$
Unit cell dimensions	$a = 15.3737(12)$ Å $\alpha = 90^\circ$ $b = 15.4790(14)$ Å $\beta = 113.003(2)^\circ$ $c = 16.1154(12)$ Å $\gamma = 90^\circ$
Volume	$3530.0(5)$ Å ³
Z	4
Density (calculated)	1.32 Mg/m ³
Absorption coefficient	0.433 mm ⁻¹
$F(000)$	1464
Data collection range	$2.63 \leq \theta \leq 29.24^\circ$
Index ranges	$-18 \leq h \leq 21$, $-21 \leq k \leq 21$, $-21 \leq l \leq 22$
Reflections collected	36183
Independent reflections	9529 [$R(\text{int}) = 0.0837$]
Observed reflections	5244 [$I > 2\sigma(I)$]
Absorption correction	multi-scan
Max. and min. transmission	0.7459 and 0.6847
Refinement method	Full
Data / restraints / parameters	9529 / 0 / 430
Goodness of fit	0.851
Final R indices [$I > 2\sigma(I)$]	$R_1 = 0.0436$, $wR_2 = 0.0702$
R indices (all data)	$R_1 = 0.101$, $wR_2 = 0.0818$
Largest diff. peak and hole	0.286 and $-0.528 e.\text{Å}^{-3}$

Crystal data and structure refinement for complex **25**

Formula	$C_{36}H_{36}Cl_2N_2O_2Ti$	
Formula weight	647.47	
Size	0.33 x 0.29 x 0.11 mm	
Crystal morphology	Orange Fragment	
Temperature	173(2) K	
Wavelength	0.71073 Å [Mo- K_α]	
Crystal system	Monoclinic	
Space group	$C2/c$	
Unit cell dimensions	$a = 30.836(5)$ Å	$\alpha = 90^\circ$
	$b = 8.2511(6)$ Å	$\beta = 126.83(3)^\circ$
	$c = 15.442(2)$ Å	$\gamma = 90^\circ$
Volume	3145.0(7) Å ³	
Z	4	
Density (calculated)	1.367 Mg/m ³	
Absorption coefficient	0.478 mm ⁻¹	
$F(000)$	1352	
Data collection range	$3.17 \leq \theta \leq 29.78^\circ$	
Index ranges	$-41 \leq h \leq 42, -10 \leq k \leq 9, -20 \leq l \leq 15$	
Reflections collected	12084	
Independent reflections	3817 [$R(\text{int}) = 0.0322$]	
Observed reflections	3080 [$I > 2\sigma(I)$]	
Absorption correction	multi-scan	
Max. and min. transmission	1 and 0.86393	
Refinement method	Full	
Data / restraints / parameters	3817 / 0 / 197	
Goodness of fit	1.039	
Final R indices [$I > 2\sigma(I)$]	$R_1 = 0.0388, wR_2 = 0.0804$	
R indices (all data)	$R_1 = 0.0555, wR_2 = 0.0872$	
Largest diff. peak and hole	0.406 and $-0.367 e.\text{Å}^{-3}$	